Spring 2016

# Mutlifunctional platforms for gene and drug delivery for cancer therapy

Jeffery J. Ambrose Jr.
*Louisiana Tech University*

# MUTLIFUNCTIONAL PLATFORMS FOR GENE AND DRUG DELIVERY FOR CANCER THERAPY

By

Jeffery J. Ambrose Jr., B.S.

A Dissertation Presented in Partial Fulfillment
of the Requirements of the Degree of
Doctor of Philosophy

COLLEGE OF ENGINEERING AND SCIENCES
LOUISIANA TECH UNIVERSITY

May 2016

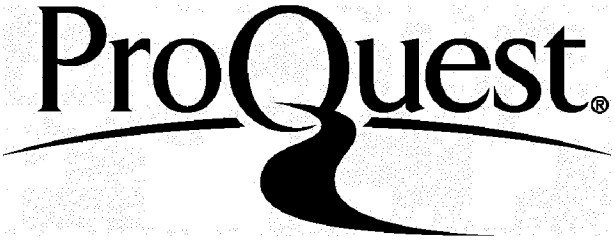

LOUISIANA TECH UNIVERSITY

**THE GRADUATE SCHOOL**

4-25-16

Date

We hereby recommend that the dissertation prepared under our supervision by Jeffery J. Ambrose Jr. B.S.

entitled MUTLIFUNCTIONAL PLATFORMS FOR GENE AND DRUG DELIVERY FOR CANCER THERAPY

be accepted in partial fulfillment of the requirements for the Degree of Doctor of Philosophy in Biomedical Engineering

Supervisor of Dissertation Research

Head of Department

Biomedical Engineering

Department

Recommendation concurred in:

Advisory Committee

**Approved:**

Director of Graduate Studies

**Approved:**

Dean of the Graduate School

Dean of the College

GS Form 13a
(6/07)

# ABSTRACT

The National Cancer Institute and the American Cancer Society estimate that 1.6 million new cancer incidences and over half a million cancer related deaths occur annually [1][2]. Cancer the second most common cause of death in the United States [1], [2]. Although the causes of cancer can vary depending on cell type, all or almost all instances of cancer arise from a mutation or from an abnormal activation of the cellular genes that control cell growth and mitosis [3].

Treatment of a given cancer type depends on the subtype, stage and progression of the cancer. Varieties of cancer therapy include surgery, immunotherapy, radiation therapy, chemotherapy, hormone therapy, targeted therapy, gene therapy and stem cell transplant [4]. Some treatments help patients achieve remission, and with additional treatment, can cure the illness. Many of the available therapies have drawbacks that can negatively affect patients. Some of these drawbacks include systemic, as opposed to local, delivery of chemotherapeutic agents, pain, hair loss, reoccurrence and metastasis post-surgery.

A major goal of current research in cancer medicine is to develop novel strategies and materials to halt the advance of cancer and its potential metastasis. This goal can be achieved by employing strategies that can localize treatments to affected areas, sustaining drug release to these areas, and destabilizing cellular processes that affect cell-drug interaction.

The focus of this dissertation was to design and develop novel injectable and implantable applications for gene and chemotherapeutic cancer treatment. The use of naturally occurring materials can improve gene and drug delivery characteristics *in vivo*. The research aimed to establish halloysite nanotubes as a novel delivery system for drugs and/or genes. The first stage of this goal was to analyze the drug and gene release by establish a release profile from halloysite nanotubes. The next stage was *in vitro* assay to determine the transfection efficiency of pIRES2-EGFP loaded Halloysite Nanotubes (HNTs), and the and *in vitro* cell proliferation and cytotoxicity assay of methotrexate-loaded HNTs. Results indicate that methotrexate-or pIRES2-EGFP loaded nanotubes, and composite films can boost transfection efficiency and reduce cancer cell growth and proliferation. Nanotubes showed promise in gene delivery as they enhanced the transfection efficiency of commonly used transfection reagents. Nanotubes and nanotube-imbedded films show promise as novel chemotherapeutic treatments as the provided a platform for sustained and localized drug delivery *in vitro*.

# APPROVAL FOR SCHOLARLY DISSEMINATION

The author grants to the Prescott Memorial Library of Louisiana Tech University the right to reproduce, by appropriate methods, upon request, any or all portions of this Dissertation. It is understood that "proper request" consists of the agreement, on the part of the requesting party, that said reproduction is for his personal use and that subsequent reproduction will not occur without written approval of the author of this Dissertation. Further, any portions of the Dissertation used in books, papers, and other works must be appropriately referenced to this Dissertation.

Finally, the author of this Dissertation reserves the right to publish freely, in the literature, at any time, any or all portions of this Dissertation.

Author _____

Date _____

# DEDICATION

To the head of my life, my Lord and Savior Jesus Christ, my parents, Jeffery Ambrose Sr. and Dianne Galatas, brothers, Julian Ambrose and Justin Ambrose, grandparents, Marie Ortiz, Donald Galatas, Joseph Ambrose, Sr. and Florestine Ambrose.

# TABLE OF CONTENTS

# LIST OF TABLES

# LIST OF FIGURES

# ACKNOWLEDGMENTS

First and foremost, I would like to express a tremendous amount of gratitude to my mentor, Dr. David K. Mills, for his constant support in defining my dissertation. His guidance and encouragement has fueled my drive to complete my doctoral degree. My experiences as a member of his lab have taught me how to excel on both the academic and professional level.

I would also like to thank my advisory committee members Drs. William Wolf, Steven A. Jones, Teresa Murray and Bryant Hollins for their support and assistance with my research and matriculation. I would like to mention Dr. Alfred Gunasekaran and Dr. Jibao He for their help with electron microscopy imaging and Dr. Rebecca Giorno for her assistance with the bacterial replication of plasmids. I also thank Dr. Yuri Lvov for allowing me to use various instruments in his laboratory for characterization and Dr. Scott Ray who assisted in the statistical analysis of data. Dr. James Spaulding has also helped me troubleshoot common lab instrumentation, as well as, cell culture instruments.

I would not have been able to achieve any of this without the love and support of my family and friends. My parents, Dianne Galatas and Jeffery Ambrose, Sr., have continued to support me spiritually mentally and financially throughout my academic matriculation. They have been with me through the ups and downs and have made sure I was steadfast in my journey. I would also like to thank my brother, Julian Ambrose, who has had a continued interest in my work and also taught me how to use adobe Photoshop.

I would like to thank all of the civil rights activist who paved the way for me and take a special mention of my grandmother Marie Ortiz (formerly Galatas) whose work in the civil rights movement allowed me to be here today. A special thanks goes out to my undergraduate advisor, Dr. Murty Kambhampati, who encouraged me to pursue a Ph.D.

I would like to extend thanks to my lab members, especially Mr. Chris Boyer, Mr. Lin Sun and Dr. Jeff Weisman, for supporting and assisting me on these projects and through trying times. I would like to thank Udaybhanu Jammalamadaka and Mr. Karthik Tappa for their help with electron microscope imaging. I would also like to extend thanks to Mr. Payam Khoshkenar and Mortezza Razoulin for their assistance with fabrication, characterization and cellular assays. Thank you to you all and to all the family, friends and colleagues that contributed to my experiences at Louisiana Tech.

# CHAPTER 1

# INTRODUCTION AND BACKGROUND

The National Cancer Institute and the American Cancer Society estimate that 1.6 million new cancer incidences and over half a million cancer related deaths occur annually [1][2]. Cancer the second most common cause of death in the United States [1] [2]. Although the causes of cancer can vary depending on cell type, all or almost all instances of cancer arise from a mutation or from an abnormal activation of the cellular genes that control cell growth and mitosis [3].

Treatment of a given cancer type depends on the subtype, stage and progression of the cancer. Varieties of cancer therapy include surgery, immunotherapy, radiation therapy, chemotherapy, hormone therapy, targeted therapy, gene therapy and stem cell transplant [4]. Some treatments help patients achieve remission, and with additional treatment, can cure the illness. Many of the available therapies have drawbacks that can negatively affect patients. Some of these drawbacks include systemic, as opposed to local, delivery of chemotherapeutic agents, pain, hair loss, reoccurrence and metastasis post-surgery.

A major goal of current research in cancer medicine is to develop novel strategies and materials to halt the advance of cancer and its potential metastasis. This goal can be achieved by employing strategies that can localize treatments to affected areas, sustaining

drug release to these areas, and destabilizing cellular processes that affect cell-drug interaction.

## 1.1 Cancer and Therapies

Cancer, also referred to as malignant tumors or malignant neoplasm, is a generic term used to describe a variety of illnesses caused by mutations and/or disruptions in cellular machinery that cause cells to multiply uncontrollably and invade other tissues. Generally, cell growth, damage repair, and death within the body are highly ordered. Malignant neoplasm can disrupt this order by allowing cells to live past their normal cell death and multiply incessantly. Cancerous cells multiply to form masses called malignant tumors which can invade surrounding tissues and metastasize, a term used to describe the circulation and development of malignant tumors distant from the primary site of malignant neoplasm. Cancerous tumors can further disrupt the body's natural order by syphoning off nutrients to support their own growth and creating abnormalities in surrounding tissues. In this chapter, I will discuss different types of cancer, their causes, and the current treatment modalities.

Several cell lines were chosen based on the clinical relevance of the research outlined in this dissertation. Osteosarcoma, breast cancer and prostate cancer were chosen due to potential applications of halloysite nanotubes for gene delivery, drug delivery and blow sprayed chitosan films for adjuvant delivery of chemo therapeutic agents. Drug or gene loaded halloysite nanotubes could potentially be injected into tumors to shrink them and drug loaded films may be used to coats sites where tumors have been removed.

### 1.1.1 Osteosarcoma

Osteosarcoma is the most common primary bone cancer. It is an aggressive neoplasm that arises from primitive bone forming mesenchymal cells. Osteosarcoma is most prevalent in children and young adults, although it can affect a person of any age. Around 1000 new cases occur per year and more than 400 of those new cases are in patients under the age of 18 [5]. Most osteosarcomas affect people between the ages of 10-30, with the most affected group being teens. In addition at least 10% of the cases affect people over the age of 60 [6].

Osteosarcoma occurs most frequently in the metaphyseal portion of tubular long bones with 42% incidence in the femur, 19% in the tibia and 10% in the humerus. Around 8% of all cases affect the skull and jaw, while another 8% arise in the pelvis [7].Subtypes of osteosarcoma are differentiated by grade:

1. High grade is the fastest growing grade of the osteosarcomas. They do not exhibit normal morphology of bone and many can be observed in mitosis. High-grade osteosarcomas are the most common osteosarcoma affecting youths and there are many different types. The most common are osteoblastic, chondroblastic and fibroblastic. Other types can include mixed, small cell, telangiectatic and pagetoid (a tumor resulting from Paget disease of the bone) and post-radiation (a tumor resulting from radiation therapy) [8].
2. Intermediate grade falls between the high grade and low grade. The most common type is periosteal (just cortical intermediate grade) [8].
3. Low grade is the slowest growing form, and has morphology closer to that of normal bone. Some of the more common low-grade osteosarcomas include

periosteal (juxta cortical low grade) and intramedullary or intraosseous well differentiated (low-grade central) [8]. See **Table 1-1**.

**Table 1-1:** Osteosarcoma types [9].

| **Osteosarcoma Types** |
|---|
| Central |
| High-grade |
| Conventional |
| Telangiectatic |
| Small cell |
| Epithelioid |
| Osteoblastoma-like |
| Chondroblastoma-like |
| Fibrohistiocytic |
| Giant cell–rich |
| Low-grade |
| Low-grade central |
| Fibrous dysplasia–like |
| Desmoplastic fibroma–like |
| Surface |
| Low-grade |
| Parosteal |
| Intermediate-grade |
| Periosteal |
| High-grade |
| Dedifferentiated parosteal |
| High-grade surface |
| Intracortical |
| Gnathic |
| Extraskeletal |
| High-grade |
| Low-grade |

Osteosarcoma is described as malignant tumors of the connective tissue that can give rise to bone. Osteosarcoma retains the ability to produce fibrous tissue and cartilage matrix. Histologically, it is more similar to bone fracture or fracture callus than other differentiated bone tumors. The traditional method of classification for osteosarcoma has led to three subdivisions: osteoblastic, chondroblastic and fibroblastic. However,

osteosarcomas typically exhibit all three cell types in varying amounts. Classification generally means 50% or more of a particular cell type is present.

Osteosarcoma typically affects the medullary cavity of the metaphysis of a growing long tubular bone, but it also can arise at the surface, cortex and even extra-skeletal sites. Osteosarcomas on the bone surface are 20 times less common then their medullary counterparts [9]. Patients with bone surface osteosarcoma are on average a decade or more, older than those with osteosarcomas of medullary origin. Low and high grade can be present throughout the osteosarcoma. However, when they are of medullary origin they are most likely high grade.

Symptoms of osteosarcoma are generally nonspecific; the most common symptom is pain. At first the pain can be inconsistent but over time it worsens and can become constant. Often, if it affects the lower extremities, it can cause a limp. The pain can be so excruciating at times it can interrupt sleep and prompt affected persons to seek medical attention. Another common symptom is swelling, which results in a firm and almost always tender mass in the affected bone region. This swelling can also lead to a limp, loss of function and decreased range of motion. These symptoms are common in active children and may be thought to arise from some other type of injury complicating diagnosis. Although osteosarcomas can cause bones to weaken, fractures are not common. Rare forms of osteosarcomas tend to weaken bones and cause fractures.

Diagnosis usually begins with a physical examination of the bone to see if a tumor or abnormal mass is near the bone. If an abnormal mass is observed, the next step is usually imaging tests followed by a biopsy. Imaging tests help elucidate whether the suspicious mass is a tumor, how far it has spread, where it was derived and whether

treatment is working. The first imaging examination is usually a bone x-ray. An x-ray will strongly suggest whether a mass is a tumor versus some type of infection. Magnetic resonance imaging gives a more detailed analysis of the affected region and can help to identify the progression, as well as, whether there is smaller tumor in close proximity to the major tumor mass. CT scans, chest X-rays and bone scans can also be used to determine the progression of the cancer, whether it has grown into nearby tissue or bone and whether or not it has spread to the lungs. While imaging may strongly suggest that the patient may be suffering from osteosarcoma, a biopsy is necessary to confirm that the abnormality is osteosarcoma. A blood test may also be administered, as it can provide useful information about the progression of osteosarcoma.

Great advances have recently been made in the treatment of osteosarcoma. Current and cutting edge treatments will be reviewed briefly in this section and more thoroughly in the cancer treatments section. In the 1960's, amputation was the major mode of treatment for osteosarcomas, the survival rate post diagnosis was 2 years and amputation was associated with a 5 year survival rate of less than 20% [8][5]. Current treatments include surgery, chemotherapy and radiation therapy. Typically surgeries fall into three categories, including limb salvage surgery (depending on the size), tumor excision (depending on whether it has invaded surrounding tissues) and amputation. Most regular treatments combine chemotherapy and surgery. Several groundbreaking strategies improved outcomes drastically by adding adjuvant and neoadjuvant chemotherapies increasing long term survival rates to nearly 70% [5]. Furthermore, surgical advancements in limb salvage surgeries have made amputation a rarity. For localized pediatric osteosarcoma, high dose methotrexate, doxorubicin and cisplatin are the

standard for cooperative group clinical trials [5]. For young adults, less is known about how the treatment and pathology of the illness affect survival, but age is a prognostic factor for osteosarcoma as well as other cancers [5].

Osteosarcoma occurs slightly more in men than in women and in African Americans than in whites. People who have been subjected to radiation therapy, as well as those who have a noncancerous bone disease are also slightly more likely to develop osteosarcoma (e.g. Paget's disease) [8][9]. Also people with rare inherited bone cancer syndromes have an increased risk of developing osteosarcoma, these illnesses can include:

1. The Li-Fraumeni syndrome can be attributed to the TP53 tumor suppressor gene. This syndrome increases the risk of develop certain types of cancer, including breast cancer, brain tumors, osteosarcoma, and other types of sarcoma.
2. Retinoblastoma is a rare juvenile cancer of the eye. Many children have the inherited form of retinoblastoma where all the cells of the body have a mutation in the RB1 gene. Children affected by retinoblastoma are more likely to develop bone or soft tissue sarcomas, including osteosarcoma. When radiation therapy is used for retinoblastoma treatment, the risk of osteosarcoma in the bones around the eye increases.
3. Rothmund-Thomson syndrome is the result of abnormal changes in the REQL4 gene. Children with this syndrome tend to have a stunted growth and typically have skeletal problems and rashes. They also are more likely to develop osteosarcoma.

### 1.1.2 Prostate Cancer

Prostate cancer is a carcinoma that that develops in the prostate gland of the male reproductive system [10]. Prostate cancer is the second most common cancer affecting men in the United States. In 2015 over 220,000 new cases of prostate cancer will be reported and over 27,000 men will die from prostate cancer [11]. One in seven men will have prostate cancer in their lifetime [11]. Prostate cancer is a disease that primarily affects older men and it is uncommon for a man to develop it before the age of 40. 6 out of 10 men who have prostate cancer are over the age of 65 [11]. In the U.S., it is more common in African American men than in white men and almost 99% of cases occur in men over the age of 50.

Prostate cancer develops when the rates of cell death and cell division are not equal and can in turn lead to tumor growth [12]. After the initial transformation, cells can undergo additional mutations that contribute to tumor growth, progression and eventually metastasis [12]. 95% of all prostate cancers are adenocarcinomas. 4% have transitional morphologies and are derived from urethral lining of the prostatic urethra and an even smaller number neuroendocrine morphology and are believed to be derived from neuroendocrine stem cells normally in the prostate [12].

Adenocarcinoma of the prostate gland can arise in several locations throughout the prostate. 70% of the time it arises in the peripheral zone, 15-20% in the transition zone and 15-20% in the central zone [12]. As it spreads, it invades the capsule medially and spreads by direct extension through vascular and lymphatic channels. More aggressive tumors invade the seminal vesicles and bladder and can cause urethra obstructions. As the cancer metastasizes it can invade bones of the pelvis, spine (lumbar and thoracic) femur,

ribs and sternum. As it viscerally metastasizes it commonly invades the lungs, liver and adrenal glands.

Prostate cancer has been called the 'silent killer' because often times it is asymptomatic. Most are slow growers and often go unnoticed because they are symptomless or have very mild symptoms. More advanced cases typically have symptoms including pain and/or difficulty urinating (20-25%), blood in urine (10-15%), fecal incontinence and erectile dysfunction. Pain in the hips, back, chest or bones can indicate that the cancer has spread. As the tumor grows, it can begin to press against the spine, resulting in weakness in the lower extremities (20-40%) and/or a weakened bladder control [13][12]. Metastatic symptoms can include weight loss from lack of appetite, bone with or without fracture due to the cancers affinity for bone and back and leg pain due to obstruction of local venous and lymphatic systems resulting in edema [12]. Also ureteral obstruction can occur due to local prostate growth, nodal metastasis and other factors. The presence of one or more of these symptoms is not a specific indicator of prostate cancer, and over half of men affected are symptomless.

Several diagnostic methods are used for prostate cancer, but only biopsy provides a definitive diagnosis. In most cases, a patient is symptomless; therefore, the American Cancer Society recommends a prostate examination for highest risk men at age 40, high risk men at age 45 and average risk men at age 50 annually.

Staging describes the process of determining the amount of cancer present throughout the body and where it is located. Staging can be clinical, which is determined during the patient's diagnosis, or pathological, which is determined by examination of surgically removed tissue. A detailed report on staging can be reviewed at the American

Cancer Society's webpage. The physical examination typically involves a prostate specific antigen blood test (PSA) and a digital rectal exam. The American Cancer Society states "Men with a PSA level between 4 and 10 have about a 1 in 4 chance of having prostate cancer. If the PSA is more than 10, the chance of having prostate cancer is over 50%," it is then up to the doctor's discretion at what level to perform a biopsy. In men diagnosed with prostate cancer, the results from a PSA can be used along with tumor grade and physical examination to determine if other tests are needed. The results can also be useful in staging as a high PSA number can indicate the metastasis of prostate cancer. Digital rectal examinations (DRE) are administered to check for abnormalities, and the number and timing of abnormalities can indicate metastasis. Biopsy is the best test option, as it is a confirmatory test. The procedure usually uses a transurethral ultrasound to pinpoint the area for biopsy and get a general image of the prostate. Prostate MRI provides better resolution when imaging the prostate and is the standard for imaging due to the TRUS's resolution issues.

The Gleason score is the most commonly used system to grade prostate cancer. The Gleason score is determined by studying biopsy under low power magnification. Score is calculated by adding the grades (1-5) of the two most common tumor growth patterns. The range is between 2 and 10 with 2 being the least aggressive and 10 being the most aggressive. The grades are based on how similar the cells look to unaffected glandular tissue. A grading of 1 indicates a near normal pattern, and 5 indicates a highly abnormal pattern with little or no glandular similarity. The scoring system is as follows:

1. A score of 2-4 is considered low grad or well differentiated [12].
2. A score of 5-7 is considered moderate grade or moderately differentiated [12].

3. A score of 8-10 is considered high grade with little to no differentiation [12].

Glandular architecture evaluation by Gleason score is the most widely used histological assessment for grading prostate cancer, although other histological changes such as cell and nuclear morphology, neuroendocrine differentiation, and vascularity can have prognostic significance [12].

Cancer may be linked to several some precancerous conditions. Prostatic intraepithelial neoplasia (PIN) is a possible precancerous end of morphology of cellular proliferation that presents itself in prostatic ducts, ductules, and acini [12]. Low grade PIN cells have almost identical morphology to cells of an unaffected prostate, while high grade PIN cells have a morphology that differs strongly from normal cells. The presence of PIN cells can begin as early as the late 20's of an adult male and about half of males have this condition by the age of 50. Low grade PIN cells do not necessarily develop into prostate cancer, and the importance of low grade PIN in the development of prostate cancer has not been determined. Patients with high grade PIN, have a 20% chance of developing cancer in another part of their prostate, and these patients are generally monitored [13][12]. Proliferative Inflammatory Atrophy (PIA) is another precursor to prostate cancer. Cells of the prostate are smaller than normal cells and inflammation can be observed. Many researchers believe this condition can result in high grade PIN and even prostate cancer [13]. Another condition that may suggest the development of prostate cancer is atypical small acinar proliferation (ASAP). In this condition, cells appear to be cancerous but are often too few to make that assumption. ASAP indicates a high likelihood of cancer.

TNM staging is the most widely used system for staging, and can be useful in the treatment process. The staging system is based on five key elements [13]:

1. The extent of the primary tumor (T category)
2. Whether the cancer has spread to nearby lymph nodes (N category)
3. The absence or presence of distant metastasis (M category)
4. The PSA level at the time of diagnosis
5. The Gleason score, based on the prostate biopsy (or surgery)

The most common treatment modalities are surgery, chemotherapy, radiation therapy, cryotherapy, and gene therapy and vaccine treatment. Treatment often involves a combination of said treatment and can vary based on patient demographics. Another important factor involving demographics and family history is the level of risk factor for the patient. Risk factor, along with grading and staging, can determine how aggressive the treatment needs to be. Here I will discuss, in general, some treatment modalities commonly used to treat prostate adenocarcinoma. The main surgical method for prostate cancer is through a radical prostatectomy. This procedure involves the removal of the entire prostate gland and some of the surrounding tissues. Prostatectomy may involve full or partial removal of the prostate gland and surrounding tissues [12], [13]. Laparoscopic approaches are noninvasive techniques, which use small incisions and laparoscopic tools performed by specialized surgeons to remove the prostate gland. This procedure can often involve the surgeon either holding the tools directly, or using a robotic assisted arm to hold tools and precisely remove tissues. Cryotherapy involves the freezing of tissues to destroy affected cell. This procedure is carried out with cold gas to flash freeze the tissue, and transrectal ultrasound (TRUS) is used to target cancerous tissue. A catheter is

implemented to help drain necrotic tissue over a 3 week period. Common side effects of surgical procedures include incontinence, impotence, changes in orgasm, lymphedema, change in penis length, and hernia. Many of these side effects are treatable or manageable.

Radiation therapy uses high energy radiation to destroy cancer cells. The two main types of radiation therapy are external beam radiation (EBRT) and brachytherapy (internal radiation). EBRT uses a focused beam of radiation to kill cancer cell and may also be used in bone to eliminate bone metastasis. Brachytherapy uses a radioactive seed, millimeters in size, implanted into the prostate to destroy cells. It may be used as the first treatment for low-grade localized prostate cancer and has cure rates comparable to those of radical prostatectomy. Brachytherapy may be paired with hormone treatment as part of the first treatment for localized cancer and micro-metastasis into surrounding tissues. For recurrent cancer, cancer that is not fully removed, or advanced cancer, brachytherapy may reduce tumor size and provide relief from present and possible future symptoms [12], [13]. Side effects are similar to surgery but may also include bladder problems, bowel problems and fatigue.

Hormone therapy, referred to as androgen deprivation therapy (ADT) or androgen suppression therapy, is used to reduce levels called androgens in the body, or to stop them from affecting the growth of prostate cancer cells. Testosterone and dihydrotestosterone (DHT) are the main androgens, the majority of which come from the testicles and adrenal glands [12], [13]. This treatment can slow the growth rate and shrink tumors of the prostate but alone does not cure prostate cancer. ADT may be used neoadjuvantly to shrink cancer before radiation therapy or in tandem with radiation

therapy. In addition, this treatment may be used if the cancer has spread, is recurrent, or remains following another procedure [13]. Many types of hormone therapy can be used to treat prostate cancer. Some therapies lower the levels of testosterone or other androgens, while others block the action of those hormones. Side effects are: loss of libido, hot flashes, breast tenderness and growth of breast tissue, osteoporosis which can lead to broken bones, anemia, decreased mental sharpness, and loss of muscle mass, weight gain, fatigue, increased cholesterol and depression.

Chemotherapy is an approach that delivers anti-cancer drugs orally or through intravenous injection. These drugs can travel through the bloodstream and throughout the body, making them useful for treating cancers that have metastasized. It is typically used when prostate cancer has invaded tissues surrounding the prostate gland or that have metastasized. Chemo is not a standard treatment for early prostate cancer and may be used when hormone therapy is ineffective. Some studies show it could be helpful if given for a short time after surgery [13]. Chemotherapy is generally administered in cycles with treatment being followed by a rest period to allow the body time to recover. For prostate cancer, chemotherapeutics are administered one at a time. Some common chemotherapeutic agents used include docetaxel (Taxotere®), mitoxantrone (Novantrone®), doxorubicin (Adriamycin®), etoposide (VP-16), vinblastine (Velban®) and paclitaxel (Taxol®) [13]. In most cases, the first chemo drug given is docetaxel, combined with the steroid drug prednisone. This combination is also the standard for men with castrate resistant prostate cancer [12]. If this drug-steroid combination does not work, mitoxantrone had been the standard second line of treatment but research has indicated that cabazitaxel has a statistically significant advantage [12].

Sipuleucel-T (Provenge®) is a cancer vaccine that boosts the immune system to target and destroy prostate cancer cells on a systemic level. This gene therapy is typically used after subsequent hormone therapy is rendered ineffective. This vaccine is engineered specifically for each patient by using white blood cells harvested from the patient. Cells are then exposed to prostatic acid phosphatase (PAP). The cells are then reintegrated intravenously. This treatment is administered to the patient 3 times over a one month period. These modified immune cells induce a response from the host's immune system cells to attack the prostate cancer. The vaccine does not stop cancer growth but increases the patient's life span by several months on average. The side effects of chemo and gene therapy will be discussed in the Current Treatment section.

### 1.1.3 Breast Cancer

Breast cancer is cancer that develops in the breast. In 2016 alone there will be over 230,000 new cases of invasive breast cancer diagnosed in women, over 60,000 new cases of carcinoma in situ (CIS) diagnosed in women (non-invasive and earliest form) and about 40,000 women will die from breast cancer. As breast cancer can be genetically linked a woman is more likely to develop breast cancer if other women in her family have the disease.

The female breast is primarily made up of lobules, ducts and stroma (comprised of connective tissue around ducts and lobules, blood and lymphatic vessels) [14]. Breast cancer is a malignant neoplasm that begins in the lobules or ducts of the breast and can invade surrounding tissue and or metastasize to other parts of the body. Ductal carcinoma accounts for 50-80% of reported cases and lobule carcinoma is the second most common accounting for 5-15% of the cases. When discussing breast cancers it is

important to understand lymphatic system of the breast in order to fully comprehend how these cancers spread. Most lymphatic vessels of the breast connect via axillary nodes located under the arm, while some connect via internal mammary nodes of the chest or supraclavicular and infraclavicular nodes. Most breast cancers are carcinomas of the epithelial cells and adenocarcinomas, which affect glandular tissue. Other types of cancers that occur in breast are sarcomas, which start in the muscle, fat and connective tissue. In most cases, a tumor of the breast can be a combination of these different phenotypes and a mixture of invasive and cancer in situ.

Invasive breast carcinoma is characterized as malignant epithelial tumors that invade surrounding tissues and tend to metastasize [15]. Most of them are adenocarcinoma, which may arise from the mammary parenchymal epithelium, specifically the terminal duct lobular unit. They may have a wide range of phenotypes and morphologies and particular types have select histopathology and clinical characteristic. The main type of breast cancer accounting for 50-80% of all cases is invasive ductal carcinoma (IDC) [15][16]. The carcinoma begins in the milk duct of the breast, pierces through the wall of the duct and invades the fatty tissue of the breast. As this occurs, the cancer may be able to metastasize to other parts of the body via the lymphatic system. The second most common type of breast cancer occurs in the milk producing lobules of the breast and is called invasive lobular carcinoma. Similarly to IDC it can metastasize via the lymphatic system of the breast. Additionally it may be more difficult to detect by mammogram. See **Table 1-2:** Frequency and Survival Rates of different types of Invasive Breast Cancer [15], [16]

**Table 1-2:** Frequency and Survival Rates of different types of Invasive Breast Cancer [15], [16].

| Histopathological type of invasive breast carcinoma | Frequency | 10-year overall survival rate |
|---|---|---|
| Invasive ductal carcinoma not otherwise specified (IDC NOS) | 50–80% | 35–50% |
| Invasive lobular carcinoma (ILC) | 5–15% | 35–50% |
| Adenoid cystic carcinoma | 0.1% | 90–100% |
| Apocrine carcinoma | 0.3–4% | Like IDC NOS |
| IDC with osteoclastic giant cells | Unknown | Like IDC NOS |
| Medullary carcinoma | 7% | 50–90% |
| Metaplastic carcinoma | <5% | Unknown |
| Micropapillary carcinoma | <3% | Unknown |
| Mucinous carcinoma | <5% | 80–100% |
| Neuroendocrine carcinoma | 2–5% | Unknown |
| Tubular carcinoma | 1–6% | 90–100% |

Usually the first symptom of breast cancer is a lump or mass with irregular edges that feels distinctly different from the rest of the breast tissue. Lumps can also be found in the lymph nodes of the armpits. More than 80% of cases are found when a woman discovers a lump [14], [17]. One breast may have a thickening when compared to the other, or one breast may become larger than the other. Other symptoms can include change in the position of the nipple, inversion of the nipple, discharge from the nipple, constant pain in the breast or armpit, and swelling or rash in the breast or armpit [14]. In early stages, the lump may move freely and in more advanced stages the lump may adhere to the chest wall or skin [17]. Inflammatory breast cancer can result in the breast becoming warm, red and swollen, the skin may appear to be dimpled and leathery, possessing the texture of an orange.

The screening process for breast cancer starts with a physical examination. If abnormalities are discovered during the initial screening process additional test will be performed. The next screen is usually an imaging test called a mammogram. The breast is pressed between two plates and X-ray images are taken from two different angles. Other imaging tests a physician may order are breast ultrasound, and an MRI. The MRI is

typically used in tandem with a mammogram to judge disease progression, to screen if the cancer has spread to the other breast, as well as, to help to determine the size of the mass. If imaging does not show a mass and the physician can still feel a lump, a biopsy is done to confirm whether the mass is cancerous or not. The next step following imaging test is a biopsy, a test that confirms the presence of cancerous tissue. Different types of biopsies include fine needle aspiration, which is the least invasive and can also be guided by ultrasound, core needle biopsy, which provides a larger sample and can be vacuum assisted, and open biopsy, which is rarely done. A lymph node biopsy can also be done if the lymph nodes of the arm pit are enlarged.

Breast cancer can be further classified. One classification is based on the presence of estrogen and progesterone receptors (ER+ and PR+), as estrogen and progesterone can fuel the growth of breast cancers. Another classification is based on the status of HER2 gene, the presence of which can indicate greater than normal amount of HER2 protein, which usually is associated with a more aggressive cancer type. The term "triple negative" refers to the status when the tumor cell is both hormone receptor negative (PR- and ER-) and HER2-. Other classifications are based on ploidy, proliferation, and gene type and patterns as well as gene expression.

The staging of breast cancer follows the American Joint Committee on Cancer TNM staging. Treatment can depend on the stage of the cancer, as well as, the progression of the disease. Treatment can also be split into two groups:

1. Local treatment applies therapy directly to the tumor, surgeries and radiation therapy.

2. Systemic treatment can reach cancerous cell throughout the body and usually administered orally or intravenously. Examples include chemotherapy, targeted therapy, and hormone and gene therapy.

Surgery is often the first line of treatment for localized breast cancers. Surgical tumor removal can be either breast-conserving or mastectomy [14][17]. The breast can be reconstructed at the same time as surgery or later. Surgery is also used to check the lymph nodes under the arm for cancer spread [14], [17]. Options for this include a sentinel lymph node biopsy and an axillary (armpit) lymph node dissection. With Stage 1, invasive cancer mastectomy and breast conservation therapy with radiation are comparable in terms of remission rate, but it is important that physicians remove all cancerous tissue. Prior to surgery chemotherapy can be used to shrink the tumor and this approach may enable the use of breast conserving surgery rather than mastectomy. Post-mastectomy many women can opt in for breast reconstructive surgery.

Radiation therapy is typically given to kill cancer cells near the site where a tumor was removed including nearby lymph nodes. It may also be administered in patients where cancer has spread to others areas like the bone or brain. The most common type of radiation therapy given to women with breast cancer is external beam radiation. If breast conservation therapy is done, the entire breast gets radiation and an extra boost is given to the area of the breast where the cancer was removed. It is usually given after the patient has healed from surgery, and if given after chemotherapy it usually follows a recovery period [14], [17]. It is only given for a few minutes at a time 5 days a week for 5 days at a time. Side effects include numbness, pain, and nerve damage, fatigue, swelling and blistering. Alternatively, internal beam radiation treatment can be given for 5 days, after

which the pellets are removed. This technique has comparable side effects to those of external beam radiation.

Chemotherapy is used to kill rapidly growing cancer cells or to slow replication. It is usually given along with surgery or radiotherapy because it cannot kill cancer alone. Treatment is usually given for one day followed by 2 weeks of recovery, orally or intravenously. Adjuvant chemo is given after surgery as a safeguard to kill any cancer cells that have been left behind [14]. Neo adjuvant chemo is administered pre surgery to shrink the tumor and or to see how the cancer responds to chemotherapy [17]. Chemotherapeutic drug are most effective when given in combination. Some common combinations include doxorubicin, epirubicin or paclitaxel in combination with fluorouracil or carboplatin [14]. Chemotherapeutics may be used alongside drugs that target HER2 to enhance their effects. Trastuzumab or Pertuzumab is given along with a taxane [14], [17]. Side effects include hair loss, fatigue, nausea, mouth sores and because of possible affects to bone marrow increased chance of infections and bruising.

Hormone therapy is another systemic treatment that can be used like chemo therapy adjuvant or neoadjuvant to decrease risk of reoccurrence and to shrink the tumors. They can be used to block estrogen and progesterone, hormones known to have an effect on the aggressiveness and growth of cancer cells. These treatments are used on ER+ and PR+ cancers and can either lower production of the enzymes or block receptors in ER and PR positive cancers. Such treatment is ineffective on ER- and PR- breast cancers. Tamoxifen is a drug commonly used that blacks estrogen receptors. It acts as an anti-estrogen in breast cancer cells and has the effect of estrogen in other tissue [17]. Because of this feature tamoxifen belongs to a class of drug called selective estrogen

receptor modulators. Its side effects include hot flashes, vaginal dryness, fatigue and mood swings [14]. In premenopausal women, it can lead to bone thinning, but in post-menopausal women it can have the opposite effect. Other commonly used hormone drugs include toremifene, letrozole and anastrozole [14], [17]. Chemotherapies, hormone therapies, gene therapies and targeted therapies will be discussed in the current treatments for cancers later.

## 1.2 Multi-Drug Resistant Cancer

Off-target toxicity to adjacent healthy tissues and poor accumulation of chemotherapeutics into the tumor site are major drawbacks of free-drug chemotherapy, which will necessitate high drug doses. Consequently, emergence of multidrug resistance (MDR) gives rise to cancer progression or recurrence, which requires multiple treatment courses. Increased drug efflux mainly via transporting activity of ATP-binding cassette (ABC) family and inactivation of apoptosis pathways are major molecular mechanisms causing MDR phenotype.

### 1.2.1 Multi-Drug Resistance Mechanisms

Multi-drug resistance is a system that protects the cell against a various amount of compounds like drugs, which may have different chemical structures, and different mechanisms of intracellular activity. Complex biochemical networks of the above-mentioned pathways play a multi-factorial role in the implication of MDR, which could be intrinsic or acquired. Transporters in the body are security gates altering the molecular distribution of therapeutic agents. MDR is facilitated by the existence of several different mechanisms. It is widely known that membrane transporters account for the resistance to many of the commonly used chemotherapeutics by affecting the cellular uptake and

retention of these drugs into tumor cell. Other factors may have may contribute to MDR, such as inactivation of apoptosis pathways, but here I will describe membrane transporters and will only refer to apoptosis inactivators as they relate to transport mechanisms.

### 1.2.2 ABC Family of Transporters

Two classes of membrane transporters affect the pharmacokinetics of cellular uptake of drugs. Changes to these membrane transporters can be directly and indirectly responsible for MDR tumors. One of the classes is the adenosine triphosphate (ATP)-binding cassette super family, which is often times correlated with decreased accumulation of hydrophobic anti-cancer therapeutic drug. It pumps the drugs outward when drugs diffuse down a concentration gradient into the cells. The other superfamily is solute carrier transporters which commonly increase sensitivity to chemicals by mediating the uptake of hydrophilic anticancer agents [18]. If either one of these systems is affected it can result chemotherapeutic drug resistance.

ABC proteins are characterized by having a cytoplasmic ATP-binding domain with a specific nucleotide binding domain. They function by harvesting energy from hydrolysis so that transporters act as efflux pumps to remove various intracellular chemotherapeutic agents. ABC transporters also have a trans membrane domain which offers a binding site for substrate or chemotherapeutics which are, in turn, translocated from the cytoplasm out to the cell membrane [18].

The human ABC family proteins are divided into seven subfamilies based on binding domain organization (the number and configuration of TMDs and NBs). This family has a total of 49 members, but three members are noted for their contribution to

MDR [18], [19]. They are P-glycoprotein(p-gp:MDR1/ABC1) MDR-associated Protein (MRP1/ABCC1) and the breast cancer resistance protein (BCRP:ABCG2) [18]. All have characteristics which include the expulsion of a variety of hydrophobic compounds, decreased substrate specificity which allow for the transport of many of the major drugs used in chemotherapy and MRP1, as well as ABC2 which can remove xenobiotics and intracellular metabolites.

1.2.2.1 *P-glycoprotein (P-gp, MDR1, ABCB1)*

A member of ATP-binding cassette (ABC) family of transport is called P-glycoprotein (P-gp) which is a 70 kDa membrane bound protein and expels chemotherapeutics. In other words, reduced drug accumulation inside the cell, due to the energy-dependent drug efflux activity of P-gp is the primary cause of MDR. P-gp is a membrane bound protein consisting of 1280 amino acids. P-gp is a full transporter consisting of 2 homologous half transporters each having a TBD and NBD. [18] A linker region connects the two half transporters and this region may be important in proper communication between the subunits. If the central core is deleted, the p-gp is still expressed at levels similar to the wild type but is not functional for transport of ATP activity [18].

The P-gp transporter removes neutral and cationic hydrophobic compounds like doxorubicin vinblastine actinomycin D, daunorubicin, vincristine, etoposide and paclitaxel. The mechanism for drug transport is as follows. ATP is hydrolyzed, forming a transition state intermediate of the complex, then the drug is extruded from the P-gp and ADP dissociates from the complex. An additional ATP then binds and returns the P-gp to its original conformation to prepare for the next round of transport [18], [20].

In tumors, P-gp expression and overexpression can be caused by mutations to the p53 gene and overexpression of the p63 and or p73 gene. Upregulation of P-gp may be the result of ABCB1 promotor activation via nuclear protein MDR1 promotor enhancing factor or multiprotein complex RNA helicase I [18]. Some factors can also silence ABCB1, such as epigenetic methylation; and chromatin modifying enzymes like histone acetylates and deacetylases can also regulate ABCB1 genes. Other factors involved may include heat shock, chromosomal rearrangement, inflammation, hypoxia, toxic metabolites and ultraviolet radiation [18].

1.2.2.2 *MDR-associated Protein (MRP1, ABCC1)*

The MRP1 gene arises from chromosome 16p13.1. MDR-associated protein is a membrane bound glycoprotein with a 1,531 amino acid residue. The protein has a similar structure to that of the P-gp but the MRP1 contains an n-terminus segment, TMD0, which connects TMD1 with L0 linker region. The L0 region is absolutely necessary for transport and the TMD0 is not.

Although MRP1 behaves similarly to the P-gp (requires 2 ATPs for transport), the mechanisms for transport differ. In MRP1, the NBD1 has a higher affinity for o ATPs than NBD2 as opposed to the equal affinities between NBDs in P-gp.[18] The transport proceeds as follows. First the substrate binds to TMDs of MRP1 and then a conformational change induces ATP binding NBD1. The confirmation is further altered and enhances the binding of ATP at NBD2. Once ATP is bound at both NBDs, the substrate is transported out of the cell. Shortly after extrusion, ATP bound at NBD2 is hydrolyzed and it induces a partial conformation change which allows dissociation of the

ATP bound at NBD1. The release of ADP and inorganic phosphate brings MRP1 back to its original conformation [18].

Unlike P-gp, MRP1 expression can be found in a variety of cell types and organs. P-gp located in the apical membranes of epithelial cell, whereas MRP1 is found basolaterally and tends to pump drugs into the body rather than being excreted in bile, urine and the gut. Overexpression of MRP1 results in resistance to a wide array of drugs including doxorubicin, epirubicin, vinblastine vincristine, and etoposide. Research has shown that MRP1 requires glutathione to transport unmodified anticancer drug. MRP1 may co-transport GSH or GSH may bind to MRP1 to enhance transport of hydrophobic anticancer agents across membranes [18][21].

1.2.2.3 *Breast Cancer Resistance Protein (BCRP, ABCG2)*

The chromosome locus 4q21-4q22 is the location of ABCG2 gene and encodes for a 655 amino acid plasma membrane glycoprotein. This gene was first cloned from the drug resistant breast cancer cell line MCF7/ADVO [18][22]. ABCG2 is half the structure of P-gp containing one TMD and NBD while showing a reverse domain arrangement, i.e., NBD-TMD. Two ABG2 molecules combine to form a functioning homodyne via a sulfide bond. This bond allows ABCG2 to have 2 TMDs and NBDs so that it can function as a drug transporter [18]. ABCG2, like MRP1, is expressed ubiquitously across tissues, but most abundantly found in the liver, intestinal epithelium, placenta, and blood brain barrier and in various stem cells. Overexpression is typical in drug resistant (selective) cell lines from ovary, lung, breast, colon and gastric cancer.

The mechanism of action for the ABCG2 transporter had not been investigated as of 2009, but researchers speculate that is does not have any major difference from the

mechanisms for P-gp and MRP1. As mentioned, substrates may include similar chemotherapeutic drugs for P-gp and MRP1, as well as some molecularly targeted drugs, such as mitoxantrone, topotecan, irinotecan, methotrexate, gefitinib and imatinib. As for P-gp and MRP1, several factors control expression of ABCG2. Estrogen, progesterone and testosterone effect its expression, although data are conflicting. Expression can be upregulated by the mammary gland during lactation. Also, hypoxia regulates expression, and research has suggested that stem cells and tumor cells may be protected in hypoxic conditions from chemotherapeutics due to upregulation of ABCG2 [18][22][23].

## 1.3 Current Treatments

This section will discuss, in detail, the current treatments for osteosarcoma, prostate cancer and breast cancer. It will focus on chemotherapy, gene therapy and combination therapies used to shrink tumors that may be paired with surgical methods. Surgical methods will only be discussed when they are paired with the treatment modalities discussed below.

### 1.3.1 Chemotherapies

Chemotherapy refers to the use of anticancer drugs to shrink tumors or eliminate metastasis throughout the body. Chemotherapy is systemic and usually administered intravenously or orally. For cancers like osteosarcoma, chemotherapy is an important part of treatment. In breast cancer and prostate cancer it can be used adjuvantly when tumors are un-ressectable, to destroy any cancer cells left behind, and neoadjuvantly to shrink tumors before surgery. Chemotherapy can be used to treat the majority of cancers once they have become metastatic; however, it but does not cure cancer. Chemotherapeutic

agents are often administered in combination with surgery or other types of treatment but are most useful in shrinking tumors and destroying metastasis.

1.3.1.1 *Free Drugs*

There are a variety of free drugs that may be evaluated for patients with cancer who are seeking chemotherapy to shrink tumors in adjuvant or neoadjuvant therapies. Some of the same drugs can be administered to patients with osteosarcoma, prostate cancer or breast cancer; these drugs are doxorubicin (Adriamycin) and platinum agents (cisplatin, carboplatin) [8][13][14]. Etoposide is administered to both osteosarcoma patients and prostate cancer patients while gemcitabine may be administered to both osteosarcoma and breast cancer patients [8][13]. Docetaxel, paclitaxel, vinorelbine and mitoxantrone may be given to both prostate cancer patients and breast cancer patients [13][14]. Some other commonly administered chemotherapeutic drugs for osteosarcoma are methotrexate (given in high doses along with leucovorin to help prevent side effects), epirubicin, ifosfamide, cyclophosphamide and topotecan. Often, two or more drugs are given together. Some common combinations of drugs include high-dose methotrexate, doxorubicin, and cisplatin, doxorubicin and cisplatin, ifosfamide and etoposide and ifosfamide, cisplatin (or carboplatin) and epirubicin [8][13][14]. Some commonly administered chemo drug for prostate cancer are cabazitaxel, estramustine, and vinblastine [13]. Other chemotherapeutic drugs for breast cancer include capecitabine, liposomal doxorubicin, ixabepilone, albumin-bound paclitaxel and eribulin.

1.3.1.2 *Nanomedical Approaches*

Nanomedical approaches to cancer therapies involve the use of nanoparticles (NPs) or nanoparticulate-based systems or devices used along with drugs, genes or other

therapeutic mechanisms to treat cancer. NPs used as drug delivery vehicles are 1-300 nm particles made from polymers, lipids, proteins, viruses, or even organometallic compounds and combinations of any of these.

Polymeric nanoparticles are NPs less than a half micron in diameter formed from naturally occurring polymers (chitosan, chitin, albumin, etc.) and/or synthetic polymer (PLGA, PLA and PEG, etc.). These particles may be used to deliver DNA, proteins, cancer drugs or oligonucleotides. Gradishar *et al.* developed a nanoparticle paclitaxel formulation, where serum albumin was used as a nanocarrier [24]. This complex known as abraxane has been used for the treatment of metastatic breast cancer and has entered clinical trials for many other cancers, including small cell lung carcinoma and advanced nonhematologic malignancies. Some of the most widely used non-biodegradable synthetic polymers are *N*-(2-Hydroxypropyl) methacrylamide (HPMA) and polyethylene glycol (PEG) [25]. PK1, a conjugate of HPMA and doxorubicin, was the synthetic polymer-drug evaluated in clinical trials as an anticancer agent. Phase I clinical trials were completed in patients with a variety of tumors that were refractory or resistant to prior therapy such as chemotherapy [26]. Liang *et al.* fabricated paclitaxel-loaded nanoparticles with galactosamine conjugates to target liver cancer cells. These NPs were efficient in shrinking the size of tumors when injected into hepatoma-tumor-bearing nude mice, through the specific interaction between galactosamine and asialoglycoprotein receptors [27]. Genexol-PM (PEG-poly (D, L-lactide)-paclitaxel) is one of the first polymeric micelle formulations of paclitaxel. Phase I clinical trials and pharmacokinetic studies have been conducted in patients with advanced refractory malignancies [28].

Chitosan nanoparticles, 100 nm in diameter, have been fabricated to encapsulate of dextran-doxorubicin conjugates (DDC). In the study, mice were intravenously injected with DDC-loaded chitosan nanoparticles. DDC-chitosan nanoparticles showed a decrease in the tumor volume after 4 weekly injections. The DDC-chitosan nanoparticles were 60% as effective on tumors treated with the conjugate alone, while treatment with doxorubicin alone did not decrease the tumor volume [29]. Another group conjugated doxorubicin with PLGA and formed nanoparticles of 200–250 nm diameter with an *in vitro* release of up to 1 month. *In vivo* analysis indicated that a single injection of doxorubicin-PLGA conjugated nanoparticles inhibits tumor growth for up to 12 days, although NPs were not as effective as daily doxorubicin injections at the concentrations tested [30]. SN-38 analogs of irinotecan in lipid nanoparticles were prepared and yielded sizes of 100–375 nm diameter. It was found that the longest tumor regression and survival was seen in mice injected with nanoparticles of 375 nm in diameter (65 days survival, 1.98 mg SN-38/mouse), followed by those injected daily with Camptosar (51 days survival, 9 mg irinotecan/mouse) and then by those injected with nanoparticles of 100 nm diameter (48 days survival, 1.51 mg SN-38/mouse).

### 1.3.2 Gene Therapies

Gene therapy provides a novel approach to combating cancer at its source. Gene therapy can be used to reactivate apoptotic pathways, selectively target tumors cells, to destabilize membrane proteins that affect drug resistance and to activate pathways that may serve to boost the actions of drugs. Genes can be delivered to cells in a variety of ways even though some systems have major drawbacks. Direct injection can be a delivery pathway, but nucleic acids delivery may be blocked due degradation of nucleic

acids DNases and RNases. Viral vectors may be used for highly efficient delivery of nucleic acids but some hurdles may be faced due to safety issues, immunogenicity, low transgene and high cost. Cationic polymers and lipids show promise in the field of gene delivery as they can be adapted for large scale manufacture, have a typically low immunogenic response, and can be modified and also allow for the carrying large inserts. In addition, they can be co-loaded with drugs to allow for a co-administration of drugs and genes for localized cancer therapy.

Some ligands that have shown selective targeting to cancer cells are transferrin (Tf) and epidermal growth factor (EGF) [31]. The group designed and fabricated complexes for gene delivery with polyethylenimine (PEI) linked to PEG which were subsequently coated with either Tf or EG PEI-PEG-DNA complexes, this process yielded nanoparticulates ranging in diameter from 49 to 1200 nm. Plasmid pCMVLuc, which codes for luciferase production, was complexed with these nanoparticles for *in vivo* studies. *In vivo* studies in mice showed that the gene expression from administration of targeted systems was 10–100 higher in tumors than in other organs [32].

Liu *et al.* [33] fabricated ultra-low size calcium phosphate nanoparticles (23.5-34.5nm) for entrapping DNA molecules. *In vitro* studies demonstrated that nanoparticles efficiently encapsulated the DNA and protected it from DNase degradation. Suicide gene therapy assays, assays in which a gene is delivered to transform a pro-drug into an active drug, displayed promising results even though these nanoparticles were not tested via systemic injection. This therapy activates pathways that induce apoptosis.

Another promising approach to gene delivery is through polyelectrolyte complex (PEC) micelle based vector. PEC micelles result from interactions between PEG

conjugated oligo nucleic acids (PEGylated ODN) and a polycations (e.g. PEI). Vonarbourg et al states "The negatively charged antisense c-Raf ODN interacts with polycations to form a neutral charged hydrophobic inner core of PEC micelles, while PEG segments are localized outside the core to form a hydrophilic shell [34]." When compared to ODN alone, micelles show a grander anti-proliferative activity against ovarian cancer cells *in vitro* and *in vivo*, when injected to the tumor [34].

Kommareddy *et al.* [35] developed PEGylated modified gelatin nano-vectors for delivery of pDNA and encoding for the soluble form of the extracellular domain of vascular endothelial growth factor receptor-1 (VEGF-R1 or sFlt-1). Intravenous administration in female nude mice, bearing orthotopic MDA-MB-435 breast adenocarcinoma xenografts, showed size reduction in tumors and suppression of microvasculature to the tumor. This system has proven its effectiveness for systemically administered gene delivery vehicle in solid tumor models.

Clusterin/apolipoprotein gene is a heterodimeric ubiquitously expressed glycoprotein that may be linked to many severe physiological disturbances such as tumor formation and cancer progression [36]. Zimmermann *et al.* [37] was the first group to report siRNA-mediated silencing of the apolipoprotein (ApoB) in response to systemic delivery in non-rodent species. Stable nucleic acid lipid particles (SNALP) were composed of lipids 3-N-[(-methoxypoly(ethyleneglycol)2000)carbamoyl]-1,2-dimyristyloxy-propylamine(PEG-C-DMA), 1,2-dilinoleyloxy-N,N-dimethyl-3-aminopropane (DLinDMA), 1,2-distearoyl-sn- glycero-3-phosphocholine (DSPC) and cholesterol, in a 2:40:10:48 molar per cent ratio. SNALP containing ApoB-specific siRNA were administered by intravenous injection to cynomolgus monkeys at doses of 1

or 2.5 mg $kg^{-1}$. They reported a significant reduction in ApoB protein, serum cholesterol and low-density lipoprotein levels as early as 24 hours after treatment. Levels were sustained at low amounts for 11 days at the highest siRNA dose. Results indicated an immediate, potent and lasting biological effect of siRNA treatment. This landmark study demonstrated, for the first time, a clinically relevant systemic RNAi-mediated gene silencing in non-human primates.

### 1.3.3 Combination Therapies

Cancer is a complex illness that may result from a variety of factors depending on progression, staging type, apoptosis demodulation and angiogenesis. Consequently, treatment may involve a combination of remedies to achieve remission. It often involves chemotherapeutics, hormone modulation, gene therapy and surgeries paired to treat cancers. Hormone therapy used is before surgery to shrink the tumor, after surgery to eliminate left over cancer cells, and with advanced stages of cancer. Hormone therapy can cut off pathways that feed tumor growth and aggressiveness of cancer, thus leading to a reduction in tumor size, which aids in resection. When treating certain types of cancer, gene therapy can be paired with chemotherapeutics. Consequently, gene therapy actively or passively targets tumor cells for localized drug interaction, restores apoptotic functions, destabilize membrane proteins that lead to resistance, and/or silences genes that may be active in metastatic and more aggressive cancers. An ideal model may involve both gene/drug therapy with surgery or possibly eliminate surgery altogether. Recent advances in MDR targeting and drug localization have led to reduced tumor proliferation and size.

#### 1.3.3.1 *Hormone Therapies and Surgeries*

In prostate cancer, hormone therapy is referred to as androgen deprivation therapies. The main goal of therapy is to disrupt hormone pathways in order to inhibit their response in prostate cancer cell. It is often administered when the cancer has spread too far to be removed by surgery or radiation. It can be used neoadjuvantly to shrink tumor prior to resection or to reduce the risk of reoccurrence after surgery. Some therapies involve the removal of the testicles, which are major producers of androgens, while others rely on drugs, and/or genes that reduce androgen production or block androgens. Luteinizing hormone releasing hormone analogs (LHRH or GnRH agonist) are injected or implanted subcutaneously [10]. Some of the drugs available in the U.S. are leuprolide (Lupron®, Eligard®), goserelin (Zoladex®), triptorelin (Trelstar®) and histrelin (Vantas®) [13]. The American Cancer Society states "Degarelix is an LHRH antagonist. LHRH antagonists work like LHRH agonists, but they reduce testosterone levels more quickly and do not cause tumor flare like the LHRH agonists do." LHRH acts in the testicles, inhibiting testosterone production, but does not limit the production in the prostate and other tissues. Abirateron blocks the CYP17 enzyme, thus inhibiting other tissues from producing androgens. It may be administered to men with advanced staged castrate-resistant cancer because it may shrink or slow the growth of tumors and prolong life [13].

Another class of drugs that disrupts the action of androgens is anti-androgens. Anti-androgens bind androgen receptors, blocking androgen binding. Some anti-androgens include flutamide (Eulexin®), bicalutamide (Casodex®), and nilutamide (Nilandron®) in pill form and are taken daily [13]. These drugs are often added to

treatment if orchiectomy, an LHRH analog, or LHRH antagonist is ineffective alone. They are typically administered for a few weeks when an LHRH analog is first started to prevent a tumor flare. When anti-androgen treatment is combined with orchiectomy or with an LHRH analog as the first line hormone therapy, the therapy is called combined androgen blockade (CAB) [13]. Enzalutamide (Xtandi®) is a newer type of anti-androgen that blocks growth and division signals sent from the androgen receptor to the nucleus. In men with castrate-resistant prostate cancer, enzalutamide can lower PSA levels, shrink or slow the growth of tumors, and help men live longer. Other androgen-suppressing drugs include ketoconazole (Nizoral®), which was first used for treating fungal infections, and estrogens. Both block the production of certain hormones, including androgens, similarly to abiraterone. Ketoconazole is most often used to quickly lower testosterone levels in men diagnosed with advanced prostate cancer and an abundance of metastasis [13].

In breast cancer, hormone therapy is either used as an adjuvant therapy to help reduce the risk of the recurrence or used as a neoadjuvant therapy, to shrink tumors prior to resection. If cancer is recurrent or metastatic, cancer hormone therapy can be used. Two thirds of breast cancers are PR+ or ER+ and most types of hormone therapy for breast cancer is geared towards lowering estrogen levels, and blocking or limiting estrogen activity in breast cancer cells. These treatments are only useful in hormone receptor positive cancer types.

A commonly administered drug that blocks estrogen receptors is tamoxifen [14][38]. It can reduce the risk of developing breast cancer in women at high risk. Tamoxifen is a SERM and generally acts like an anti-estrogen in breast cells. It can also

act like an estrogen in other tissues, like the uterus and the bones. For women with hormone receptor-positive invasive breast cancer, tamoxifen can be given for 5 to 10 years after surgery to lower the chances of the cancer recurring and helping patients live longer. Tamoxifen can inhibit growth and reduce tumor size in women with metastatic breast cancer. It may also reduce the risk of a new breast cancer occurring in the other breast. Toremifene is another a SERM approved to treat metastatic breast cancer but it is not likely to work if tamoxifen has been used and stopped working. Another drug used is Fulvestrant, which blocks the estrogen receptor and also eliminates it temporarily [14], [17]. It is typically used to treat advanced metastatic breast cancer, most often after other hormone drugs. Aromatase Inhibitors (AIs) are drugs that block estrogen production in postmenopausal women. Some AIs include letrozole (Femara), anastrozole (Arimidex), and exemestane (Aromasin). They do not inhibit estrogen production in the ovaries and are only effective in postmenopausal women or in women with luteinizing hormone-releasing hormone analogs. AIs are taken daily as pills. So far, drugs in this group seem to work equally well in treating breast cancer. These drugs alone or in combination with or after tamoxifen, reduce the risk of the cancer recurring more effectively than just tamoxifen for 5 years [14][17] Ovarian ablation in pre-menopausal women is the removal or shutting down of the ovaries (ovarian oblation), which effectively makes the woman postmenopausal and may be synergistic with other hormone therapies, and is most often used to treat metastatic breast cancer. Often, ovarian ablation is carried out using drugs called LHRH analogs, such as goserelin (Zoladex®) or leuprolide (Lupron®), which disrupt the estrogen production signal. They may be used alone or in tandem with tamoxifen, aromatase inhibitors, or Fulvestrant in pre-menopausal women or

in women whose cancers do not respond to the other hormone treatments. Its major side effect is weight gain, and it is sometimes used in higher doses to reverse weight loss for people with advanced cancer. Androgens (male hormones) may rarely be considered after other hormone treatments for advanced breast cancer have been tried.

1.3.3.2 *Gene/Drug Hybrid Approaches*

Drug resistance and systemic toxicity are major issues in cancer chemotherapy. Also off-target activity can affect localized drug dosage. In combination with gene therapy, chemo drugs can be directed to and act more effectively on their target cell type at a radiometric dose. Gene delivery vectors allow targeting of specific cell types by taking advantage of interactions between cell membrane receptors and cell surface ligands. Current chemotherapeutic strategies are limited by the development of resistance and by their severe side effects.

Ligand targeting can play an essential role in targeting cancers like breast cancer. Strategies have been developed to select internalizing antibodies from phage libraries [31]. This technique identified F5 and C1 antibodies in the breast tumor cell line SK-BR-3 that bind to ErbB2 growth factor, which is overexpressed in 20– 30% of human breast carcinomas and other adenocarcinomas [39]. This study incubated antibody F5 conjugated PEG, with Doxil (commercial liposomal doxorubicin formulation from Alza) to form a coupled liposome system. The *in vivo* comparison of Doxil or F5-coupled Doxil in mice showed a faster and greater regression in tumor volume for F5-containing Doxil over unmodified Doxil [39].

In healthy tissues, the cell surface folic acid receptor is inaccessible; but in cancer cell surfaces, the receptor is expressed. The folate receptor has been successfully targeted

in *in vitro* and *in vivo* tumor models. Some studies have shown the effectiveness of folate-targeting immune therapy with a vaccine. This approach applied to positive lung metastasis in mice, showed cures in up to 56% of tumor bearing mice [40]. Cho *et al.* generated a novel folate receptor–targeted nanoparticle formulation of paclitaxel using heparin as a carrier [heparin-folate-Taxol (paclitaxel), HFT], and tested it using nude mouse animal models. This novel ternary nanoparticle HFT demonstrated more activity against the growth of tumor xenografts of human KB and paclitaxel-resistant KB derivatives than did binary heparin-Taxol or free drug (paclitaxel) [41].

Aptamers have been applied as ligands to drug delivery systems to enhance selectivity. DNA and RNA aptamers are oligonucleic acids that bear unique three-dimensional conformations capable of binding to target antigens with high affinity and specificity [42]. Animal models were used to investigate the *in vivo* efficacy of docetaxel-encapsulated poly(lactic-co-glycolic acid) nanoparticle conjugated with an aptamer to target prostate-specific membrane antigens [43]. Results showed single intratumoral injection of Docetaxel-NP-Apt bioconjugates, was able to completely reduce tumor size in five of seven LNCaP (prostate cancer) xenograft nude mice, whereas with Docetaxel-NP, only two of seven mice had complete tumor reduction. Also, Docetaxel-NP-Apt had a 100% survival rate, where Docetaxel-NP had a 57% survival rate, Docetaxel alone had a survivability of only 14%.

A serum glycoprotein, transferrin, transports iron through the blood and into cells by binding to the transferrin receptor then it is internalized via receptor-mediated endocytosis [42]. Its receptor is overexpressed in tumor tissues, making it an ideal target for tumor-specific drug delivery. Transferrin-conjugated paclitaxel-loaded PLGA

nanoparticles showed a greater inhibition of cell growth than free paclitaxel in MCF-7 and MCF-7/Adr cells [44]. Another group conjugated transferrin to liposomes to increase the transfection efficacy of p53, resulting in the sensitization of the transfected cancer cells/xenografts to ionizing radiation [45].

Ediriwickrema *et al.* synthesized a multi-layered polymer nanoparticle (MLNP), comprising of poly (lactic-co-glycolic acid) with surface poly-ethyleneimine and functional peptides, for targeted drug and gene delivery. Nanoparticle delivered camptothecin (CPT), and plasmid encoding TNF related apoptosis inducing ligand (pTRAIL) (CT MLNPs), and synergistically inhibited growth of multiple cancer cells *in vitro*.[46] They confirmed the results using the Chout-Talalay method and the combination index (CI) values at 50% inhibition ranged between 0.31 and 0.53 for all cell lines. Further, co-delivery with MLNPs resulted in a 3.1e15 fold reduction in CPT and 4.7e8.0 fold reduction in pTRAIL dosing. They observed significant growth inhibition in HCT116 *in vivo* models when compared to a monotherapy. Another group designed and fabricated double-layered microsphere consisting of a PLA shell and a PLGA core doped with chitosan nanoparticles conjugated with p53 tumors suppressor gene and DOX. These microspheres demonstrated a smooth and sustained release *in vitro* and encapsulation efficiency was not affected by DOX [47].

Overexpression of the drug efflux transporters like the P-glycoprotein is one of the major mechanisms leading to multi drug resistance. New approaches involve targeting and inactivating the P-gp via siRNA and or chemotherapeutics. To accomplish cell killing in an additive or synergistic fashion, Meng et al [48] fabricate mesoporous silica nanoparticles (MSNP) functionalized with phosphonate groups to deliver

doxorubicin (Dox) and P-gp siRNA efficiently to drug-resistant KB-V1 cancer cells. The phosphonate surface also allows for the addition of PEI as an exterior coating, which carries P-gp silencing siRNA. The dual delivery of Dox and P-gp siRNA was capable of intracellular and intranuclear drug concentration exceeding levels of free DOX alone. Results indicate that P-gp silencing by siRNA increases sensitivity to the chemotherapeutic agent DOX. Similarly, Lamrecht *et al.* [49] fabricated lipid nanocapsules [(LNC), known for inhibiting P-gp activity] loaded with etoposide. They conducted drug release studies and evaluated the efficiency of the synergistic combination in reducing cell growth *in vitro*. Release of etoposide was sustained over a period of one week. LNCs were internalized in all glioma cell types and Etoposide LNC showed a generally higher efficiency than the drug solution, while blank LNC was found to be less inhibitory than the pure drug at equivalent. This effect was found to be particle size dependent within a range of an 8- (C6) to 33-fold (F98) increased cytotoxicity for smallest particles. The mechanism of action for the inhibition of cell growth was etoposide LNC cell uptake, followed by a sustained drug release from the LNC in combination with an intracellular P-gp inhibition, ensuring a higher anticancer drug concentration inside the cancer cells.

### 1.3.4 Nanomedical Approaches to Multidrug Resistant Cancers

Off-target toxicity to adjacent healthy tissues and poor accumulation of chemotherapeutics into the tumor site are major drawbacks of free-drug chemotherapy that necessitate high drug doses. Consequently, emergence of multidrug resistance (MDR) gives rise to cancer progression or recurrence, which requires multiple treatment courses. Increased drug efflux, mainly via transporting activity of ATP-binding cassette

(ABC) family and inactivation of apoptosis pathways, are major molecular mechanisms causing MDR phenotype. Detailed surveys on MDR-involved pathways can be found in review papers [18][50][51]. The promise of nanomedicine in surmounting the MDR obstacle to effectively fight against cancer lies in the development of customizable nanovehicles equipped with four modules; namely, single/multiple chemotherapeutic drugs, chemosensitizer, imaging-aid components and targeting moiety. A multifunctional nanocarrier capable of synergizing the effect of four modules is described as "Quadrugnostic Nanostructures" by A. Shapira *et al.* [52] much of research and many clinical trials have focused on rational design of personalized and directed therapies with maximum efficacy. Controlling the action time of different modules in a "multi-weapon integrated system" is obviously important for its maximum damage potential. In similar reasoning, precise spatiotemporal control over action period of "Quadrugnostic Nanostructures" being studied extensively. Vijayaraghavalu *et al.* showed the enhanced therapeutic index achieved by sequential exposure of two drugs to drug resistant breast cancer cells [53]. The $IC_{50}$ is a measure of how effective a drug is and indicates the amount of drug necessary to inhibit biological process by half. They reported: "The sequential treatment of resistant cells, first with an epigenetic drug, decitabine (DAC), and then with doxorubicin, induces a highly synergistic effect, thus reducing the $IC_{50}$ of doxorubicin by several thousand fold." Basically, the initial drug restores sensitivity of breast cancer cells by reactivating the tumor suppressor genes, which are silenced in epigenetic alterations. Then, exposure of doxorubicin could act more effectively because the susceptibility of cancer cells is enhanced. Similarly, M. J. Lee proved that sequential inhibition of epidermal growth factor (EGFR) in a time-staggered manner, but not

simultaneous co-administration, immensely sensitizes breast cancer cells to genotoxic drugs [54]. In fact, time and order-dependent drug combinations were more effective. These two reports introduce the time scheduling of dose exposures as a new design paradigm to synthesize superior combinatorial therapeutics.

Controlling the release kinetic of payloads and their possible interactions, as well as formulating a synergistic combination of bioactive agents has been proposed to reshape the future of nanomedicine. Synthesis of sequentially releasing nanoparticles via tuning the release kinetic of each drug in a time-staggered fashion seems to be drastically promising. Kinetically discrete sequential release of multiple agents provides localized delivery of multiple drugs in a desirable time period. Inspiringly, novel multifunctional nanoparticles possessing a well-defined release pattern could efficiently rewire the cancer regulation pathways and transform drug-insensitive cells into drug-sensitive cells. Proper selection of synergistic drug ratios and precise calculation of combination doses, released with time-staggered rate, will truly impact the personalized design of combinatorial systems with maximal efficacy and minimal adverse effect. Orderly releasing quadrugnostic aimed to selectively target biochemical pathways will realize the promising era of "network nanomedicine"; Network nanomedicine needs intimate knowledge of systems biology and advanced screening technologies to monitor complex pool of signaling networks. In this section, my group is proposing the envisioned "orderly releasing multifunctional quadrugnostic" platform capable of MDR reversal and able to selectively target the biochemical networks with minimum adverse effects. As an example, some sequentially releasing nanostructures loaded with synergistic combination of multiple components will be suggested as starting points for the future advancements.

#### 1.3.4.1 *Combinatorial Nanoparticles for P-gp Downregulation*

Most of the therapeutic modalities for cancer treatment have become ineffective, mainly due to multidrug resistance (MDR) phenotype caused by various intracellular biochemical mechanisms. The adaptive response of cancer cells to present MDR is caused by an inter-connected network of numerous pathways including cellular pharmacokinetic and metabolic sequestration of drugs, drug-target interactions, and DNA repair pathways. Complex biochemical networks of the above-mentioned pathways play a multi-factorial role in implication of MDR, which could be intrinsic or acquired. Transporters in the body are security gates altering the molecular distribution of therapeutic agents. A member of ATP-binding cassette (ABC) family of transport is called P-glycoprotein (P-gp) which is a 70 kDa membrane bound protein and expels chemotherapeutics. In other words, reduced drug accumulation inside the cell due to the energy-dependent drug efflux activity of P-gp is the primary cause of MDR. The most distinctive approach used to bypass the MDR seems to be blockage of P-gp pump using P-gp inhibitor molecules. Multiple mechanisms are governing the inhibition activity of P-gp pump. In-depth investigation of driving mechanisms involved in P-gp pump activity, and its substrates/inhibitors, and structural information to design potential P-gp inhibitors can be found in literature reviews [18][20][23][55]. Co-administration of potent and long lasting P-gp inhibitor molecules with genotoxic drugs delivered by polymeric and liposomal nanocarrier have shown promising results compared to single-dose regimens. C. Sarisozen *et al.* synthesized and characterized a PEG-PE-based long-circulating micelle-based delivery systems co-loaded with a P-gp inhibitor molecule called elacridar and paclitaxel [56]. Based on their claims, elacridar/paclitaxel-co-loaded micelles showed

maximal cytotoxicity compared to both free and micellar paclitaxel. Patel *et al.* investigated co-delivery of the P-gp inhibitor, tariquidar, and cytotoxic drug, paclitaxel, into tumor cells to reverse the MDR using long-circulating liposomes [57]. Results indicate SKOV-3TR taxol resistant ovarian cancer cells treated with Tariquidar- and paclitaxel-loaded long-circulating liposomes, resensitized significantly, due to the bypassing effect of Tariquidar in blockage of P-gp pump. Simultaneous delivery of doxorubicin and Elacridar with encapsulation efficiency of 89% was reported in 2006 by Wong et al [58]. They prepared a polymer-lipid hybrid nanoparticle (PLN) formulation capable of simultaneous delivery of a cytotoxic drug, doxorubicin (Dox), and a chemosensitizer, Elacridar. Their Dox and GG918 co-encapsulated PLN formulation ((DG) n) demonstrated the greatest Dox uptake and anticancer activity to MDA435/LCC6/MDR1, a human breast carcinoma cell line. Based on their developments, drugs and structures are classified in three generations. First, second and third generation.

Third generation P-gp inhibitors developed rationally based on structure-activity relationships and have shown the most potent efficacy. Elacridar, Tariquidar and Zosuquidar trihydrochloride (LY335979) are third generation P-gp inhibitors, which have shown synergistic efficiency in combination with genotoxic drugs. In fact, co-loading of P-gp inhibitors with antineoplastic agents circumvent the transport activity of P-gp and reduces the MDR leading to enhanced cancer cell vulnerability and consequently, improved therapeutic efficacy. Based on the above-mentioned research, the sequential release of a P-gp inhibitor and a chemotherapeutic agent seem to be more effective, based on network systemic point of view. Evaluation of sequential vs. concurrent exposure of

free therapeutic molecules in oncology labs, stimulates the nanomedicine platforms to design sequentially releasing nanoparticles capable of dynamic rewiring of drug-insensitive cancer cells into more susceptible state. Evasion of P-gp mediated cellular efflux by initial release of P-gp inhibitor followed by second release of chemotherapeutics, seems to have drastically improved outcomes. Moreover, results of Vijayaraghavalu *et al.* trigger the fabrication of orderly releasing nanoparticles delivering epigenetic drugs and chemotherapeutics in a time-staggered manner [53]. Initial drug accumulation will resensitized the MDR cancer cells and second delivery of genotoxic drug will knock down the sensitive cells.

1.3.4.2 *Pharmaceutical Excipients for P-gp Downregulation*

Some pharmaceutical surfactants mediating the membrane lipids' integrity can cause interruption in P-gp structure. Tween 80 and Cremophor EL hindered the P-gp pump using a fluidization, while TPGS 1000 demonstrated rigidization in lipid bilayers. [59][60] Hydrophilic surface decoration using PEG 400 and PEG 1000, co-administered with fexofenadine, caused twofold increase in plasma concentration of fexofenadine. Co-administration of labra sol (P-gp inhibitor) and fen fibrate in the form of a reverse micelle has been investigated by Shire Laboratories, Inc. [60][61]. Labrasol was found as one of the best among all examined P-gp inhibitors for the delivery of digoxin and enhanced its permeability across the cell [62][63][60]. Polysorbate 80, Gelucire 44/14, Labrasol and Vitamin E TPGS have also been evaluated by SRI International for the delivery of vancomycin hydrochloride [64][65]. Synthetic subcategory of PEGs, poloxamers, dendrimers and thiomers have been extensively reviewed for their P-gp inhibitory activity [60]. When these polymers were administered with drugs, drug accumulation and

efficacy were enhanced. Branched chain fatty acids and their derivatives have been investigated by D-Pharm Ltd in term of P-gp mediated drug transport. Permeability of drugs co-administered with branched chain fatty acids on monolayer of endothelial cells of the blood brain barrier has been studied before [66][67]. Utilizing these potent excipients along with chemotherapeutics reflected less nonspecific pharmaceutical adverse effects. Prodrug derivatization of P-gp substrates appears to be another viable approach in bypassing the P-gp. Overall, improved bioavailability, enhanced sensitivity, and accurate dose formulation are beneficial when potent agents are co-administered with P-gp inhibitors. These benefits lead to a decrease the $IC_{50}$ value of drugs, consequently lowering cytotoxicity to the adjacent normal tissues. Discrete release of P-glycoprotein inhibitors and chemical molecules from sequentially released from nanoparticles masked with PEG chains. These PEG masked NPs, when modified with potent surfactants or tailored with branched chain fatty acids, could yield superior multi arrow nanostructures, thwarting P-gp pump and turning the MDR cells into a defenseless state which is more easily targeted for subsequent release of drugs.

1.3.4.3 *Combinatorial RNAi-based Nanotherapies for P-gp Downregulation*

RNA interference (RNAi) is a regulatory pathway in which an allele-specific gene regulation is inhibited by small RNA molecules, typically cleavage specific mRNA molecules. SiRNA-based therapeutics can target "non-drug gable" sites leading to blockage of gene expression. Biological pathways involved in regulatory mechanisms of siRNA have been widely investigated [68]. Vector-enabled delivery and transfection of synthetic analogs of RNAi (siRNA), miRNA mimics, or hairpin RNAs introduced RNAi-based therapeutics as an alternative nanomedicine. Stable nucleic acid lipid particle

(SNALP)-based and cyclodextrin-based nanoparticulate siRNA formulation developed by Tekmira, Alnylam, Calando, and Silence Inc. have entered Phase I trials. Several interrelated parameters are crucial in approaching the synthesis and safety evaluation of siRNA-based formulations for cell and tumor tissue targeting: 1) Toxic kinetics and distribution of formulation governed by fenestrated endothelium found in liver and spleen, 2) Size and surface characteristics affecting the formulation interaction with plasma proteins and vascular endothelium and immune system cells, 3) dosage design and administration route for different species and 4) biochemical reactions with complex hemostatic cascade and receptors are key safety checkpoints needed to be considered for optimum and desirable pharmacokinetic and pharmacodynamics. Ever-increasing "omics" technology coupled with RNAi-based screening technologies and bioinformatics advancements, opened-up new avenues in the development of individualized siRNA formulations.

1.3.4.4 *Nanoparticles with Multipronged Functionalities for MDR Reversal*

Core-shell lipid-polymer hybrid nanoparticles (CSLPHNPs) are composed of a polymeric core as mechanical back-bone, a hydrophobic lipid shell, and a hydrophilic PEGylating mask. Polymer choices could be PLGA, PCL, albumin or dextran as their biocompatibility and biodegradability have been approved. DPPC, DPTAP, DOTAP, DOPE are the most common lipid candidates which serve as a molecular fence to prevent drug leakage from polymeric core. The hydrophilic PEG chains provide chemical and serum stability, prolong the bioavailability in circulation system and can be conjugated with targeting moieties and ligands for active site specific targeting.

### 1.3.5 Electrospun Scaffolds

Electrospinning is a process used to produce fibers in a submicron to nanometer range with a controlled surface morphology [69][70]. Ultrafine fibers are generated by applying a strong electric field to a polymer solution or melt [70]. Electrospinning emerged as a novel technique over 100 years ago and has since evolved and demonstrated itself as a simple and versatile approach with a variety of potential applications. Some of the more noteworthy applications include filtration, wound dressing, protective military clothing, drug and gene delivery and tissue engineering scaffolds [70][71].

Electrospinning has a variety of applications, but drug delivery is emerging as one of its most promising uses. Electrospun fibers have high loading capacity and efficiency and may be used to deliver a variety of therapies. Simultaneously, electrospinning is a simple cost effective process, which makes it appealing for the field of drug delivery [70][71]. Electrospun fibers can be drug carriers and may be promising in localizing chemotherapeutic post op therapies [70][72] Kenawy *et al.* demonstrated an application of poly(lactic acid) and poly(ethylene-co- vinyl acetate), and a blend of these polymers, as matrices and provided a sustained release of the model drug tetracycline hydrochloride [70]. Researchers have shown that electrospun nanofibers can be successfully used to control drug release profiles, such as immediate, smooth, pulsatile, delayed, and biphasic releases [73][70] [74]. In addition, other drugs ranging from antibiotics, chemotherapeutics, nucleic acids, aptamers and proteins have been doped into electrospun fibers.

### 1.3.5.1 *Polymers with Potential for Drug Delivery*

Synthetic and natural polymers and hybrids have been used to synthesize electrospun fibers. Natural fibers show good cytocompatibility and cell adhesion, and also some intrinsic antibacterial and clinical properties. Synthetic polymers have flexibility in modification and synthesis, but lack some of the properties natural polymers have in cell affinity. Hybrid polymers can harness properties of both synthetic and natural polymers while limiting the drawbacks. Many natural polymers, such as polysaccharides (cellulose, chitin, chitosan and dextrose), proteins (silk, collagen and gelatin, DNA, and biopolymer derivatives and composites are reportedly being used in electrospinning [70], [75], [76]. Lipofectamine is a commercially available transfection reagent produced by Invitrogen [77]. It is a cationic liposome formulation that forms complexes with nucleic acids allowing them to pass the cell membrane. Cationic lipids are fused with a neutral co-lipid and when complexed with DNA the cationic liposomes fuse with the plasma membrane transporting the DNA to the cytoplasm for replication and expression. Lipofectamine may additionally carry the DNA to the nucleus. This system was invented by Yonglian Chu *et al.* [78] Electrospinning of polysaccharides such alginate chitosan, chitin cellulose, starch, dextran and heparin for tissue engineering, wound healing and drug delivery was investigated by Lee *et al.* [70][79]. Research has shown that electrospun chitosan and quartnernized derivatives have anti-cancer properties and show promise in the field of drug delivery. These properties were demonstrated *in vitro* against HeLa, Hep3b and SW480 cells [70]. Biodegradable synthetic polymers also warrant attention as they do not have to be removed by a second surgery following implantation. Polymers like PLA, PCL, PLGA, PEI and PCLA have been extensively

studied in fiber fabrications because they have desirable properties for drug delivery and tissue engineering [70] [71]. Altering composition and polymer blends of biodegradable synthetic polymers can limit degradation and offer a tailored release of drugs. Hybrid fibers made of natural and synthetic polymers may show the most favorable properties. The synthetic polymers can be used to add mechanical properties. Park *et al.* designed a novel fiber by electrospinning a hybrid blend consisting of poly(glycolic acid) (PGA) and chitin.[80] Results indicated that PGA in PGA/Chitin blend degrades faster than PGA alone, which may be attributed to the hydrodrophilicity of chitin. PGA/chitin blend also show a promising amount of cell attachment for human fibroblast when compared to PGA alone. Additionally, natural, synthetic and hybrid polymer fibers can be functionalized with bioactive molecules to facilitate the desired cellular response.

1.3.5.2 *Scaffolds Doped with Chemotherapeutics Drugs and Antibiotics*

Antibacterial and antimicrobial agents are the most ideal biocides for loading into in nanofibers for wound healing. Ignatova *et al.* explored a variety of biocides, such as tetracycline hydrochloride, ciprofloxacin, levofloxacin, and moxifloxacin, and anti-bacterial agents (e.g., 8-hydroxyquinoline derivatives, itraconazole, benzalkoniumchloride (BC), fusidic acid or silver nanoparticles) doped nanofibers for wounds [21] [81]. PLGA, and PLA were commonly used as carriers, along with natural polymer blends to regulate biodegradability and the hydrophilic nature of the fibers, resulting in the modulation of drug release. Kenawy *et al.* conducted pilot research on drug eluting nanofibers using tetracycline hydrochloride as a model drug and poly (ethylene-co-vinyl acetate), poly (lactic acid) and their blends as polymeric carriers. These experiments demonstrated that drug release profiles were influenced by the nature

of the polymer and drug content. The results demonstrated that drug release behavior was influenced by the nature of polymeric carrier and drug content. The drug release profile for a 50/50 electrospinning blend with a relatively low drug concentration (5 wt. %) was smooth and regulated, whereas a higher drug concentration (25 wt. %) resulted in a rapid release. The more rapid release may be caused by surface-segregation of the drug.

Electrospun mesh has shown promise in the area of localized administration of chemotherapeutic drugs. Doxorubicin (Dox), paclitaxel (PTX), platinum complexes [67], and dichloroacetate have been electrospun into fibers and used for postoperative local chemotherapy [21]. A water-in-oil emulsion was used to electrospin ultrafine Dox-containing PEG–PLLA fibers where the aqueous phase contained the water-soluble drugs while the oily phase was a chloroform solution of PEG–PLLA. The resulting fiber completely encapsulated Dox and results indicated that the Dox was entirely encapsulated inside the electrospun fibers [82]. In later research, the group succeeded in the co-encapsulation of both hydrophobic PTX and hydrophilic Dox, simultaneously, into PEG–PLA nanofiber mats by the emulsion-electrospinning method, and realized drug co-administration [70]. Xie *et al.* synthesized cisplatin-loaded PLA/PLGA (30/70) fibers for long-term sustained delivery of cisplatin to treat C6 glioma *in vitro* [83]. They achieved a drug encapsulation efficiency of more than 90% and the cisplatin-loaded fibers sustained release for over 75 days without initial burst release.

1.3.5.3 *Sustained and Localized Drug Delivery*

Most of the past research in biomedical applications of electrospinning has been geared towards the parameters and electrospinning technique, loading method and their application in tissue-engineering scaffold and wound healing. The application of novel

electrospun fiber mats for localized chemotherapy became popular only recently. When compared to systemic dosage forms like liposomes, micelles, and nanoparticles, electrospun mats can reduce systemic toxicity by localizing drug concentrations. Local drug administration is a favorable choice of treatment for post-surgical cancer reoccurrence prevention and may prove useful in treating unresolvable tumors. Lui *et al.* tested DOX encapsulated PLLA nanofibers against secondary hepatic carcinoma and results indicated the majority of the drug diffused into the tumor site beneath the fibers [72]. This application greatly reduced tumor growth with little effect on other organs. Ranganath *et al.* did a similar study replacing DOX with paclitaxel to test the post-surgery chemotherapeutic effects [70] against malignant glioma. Other groups such as Liu *et al.* incorporated dichloroacetate (DCA) into the polylactide (PLA) non-woven fabrics by electrospinning [84]. Liu *et al.* implanted DCA-loaded electrospun mats to cover the solid tumor. A total tumor suppression degree of 96% was achieved in fewer than 19 days and solid subcutaneous tumors completely disappeared from 50% of the tumor-bearing mice and fewer side effects were observed [84].

1.3.5.4 *Extending Delivery with Embedded Nanoparticles*

As discussed above electrospun fibers and mats have shown great promise in the fields of drug delivery and cancer therapy. They provide a platform for localized delivery of drugs for antibacterial and anticancer treatments. The polymer concentrations and the blend of drug release, can be varied to modulate biodegradability. When implanted and after the mats have degraded, embedded nanoparticles containing drugs can provide sustained a drug release. The mats also may help to localize chemotherapeutic bearing nanoparticles in the tumor site or tumor resection site. Various nanoparticles and

naturally occurring clays can be incorporated into electrospun fibers to modulate release. PLGA nanoparticles, iron oxide NPs, halloysite nanotubes, chitosan nanoparticles and more have been incorporated to add mechanical properties and to modulate drug release. Amna *et al.* fabricated camptothecin/iron(III) oxide (CPT/$Fe_2O_3$)-loaded poly(D,L-lactide-co-glycolide) (PLGA) composite mats to modulate the CPT release and to improve the structural integrity and antitumor activity of the released drug [85]. Pristine PLGA did not exhibit noteworthy cytotoxicity; conversely, the CPT/$Fe_2O_3$ composite fibers inhibited C2C12 cells significantly. Yu *et al.* encapsulated DOX using inorganic rod-like nano-hydroxyapatite (n-HA) as a carrier and mixed with poly(lactic-*co*-glycolic acid) (PLGA) solution to fabricate electrospun hybrid nanofibers [86]. The loaded DOX n-HA PLGA nanofiber hybrids demonstrated a sustained release profile, and non-compromised antitumor activity towards the growth inhibition of KB cells. Tada *et al.* developed a dual drug delivery system where chitosan films were embedded with fluorescent paclitaxel doped PLGA nanoparticles and carboxyflourescin (a hydrophilic drug model) [87]. Chitosan films containing CF and FPTX-loaded PLGA NPs showed a biphasic release profile. In the first phase, 78% of CF and 34% of NPs were released within few days. In the second phase, the release was slower, showing an additional release of 22% of CF and 18% of NPs after 3 weeks. FPTX-loaded PLGA NPs showed the release of 19.8% of total drug in 2 days, and no additional release was detected in the next 26 days. Qi *et al.* used tetracycline hydrochloride (TCH)-loaded halloysite nanotubes/poly(lactic-co-glycolic acid) composite nanofibers (TCH/HNTs/PLGA), and investigated drug release and antibacterial activity of this delivery system [88]. The nanofibers were cytocompatible, and the TCH/HNTs/PLGA composite nanofibers

sustained a release of the antibacterial drug TCH for 42 days while displaying antimicrobial activity solely associated with the encapsulated TCH drug. Research has demonstrated that embedding nanoparticles in films, fibers, and mats can add beneficial mechanical properties, localize drug dosage, and sustain long term release for drug delivery in antibiotic and chemotherapeutic applications.

# CHAPTER 2

# ENHANCED NANOPARTICULATE STRATEGIES FOR NOVEL CANCER THERAPIES

Cancer is referred to as a malignant neoplasm, resulting from abnormalities in morphology and cell growth and death cycles. Depending on the stage, progression and amount of metastasis, a variety of treatments can be employed. These treatments can include, but are not limited to chemotherapy, hormone therapy, gene therapy, and radiation therapy, although therapy most commonly involves the surgical removal of tumors. Clinically available treatments are used to shrink, slow growth, remove, or destroy tumors and have many drawbacks.

The term cancer therapy describes the use of surgery, chemotherapy, gene therapies, or other bioactive molecules to remove, shrink or destroy cancerous tissue (malignant neoplasms). Once the type of cancer is identified and staged, one or more of the aforementioned treatment strategies may be employed. Chemotherapeutics, genes, and bioactive molecules may be employed to selectively target, shrink, or stop and destroy tumors and metastasis. Depending on the cell type, size, degree of metastasis, and biomarkers expressed, a therapy can be developed to localize and enhance treatment at a safe and effective dosage.

Most of the clinically available treatment modalities do not target cancer cell types and require high doses which lead to systemic cytotoxicity that affect adjacent tissues. These treatments may also require multiple injections over a prolonged time period. In order to sustain localized drug release, I propose the combination of nanoparticles and films to compensate for drawbacks. In addition nanoparticles can be complexed with bioactive molecules that target drug resistant cancer cell types. These particles would selectively target and kill drug resistant cancer cells. Drug releasing NPs and NP-embedded films, with modified surface properties, hold promise in fulfilling criteria for effective and targeted cancer therapies.

Nanomedicine is an emerging field that combines the use of nanoparticles and/or nanoscale architecture with drugs, genes and bioactive molecules to initiate a cellular response based on the infirmity. Cancer, its progression, and the development of drug resistance result from a variety of factors. Cancer therapy requires a tailored approach, based on tissue type and progression, to localize and sustain cell death in affected tissues. Nanomedicine may be used to attack cancer at its core, delivering targeted therapies to destroy tumors and metastasis.

Recent advances in the field of nanomedicine for cancer therapy have yielded polymeric nanoparticle-based treatment modalities capable of selectively targeting multidrug resistance and localizing drugs in cancerous tissues. Natural, synthetic and hybrids can be used to synthesize nanoparticle and microfilms/fibers. By applying engineering principles and the properties of polymers, we can design a system where cancer targeting drug-NPs, combined with bioactive films and meshes, can be provide a localized and sustained drug delivery to tumors and metastasis. This approach can be

used for in situ drug delivery to significantly reduce and/or eliminate systemic cytotoxicity therefore eliminating many severe side effects.

Targeted nanoparticles or nanoparticulate-embedded films can be employed as a means of delivery for chemotherapeutics and genes to target apoptotic pathways and selectively, rather than systemically, induce cell death in cancer cells. Films and NPs may also be used post surgically to reduce or eliminate the risk of recurrence. Materials should be biocompatible to reduce the risk of side effects and should also possess certain mechanical properties. Said properties may be manipulated to modulate biodegradability and facilitate a sustained release of drugs or genes.

## 2.1 Rationale behind the Three Integrated Projects

This chapter describes the three integrated and interrelated projects that focus on localized, sustained and targeted chemotherapy for the treatment of cancer by applying principles of nanomedicine, gene therapy and chemotherapy. All three projects use drug-doped nanoparticles, plasmid-doped nanoparticles, and enhanced bioactive films to present a localized treatment for cancer, especially drug resistant forms.

The first project attempted to establish Halloysite Nanotubes (HNTs) as a gene delivery platform. The project attempted to deliver plasmids to cancer cells as a means to induce a cellular response. HNTs contained the gene of choice. The HNTs' efficacy for gene delivery would be analyzed first *in vitro*.

The second project attempted to delivery drugs to cancer cells as a means to inhibit growth and induce apoptosis. HNTs contained the drug choice. The HNTs' efficacy for drug delivery would be analyzed first *in vitro*.

In the third project, films were made from chitosan, through a novel method termed solvent evaporation air-brushing. These films, enhanced with nanoparticles, were used as an in situ delivery of chemotherapeutic agents. In the following studies, chitosan films would hold HNTs in their network and the release would be sustained and extended when compared to chitosan films alone. With this design, changing the chemotherapeutic agent loaded into HNTs and adding a P-gp blocker to the polymer itself can modify films.

Certain types of cancers require different types of targeting modalities. If osteosarcoma cells are the targets, methotrexate can be used to inhibit proliferation and stop cell growth. HNTs, loaded with methotrexate, could then be directly injected into the tumor, or applied to the tumor surface using a HNT-chitosan film.

In conclusion, chitosan films would aid in localizing the delivery of drugs to cancerous tissues. If the objective is to reduce side effects resulting from systemic drug and gene treatments and extending drug/gene release, HNT-chitosan films can be used. **Figure 2-1** illustrates the rationale behind the three related projects. The following sections describe the projects in detail.

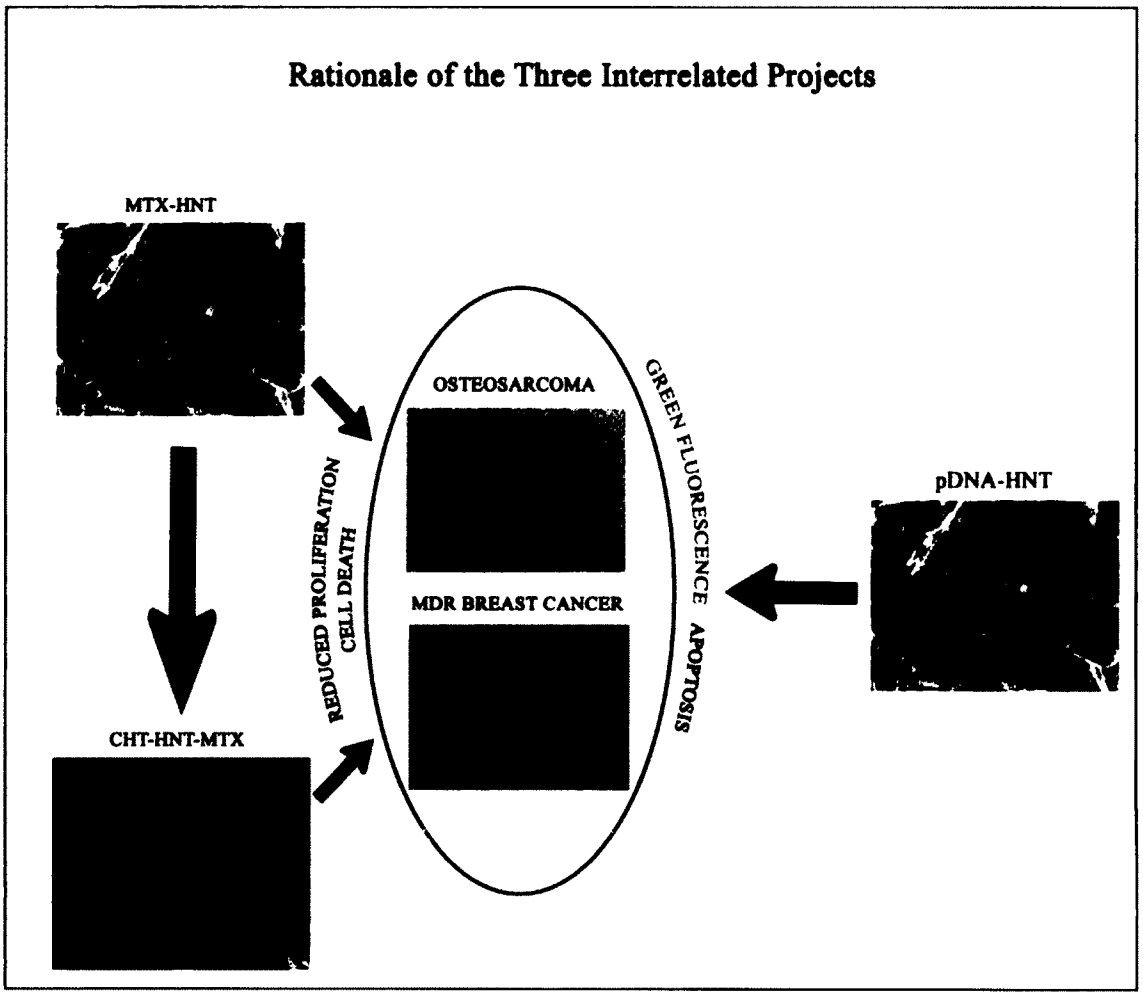


**Figure 2-1:** Graphical representation of the rationale behind the three interrelated projects[50].

## 2.2 HNTs: A New Platform for Delivery of Genes for Cancer Therapy

HNTs are ideal for gene delivery because they can provide a protective container and provide a sustained release of agents over time [89][90]. Halloysite particles are double-layered aluminosilicates which have a hollow tubular structure with an inner diameter of 15 nm and an external diameter of 50-70 nm [90]. Their lengths can be up to 1 micron. HNTs naturally occur and hold several properties that may make them useful in a variety of applications. They have a high loading capacity, can be loaded with a

variety of chemicals and can sustain an extended and controlled release over time. Polymers can be enhanced with HNTs, resulting in a prolonged delivery of chemical agents and enhanced strength, while providing thermal stability and adding surface roughness. HNTs are cytocompatible and are already being used in many health-related fields [90].

HNTs show promise as they can provide a sustained release when localized in the affected tissues. They can act as a nanocarrier for proteins, enzymes, nucleic acids and other bioactive materials. They provide protection from RNases and DNases, other degradation proteins, and heat, and they can house a number of small molecule biocatalysts.

In the first project, HNTs were loaded with plasmid IRES2-EGFP to evaluate gene release and transfection efficiency *in vitro*. Studies were aimed at showing whether HNTs were capable of sustaining release and acting effectively *in vitro*. After suitable 7-day release profiles were obtained, HNTs doped with plasmids were assessed *in vitro* to discover if they performed suitably.

In our preliminary studies, HNTs were loaded with antibiotics or methotrexate, and showed promising results. Studies indicated a biphasic release profile, which was sustained for more than 7 days. Subsequently, HNTs were tested *in vitro*. In bacterial culture, HNTs doped with antibacterial agents inhibited bacterial growth of *Escherichia Coli* and *Staphylococcus aureus*. In mammalian *in vitro* studies, HNTs loaded with pIRES2-EGFP enhanced lipofectamine transfection in CRL-2836 murine osteosarcoma. Lipofectamine is commonly used alone for transfection and the concentration used is typically based on the concentration of DNA and cell density. The results indicate that

gene-doped HNTs may be either applied directly or embedded in films for localized cancer therapy. **Figure 2-2** shows a graphical representation of the use of HNTs for gene delivery.

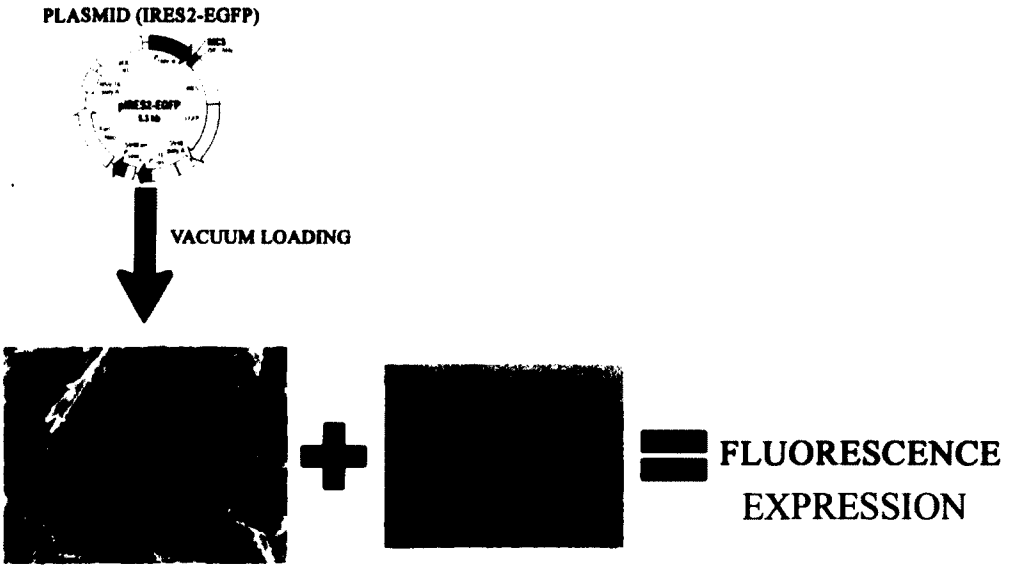


**Figure 2-2:** Graphical representation of the use of HNTs for gene delivery.

## 2.3 HNTs: A New Platform for Delivery of Drugs for Cancer Therapy

HNTs are ideal for drug delivery because they can provide a protective container and a sustained release of agents over time [89][90]. HNTs' geometrical structure and surface charges make them an ideal nanocontainer for drugs, bioactive macromolecules, and polymers, for sustained and extended releases [91][89]] [12-14]. Recent studies showed HNTs biocompatibility with several cell types such as mesenchymal stem cells, fibrochondrocytes, osteoblasts, and human dermal fibroblasts (up to concentrations of 0.1 mg/ml) [90][92]. Polymers can be enhanced with HNTs, resulting in a prolonged delivery

of chemical agents and enhanced strength while providing thermal stability and adding surface roughness.

In the second project, HNTs were loaded methotrexate to evaluate release profile for drug and proliferation inhibition *in vitro*. Studies were aimed at showing whether HNTs could sustain release and act effectively *in vitro*. After obtaining suitable 7-day release profiles, HNTs doped with drugs were assessed *in vitro* to discover if they performed suitably.

In our preliminary studies, HNTs were loaded with antibiotics or methotrexate, and showed promising results. HNTs loaded with resveratrol with subsequent surface modifications was able to deliver the drug to cancer cells [93]. The results indicate that drug-doped HNTs may either be applied directly or be embedded in films for localized cancer therapy. **Figure 2-3** shows a graphical representation of the use of HNTs for drug delivery.

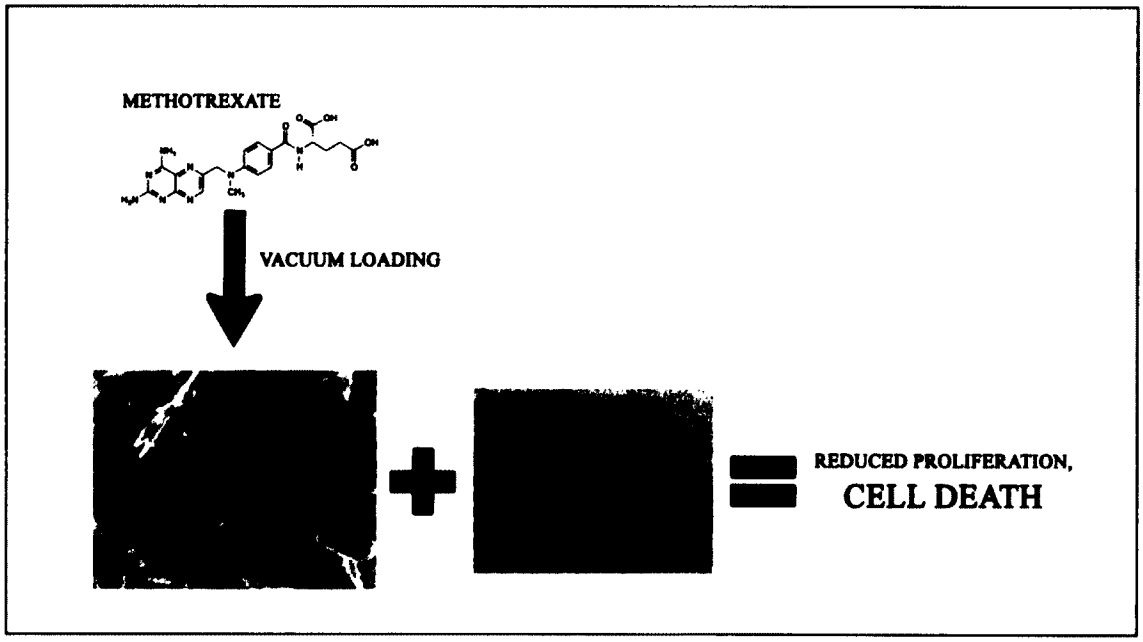


**Figure 2-3:** Graphical representation of the use of HNTs for drug delivery.

## 2.4 Air-Brushed HNT-Doped Chitosan Films for Sustained and Localized Delivery of Methotrexate

The objective of this study was to investigate the potential of methotrexate loaded HNT doped chitosan films and fiber synthesized via a novel air brushed solvent evaporation method for cancer therapy. The main goal was of this research was to develop a novel system for localized delivery of chemotherapeutics for a sustained release that inhibited tumor growth.

During this study, HNTs were loaded with methotrexate, mixed with chitosan and air brushed into a film with nanoscale architecture. Various imaging techniques (SEM) and material tests were used to determine material properties. Drug-loaded chitosan films and HNT-chitosan were then assessed to determine loading capacity and release profile.

HNT-chitosan films were sprayed onto the wells of 12-well tissue culture dishes. Chitosan films and HNT-chitosan composite films were first assessed to determine

whether they had an anti-proliferative effect on CRL-2836 murine osteosarcoma. Drug loaded chitosan films and drug-loaded HNT-chitosan composites were used *in vitro* to comparatively assess their inhibition of cell growth in ATCC cell line CRL-2836 murine osteosarcoma. **Figure 2-4** is the experimental design and concept for air-brushed HNT-doped chitosan films for sustained and localized delivery of methotrexate.

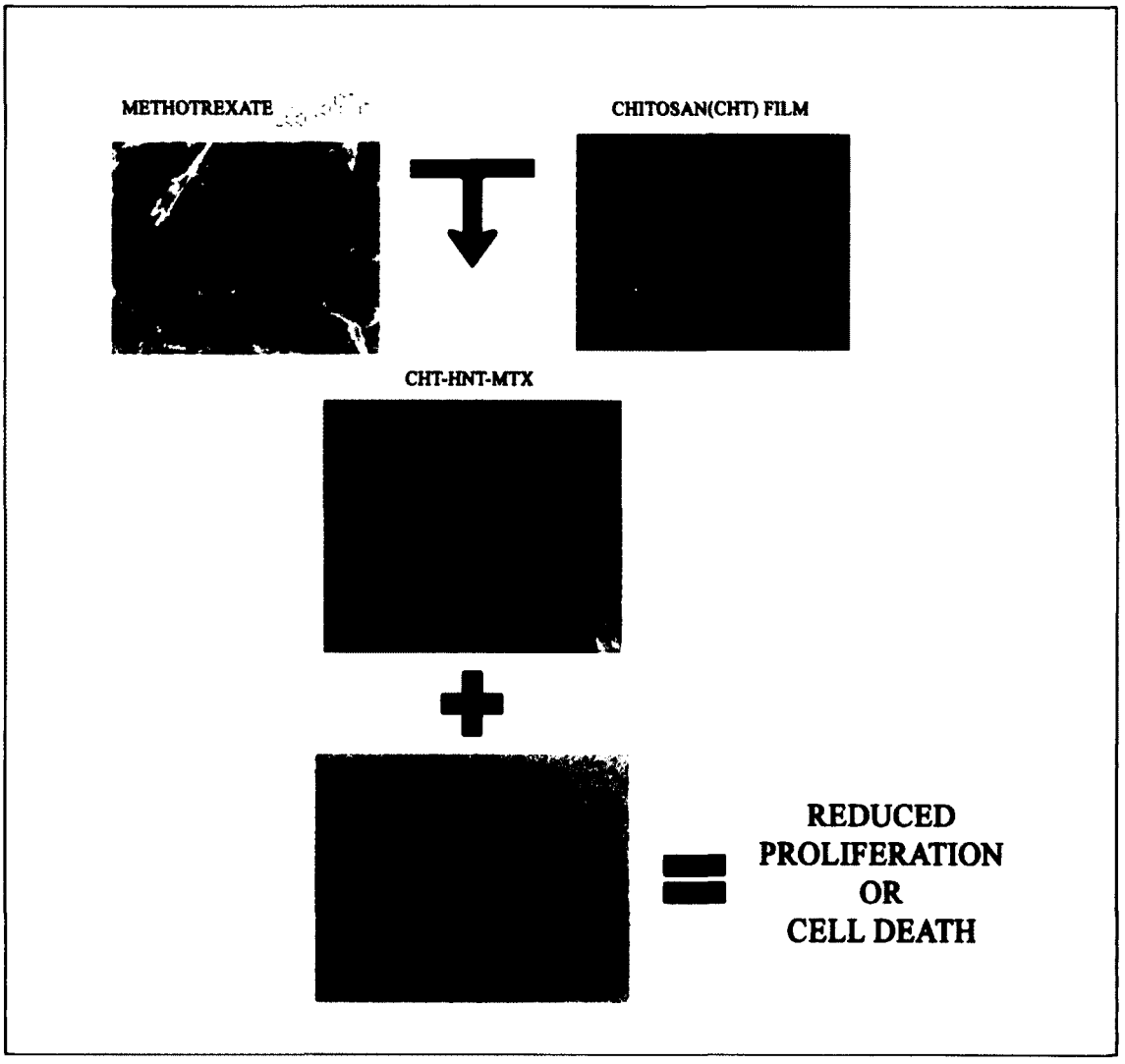


**Figure 2-4:** Experimental design and concept for Air-Brushed HNT doped chitosan films for sustained and localized delivery of methotrexate.

## 2.5 Objective of the Projects

The objectives of all three projects are to design two cytocompatible systems capable of sustaining gene and drug release, to localize drug administration, and to target cancerous tissue and metastasis. The detailed objectives of the individual projects are as follows:

1. To obtain an extended and controlled release of genes and chemotherapeutic drugs from HNTs.
2. To obtain an extended and controlled release of chemotherapeutic drugs from HNTs.
3. To obtain a sustained and extended release of chemo drugs and genes from nanoparticles and films enhanced with nanoparticles.
4. To evaluate whether HNTs can be used for plasmid transfection.
5. To evaluate whether HNTs, loaded with drugs can be used to elicit a inhibit cell growth and induce cell death.
6. To design HNT-chitosan films with chemotherapeutic drugs loaded in them to inhibit cell growth and induce cell death
7. To investigate material properties and characterize nanoparticles, drug- and gene-loaded nanoparticles, and films.

# CHAPTER 3

# INSTRUMENTATION AND METHODS

The current chapter details the instrumentation and methods used for HNT and nanoparticle loading, nanoparticle and film preparation, material characterization of films and nanoparticles, and cellular response to drug or gene loaded nanoparticles and films.

## 3.1 Instruments

Instruments are integral in investigating nanoparticle and film properties. The following subsections describe the instruments used in this dissertation. The instruments and types of data they produce are listed below.

### 3.1.1 HITACHI S 4800 Field Emission Scanning Electron Microscope

HITACHI S 4800 Field Scanning Electron Microscope (FE-SEM) (**Figure 3-1**) was used to image HNTs, chitosan films and double-layered PLGA-Lipid nanoparticles. The high magnification attained allowed for a close comparison of the surface morphologies of chitosan films and chitosan-HNT films. The comparison helped to assess the surface properties and to predict the behavior of the films in *in vitro* conditions.

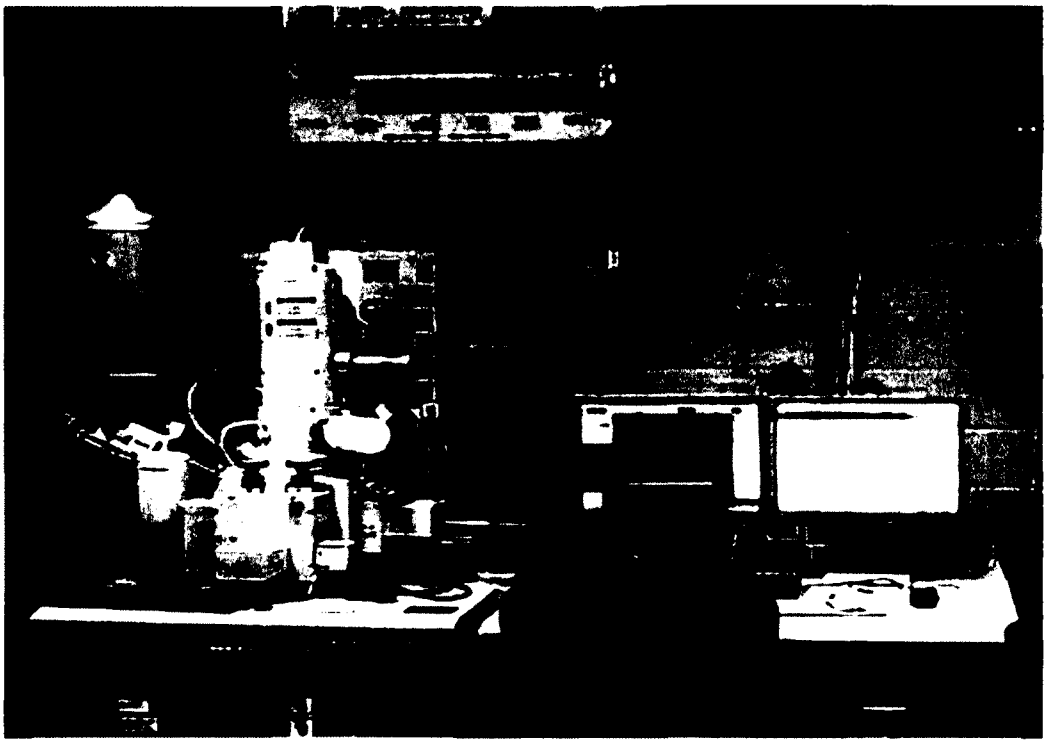

**Figure 3-1:** HITACHI S 4800 FE-SEM at Institute of Micromanufacturing, Louisiana Tech University [94].

### 3.1.2 Tecnai G2 F30 TWIN 300 kV/FEG Transmission Electron Microscope

Tecnai G2 F30 TWIN 300 kV / FEG Transmission Electron Microscope (TEM) (**Figure 3-2**) was used to image HNTS. The high magnification attained via TEM allowed for a comparison of morphologies of halloysite nanotubes.

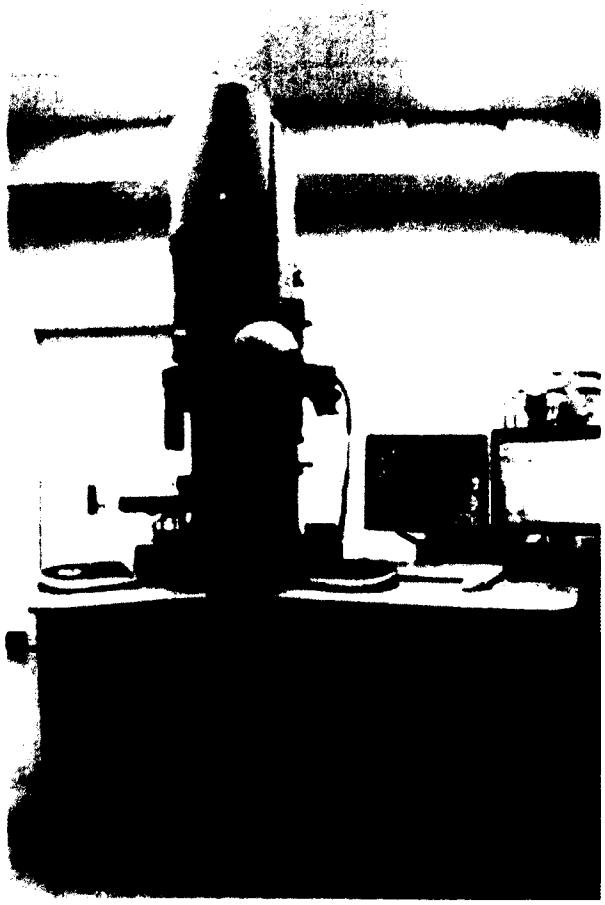

**Figure 3-2:** Tecnai G2 F30 TWIN 300 kV / FEG Transmission Electron Microscope at CIF Microscopy lab, Tulane University [95].

### 3.1.3 Brookhaven Instruments ZetaPlus Potential and Particle Size Analyzer

Brookhaven Instruments ZetaPlus Potential and Particle Size Analyzer (**Figure 3-3**) were used to characterize HNTs. The instrument operates on dynamic light scattering principles; subsequently, it provides the average particle size and average zeta potential. This instrument was used to determine the zeta potential and particle size of HNTs, methotrexate-loaded HNTs and plasmid-loaded HNTs.

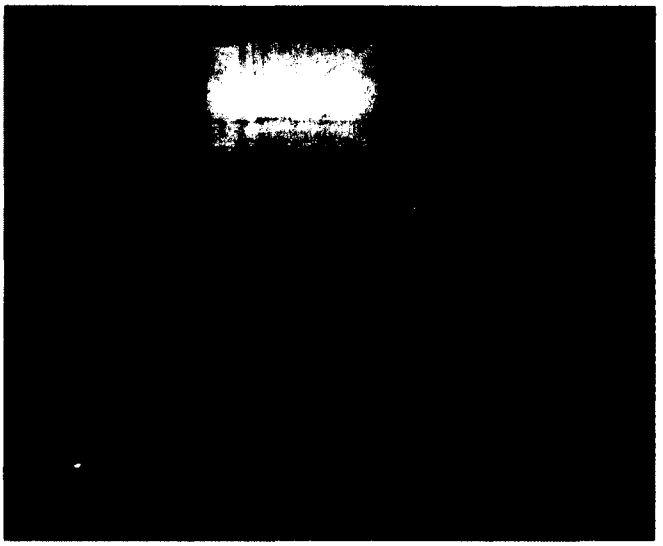

**Figure 3-3:** Brookhaven Instruments ZetaPlus Potential and Particle Size Analyzer IFM, Louisiana Tech University [96].

### 3.1.4 NANODROP 2000 Spectrophotometer

The NANODROP 2000 spectrophotometer (**Figure 3-4**), from Thermo Scientific, is a UV-VIS spectrophotometer, which uses a μl volume samples for DNA, RNA, protein, and various fluorescently active drugs or chemicals. This instrument analyzes samples over a short period of time. Cuvettes can be used for dilute samples, or the pedestal can be used to analyze samples, while the data are reported in the form of graphs and absorbance values through the software [97].

The NANODROP 2000 spectrophotometer (**Figure 3-4**) was used to measure samples for the drug release studies. The NANODROP 2000 used for this research was located in the common second floor lab in the Biomedical Engineering building, Louisiana Tech University.

**Figure 3-4:** Thermo Scientific NANODROP 2000 spectrophotometer.

### 3.1.5 Qubit® 2.0 Fluorometer

The Qubit® 2.0 fluorometer (**Figure 3-5**) is a benchtop fluorometer used to quantify DNA, RNA, and protein, using the highly sensitive and accurate fluorescence-based Qubit™ quantitation assays.The Qubit® 2.0 fluorometer uses the latest illumination and detection technologies to attain the highest sensitivity and allows the use of as little as 1 μL of sample to still achieve high levels of accuracy, even with very dilute samples [98].

The Qubit® 2.0 fluorometer (**Figure 3-5**) was used to analyze samples from DNA release studies. The Qubit® 2.0 Fluorometer used is located in the second floor Mills laboratory in the biomedical building.

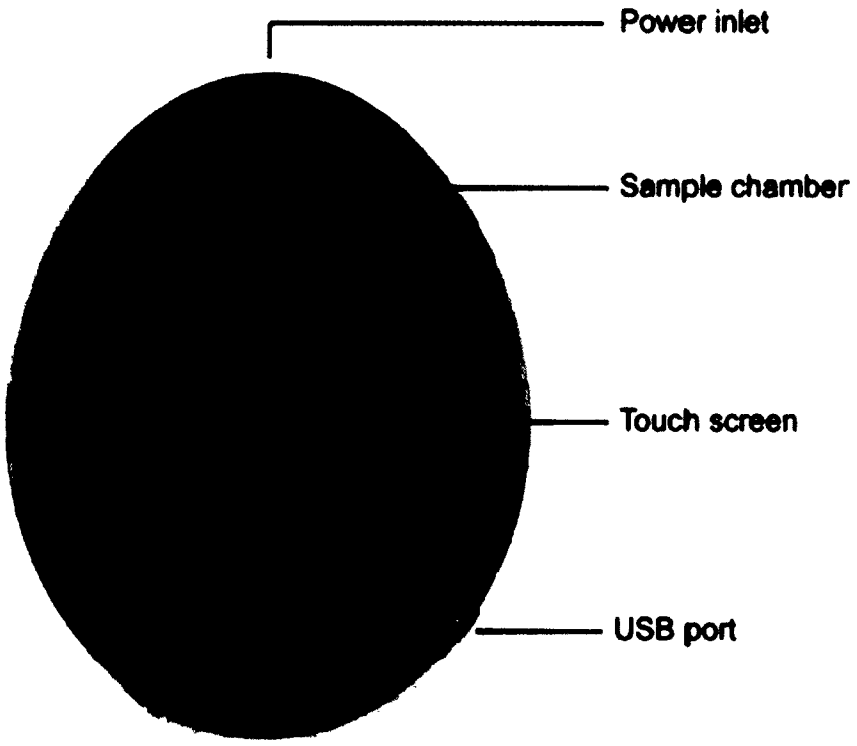


**Figure 3-5:** Qubit® 2.0 Fluorometer.[98]

### 3.1.6 Multiscan Spectrum Absorbance Microplate Reader

The absorbance microplate reader acts similarly to a spectrophotometer, but the stage on which the samples are mounted for analysis differs. This stage can read 12-well plates or similar plates that are used for cell culture.

For the quantification of cell proliferation via XTT assay, a Thermo Scientific Multiskan spectrum absorbance microplate reader was used (**Figure 3-6**). The assays were done in a 12-well plate specifically treated with XTT cell Proliferation assay.

**Figure 3-6:** Thermo scientific Multiskan spectrum absorbance microplate reader Decoster laboratory, Louisiana Tech University.

### 3.1.7 Olympus BX51 Epifluorescence Microscope

The Olympus BX51 epifluorescence microscope (**Figure 3-7**) images cells live/dead or in the fixed state. The microscope has a filter for different fluorescent dyes such as DAPI, Alexa Fluor Red, FITC, and TRITC. This microscope can also image the cells in phase contrast mode when the UV lamp is turned off. The images are captured in high definition and can be taken at 10X, 20X or 40X magnifications. To visualize the cells stained with live/dead fluorescent dyes and green fluorescence protein expression

we used 10X and 20X magnifications. The composite films and the seeded cells were also imaged on the phase contrast mode.

**Figure 3-7:** Olympus BX51 epifluorescence microscope in BME microscopy lab, Louisiana Tech University.

### 3.1.8 TCP Global Master Airbrush Model G22 Airbrush Set and Compressor

TCP Global Master Airbrush Model G22 Airbrush Set and Compressor (**Figure 3-8**) were used to spray chitosan films and composite HNT-chitosan films. This device is commonly used in airbrush paintings. The air-brush system settings were altered and used with polymer solutions to prepare different films.

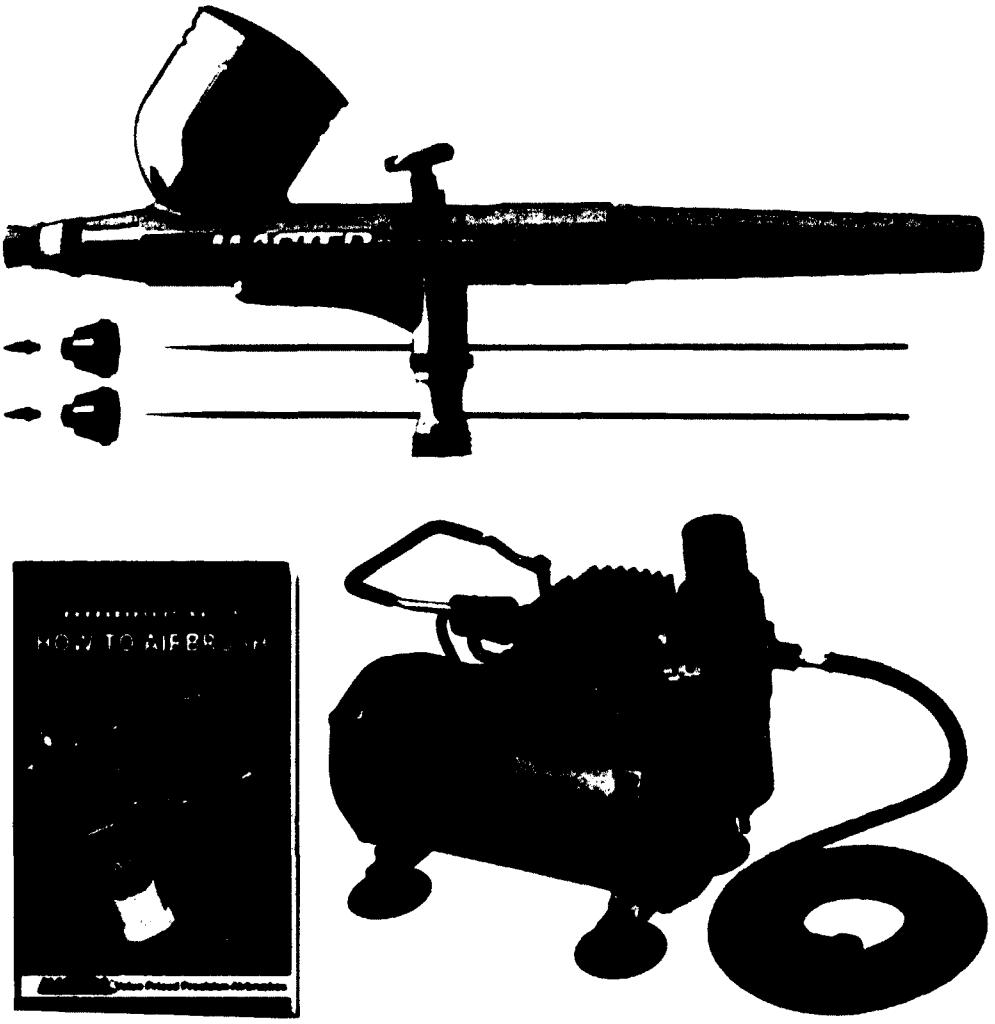

**Figure 3-8:** Master Performance G222 Airbrush Kit with Master Compressor TC-20 & Air Hose [99].

## 3.2 Methods

The methods used to load HNTs, prepare films, characterize samples, and perform the biochemical assays used to determine cellular responses from each system are detailed in the Section 3.2.1.

### 3.2.1 Vacuum Loading of Halloysite

HNTs were loaded with plasmid IRES2-EGFP and the chemotherapeutic drug methotrexate. The basic protocol for vacuum loading remained the same, with concentrations differing based on what was being loaded. For sterilization purposes, HNTs were autoclaved for 45 minutes. Aseptic conditions were maintained throughout the loading process.

#### 3.2.1.1 *Loading HNTs with Plasmids*

Plasmid IRES2-EGFP was obtained from Clontech, Mountainview, California. Stock solution was obtained through bacterial replication and purified using Gene JET plasmid miniprep kit available at ThermoFisher Scientific, Grand Island, New York. Kits yielded plasmid solution with a final concentration of 1μg/μl. This plasmid solution was prepared under sterile conditions and diluted with sterile elution buffer.

After autoclave sterilization, HNTs were vortexed for 15 minutes with prepared concentrations of pIRES2-EGFP. Separate 1 mg aliquots of HNTs were loaded with 1 μg of plasmid, 5 μg of plasmid, and 10 μg of plasmid. A 100 μL volume of elution buffer was added to each sample and the resultant solution was kept in a vacuum chamber under sterile conditions for 48 hours with intermittent vacuum applied to it at 30 inHG. After 48 hours, the HNTs loaded with IRES2-EGFP were vacuum-dried for 3 hours and stored at 4 °C.

#### 3.2.1.2 *Loading HNTs with Methotrexate*

Methotrexate was obtained from Sigma Aldrich, St. Louis, Missouri. A stock solution was prepared according to the manufacturer's instructions. A solution was

prepared at 4 mg/ml concentration in a 20% acetone. All solutions were prepared with sterile diluents and under aseptic conditions.

After autoclave sterilization, HNTs were vortexed for 15 minutes with prepared concentrations of methotrexate. One gram of HNTs was loaded with 100 mg of methotrexate. The resultant solution was kept in a vacuum chamber under sterile conditions for 48 hours with intermittent vacuum applied to it at 30 inHg. After 48 hours, the HNTs loaded with methotrexate were dried in a vacuum oven at 20 inHg of pressure and 100 °C for 1 hour until completely dry.

### 3.2.2 Preparation of Chitosan Films

To blow-spray chitosan microfilms, a 3% chitosan solution was prepared. Chitosan was diluted in a 3% acetic acid solution with magnetic stirring. The chitosan/acetic acid solution was subsequently diluted in acetone and the resultant solution was diluted in DMSO. The resultant solution of 3% chitosan, 1% acetic acid, 33.3% acetone, and 33% DMSO was homogenized for 5 minutes at 500 rpm and for 5 minutes at 800 rpm. The resultant solution's pH was adjusted to 3 for 30 minutes with magnetic stirring, as chitosan crosslinks at an acidic pH, and then returned to pH 7. The addition of acetone allowed for solvents to evaporate during the spraying and drying process and yielded a clean smooth film, while DMSO acted as a curing agent. In the next step, the unloaded HNTs or MTX-loaded HNTs were added to the chitosan solution and the resultant HNT-chitosan mixture was sonicated for 5 minutes to disperse HNTs. A separate solution of chitosan was prepared with a MTX concentration of 1 mg/ml.

The solutions were loaded in the reservoir of the Master Airbrush G22 equipped with a 0.5 mm needle and sprayed at 30 psi of pressure. A 100 µl aliquot of each solution

was sprayed into the wells of a 12 well plate. The films were allowed to dry for 15 minutes before UV sterilization.

### 3.2.3 Zeta Potential and Particle Size

Plain halloysite, IRES2-EGFP-loaded halloysite, or methotrexate-loaded halloysite surface potentials were analyzed by microelectrophoresis (ZetaPlus Potential Analyzer, Brookhaven Instruments). Diluted aqueous dispersions of IRES2-EGFP – loaded halloysite, or methotrexate-loaded halloysite (ca. 1 μg/mL), were transferred into the special cuvette, and electric field was applied across the suspension, causing the movement of negatively charged halloysite toward the cathode. Surface electrical potential of the particles was determined by Smoluchowski formula using particle speed measured with dynamic light scattering (all included in the instrument software). The instrument also allowed for average particle size measurement based on dynamic light scattering (all included in the instrument software).

### 3.2.4 SEM/TEM Preparation

The following subsections describe preparation of HNTs and chitosan films for SEM and TEM. The basic protocol remained the same for both types of nanoparticle but differed for chitosan films. The SEM in IFM was used for imaging and the TEM ate Tulane University was used for imaging nanoparticles and features.

#### 3.2.4.1 *Sample Preparation for FE-SEM*

HNT samples were added to carbon tape and imaged with a Hitachi Field Emission Scanning Electron Microscope. Surface features and morphology were observed. Chitosan films were sprayed onto 1x1 mm square silicon wafers and allowed to dry for 15 minutes at room temperature

3.2.4.2 *Sample Preparation for TEM*

Transmission Electron Microscopy (TEM) images were recorded with a Tecnai G2 F30 TWIN 300 kV / FEG Transmission Electron Microscope at CIF Microscopy lab, Tulane University. The microscope operated at an accelerating voltage of 100-200 kV. We prepared samples for analysis by dropping a dilute HNT dispersion in water onto carbon-coated copper grids and allowing water to evaporate.

3.2.5 Release Profile Studies

The release profiles for methotrexate and plasmids were done under simulated physiological conditions. Release profiles for plasmid DNA were obtained from loaded HNTs. Plasmid-loaded HNTs were suspended in nuclease-free water with uniform agitation on a vortex. At set time points, HNTs were centrifuged at 13k rpm for 5 minutes and 200 µl of nuclease free water was completely removed and collected from HNT suspension and replaced with 200 µl fresh nuclease free water.

For plasmid release profile (pIRES2-EGFP), the samples were collected for 24 hours over 7 days. Qubit® dsDNA HS and BR Assay Kits were used to determine the concentrations of the stored samples. The Qubit® dsDNA HS (high sensitivity) and BR (broad range) assay kits were custom made for double stranded DNA and were obtained from Invitrogen (Carlsbad, CA). The kits bind a fluorescent dye to DNA and allow the concentration to be read on Qubit® 2.0 fluorometer. The concentration of DNA is given based on the fluorescence measurements and exported directly into an Excel file.

Release profiles for methotrexate were obtained from HNTs, chitosan films, and chitosan-HNT composite films. MTX loaded HNTs were suspended in 2 ml Hank's Balanced Salt Solution (HBSS) and put on a rocker for uniform agitation. At set time

points, HNTs were centrifuged at 3k rpm for 5 minutes, and 2 ml of HBSS was completely removed, collected from HNT suspension and replaced with 2 ml of fresh HBSS. Samples were taken and stored at 4 °C for further analysis.

Drug-loaded chitosan and chitosan-HNT films were sprayed onto the well of a 12-well tissue culture dish. Then 2 ml of HBSS were added, and the plate was put on a rocker for uniform agitation. At set time points, 2 ml of HBSS were completely removed, collected and replaced with 2 ml of fresh HBSS. Samples were taken and stored at 4 °C for further analysis. All release profile experiments were performed at room temperature.

Samples were read using UV/VIS NANODROP spectrophotometer at 300 nm. Since, methotrexate is photometrically active, concentrations were estimated by comparing UV/VIS spectra to UV/VIS spectra standards for methotrexate.

### 3.2.6 Cell Assays

Biochemical assays were used to quantify cellular responses to HNTs, DBL-NPs and chitosan films. Lab plastics and 96-well plates were purchased from MidSci, St. Louis, MO. Dulbecco's Phosphate Buffered Saline (DPBS), Dulbecco's Modified Eagle's Medium (DMEM), fetal bovine serum (FBS), Live/Dead Viability/Cytotoxicity kit and penicillin-streptomycin-amphotericin (PSA) antibiotics were obtained from Life Technologies, Carlsbad, CA

#### 3.2.6.1 *Transfection*

Transfection was used to determine the loading and delivery capacity for HNTs and was compared to common transfection agent Lipofectamine.

3.2.6.1.1 HNT-Plasmid Complexes

*In vitro* transfection efficiency studies of Plasmid IRES2-EGFP-loaded HNTs were carried out to determine whether HNTs are able to deliver plasmid to the cell. Murine osteosarcoma were seeded in 96 well tissue culture dishes (MidSci, St. Louis, MO) with serum free Dulbecco's Modified Eagle Medium. Plasmid IRES2-EGFP-loaded HNTs were added with cells at the time of seeding and incubated 24 hours. Lipofectamine was diluted in serum free DMEM and Plasmid IRES2-EGFP-loaded HNTs were diluted in serum free DMEM. These solutions were combined, mixed and incubated for 5 minutes. These Lipofectamine Plasmid IRES2-EGFP-loaded HNTs complexes were then added with cells at the time of seeding. The media was changed to media with serum and cells were evaluated for EGFP expression after 24, 48, 96 and 144 hours. At 72 hours, transfected cells were split from the 96-well and seeded into a 24-well plate for further analysis. The negative controls was free plasmid DNA and the positive control was Lipofectamine.

3.2.6.1.2 Lipofectamine

To prepare for transfection, cells were seeded and allowed to adhere for 4 hours prior to Lipofectamine treatment. Lipofectamine was used as a positive control for plasmid transfection because it is known to have a high transfection efficiency. The manufacturer's protocol was followed for transfection. Lipofectamine was diluted in serum free DMEM and pDNA was diluted in serum free DMEM. These solutions were combined, mixed and incubated for 5 minutes. DNA-lipid complexes were then add to cells and incubated for 24 hours. The media was changed at 24 hours and EGFP

expression was evaluated after 24, 48, 96, and 144 hours. At 72 hours, transfected cells were split from the 96-well into a 24-well plate for further analysis.

3.2.6.2 *XTT Cell Proliferation Assay*

This assay is based on the ability of viable cells to reduce tetrazolium dye. In these experiments, osteosarcoma cells were used. For methotrexate-loaded HNTs, cells were seeded in 96-well plates and allowed to adhere, and the MTX-HNTs were added to well containing cells. There were two sets of controls, untreated cells and cell exposed to drug-free HNTs. For chitosan films, cells were seeded in 12-well plates containing drug free chitosan composite films and MTX loaded chitosan composite films. Cells were tested at 24, 72, 120 and 168 hours. The XTT assay protocol supplied by the manufacturer (Sigma-Aldrich) was followed. After aspiration of medium, 100 μL of buffer were added to each well along with 20 μL of XTT solution. Photometric absorption of each well was measured at 450 nm and 690 nm after 4 hours of incubation. After completing the XTT assay, a live/dead cytotoxicity assay was conducted on additional wells of each category on the same plate.

3.2.6.3 *Live/Dead*

A live/dead cytotoxicity kit cat. No. L3224, obtained from Thermo Fischer, Waltham, MA, was used for testing. The protocol supplied by the manufacturer was used for the assay. The dyes were diluted to 2 μM solutions and were added to the test wells. Fluorescence microscopy was used to image live and dead cells after they were incubated for 30 minutes in the dye solutions.

# CHAPTER 4

# USE OF HNTS FOR GENE DELIVERY IN CANCER THERAPY

## 4.1 Introduction

HNTs are ideal for gene delivery because they can provide a protective container and a sustained release of agents over time [89][90]. Halloysite particles are double-layered aluminosilicates which have a hollow tubular structure with an inner diameter of 15 nm and an external diameter of 50-70nm [90]. Their lengths can be up to 1 micron. HNTs naturally occur and hold several properties that may make them useful in a variety of applications. They have a high loading capacity, can be loaded with a variety of chemicals and can sustain an extended and controlled release over time. Research has yet to establish HNTs efficacy for delivery plasmid DNA to cells.

For osteosarcoma patients who have received chemotherapy alone have a 100% recurrence rate without surgical resection [100], [101]. Even though recent advances have led to increased rates of limb sparing therapy, patients are still at risk of recurrence. While surgical abscission can physically remove clinically detectable tumor masses, systemic chemotherapy or gene therapy can inhibit micrometastasis before and/or after surgery. For the treatment of osteosarcoma, many of the research efforts are directed at reducing the risk of recurrence following surgical resection. One of the major challenges faced by chemotherapy and gene therapy is the inability to sustain and/or localize drug release in targeted cell types.

To address this challenge, HNTs loaded a plasmid pIRES2-EGFP expressing the green fluorescence protein is the method being proposed. HNTs have a cylindrical structure with concentric aluminosilicate layers and negatively charged surface and positively charged lumen [102]. HNTs' unique structure makes them ideal for loading a variety of charge molecules [103]. Past research has shown HNTs can be used to deliver chemotherapeutic agents, as well as, bioactive molecules like anti-infective agents, proteins, etc. in a sustained manner [103][93].

The hypothesis of this project was that HNTs would act as an efficient delivery vector for genes, such as pIRES2-EGFP, for a sustained release. If effective for plasmid delivery, the model vector pIRES2-EGFP would be replaced with a plasmid that induces apoptosis.

## 4.2 Methods and Materials

All the plastic wares, such as, syringes, centrifuge tubes, microcentrifuge tubes, tissue culture plates, and pipettes, were purchased from Mid Scientific, St. Louis, MO. Cell culture media, buffers, and serum Life Technologies, Grand Island, NY. HNTs were obtained from Sigma-Aldrich, St. Louis, MO, and pIRES2-EGFP was obtained from Clontech, Mountainview, CA. Plasmid purification kits, elution buffer and nuclease-free water were obtained from Thermo Fisher Scientific, Waltham, MA. Murine osteosarcoma cells CRL-2836 were obtained from ATCC, Manassas, VA. The Qubit® dsDNA HS and BR assay kits were custom made for double stranded DNA and were obtained from Invitrogen (Carlsbad, CA).

### 4.2.1 Release study

A release study was carried out to understand the elution of plasmid DNA from HNTs. These studies provided an analysis of the release of gene from HNTs.

#### 4.2.1.1 *Plasmid DNA*

The release profile study for pIRES2-EGFP was done to understand the release of plasmid DNA from HNTs. As the amount of plasmid eluted fell in the range of nanograms and micrograms, the custom made Qubit® dsDNA HS (high sensitivity) kit was used. The Qubit® dsDNA HS kit with the Qubit® 2.0 from Invitrogen can estimate the amount of DNA as low as 10 pg/μl. The details of sample collection and the overall procedure are provided in section 3.2.6.

### 4.2.2 Cell Culture and Seeding

An osteosarcoma cell line was the model used to study transfection efficiency of plasmid loaded HNTs. Osteosarcoma cells were plated in 25 $cm^2$ tissue culture flasks, and incubated at 37 °C under humidified 5% $CO_2$ and 95% air in complete DMEM containing 10% FBS and 1% PSA. Subconfluent cells were passaged with 0.25% trypsin, collected by centrifugation, suspended in complete DMEM and cultured at a 3:1 split into 25 $cm^2$ tissue culture flasks. These cultures were *in vitro* transfection efficiency tests.

#### 4.2.2.1 *Green Fluorescence Imaging for Transfection Efficiency*

A transfection efficiency study was carried out to determine if HNTs were able to act as a vector for the delivery of plasmid DNA. Cells were seeded into a 96-well tissue culture dish and allowed to adhere and reach 80% confluency. HNT-plasmid complexes were added to the cells as described in Section 3.2.7.1.1. Controls did not receive plasmid complexes. Negative controls received free plasmids and positive controls receive

plasmid-lipofectamine complexes as detailed in Section 3.2.7.1.2 (see **Table 4-1**). The wells were evaluated after 24, 48, 96, and 144 hours, using the Olympus BX51 fluorescent microscope with FITC filter. Image fluorescence was quantified using Image J software.

**Table 4-1:** Platemap for Transfecion Assay.

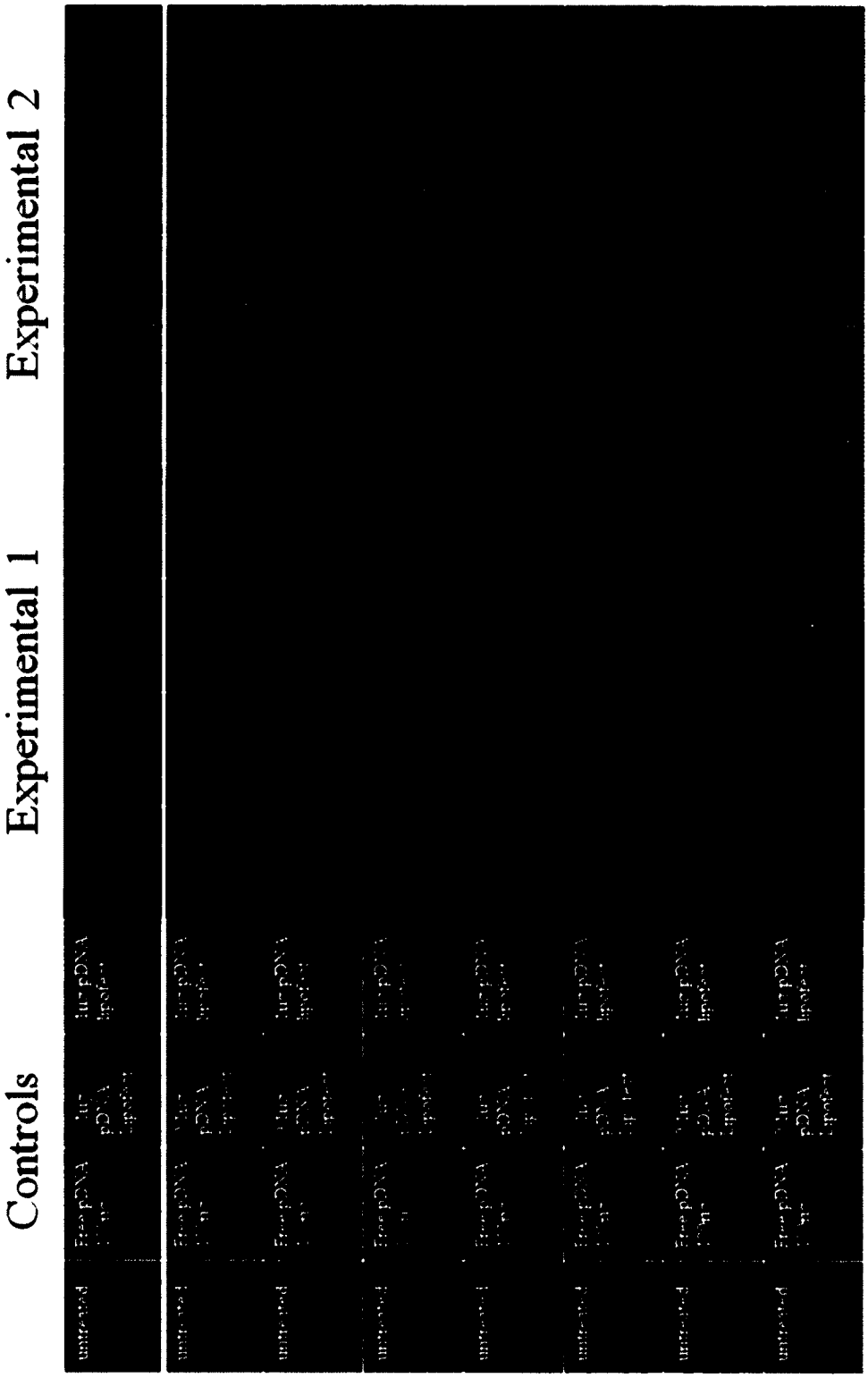

### 4.2.3 Zeta Potential/Particle Size Analysis

To characterize the HNTs, average size and charge measurements, were taken.

#### 4.2.3.1 *Zeta Potential and Particle size*

The halloysite surface potential was analyzed under microelectrophoresis (ZetaPlus potential analyzer, Brookhaven Instruments). A diluted aqueous dispersion of halloysite was prepared and analyzed as described in Chapter 3, Subsection 3.2.4. The instrument also provided average particle size measurements, based on dynamic light scattering.

## 4.3 Results and Discussion

### 4.3.1 Release Profile Study of pIRES2-EGFP from HNTs

The release profile study of pIRES2-EGFP from HNTs was done to estimate the amount of plasmid eluted from the HNTs for a period of 24 hours and over seven days. This study was carried out to determine if HNTs could be loaded with plasmids and elute enough plasmid DNA to efficiently transfect cells *in vitro*. The graph showing the release profile study for pIRES2-EGFP for 24 hours is given in **Figure 4-1**.

Figure 4-1 shows the trend of the pIRES2-EGFP release over 24-hours at the three different loading concentrations. This release was achieved for the vacuum-loaded HNTs in nuclease free water at room temperature. The amount of pIRES2-EGFP release was estimated by the Qubit® dsDNA HS kit and reading the sample on the Qubit® 2.0 fluorometer. The experiment was repeated three times to reduce error and to check for reproducibility of results. The values are the mean of reading of pIRES2-EGFP release from HNTS at the respective time points from the 3 repetitions of the experiment. The error bars reflect the standard deviation.

The graph shows the cumulative release profile of the plasmid for 24 hours in the nanogram to microgram range which is comparable to the amount used *in vitro* with Lipofectamine.

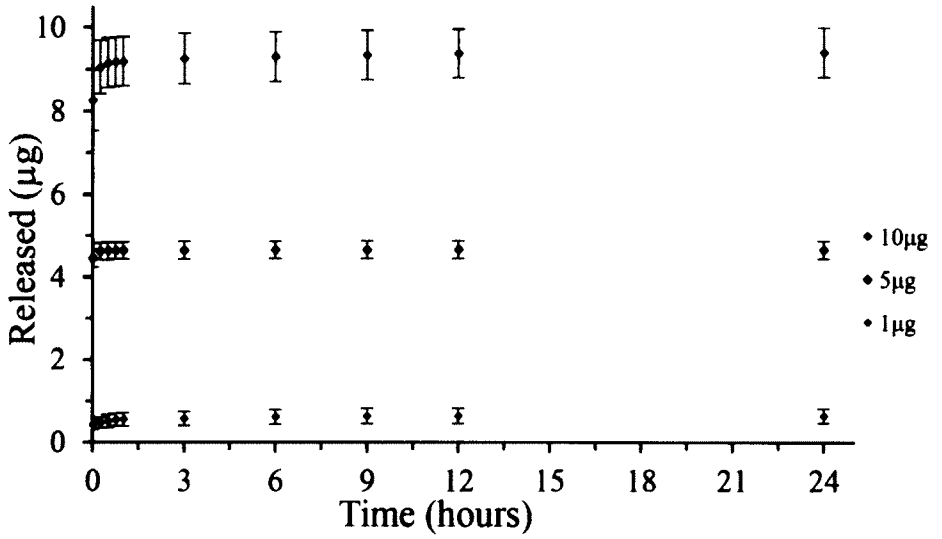


**Figure 4-1:** Mean Cumulative Release profile of pIRES2-EGFP from HNTs for 24 hours mean of n = 9 for each concentration +/- standard deviation.

The graph of the release profile study for pIRES2-EGFP from HNTs for seven days is given in **Figure 4-2**. The release profile study of pIRES2-EGFP from HNTs was extended to seven days. The experiment was repeated three times to reduce error and to check for reproducibility of the results. The values are the means of the readings of pIRES2-EGFP from HNTs at the respective time points recorded from the repetitions of the experiments. The error bars reflect the standard deviation.

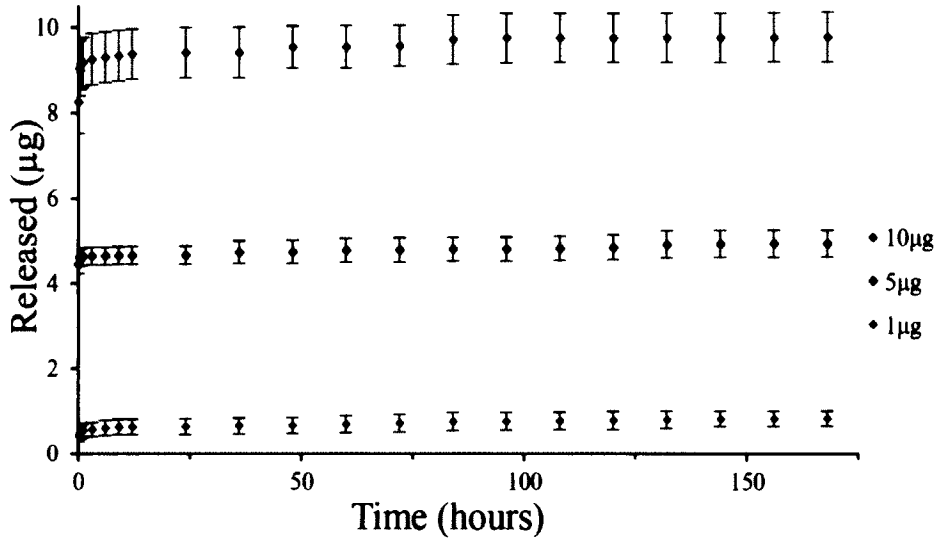


**Figure 4-2:** Mean Cumulative Release profile of varying concentrations of pIRES2-EGFP from HNTs for seven days mean of n = 9 for each concentration +/- standard deviation.

The release of pIRES2-EGFP from HNTs was extended and sustained for seven days. In the first 24 hours, from the three different samples, a mean of 78.7% ± 7.1% of loaded plasmid was released and after seven days, an average 93.7% ± 8.2% of loaded plasmid was released. The release for 24 hours and seven days were in the nanogram and microgram range for all samples and well within the range of DNA concentrations required for commonly used transfection reagents like Lipofectamine.

The release profile of pIRES2-EGFP from HNTs suggests that the majority of the plasmid was localized or wrapped around the surface of HNTs. The initial burst release was mainly from the surface localization of the plasmid. Even with the majority of the plasmids being localized on the surface of the HNTs, the release is in nano and micrograms, which is well within the range of DNA concentrations required for commonly used transfection reagents like Lipofectamine. Results obtained from the seven-day release profile are promising. The majority of plasmid DNA is released in the

first 24 hours, but HNTs release plasmid DNA continuously over a seven-day period, as opposed to Lipofectamine which is typically only stable for transfection for 24-48 hours. A sustained release of plasmid DNA is beneficial because loaded HNTs can be injected once and sustain a release in the cancerous tissues for more than seven-days therefore reducing the need for multiple injections. This approach may have a further advantage in that HNTs with DNA localized on the surface could be coated with lipids or polyelectrolytes to increase cellular uptake and modulate release.

The release of pIRES2-EGFP was not extended beyond seven days as *in vitro* experiments would only focus on the first seven days and primarily on the first 48 hours. The comparison of the three loaded volumes, 1, 5, and 10 μg, demonstrated HNTs could sustain a release of low and high concentration for more than seven day; however, HNTs released the plasmids slightly faster when loaded with a higher volume. Results indicated that 10 μg plasmid DNA would be loaded into 1 mg HNTs for *in vitro* experiments as the sample would be split into aliquots that corresponded to concentrations needed to transfect cells cultured in a 96-well tissue culture dish. Further analysis of surface adsorption was done using particle size measurements in Section 0.

### 4.3.2 Transfection Assay

Transfection assay result for 4 groups were compared for:

1. Free pIRES2-EGFP
2. pIRES2-EGFP complexed with Lipofectamine
3. pIRES2-EGFP-loaded HNTs
4. pIRES2-EGFP-HNT-Lipofectamine

This comparison was done to investigate the potential of HNTs as a transfection agent and also to determine if they enhanced the transfection efficiency of Lipofectamine. Following transfection, the plates were analyzed after 24 and 48 hours, as green fluorescence protein (GFP) is fully expressed at 48 hours. The cells were split from the 96-well to a 24-well at 72 hours to allow for growth and further analysis of the transfection efficiency. The cells were then analyzed after 96 and 144 hours.

Transfection efficiency was determined by the mean fluorescence area in a plate. Eight images were randomly selected from each well, four from the edge and four from the center, for processing. Image j was used to measure the amount of fluorescent area and calculate the fluorescence percentage in each group. IBM SPSS software and a paired t-test were used for statistical analysis. Results of paired t-test are seen in **Table A-51** of the appendix. **Figure 4-3**, **Figure 4-6**, **Figure 4-9** and **Figure 4-12** show the average fluorescent percentage of each group after 24, 48, 96, and 144 hours, respectively. Images that represent the amount of average fluorescence among the group are shown in **Figure 4-4** and **Figure 4-5** for 24 hours, **Figure 4-7** and **Figure 4-8** for 48 hours, **Figure 4-10** and **Figure 4-11** for 96 hours, and **Figure 4-10** and **Figure 4-11** for 144 hours.

**Figure 4-3** shows the mean fluorescence area percentage after 24 hours ± standard deviation. As expected, control groups for untreated and free DNA show no fluorescence. Fluorescence percentage for Lipofectamine transfection with 100 ng and 1 μg of pIRES2-EGFP are 44.9% ± 19% and 55% ± 4.5% respectively. All groups with HNT-pIRES2-EGFP show little to no fluorescence. HNT-pIRES2-EGFP-Lipofectamine groups for 100 ng and 2 μg pIRES2-EGFP have minimal fluorescence by comparison to controls. The 1 μg and 500 ng HNT-pIRES2-EGFP-Lipofectamine groups were less

effective when compared to controls but showed a transfection efficiency of 8.5% ±1.8% and 27% ±3.7%, respectively.

At 24 hours Lipofectamine transfection with 100 ng and 1 μg of pIRES2-EGFP, and 1 μg and 500 ng HNT-pIRES2-EGFP-Lipofectamine groups showed a significant difference from the untreated control at α = .05 (Appendix **Table A-5**). Lipofectamine transfection with 100 ng differed significantly from Lipofectamine transfection with 1 μg of pIRES2-EGFP. 1 μg differed significantly from 500 ng HNT-pIRES2-EGFP-Lipofectamine at α = .05 (Appendix **Table A-5**).

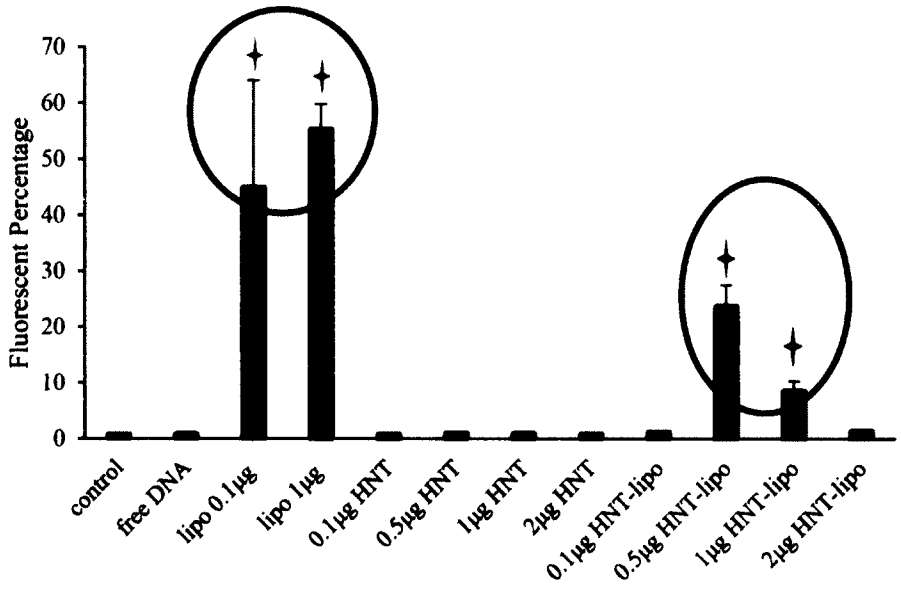


**Figure 4-3:** Mean Fluorescence Area Percentage of n = 8 images ± at standard deviation 24 hours. Statistical analysis was applied with IBM SPSS 22.0 at α = .05, and the red stars indicate no significant difference exists two groups encircled are compared and the black stars indicate significant difference exists when encircled groups are compared.

In **Figure 4-4** the images for 24 hours are shown. A and B are controls that are untreated and treated with Free DNA respectively; C and D are positive controls for Lipofectamine with 100 ng and 1μg of pIRES2-EGFP respectively. **Figure 4-4** E, F, G and H show HNTs with 100 ng, 500 ng, 1 μg and 2 μg pf pIRES2-EGFP respectively.

The image for 100ng pIRES2-EGFP-HNT agrees with the graph and shows that E has no fluorescent cells (compare **Figure 4-3** with **Figure 4-4** E). 500ng pIRES2-EGFP-HNT and 1μg pIRES2-EGFP-HNT have few fluorescents cells (less than 5%) when compared to the Lipofectamine controls (~50%) while 2μg pIRES2-EGFP-HNT has no living fluorescent cells as the one cell that is fluorescent does not have the morphology of a healthy cell (compare **Figure 4-3** with **Figure 4-4** F and G).

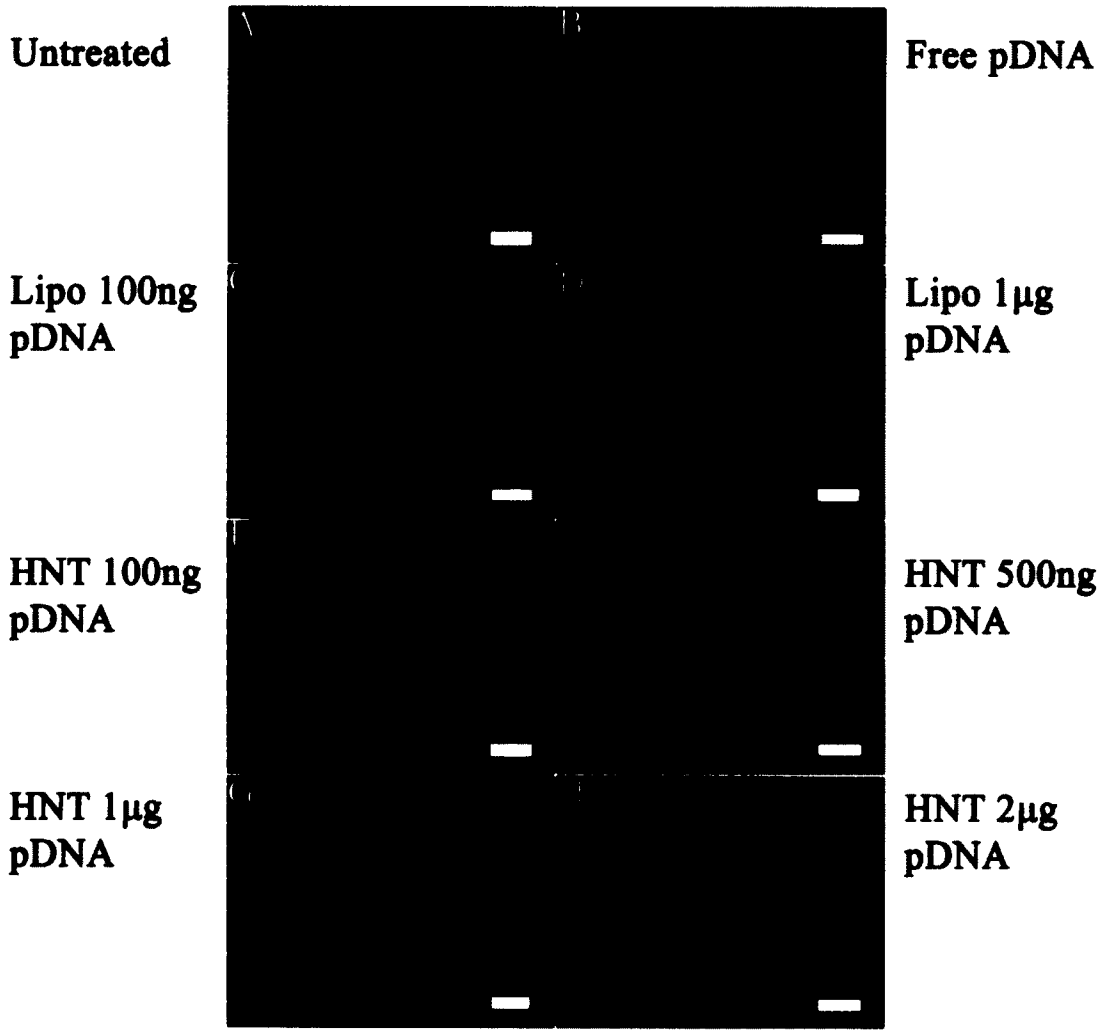


**Figure 4-4:** 24 Hours Fluorescent Images for HNT-pIRES2-EGFP. Scale bar indicates 200μm A and B are Negative controls. C and D are positive controls A) Control 1 untreated; B) Control 2 free DNA; C) Control 3 100 ng pIRES2-EGFP with Lipofectamine.; D) Control 4 1μg pIRES2-EGFP with Lipofectamine; E) Experimental 1 100 ng pIRES2-EGFP with HNT; F) Experimental 2 500ng pIRES2-EGFP with HNT; G) Experimental 3 1μg pIRES2-EGFP with HNT; H) Experimental 4 2μg pIRES2-EGFP with HNT.

In **Figure 4-5** the images for 24 hours are shown. A-D are the same controls shown in Figure 4-4 A-D. **Figure 4-5** E, F, G and H show Lipo-HNTs with 100 ng, 500 ng, 1 μg and 2 μg pIRES2-EGFP, respectively. The images agree with the graph and show that 100ng pIRES2-EGFP-Lipo-HNT and 2μg pIRES2-EGFP-Lipo-HNT have few fluorescent cells (less than 5 %) (Compare **Figure 4-3** with **Figure 4-5** E and H). 500ng pIRES2-EGFP-Lipo-HNT and 1μg pIRES2-EGFP-Lipo-HNT have fewer fluorescents cells (~25% and ~10 % respectively) when compared to the Lipofectamine controls (~50%) while 2μg pIRES2-EGFP-Lipo-HNT has no living fluorescent cells as the one cell that is fluorescent does not have the morphology of a healthy cell (Compare **Figure 4-3** with **Figure 4-5** F and G).

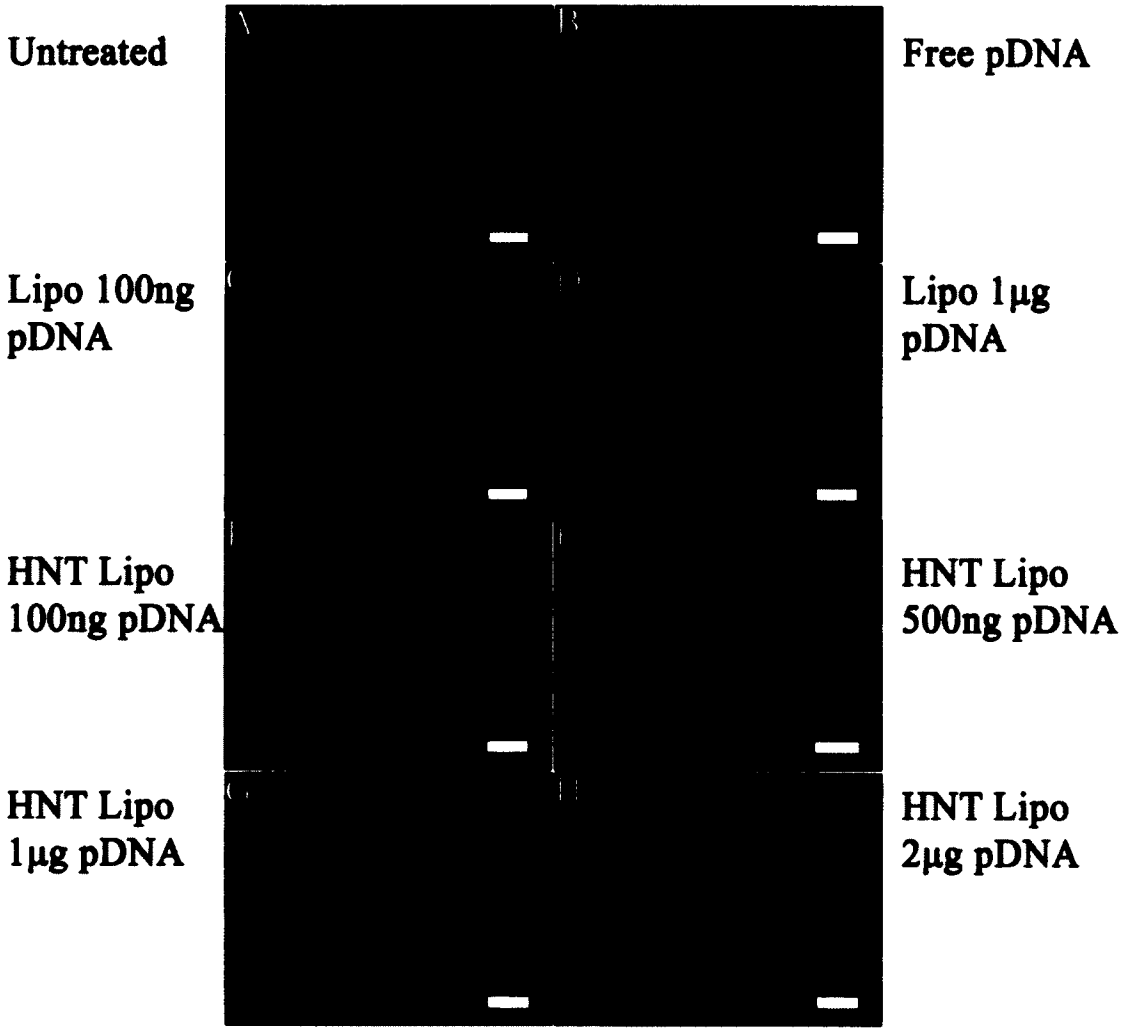


**Figure 4-5:** 24 Hours Fluorescence Images for HNT-Lipo-pIRES2-EGFP. Scale bar indicates 200μm. A and B are Negative controls (also shown in figure 4-4). C and D are positive controls (also shown in figure 4-4). A) Control 1 untreated; B) Control 2 free DNA; C) Control 3 100 ng pIRES2-EGFP with Lipofectamine; D) Control 4 1μg pIRES2-EGFP with Lipofectamine; E) Experimental 5 100 ng pIRES2-EGFP with HNT and Lipofectamine; F) Experimental 6 500ng pIRES2-EGFP with HNT and Lipofectamine; G) Experimental 7 1μg pIRES2-EGFP with HNT and Lipofectamine; H) Experimental 8 2μg pIRES2-EGFP with HNT and Lipofectamine.

**Figure 4-6** show the mean fluorescence area percentage at 48 hours ± standard deviation. As expected, control groups for untreated and free DNA show no fluorescence. Fluorescence percentages for Lipofectamine transfection with 100 ng and 1μg of pIRES2-EGFP are 65.8% ± 11.7% and 66.2% ± 8.7% respectively. All groups with HNT-pIrES2-EGFP show little to no fluorescence at all. HNT-pIrES2-EGFP-Lipofectamine groups for 100 ng and 2 μg pIRES2-EGFP have minimal fluorescence by comparison to controls. 1 μg and 500 ng HNT-pIrES2-EGFP-Lipofectamine group were less effective when compared to controls but showed a transfection efficiency of 6.2% ±2% and 60.8 % ± 19.9 % respectively.

At 48 hours Lipofectamine transfection with 100 ng or 1 μg of pIRES2-EGFP, and 500 ng HNT-pIRES2-EGFP-Lipofectamine groups showed a significant difference from the untreated control at $\alpha = .05$ (Appendix **Table A-5**). Lipofectamine transfection with 100 ng or 1 μg of pIRES2-EGFP, and 500 ng HNT-pIRES2-EGFP-Lipofectamine groups did not differ significantly difference from each other. Lipofectamine transfection with 100 ng differed significantly from Lipofectamine transfection with 1 μg of pIRES2-EGFP. 1 μg differed significantly from 500 ng HNT-pIRES2-EGFP-Lipofectamine at $\alpha = .05$ (Appendix **Table A-5**).

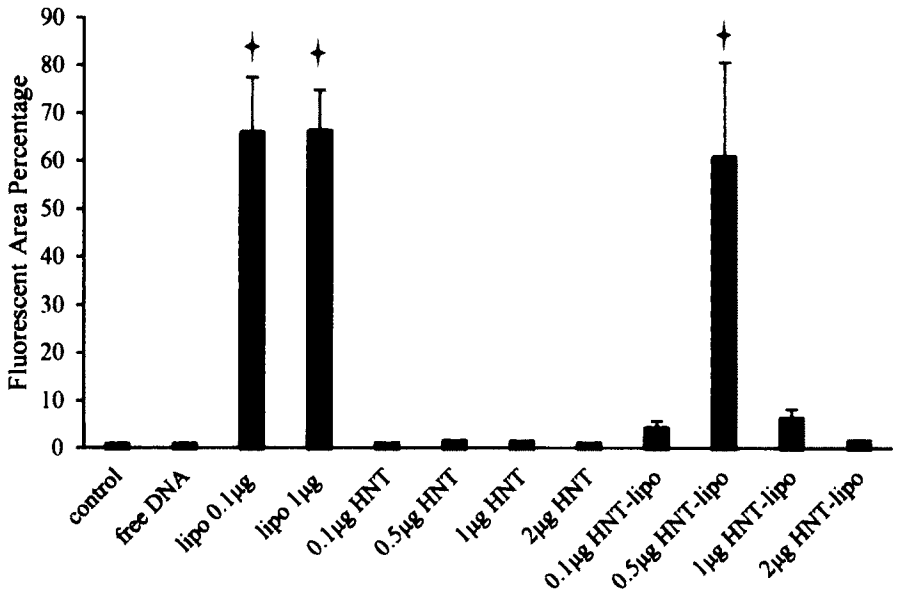


**Figure 4-6:** Mean Fluorescence Area Percentage of n = 8 images ± at standard deviation at 48 hours. Statistical analysis was applied with IBM SPSS 22.0 at $\alpha = .05$, The red stars indicate no significant difference exists between groups compared lipo 0.1 µg, lipo 1µg and 0.5µg HNT-Lipo.

In **Figure 4-7** the images for 48 hours are shown. A and B are controls that are untreated and treated with Free DNA; C and D are positive controls for Lipofectamine with 100 ng and 1 µg of pIRES2-EGFP, respectively. **Figure 4-7** E, F, G and H show HNTs with 100 ng, 500 ng, 1 µg and 2 µg pIRES2-EGFP respectively. 500ng pIRES2-EGFP-HNT and 1µg pIRES2-EGFP-HNT have fewer fluorescents cells (less than 10 %) when compared to the Lipofectamine controls (~80%) while 100ng pIRES2-EGFP-HNT and 2µg pIRES2-EGFP-HNT have no living fluorescent cells as cells that are fluorescent do not have the morphology of a healthy cells.

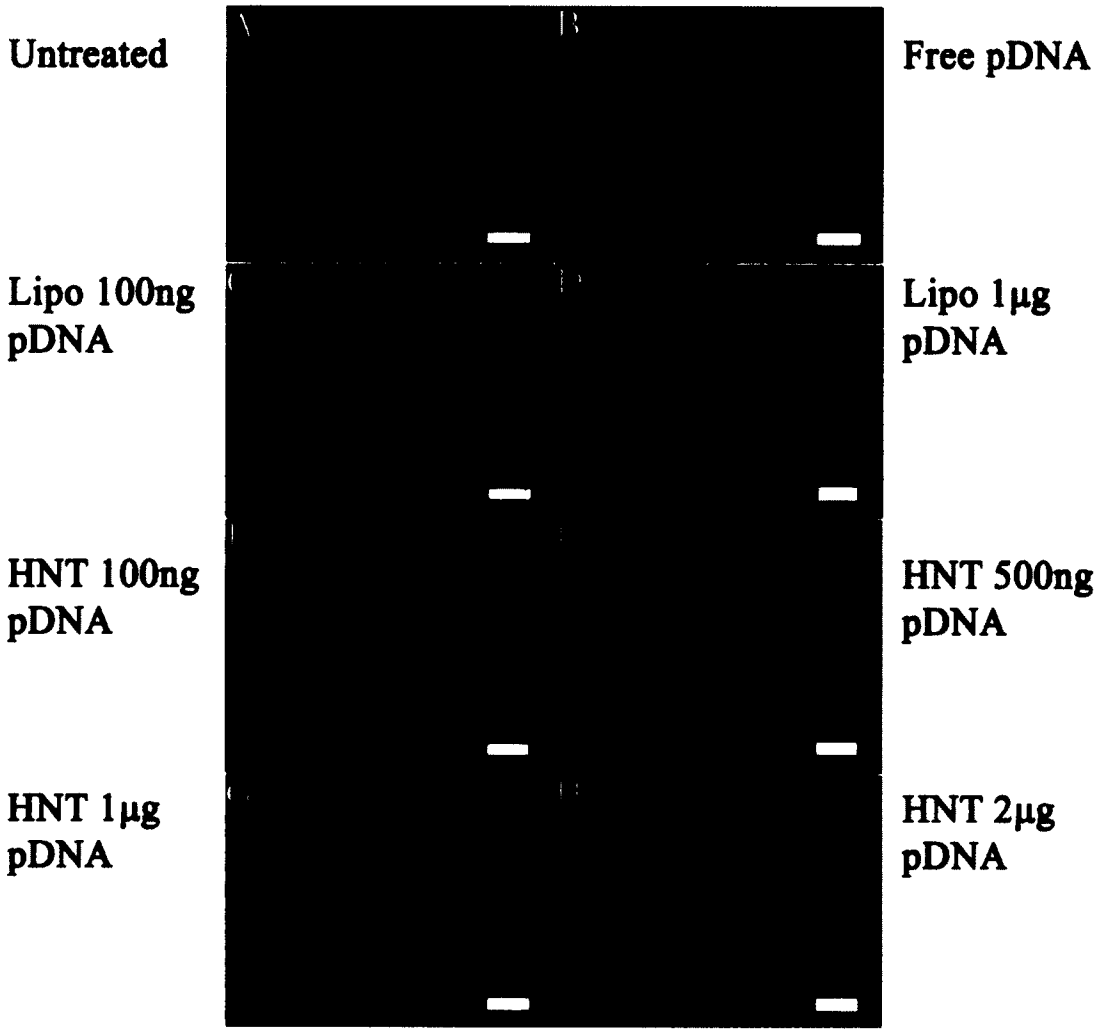


**Figure 4-7:** Fluorescence Images at 48 Hours for HNT-pIRES2-EGFP. Scale bar indicates 200μm. A and B are Negative controls C and D are positive. A) Control 1 untreated; B) Control 2 free DNA; C) Control 3 100 ng pIRES2-EGFP with Lipofectamine; D) Control 4 1μg pIRES2-EGFP with Lipofectamine; E) Experimental 1 100 ng pIRES2-EGFP with HNT; F) Experimental 2 500ng pIRES2-EGFP with HNT; G) Experimental 3 1μg pIRES2-EGFP with HNT; H) Experimental 4 2μ pIRES2-EGFP with HNT.

**Figure 4-8** shows the images for 48 hours A-D are the same controls shown in Figue 4-7 A-D. **Figure 4-8** E, F, G and H show Lipo-HNTs with 100 ng, 500 ng, 1 μg and 2 μg pIRES2-EGFP, respectively. The images agree with the graph and show that 100ng pIRES2-EGFP-Lipo-HNT and 2μg pIRES2-EGFP-Lipo-HNT have few fluorescent cells (less than 5 %) (Compare **Figure 4-6** with **Figure 4-8** E and H). 500ng pIRES2-EGFP-Lipo-HNT has a comparable amount of fluorescent cells (~70%) to lipofectamine control (~80%) and 1μg pIRES2-EGFP-Lipo-HNT has fewer fluorescents cells (~10 % respectively) when compared to the Lipofectamine controls.

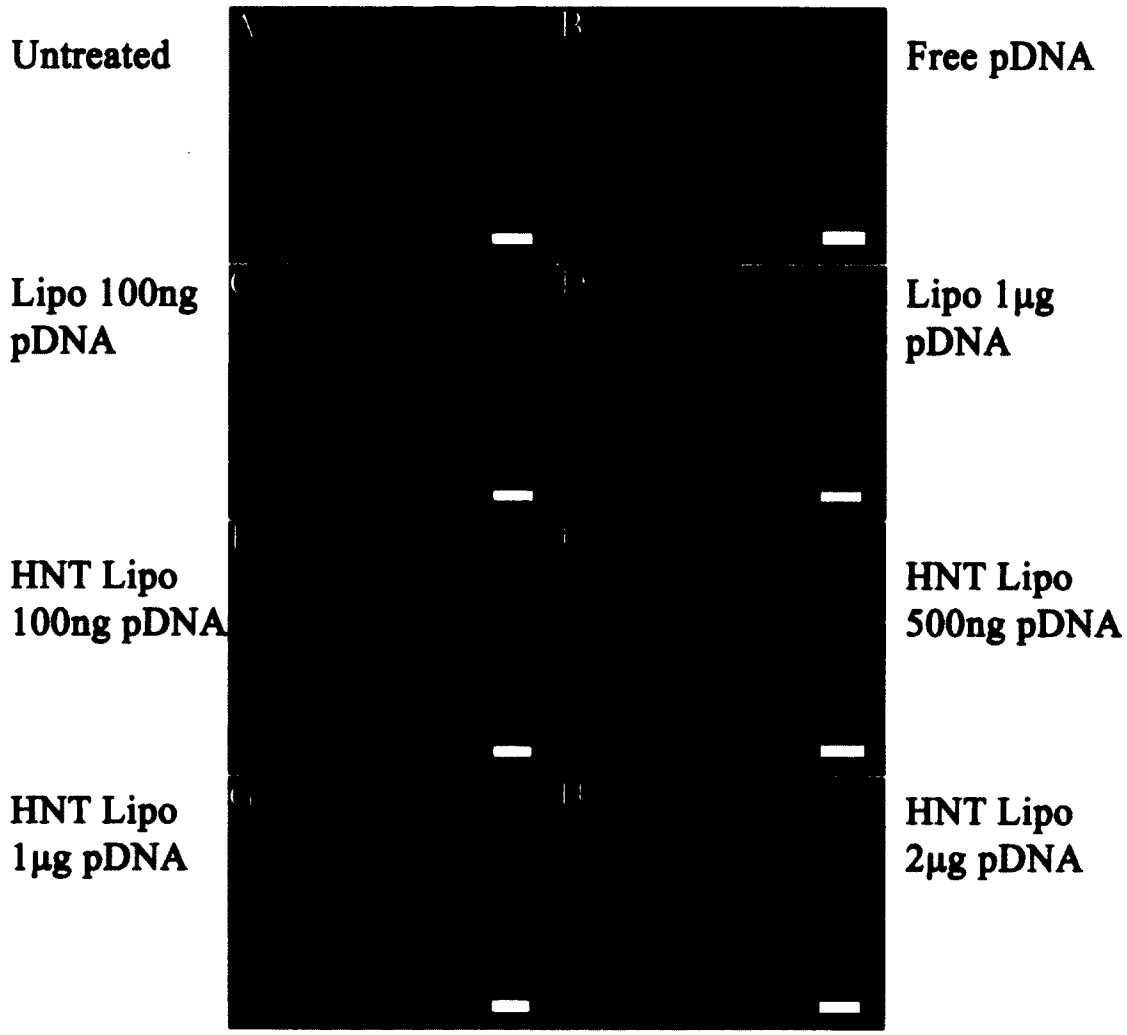


**Figure 4-8:** Fluorescence Images at 48 hours for HNT-Lipo-pIRES2-EGFP. Scale bar indicates 200μm. A and B are Negative controls (also shown in figure 4-7). C and D are positive controls (also shown in figure 4-7). A) Control 1 untreated; B) Control 2 free DNA; C) Control 3 100 ng pIRES2-EGFP with Lipofectamine; D) Control 4 1μg pIRES2-EGFP with Lipofectamine; E) Experimental 5 100 ng pIRES2-EGFP with HNT and Lipofectamine; F) Experimental 6 500ng pIRES2-EGFP with HNT and Lipofectamine; G) Experimental 7 1μg pIRES2-EGFP with HNT and Lipofectamine; H) Experimental 8 2μg pIRES2-EGFP with HNT and lipofectamine.

**Figure 4-9** shows the mean fluorescence area percentage at 96 hours ± standard deviation. As expected, control groups for untreated and free DNA show no fluorescence. Fluorescence percentage for Lipofectamine transfection with 100 ng and 1 μg of pIRES2-EGFP are 18.5%±14.6% and 53.2%±29.7%, respectively. All groups with HNT-pIRES2-EGFP show little to no fluorescence. HNT-pIrES2-EGFP-Lipofectamine groups for 100 ng and 2 μg pIRES2-EGFP- have minimal fluorescence compared to controls. The 1 μg and 500 ng HNT-pIRES2-EGFP-Lipofectamine groups were less effective than controls but showed a transfection efficiency of 12%±5.3% and 49.7%±14.1%, respectively.

At 96 hours Lipofectamine transfection with 100 ng or 1 μg of pIRES2-EGFP, and 500 ng or 1 μg HNT-pIRES2-EGFP-Lipofectamine groups showed a significant difference from the untreated control at $\alpha = .05$ (Appendix **Table A-5**). Lipofectamine transfection with 1 μg of pIRES2-EGFP, and 500 ng HNT-pIRES2-EGFP-Lipofectamine groups did not differ significantly difference from each other. Lipofectamine transfection with 0.1 μg of pIRES2-EGFP, and 1 μg HNT-pIRES2-EGFP-Lipofectamine groups did not differ significantly difference from each other. Lipofectamine transfection with 100 ng differed significantly from Lipofectamine transfection with 1 μg of pIRES2-EGFP. 1 μg differed significantly from 500 ng HNT-pIRES2-EGFP-Lipofectamine at $\alpha = .05$ (Appendix **Table A-5**).

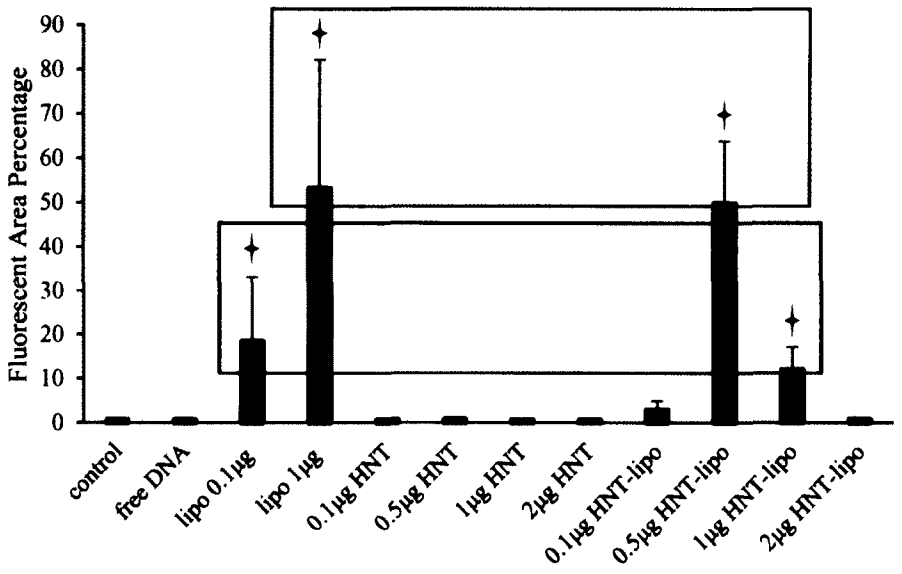


**Figure 4-9:** Mean Fluorescence Area Percentage of n = 8 images ± at standard deviation at 96 Hours. Statistical analysis was applied with IBM SPSS 22.0 at $\alpha = .05$, and the red stars indicate no significant difference exists between enclosed groups.

**Figure 4-10** shows the images for 96 hours. Figure 4-10 A and B are controls that are untreated and treated with Free DNA, respectively. C and D are positive controls for Lipofectamine with 100 ng and 1 μg of pIRES2-EGFP, respectively. **Figure 4-10** E, F, G and H show HNTs with 100 ng, 500 ng, 1 μg and 2 μg pIRES2-EGFP, respectively. HNTs with 100 ng, 500 ng, and1 μg have minimal fluorescence when compared to the Lipofectamine controls (~80% for 1 μg and 50% for 100 ng) while HNTs with 2 μg pIRES2-EGFP has no living fluorescent cells as cells that are fluorescent do not have the morphology of a healthy cells.

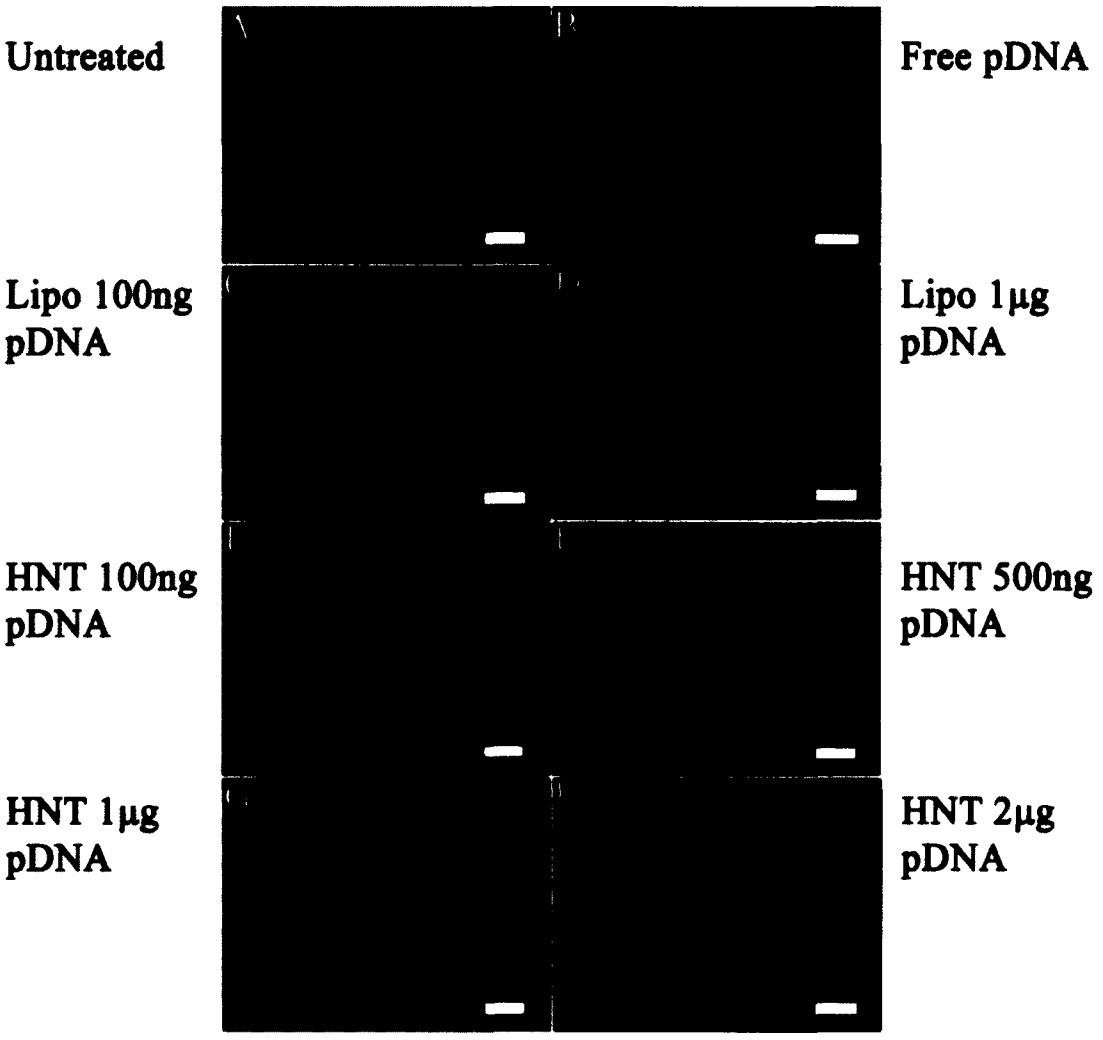


**Figure 4-10:** Fluorescence Images at 96 Hours for HNT-pIRES2-EGFP. Scale bar indicates 200μm. A and B are Negative controls. C and D are positive controls . A) control 1 untreated; B) control 2 free DNA; C) Control 3 100 ng pIRES2-EGFP with Lipofectamine; D) Control 4 1μg pIRES2-EGFP with Lipofectamine; E) Experimental 1 100 ng pIRES2-EGFP with HNT; F) Experimental 2 500ng pIRES2-EGFP with HNT; G) Experimental 3 1μg pIRES2-EGFP with HNT; H) Experimental 4 2μ pIRES2-EGFP with HNT.

**Figure 4-11** shows the images for 96 hours. A and B are controls that are untreated and treated, respectively, with free DNA; C and D are positive controls for Lipofectamine with 100 ng and 1 μg of pIRES2-EGFP, respectively. **Figure 4-11** E, F, G

and H show Lipofectamine-HNTs with 100 ng, 500 ng, and 1 μg and 2 μg of pIRES2-EGFP respectively. The images agree with the graph and show that Lipofectamine-HNTs with 100 ng and 2 μg pf pIRES2-EGFP have few fluorescent cells (less than 5 %) (Compare **Figure 4-9** with **Figure 4-11** E and H). Lipofectamine-HNTs with 500 ng of pIRES2-EGFP has a comparable amount of fluorescent cells (~70%) compared to the Lipofectamine controls (~80% for 1 μg and 50% for 100 ng) and Lipofectamine-HNTs with 1 μg of pIRES2-EGFP has fewer fluorescents cells (~10 % respectively) when compared to the Lipofectamine controls. Lipofectamine-HNTs with 1 μg of pIRES2-EGFP has fewer living cells, and the majority (90%) are fluorescent but are enlarged.

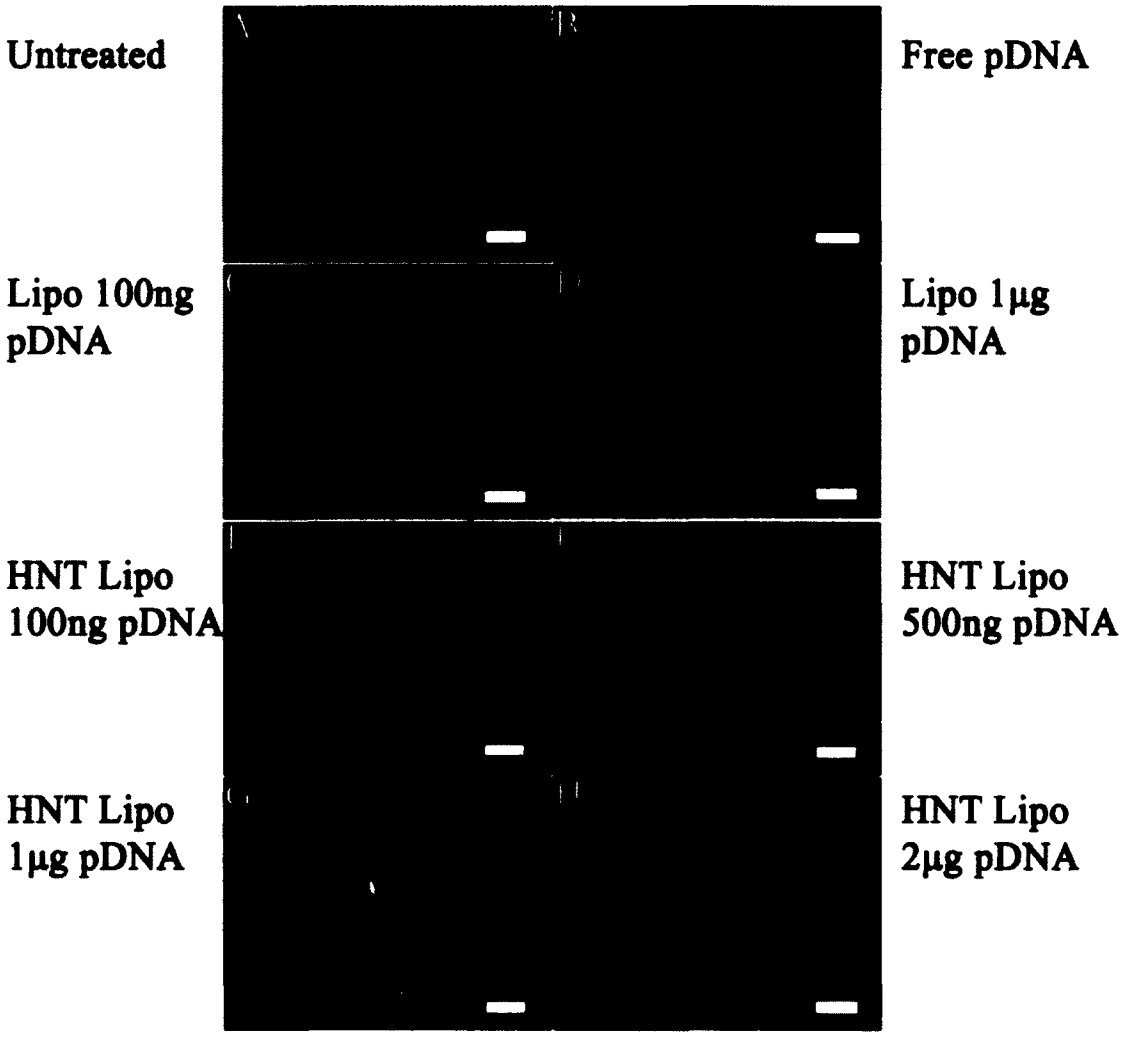


**Figure 4-11:** Fluorescence images 96 Hours for HNT-Lipo-pIRES2-EGFP. Scale bar indicates 200μm. A and B are Negative controls (also shown in figure 4-10). C and D are positive controls (also shown in figure 4-10). A) control 1 untreated; B) control 2 free DNA; C) Control 3 100 ng pIRES2-EGFP with Lipofectamine; D) Control 4 1μg pIRES2-EGFP with Lipofectamine; E) Experimental 5 100 ng pIRES2-EGFP with HNT and Lipofectamine; F) Experimental 6 500ng pIRES2-EGFP with HNT and Lipofectamine; G) Experimental 7 1μg pIRES2-EGFP with HNT and Lipofectamine; H) Experimental 8 2μg pIRES2-EGFP with HNT and Lipofectamine.

**Figure 4-12** shows the mean fluorescence area percentage at 144 hours ± standard deviation. As expected, control groups for untreated and free DNA show no fluorescence. Fluorescence percentages for Lipofectamine transfection with 100 ng and 1 μg of pIRES2-EGFP are 22% ± 13.3% and 38.8% ± 19.1% respectively. All groups with HNT-pIRES2-EGFP show little to no fluorescence. HNT-pIRES2-EGFP-Lipofectamine group for 2 μg pIRES2-EGFP have minimal fluorescence by comparison to controls. 1 μg, 500 ng and 100 ng HNT-pIRES2-EGFP-Lipofectamine groups were less effective when compared to controls but showed a transfection efficiency of 4.1%± 2.6%, 28.2 %±11.9 % and 2.5%±1.6%, respectively.

At 144 hours Lipofectamine transfection with 100 ng or 1 μg of pIRES2-EGFP, and 500 ng HNT-pIRES2-EGFP-Lipofectamine groups showed a significant difference from the untreated control at $\alpha = .05$ (Appendix **Table A-5**). Lipofectamine transfection with 1 μg of pIRES2-EGFP, and 500 ng HNT-pIRES2-EGFP-Lipofectamine groups did not differ significantly difference from each other. Lipofectamine transfection with 0.1 μg of pIRES2-EGFP, and 500 ng HNT-pIRES2-EGFP-Lipofectamine groups did not differ significantly difference from each other. Lipofectamine transfection with 0.1 μg of pIRES2-EGFP, and 1 μg HNT-pIRES2-EGFP-Lipofectamine groups differed significantly from each other. Lipofectamine transfection with 100 ng differed significantly from Lipofectamine transfection with 1 μg of pIRES2-EGFP. 1 μg differed significantly from 500 ng HNT-pIRES2-EGFP-Lipofectamine at $\alpha = .05$ (Appendix **Table A-5**).

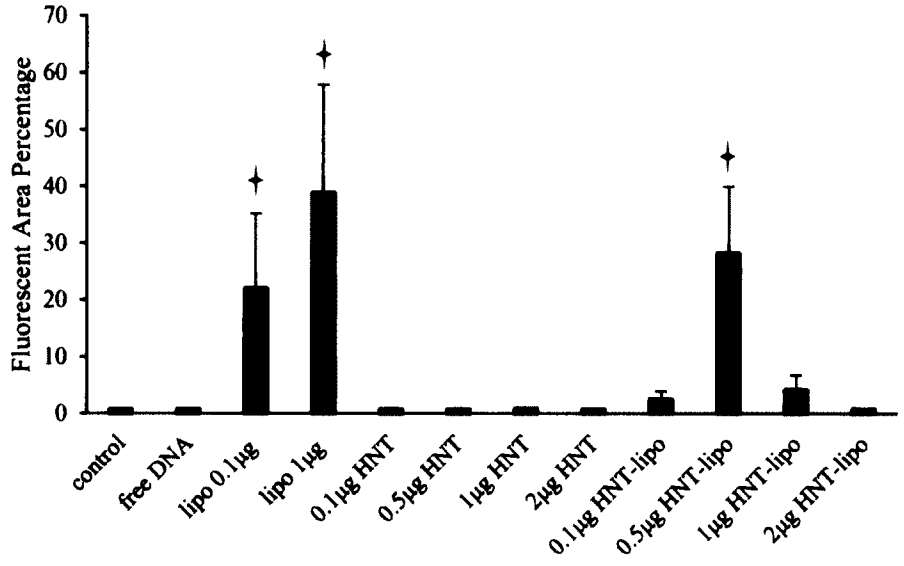


**Figure 4-12:** Mean Fluorescence Area Percentage of n = 8 images ± standard deviation at at 144 Hours. Statistical analysis was applied with IBM SPSS 22.0 at $\alpha$ = .05, and the red stars indicate no significant difference exists between lipo 0.1μg and lipo 1μg with 0.5μg HNT-lipo group.

**Figure 4-13** shows the images for 144 hours. A and B are controls that are untreated and treated with free DNA respectively; C and D are positive controls for Lipofectamine with 100 ng and 1μg of pIRES2-EGFP respectively. **Figure 4-13** E, F, G and H show HNTs with 100 ng, 500 ng, 1 μg and 2 μg pf pIRES2-EGFP respectively. HNTs with 100 ng, 500 ng, 1 μg and 2 μg pf pIRES2-EGFP have minimal fluorescent when compared to the Lipofectamine controls (~70% for 1 μg 40% for 100 ng).

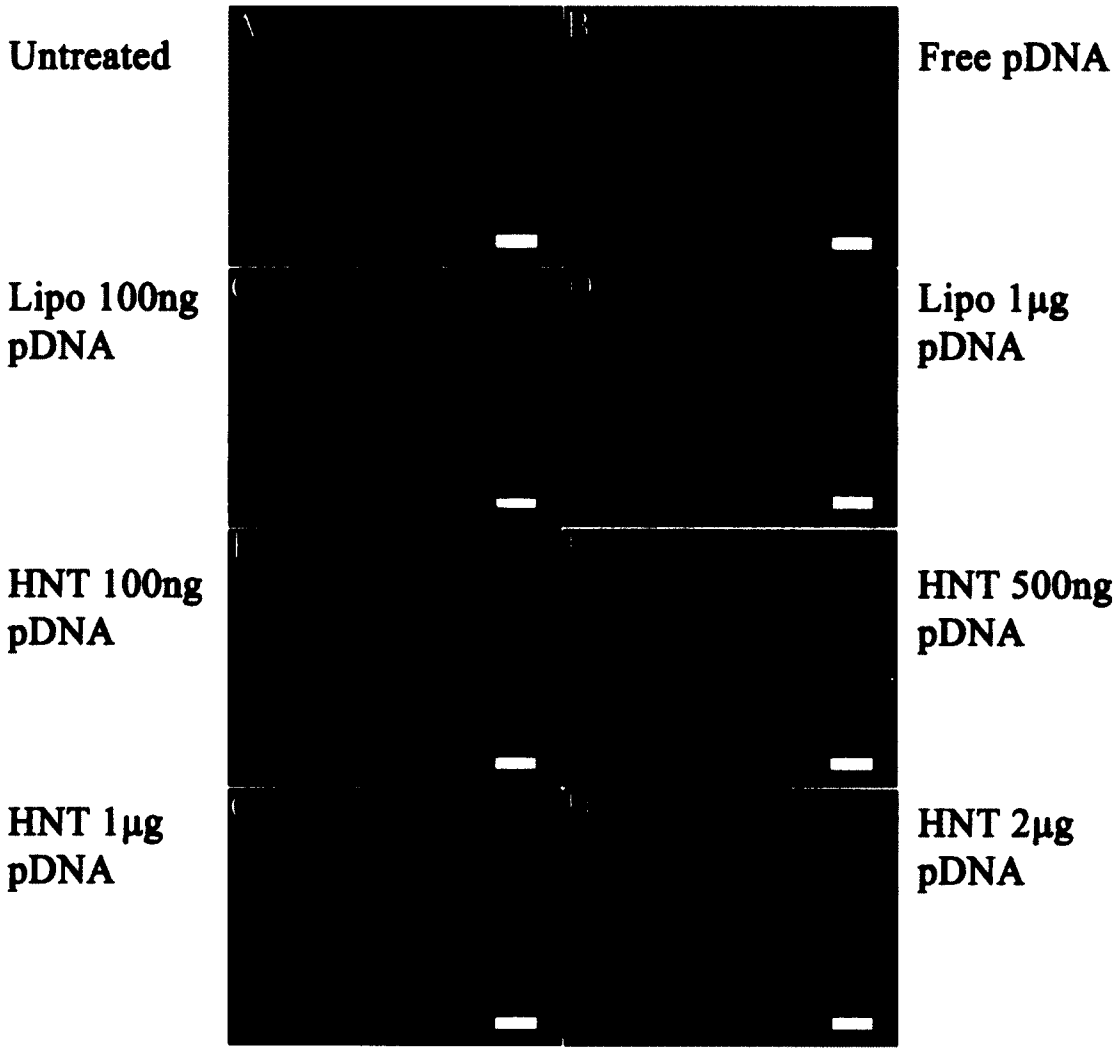


**Figure 4-13:** Fluorescence Images at 144 Hours for HNT-pIRES2-EGFP. Scale bar indicates 200μm. A and B are Negative controls. C and D are positive controls .A) control 1 untreated; B) control 2 free DNA; C) Control 3 100 ng pIRES2-EGFP with Lipofectamine; D) Control 4 1μg pIRES2-EGFP with Lipofectamine; E) Experimental 1 100 ng pIRES2-EGFP with HNT; F) Experimental 2 500ng pIRES2-EGFP with HNT; G) Experimental 3 1μg pIRES2-EGFP with HNT; H) Experimental 4 2μ pIRES2-EGFP with HNT.

**Figure 4-14** shows the images for 144 hours. A and B are controls that are untreated and treated with Free DNA respectively; C and D are positive controls for Lipofectamine with 100 ng and 1 μg of pIRES2-EGFP respectively. **Figure 4-14** E, F, G and H show Lipofectamine-HNTs with 100 ng, 500 ng, 1 μg and 2 μg pf pIRES2-EGFP respectively. The images agree with the graph and show that Lipofectamine-HNTs with 100 ng has around 10% fluorescent cells and Lipofectamine-HNTs with 2 μg has no fluorescent cells (Compare **Figure 4-12** with **Figure 4-14** E and H. Lipofectamine-HNTs with 500 ng has a comparable amount of fluorescent cells (~70%) to the Lipofectamine controls (~70% for 1 μg and 40% for 100ng) and Lipofectamine-HNTs with 1 μg has fewer fluorescents cells (~10 % respectively) when compared to the Lipofectamine controls. There are fewer living cells in G and the majority (80%) are fluorescent but are enlarged.

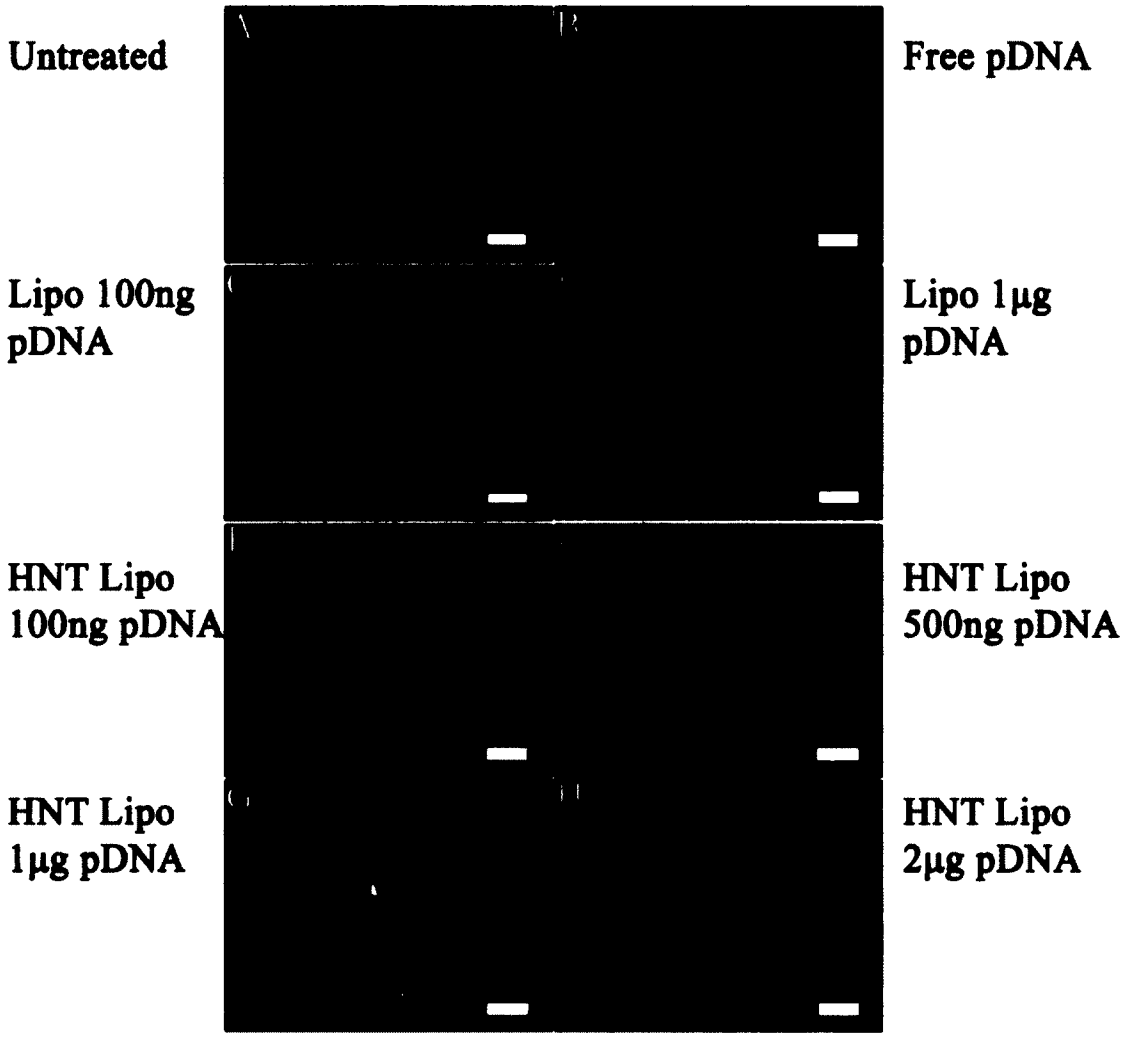


**Figure 4-14:** Fluorescence Images at 144 Hours for HNT-Lipo-pIRES2-EGFP. Scale bar indicates 200μm. A and B are Negative controls (also shown in figure 4-13). C and D are positive controls (also shown in figure 4-13) A) control 1 untreated; B) control 2 free DNA; C) Control 3 100 ng pIRES2-EGFP with Lipofectamine; D) Control 4 1μg pIRES2-EGFP with Lipofectamine; E) Experimental 5 100 ng pIRES2-EGFP with HNT and Lipofectamine; F) Experimental 6 500 ng pIRES2-EGFP with HNT and Lipofectamine; G) Experimental 7 1 μg pIRES2-EGFP with HNT and Lipofectamine; H) Experimental 8 2μg pIRES2-EGFP with HNT and lipofectamine.

### 4.3.3 Fluorescence Comparison

**Figure 4-15** shows the progression of fluorescence in all groups that exhibited EGFP expression over the 144 hour study. HNT-pIRES2-EGFP groups are not shown here because imaging and fluorescence percentage data show that HNTs alone did not effectively transfect cells. The average fluorescence in HNT-pIRES2-EGFP groups was less than 1.5 % for 24, 48, 96 and 144 hours. Image results showed that HNT-pIRES2-EGFP groups were more effective than free DNA but did not result in many cells being transfected. This low amount of transfection may be due to accumulation of plasmids on the surface of the HNTs. The majority of the plasmids were released into the media as opposed to being taken up by the cells with the HNTs. Also, in the 2 μg and 1 μg HNT-pIRES2-EGFP group, it seems that the concentration of Lipofectamine and HNTs too high, resulting in a massive cell death at time points after 24 hours. Results indicated that at up to 500 ng of pIRES2-EGFP, HNTs may be effective at raising the efficiency of Lipofectamine.

At 24 hours the 500 ng HNT-pIRES2-EGFP groups were seemingly less effective than both 1 μg and 100 ng pIRES2-EGFP Lipofectamine control groups but, at 48 hours the transfection efficiency was comparable to both Lipofectamine control groups. For 96 and 144 hours, the 500 ng HNT-pIRES2-EGFP groups yielded nearly twice the fluorescence as 100 ng group, but this higher fluorescence may be caused by the five-fold increase in the amount of pIRES2-EGFP. For 48, 96, and 144 hours 500 ng HNT-pIRES2-EGFP groups were 86% $\pm$11% fluorescent as the 1 μg pIRES2-EGFP Lipofectamine controls, which contained twice the amount of plasmid DNA.

Other groups that showed at least some effectiveness (up to 12% transection percentage) were 100 ng and 1 μg HNT-pIRES2-EGFP groups. In the 1 μg HNT-pIRES2-EGFP groups, the combination of Lipofectamine and HNTs yielded cytotoxic effects causing the majority of the cells to die. However, at 96 hours and 144 hours the majority of the cells that remained (>90%) were fluorescent.

Results of the transfection assay demonstrated, at the 500 ng pIRES2-EGFP concentration, that HNTs boosted the efficiency of transfection of Lipofectamine and were nearly as effective as Lipofectamine alone at twice the concentration of pIRES2-EGFP. Furthermore, HNTs-plasmid composite show promise as a delivery system for DNA when coated with lipids.

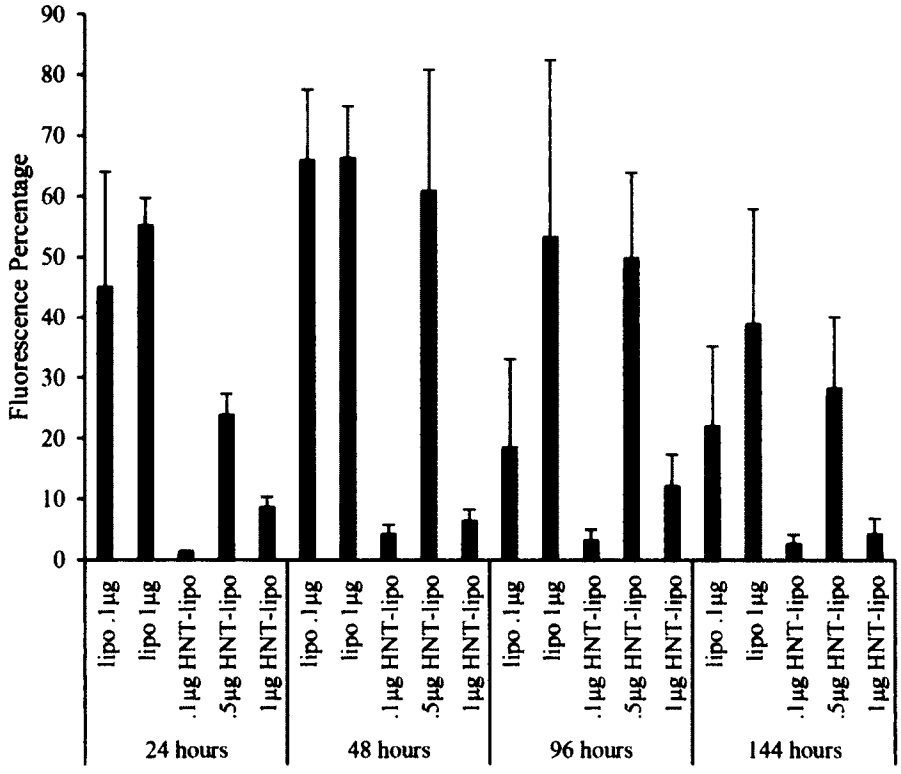


**Figure 4-15:** Mean Green Fluorescence (pIRES2-EGFP) Area Percentage comparison of n = 8 images ± standard deviation. Lipo 0.1μg, Lipo 1μg, 0.5 μg HNT-lipo and 1 μg HNT-lipo were significantly different from untreated cells at all time points.

### 4.3.4 Zeta Potential and Particle Size

The average particle size of plain HNTs and pIRES2-EGFP-loaded HNTs was measured to compare and determine if loading had an effect on particle size (**Figure 4-16**). For pIRES2-EGFP-loaded HNTs particle size was measured to determine if surface adsorption or wrapping increase particle size. Plain HNTs had an average particle size of 1522 nm ± 97.3 nm. When comparing plasmid loaded HNTs to plain HNTs there is a significant difference in size at $\alpha = 0.05$ (Appendix A **Table A-2**). On average pIRES2-EGFP-loaded HNTs were 4320 nm±609 nm in diameter. PIRES2-EGFP-loaded HNTs were almost 3 times the size of plain HNTs and this may be attributed to the plasmid DNA adhering to the surface or wrapping around HNTs. The large error may be due to the formation of aggregates during the drying process. The graph of the average particle size for plain HNTs and pIRES2-EGFP-loaded HNTs is given in **Figure 4-16**.

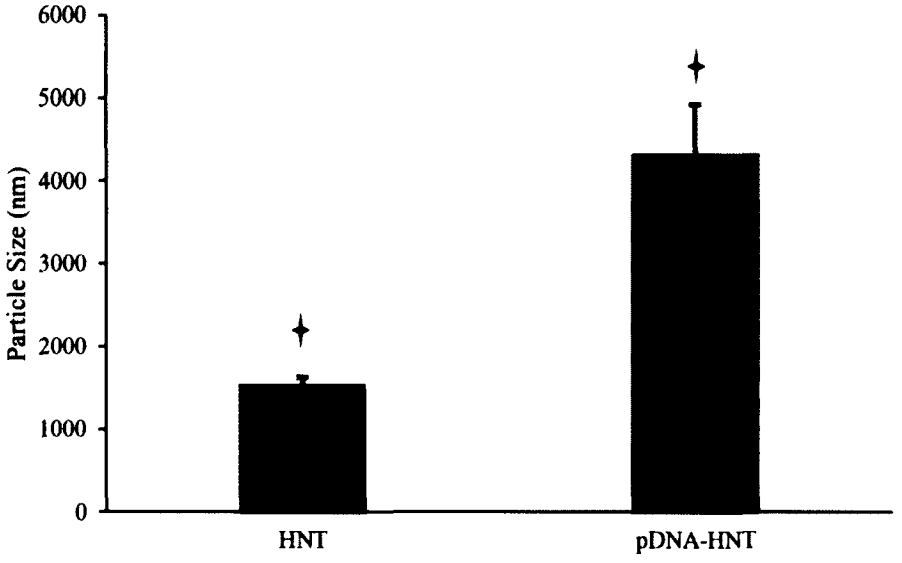


**Figure 4-16:** Mean Particle Size of n = 4 samples ± standard deviation. Black stars indicate significant difference exists between groups at $\alpha = 0.05$.

The zeta potential of plain HNTs and pIRES2-EGFP-loaded HNTs was measured to compare and determine if loading had an effect on zeta potential. For pIRES2-EGFP-loaded HNTs, zeta potential was measured to determine if surface adsorption or wrapping changed the surface zeta potential of HNTs. Results indicated that surface adsorption and /or loading of plasmid DNA caused the zeta potential to decrease slightly. The zeta potential of plain HNTs was -41.6±3mV and pIRES2-EGFP-HNT was -51.4±2.1 mV. The graph of the zeta potential for plain HNTs and pIRES2-EGFP loaded HNTs is given in **Figure 4-17**.

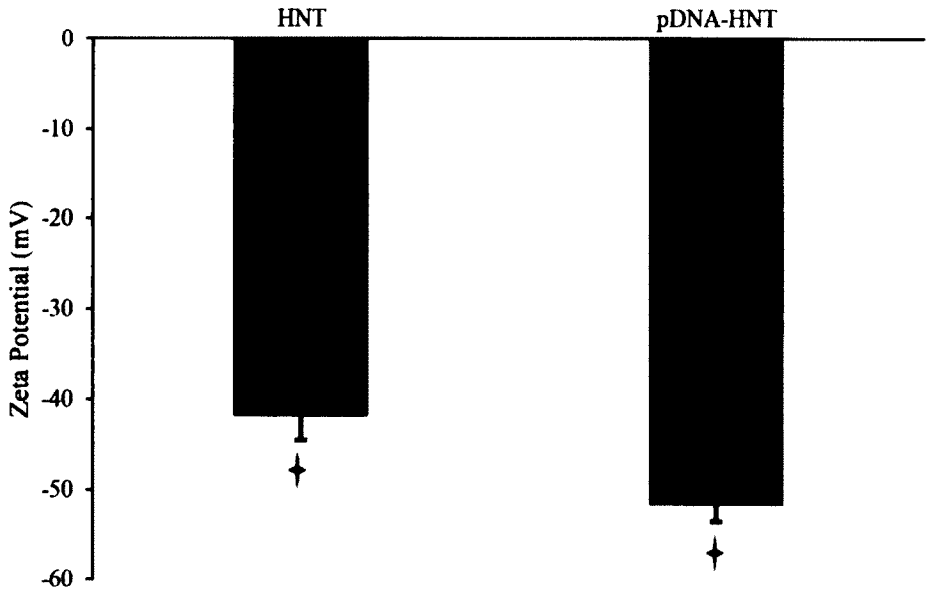


**Figure 4-17:** Mean Zeta Potential of HNTs and pDNA-loaded HNTs of n = 4 samples ± standard deviations. Black stars indicate significant difference exists between groups at $\alpha = 0.05$.

# CHAPTER 5

# USE OF HNTS FOR DRUG DELIVERY IN CANCER THERAPY

## 5.1 Introduction

Osteosarcoma patients who have received chemotherapy alone have a 100% recurrence rate without surgical resection [100], [101]. Even though recent advances have increased the rates of limb sparing therapy, patients are still at risk of recurrence. Tumor recurrence can be greater than 90% in patients who have not been clinically diagnosed with metastasis and have received surgical resection of the primary malignancy with no adjuvant chemotherapy [7][101] [104]. While surgical abscission can physically remove clinically detectable tumor masses, systemic chemotherapy or gene therapy can inhibit micrometastasis before and/or after surgery. For the treatment of osteosarcoma, many of the research efforts are directed at reducing the risk of recurrence following surgical resection. One of the major challenges faced by chemotherapy and gene therapy is the inability to sustain and/or localize drug release.

To address this challenge, HNTs loaded with chemotherapeutic agent methotrexate or a plasmid pIRES2-EGFP expressing the green fluorescence protein is the method being proposed. HNTs have a cylindrical structure with concentric aluminosilicate layers and negatively charged surface and positively charged lumen [102]. HNTs unique structure makes them ideal for loading a variety of charge molecules

[103]. Past research has shown HNTs can be used to deliver chemotherapeutic agents and bioactive molecules like anti-infective agents and proteins in a sustained manner [103][93].

The hypothesis of this project was that HNTs would provide a sustained release of methotrexate to inhibit the growth of osteosarcoma.

## 5.2 Methods and Materials

All the plastic wares, such as, syringes, centrifuge tubes, microcentrifuge tubes, 12 well plates, and pipettes, were purchased from Mid Scientific, St. Louis, MO. Cell culture media, buffers, serum and LIVE/DEAD® Viability/Cytotoxicity Kit were purchased from Life Technologies, Grand Island, NY. Methotrexate, HNTs and XTT *in vitro* toxicology assay kit were obtained from Sigma-Aldrich, St. Louis, MO. Murine osteosarcoma cells CRL-2836 were obtained from ATCC, Manassas, VA.

### 5.2.1 Release Study

A release study was carried out to understand the elution of methotrexate from HNTs. These studies provided an analysis of the release of chemotherapeutic agents from HNTs.

#### 5.2.1.1 *MTX*

The release profile study for methotrexate (MTX) was done to understand the release of chemotherapeutic agents from HNTs. A calibration curve was created for MTX to compare with the drug elution profiles of the MTX loaded HNT. Three sample sets, 1 mg HNT 10% MTX, 5 mg HNT 10 %MTX and 10 mg HNT 10% MTX, were immersed in HBSS, mixed and collected for varying time period for 24 hours and seven days. For collection, samples were centrifuged and the supernatants were collected for UV-vis.

analysis (Nanodrop 2000c, ABS wavelength 300 nm.). Samples were replenished with fresh HBSS. The details of sample collection and the overall procedure are provided in Section 3.2.6.

### 5.2.2 Cell Culture and Seeding

An osteosarcoma cell line was the model used to study *in vitro* cellular response to methotrexate-loaded HNTs. Osteosarcoma cells were plated in 25 $cm^2$ tissue culture flasks, and incubated at 37 °C under humidified 5% $CO_2$ and 95% air in complete DMEM containing 10% FBS and 1% PSA. Subconfluent cells were passaged with 0.25% trypsin, collected by centrifugation, suspended in complete DMEM and cultured at a 3:1 split into 25 $cm^2$ tissue culture flasks. These cultures were used for the viability and proliferation tests.

#### 5.2.2.1 *Cell Proliferation and Viability Studies*

In these experiments, osteosarcoma cells were used. Osteosarcoma cells were seeded in 12-well plates and allowed to adhere for four hours. After osteosarcoma cells became adherent, free HNTs were added according to **Table 5-1** while negative controls were left untreated and free methotrexate and MTX-HNTs were added to a 12 plate according to **Table 5-2**. Two of each plate were prepared for each time period, 1 for XTT cell proliferation assay and 1 for live/dead cell viability assay.

**Table 5-1:** Plate Map for controls and unloaded HNTs.

| | | | |
|---|---|---|---|
| **untreated** | **1 mg HNT** | **5 mg HNT** | **10 mg HNT** |
| **untreated** | **1 mg HNT** | **5 mg HNT** | **10 mg HNT** |
| **untreated** | **1 mg HNT** | **5 mg HNT** | **10 mg HNT** |

**Table 5-2:** Plate Map for Free MTX and MTX-HNTs.

| | | | |
|---|---|---|---|
| **100 µg MTX** | **1 mg MTX-HNT** | **5 mg MTX-HNT** | **10 mg MTX-HNT** |
| **100 µg MTX** | **1 mg MTX-HNT** | **5 mg MTX-HNT** | **10 mg MTX-HNT** |
| **100 µg MTX** | **1 mg MTX-HNT** | **5 mg MTX-HNT** | **10 mg MTX-HNT** |

5.2.2.1.1 XTT Cell Proliferation

This assay is based on the ability of viable cells to reduce XTT dye. These wells were analyzed after 24, 72, 120 and 168 hours to evaluate if MTX-HNTs reduced the cell proliferation. Cells seeded in 12-well plates were treated as mentioned above (see Section 5.2.2.1). XTT assay was added as detailed in Section 3.2.7.2 and analyzed with the absorbance microplate reader at 450 nm and 690 nm wavelengths.

5.2.2.1.2 Live/Dead Cell Viability Assay

This assay was used to determine if HNT-MTX complexes resulted in cell death. Cells seeded in 12-well plates were treated as mentioned above (see Section 5.2.2.1). Live/dead assay was added as detailed in Section 3.2.7.3 and cells were imaged after 24, 72, 120 and 168 hours. Imaging was carried out using the Olympus BX51 fluorescent microscope with FITC and TRITC filters and images were processed and quantified using Image J software.

5.2.3 FE-SEM, TEM and Zeta Potential / Particle Size Analysis

For characterization of the HNTs, average size and charge measurements, and FE-SEM images were taken.

5.2.3.1 *Zeta Potential and Particle Size*

Halloysite surface potential was analyzed by using microelectrophoresis (ZetaPlus Potential Analyzer, Brookhaven Instruments). Diluted aqueous dispersion of halloysite

was prepared and analyzed as mentioned in Section 3.2.4. The instrument also allowed for average particle size measurement based on dynamic light scattering

5.2.3.2 *FE-SEM /TEM*

To visualize the morphology and surface properties of HNTs, FE-SEM and TEM images were obtained from HNT samples. The sample preparation and imaging protocols are detailed in Sections 3.2.5.1 and 3.2.5.2

## 5.3 Results and Discussion

### 5.3.1 Release Profile Study of MTX from HNTs

The release profile study of MTX from HNTs was done to estimate the amount of drug eluted from the HNTs over a period of 24 hours for seven days. This study was carried out to determine if HNTs could be loaded with MTX and elute enough to inhibit proliferation *in vitro*. The graph showing the release profile study for MTX-HNTs for 24 hours is given in **Figure 5-1**.

**Figure 5-1** shows the MTX release over 24-hours for 1 mg HNT/10%MTX, 5 mg HNT/10%MTX and 10 mg HNT/10%MTX. This release was achieved for the vacuum-loaded HNTs in nuclease free water at room temperature. The amount of MTX release calculated using an equation (**Eq. 5-1**) derived from the standard curve for MTX concentrations absorbance values obtained at 300 nm wavelength via a NANODROP 2000 Spectrophotometer.

$$y = 0.047x + 0.015\,, \qquad \textbf{Eq. 5-1}$$

where $y$ is the absorbance value and $x$ is the MTX concentration in μg.

The experiment was repeated three times to reduce error and to check for reproducibility of results. The values are the means of the readings of MTX release from HNTs at the respective time points from the 3 repetitions of the experiment. The error bars reflect the standard deviation.

**Figure 5-1** shows the cumulative sustained release of the MTX for 24 hours in the microgram to nanogram range which is comparable to the amount used for *in vitro* assays.

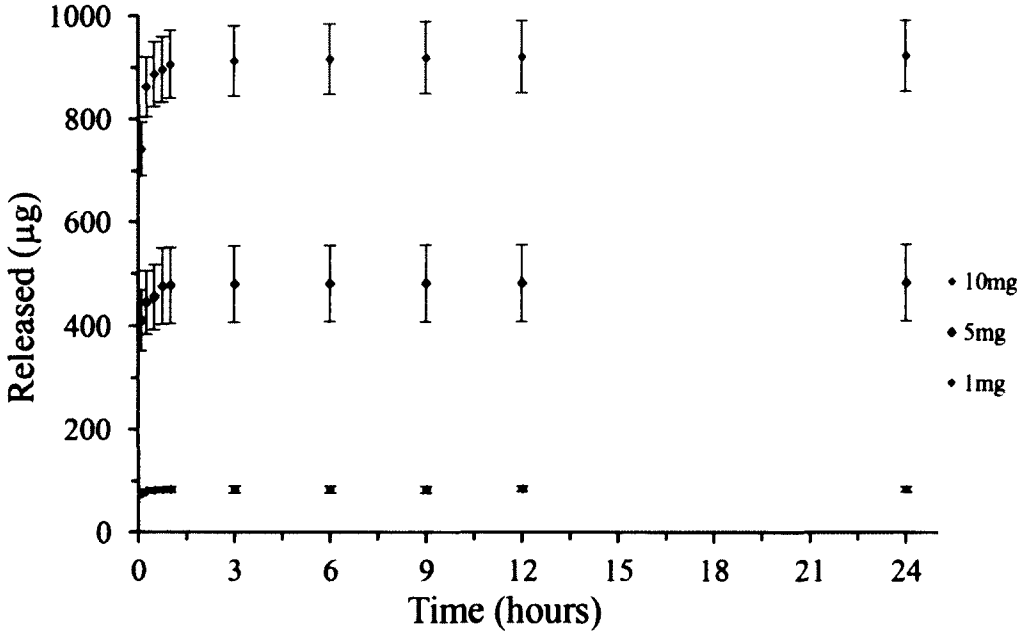


**Figure 5-1:** Mean Cumulative Release profile of MTX from HNTs for 24 hours mean of n = 9 for each concentration +/- standard deviation.

The graph of the release profile study for MTX from HNTs for 7 days is given in **Figure 5-2**. The release profile study of MTX from HNTs was extended to seven days. The experiment was repeated three times to reduce error and to check for reproducibility of the results. The values are the means of the readings of MTX from HNTs at the

respective time points recorded from the repetitions of the experiments. The error bars reflect the standard deviation.

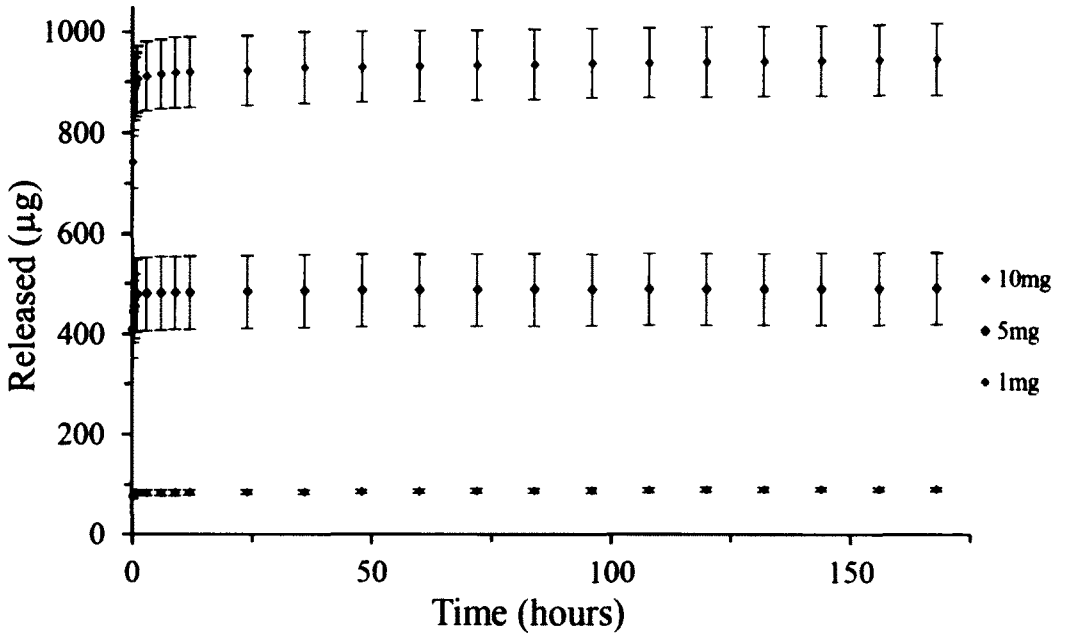


**Figure 5-2:** Release profile of MTX from HNTs for 7 days mean of n = 9 for each concentration +/- standard deviation.

The release of MTX from HNTs was extended and sustained for seven days. In the first 24 hours, from the three different samples, an average of 91.3%±6.2% of loaded MTX was released and after seven days an average 94.7% ±3.6% of loaded MTX was released. The release for 24 hours and over seven days was in the microgram and nanogram range for all samples and well within the range of MTX concentrations required for common *in vitro* assays.

The release profile of MTX from HNTs suggests that the majority of drug localized on the surface of HNTs. The initial burst release was mainly due to the suface localization of the MTX. Even with ~80% of the drug being localized on the surface of

the HNTs the release is in nano and micrograms, which is well within the range of MTX concentrations required for a cellular response in *in vitro* assays. Results obtained from the seven-day release profile are promising, as HNTs release MTX continuously, even with the majority released in the first 24 hours, as opposed to free drug which may be metabolized by the cells within the first 2-3 days. A sustained release of MTX is beneficial because loaded HNTs can be injected once and sustain a release in the cancerous tissues for more than seven days, reducing the need for more injections.

The release studies of MTX was not extended beyond seven days as *in vitro* experiments would only focus on the first seven days and primarily on the first 3- 5 days. The comparison of the three loaded volumes, 1, 5, and 10 mg HNTS with 10% MTX, demonstrated HNTs could sustain a release of low and high concentration for more than seven days, and the release profile did not differ significantly when using different amounts of HNT. Surface potential and surface adsorption were further analyzed using zeta potential and particle size measurements in Section 5.2.3.1.

### 5.3.2 Cell Culture and Seeding

#### 5.3.2.1 *Cell Proliferation*

A cell proliferation assay was performed to ascertain whether HNT loaded with MTX were capable of inhibiting the proliferation of osteosarcoma cells. The negative control for this experiment was untreated cells. The cell proliferation of osteosarcoma cells incubated with MTX loaded HNTs was compared to with proliferation of osteosarcoma cells treated with drug free HNTs and free MTX. Following seeding and incubation, the plates were analyzed after 24, 72, 120 and 168 hours via XTT cell proliferation assay. The media was changed in all plates at 72 and 120 hours, as cells in

the control well were becoming confluent and the cells had used the majority of nutrients in the media.

After absorbance was measured, the data were exported to Excel files. The data were subsequently processed and normalized based on the absorbance at each time point of the untreated. IBM SPSS software and a two-tailed paired t-test were used for statistical analysis (Appendix A **Table A-4**). **Figure 5-3** to **Figure 5-6** show graphs of the cell proliferation from 24-168 hours.

**Figure 5-3** shows the proliferation after 24 hours. After 24 hours, the drug had yet to affect cellular proliferation in the groups treated with free drug, 1 mg HNT, 5 mg HNT-MTX and 10 mg HNT. The 1 mg HNT group showed a higher level of proliferation than any other group, and this level may indicate that osteosarcoma cells proliferate more in the presence of low concentrations of HNT. As the concentration of drugs was higher in 5 mg HNT-MTX (500 μg) and 10 mg HNT-MTX (1 mg) proliferation had begun to be inhibited. Also, cells exposed to 10 mg of HNT were not growing as well as other plain HNT groups, which may suggest that HNTs at this concentration have a negative effect on growth.

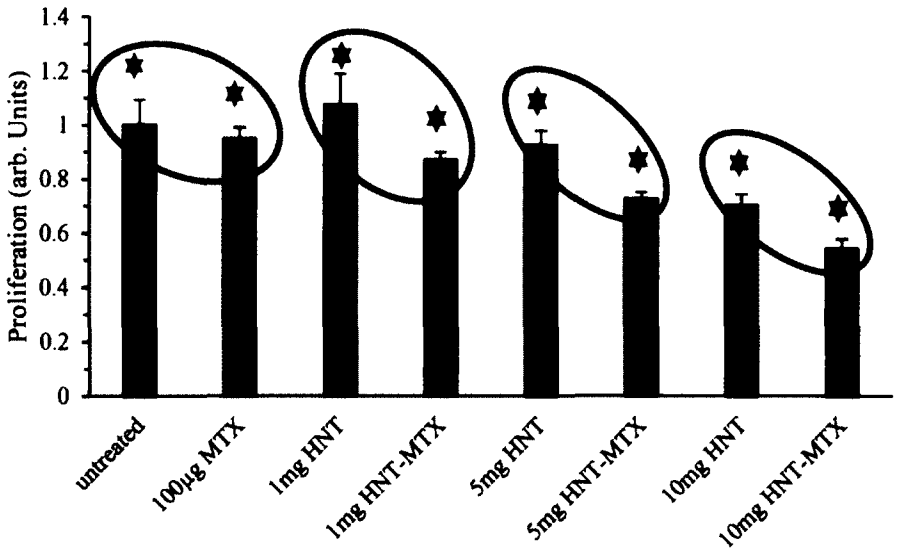


**Figure 5-3:** Mean Cell Proliferation at 24 hours of n = 9 ± standard deviation. Statistical analysis was applied with IBM SPSS 22.0 at α = .05, and the red stars indicate no significant difference exists two groups encircled are compared and the black stars indicate significant difference exists when encircled groups are compared.

**Figure 5-4** shows the proliferation after 72 hours. After 72 hours the drug began to affect cellular proliferation in all MTX-treated groups. The 1 mg HNT group showed a higher level of proliferation than any other group except the untreated control. The 1 mg HNT-MTX group showed the most proliferation reduction when compared to 1 mg of plain HNT, reducing proliferation by nearly half. The 1 mg HNT-MTX was as effective as the 100 µg of MTX at inhibiting proliferation.

The 5 mg HNT-MTX reduced proliferation by nearly 60%; however 5 mg plain HNT was shown to reduce proliferation by ~50%, therefore it became difficult to determine if the effect was brought on by MTX or the HNTs. The 10 mg HNT-MTX and 10mg plain HNT sets behaved similarly. The 10 mg HNT-MTX group showed the highest reduction in proliferation. Results indicate that the presence of MTX in this group had little effect by comparison of the 10 mg groups. After 72 hours we continue to see

that 5 and 10 mg of HNTs negatively affect the proliferation of osteosarcoma. At 72 hours, the media was changed as it had begun to change colors indicating cells had absorbed the majority of the nutrients. Also, in the 100 μg MTX set the media was replaced with media containing 100 μg MTX to maintain the proliferative ability.

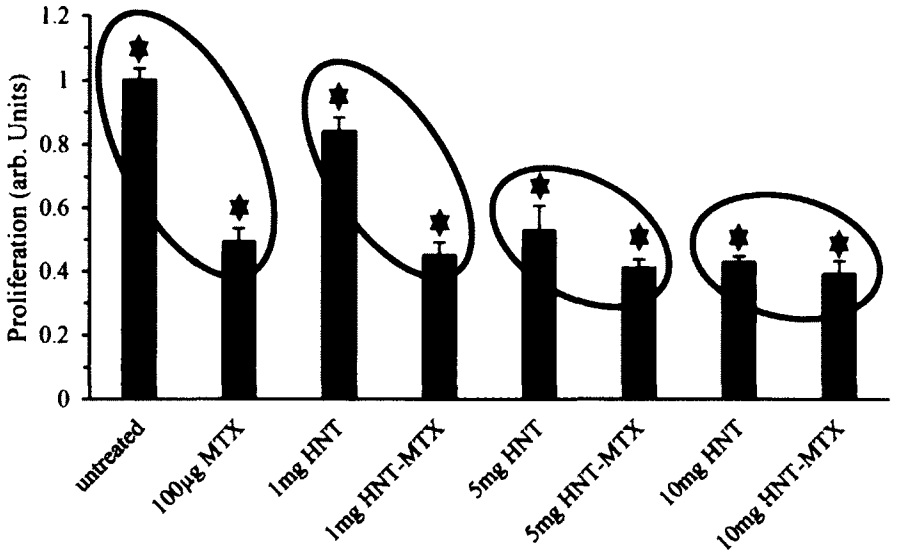


**Figure 5-4:** Mean Cell Proliferation at 72 hours of n = 9 ± standard deviation. Statistical analysis was applied with IBM SPSS 22.0 at α = .05, and the black stars indicate significant difference exists when encircled groups are compared.

**Figure 5-5** shows the proliferation after 120 hours. After 120 hours, the drug continued to affect cellular proliferation in the groups in all treated groups. Also, the media change at 72 hours caused proliferation to increase slightly in all groups, except 10 mg HNT and 10 mg HNT-MTX. The 1 mg HNT group showed the highest level of proliferation. The case with 1 mg HNT-MTX showed greater proliferation reduction than the case of 1 mg of plain HNT, reducing proliferation by nearly half. The 1 mg HNT-MTX inhibited proliferation more effectively than the 100μg of MTX, and at this point, the majority of the drug had been released from MTX-loaded HNTs.

The 5 mg HNT-MTX reduced proliferation by nearly 60% and 5 mg plain HNT reduced prolife by ~30%, and we began to see a significant difference between these two groups. The 10 mg HNT-MTX and 10 mg plain HNT sets behaved similarly, and even though the 10 mg HNT-MTX showed the highest reduction in proliferation, the presence of MTX in this group had little effect in comparison to the 10 mg groups, only making a difference of ~10% in cell proliferation. After 120 hours, 10 mg of HNTS continued to negatively affect the proliferation of osteosarcoma. At 120 hours, the media was changed as it had begun to change colors indicating cells had absorbed the majority of the nutrients. Also, in the 100 μg MTX set, the media was replaced with media containing 100 μg MTX to maintain the proliferative ability.

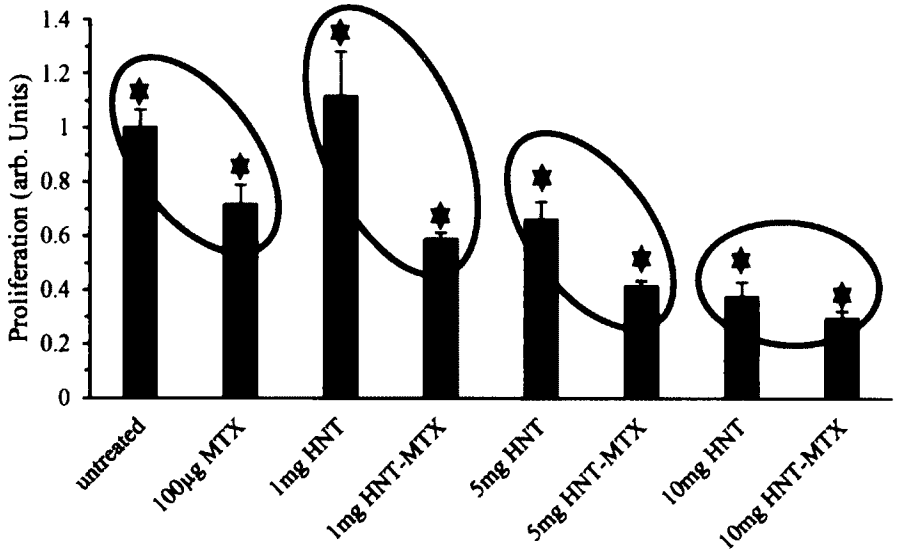


**Figure 5-5:** Mean Cell Proliferation at 120 hours of n = 9 ± standard deviation. Statistical analysis was applied with IBM SPSS 22.0 at $\alpha = .05$, and the black stars indicate significant difference exists when encircled groups are compared.

**Figure 5-6** shows the proliferation after 168 hours, the final time point. After 168 hours the drug continued to affect cellular proliferation in all treated groups. The 1 mg HNT group (73% proliferation) showed a higher level of proliferation than any other

group, except the control. The 1 mg HNT-MTX group showed more proliferation reduction than 1 mg of plain HNT and untreated controls. The 1 mg HNT-MTX group reduced proliferation by more than half when compared to 1 mg HNT and by nearly 60% when compared to untreated control. The 1 mg HNT-MTX group continued to be more effective at proliferation inhibition than the 100 μg of MTX, and at this point the majority (80%) of the drug had been released from MTX-loaded HNTs. The 5 mg HNT-MTX case reduced proliferation by nearly 80%, and 5 mg plain HNT was reduced proliferation by ~60%, and these two groups continue to differ significantly, but the 5 mg still negatively affects cell proliferation. The 10 mg HNT-MTX case had highest reduction in proliferation (82%). When the 10 mg HNT-MTX and 10 mg plain HNT cases were compared the presence of MTX in this group had little effect by comparison of the 10 mg groups only making a difference of ~9% in cell proliferation. After 168 hours, 5 mg and 10 mg of HNTS negatively affected the proliferation of osteosarcoma.

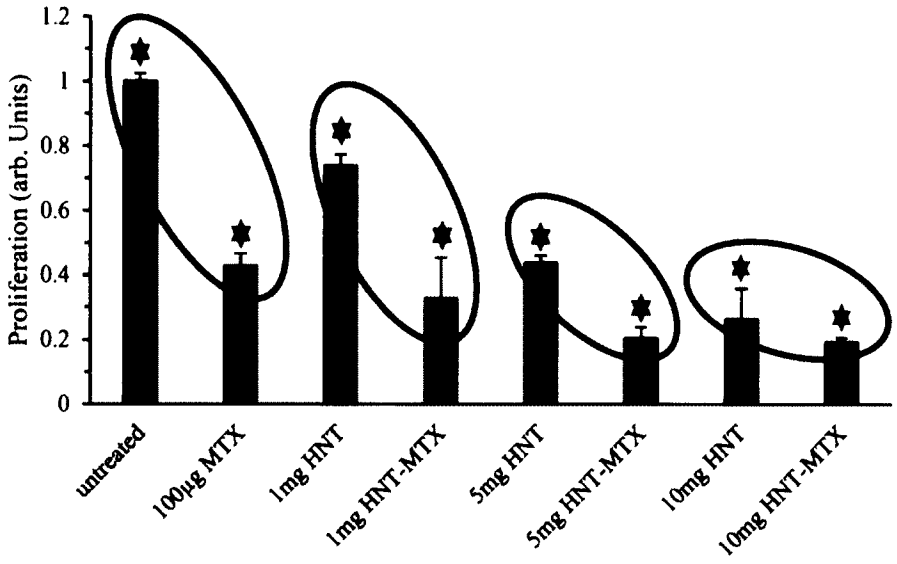


**Figure 5-6:** Mean Cell Proliferation at 168 hours of n = 9 ± standard deviation. And the red stars indicate no significant difference exists two groups encircled are compared and the black stars indicate significant difference exists when encircled groups are compared.

**Figure 5-7** compares cell proliferation over the seven-day period (168 Hours). Even though 5 mg HNT-MTX and 10 mg HNT-MTX showed the largest reductions in proliferation over the seven-day period, 5 and 10 mg of plain HNT significantly reduced the cellular proliferation and limited the response shown in the drug released in the HNT-MTX groups. All groups were more effective than free MTX at every time point which may indicate that HNTs can better localize the drug at the cell than drug diluted in the media. The 1 mg HNT-MTX showed a higher reduction in proliferation when compared to 1 mg HNTs, by reducing proliferation by more than 60% by Day 7. Cell growth seemed to be stimulated by 1 mg of HNTs until cells became confluent, and at confluency 1 mg HNTs show the lowest reduction in proliferation of all HNT groups. Cell proliferation was affected by 1 mg HNTs least when it was administered alone and

yielded the most anti-proliferative effect when loaded with methotrexate. The most effective delivery dose *in vitro* means the best drug response with the least side effects.

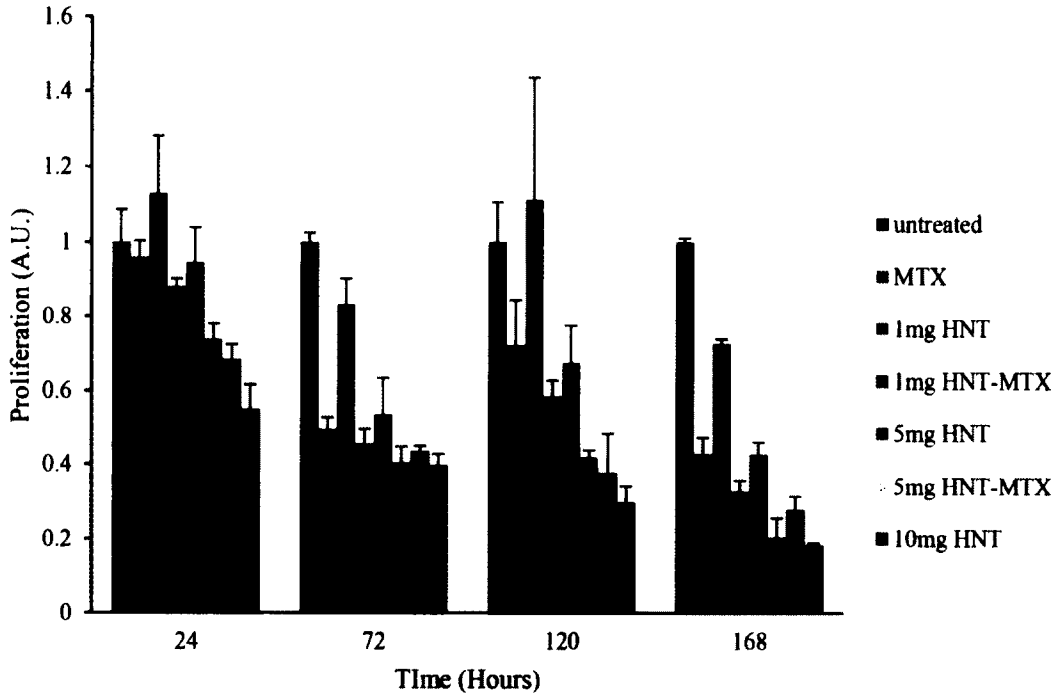


**Figure 5-7:** Seven Day Mean Proliferation Comparison normalized by untreated cells proliferation.

5.3.2.2 *Live/Dead*

A live/dead cell viability assay was performed to determine whether HNT loaded with MTX were inducing cell death in osteosarcoma cells. The live/dead assay images of osteosarcoma cells incubated with MTX-loaded HNTs were compared to with live/dead images of osteosarcoma cells treated with HNTs and free MTX. The negative control for this experiment was untreated cells. Following seeding and incubation, the plates were treated with the live/dead cell viability assay kit and imaged after 24, 72, 120 and 168 hours via the Olympus BX51 fluorescent microscope with FITC and TRITC filters. The

media was changed in all plates after 72 and 120 hours because cells in the control wells were becoming confluent and the cells had used the majority of nutrients in the media.

The images were saved and processed with ImageJ software. **Figure 5-8** to **Figure 5-15** show live/dead images results from 24-168 Hours.

Osteosarcoma cells in monolayer culture proliferated and became nearly confluent within the first 24 hours with little cell death observed (see **Figure 5-8** A-C). Osteosarcoma cells were also unaffected by the addition of HNTs (**Figure 5-8** D-L). Cells proliferated and achieved confluence comparable to normal, untreated cells (Compare B and C with **Figure 5-8** E, H, K and F, I, L).

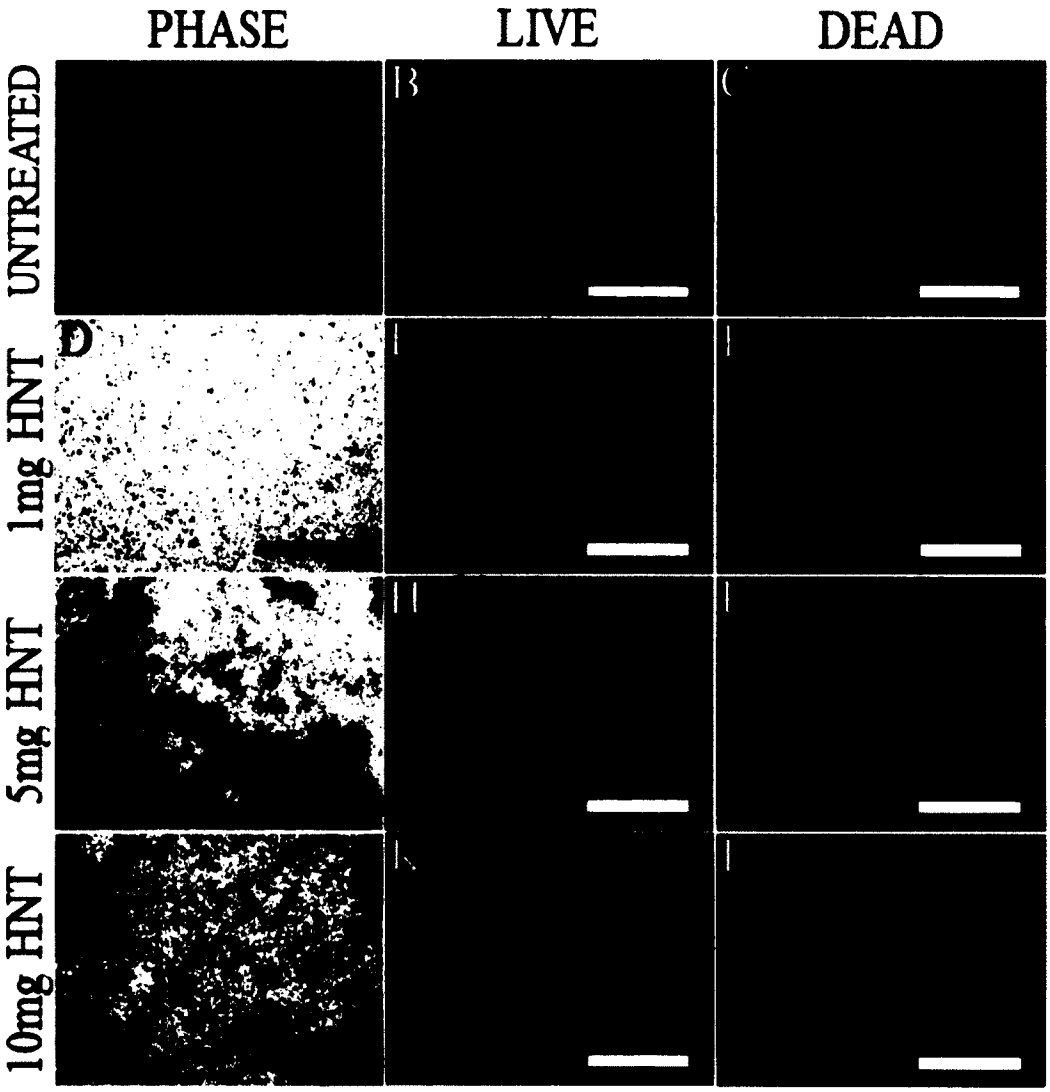


**Figure 5-8:** Cytotoxic response to HNTS at 24 Hours Scale bars represent 500μm. (A-C) Group 1: Osteosarcoma cell cultures with no HNT addition. (D-F) Group 2: Osteosarcoma cells exposed to 1 mg HNTs. (G-I) Group 3: Osteosarcoma cells exposed to 5 mg HNTs. (J-L) Group 4: Osteosarcoma cells exposed to 10mg HNTs. A, D, G and J = Phase contrast; B, E, H and K = Live Dead assay showing live cells (green); C, F, I and L = Dead assay showing dead cells (red). The brown coloration in D, G and J is caused by the high concentration of HNTs. Haze shown in some of the images is also due to high concentrations of HNTs.

HNTs are seen clearly as particulate material (**Figure 5-9** D, G and J). At 24 hours, in MTX-treated groups, the cellular response was very different from untreated cells and cell growth was reduced (**Figure 5-9**A-C). At 24 hours, in Group 2, osteosarcoma cells exposed to 1 mg MTX-HNTs showed a similar reduction in cell growth, as compared to free MTX-treated cells (**Figure 5-9** D-F). At 24 hours, in Group 3, osteosarcoma cells exposed to 5 mg MTX-HNTs showed a greatest reduction in cell growth as compared to the MTX group and the 1 mg MTX-HNT group (**Figure 5-9** G-I). After 24 hours, in Group 4, osteosarcoma cells exposed to 10 mg MTX-HNTs showed the greatest reduction in cell growth as compared to the MTX group, the 5 mg MTX-HNT group, and the 1 mg MTX-HNT group (**Figure 5-9** J-l). However, only a few dead cells were observed in all groups (**Figure 5-9** C, F, I and L).

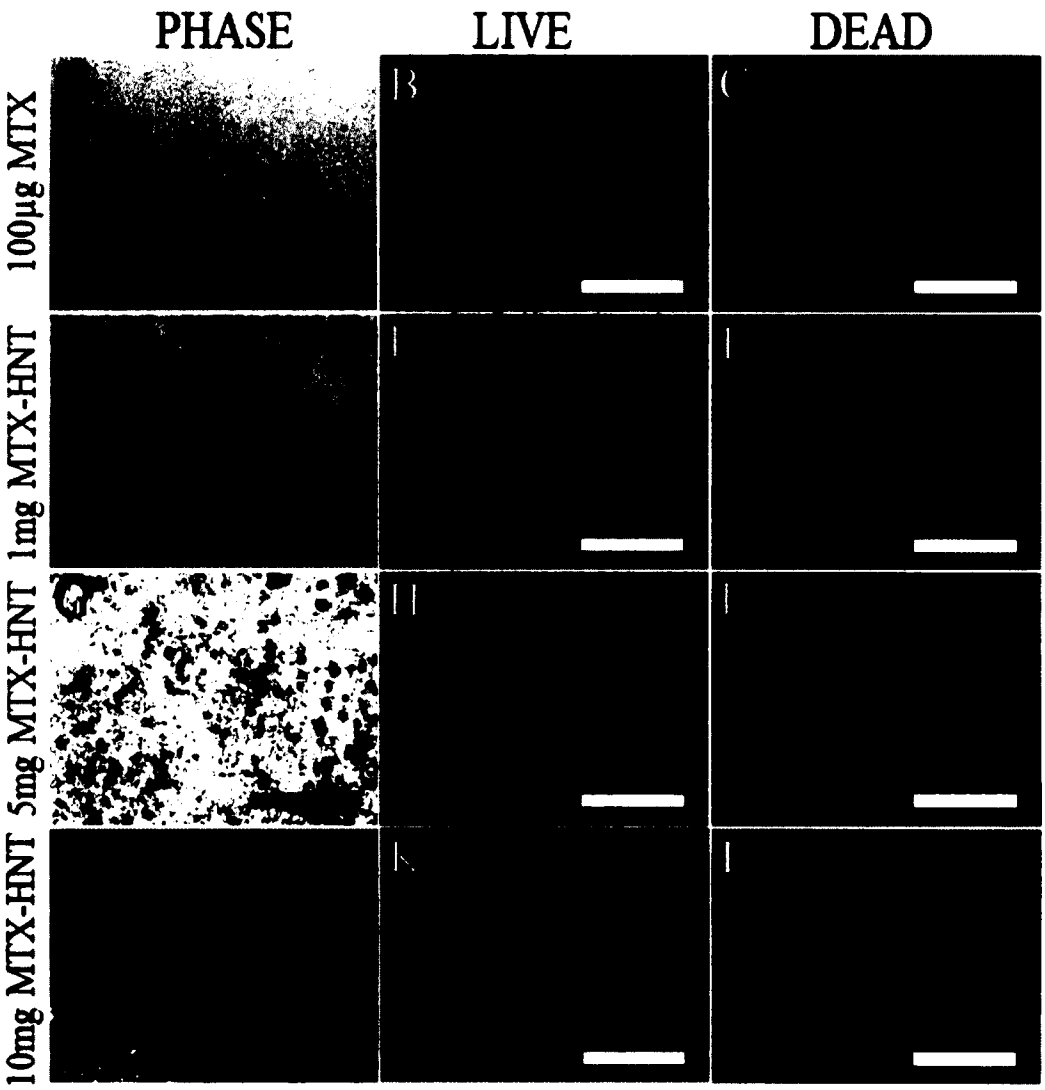


**Figure 5-9:** Cellular response to MTX and MTX-loaded HNTs at 24 Hours Scale bars represent 500µm. (A-C) Group 1: Osteosarcoma cell cultures with MTX (100 µg) addition. (D-F) Group 2: Osteosarcoma cells exposed to 1mg MTX-HNTs. (G-I) Group 3: Osteosarcoma cells exposed to 5 mg MTX-HNTs. (J-L) Group 4: Osteosarcoma cells exposed to 10mg MTX-HNTs. A, D, G and J = Phase contrast; B, E, H and K = Live Dead assay showing live cells (green); C, F, I and L = Dead assay showing dead cells (red). The brown coloration in D, G and J is caused by the high concentration of HNTs. Haze shown in some of the images is also due to high concentrations of HNTs.

Osteosarcoma cells in monolayer culture proliferated and became confluent within 2-3 days with little cell death observed (see **Figure 5-10**, A-C). Osteosarcoma cells were also unaffected by the addition of HNTs (**Figure 5-10**, D-L). Cells proliferated and achieved confluence comparable to normal, untreated cells (Compare **Figure 5-10** B and C with **Figure 5-10** E, H, K and F, I, L).

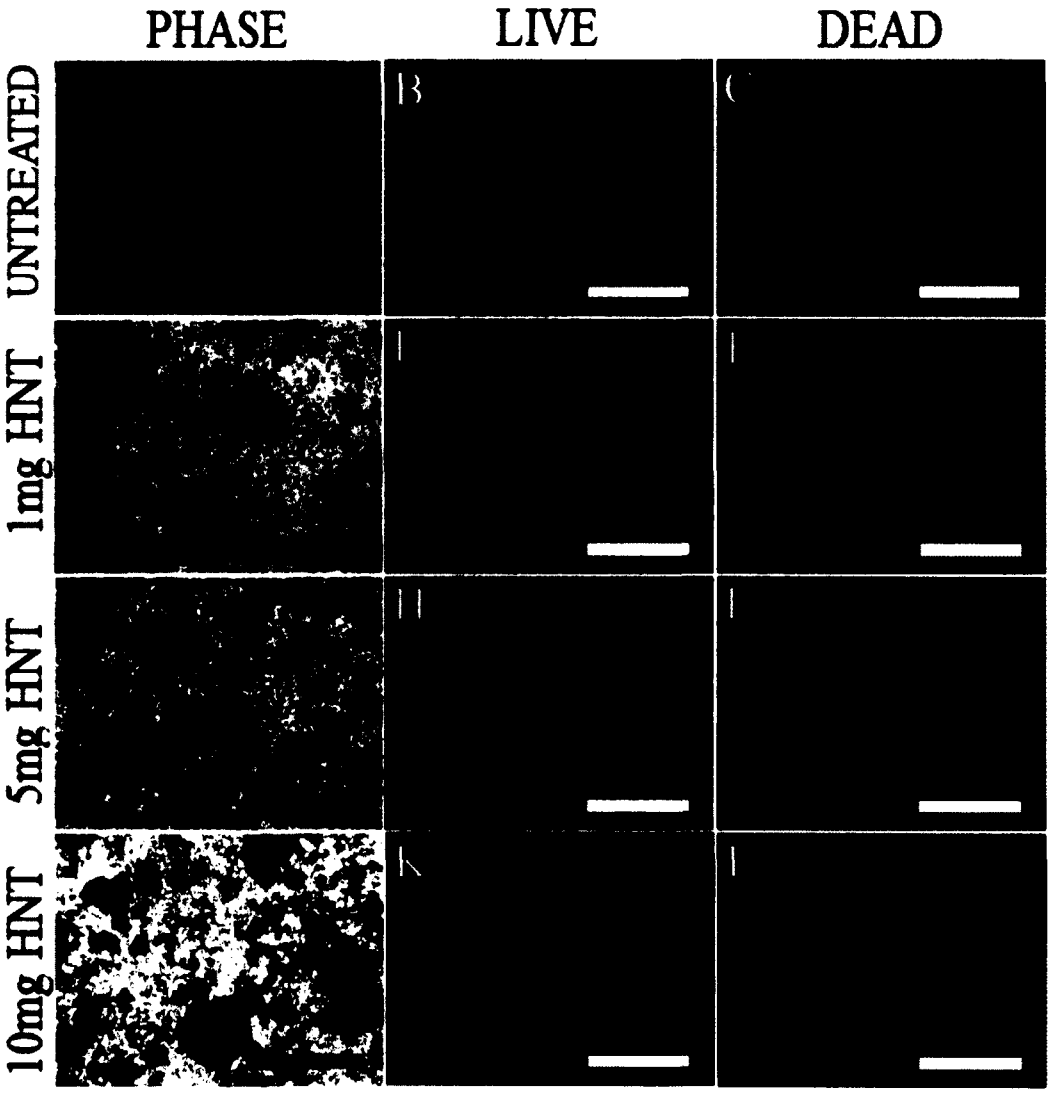


**Figure 5-10:** Cytotoxic response to HNTS at 72 Hours Scale bars represent 500μm. (A-C) Group 1: Osteosarcoma cell cultures with no HNT addition. (D-F) Group 2: Osteosarcoma cells exposed to 1 mg HNTs. (G-I) Group 3: Osteosarcoma cells exposed to 5 mg HNTs. (J-L) Group 4: Osteosarcoma cells exposed to 10 mg HNTs. A, D, G and J = Phase contrast; B, E, H and K = Live Dead assay showing live cells (green); C, F, I and L = Dead assay showing dead cells (red). The brown coloration in D, G and J is caused by the high concentration of HNTs. Haze shown in some of the images is also due to high concentrations of HNTs.

After 72 hours, in MTX-treated groups the reduction in cell growth was much greater than at 24 hours (**Figure 5-11** A-C). After 72 hours, in Group 2, osteosarcoma

cells exposed to 1 mg MTX-HNTs showed a marked reduction in cell growth as compared to untreated controls cells and cells treated with free MTX (**Figure 5-11** D-F), this reduction was even greater than the reduction seen at 24 hours. At 72 hours, in Group 3, osteosarcoma cells exposed to 5 mg MTX-HNTs showed a greater reduction in cell growth as compared to the MTX group and the 1 mg MTX-HNT group and was greater than the reduction seen at 24 hours (**Figure 5-11** G-I). At 72 hours, in Group 4, osteosarcoma cells exposed to10 mg MTX-HNTs showed the greatest reduction in cell growth as compared to the MTX group, the 5 mg MTX-HNT and the 1 mg MTX-HNT group but was similar to the cell growth at 24 hours (**Figure 5-11** J-L). However, only a few dead cells were observed in all groups (**Figure 5-11** C, F, I and L).

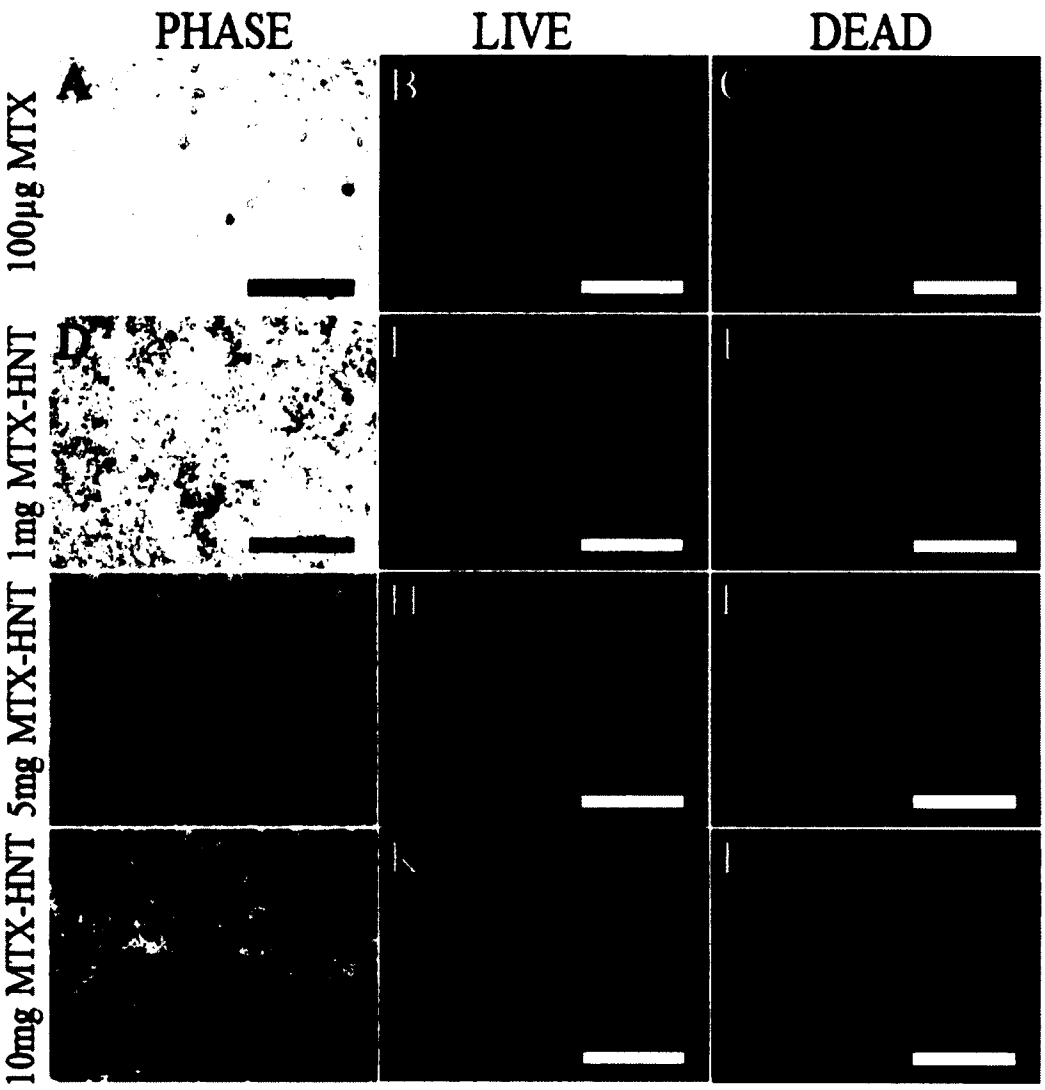


**Figure 5-11:** Cellular response to MTX and MTX-loaded HNTs at 72 Hours Scale bars represent 500µm. (A-C) Group 1: Osteosarcoma cell cultures with MTX (100 µg) addition. (D-F) Group 2: Osteosarcoma cells exposed to 1mg MTX-HNTs. (G-I) Group 3: Osteosarcoma cells exposed to 5 mg MTX-HNTs. (J-L) Group 4: Osteosarcoma cells exposed to 10 mg MTX-HNTs. A, D, G and J = Phase contrast; B, E, H and K = Live Dead assay showing live cells (green); C, F, I and L = Dead assay showing dead cells (red). The brown coloration in D, G and J is caused by the high concentration of HNTs. Haze shown in some of the images is also due to high concentrations of HNTs.

Osteosarcoma cells in monolayer culture continued to proliferate and maintained confluency after 120 hours with little cell death observed (see **Figure 5-12** A-C). Osteosarcoma cells also began to show the effects of the addition of HNTs (**Figure 5-12** D-L). Cells proliferated and achieved confluence comparable to normal, untreated cells (Compare **Figure 5-12** B and C with **Figure 5-12** E, H, K and F, I, L), but the HNT groups may have many more dead cells.


**Figure 5-12:** Cytotoxic response to HNTS at 120 Hours Scale bars represent 500μm (A-C) Group 1: Osteosarcoma cell cultures with no HNT addition. (D-F) Group 2: Osteosarcoma cells exposed to 1 mg HNTs. (G-I) Group 3: Osteosarcoma cells exposed to 5 mg HNTs. (J-L) Group 4: Osteosarcoma cells exposed to 10mg HNTs. A, D, G and J = Phase contrast; B, E, H and K = Live Dead assay showing live cells (green); C, F, I and L = Dead assay showing dead cells (red). The brown coloration in D, G and J is caused by the high concentration of HNTs. Haze shown in some of the images is also due to high concentrations of HNTs.

After 120 hours, in MTX-treated groups, the reduction in cell growth was even greater than at 72 hours (**Figure 5-13** A-C). After 120 hours, in Group 2, osteosarcoma cells exposed to 1 mg MTX-HNTs showed a marked reduction in cell growth as compared to untreated controls cells and cells treated with free MTX (**Figure 5-13** D-F). This reduction was even greater than the reduction seen after 72 hours. At 120 hours, in Group 3, osteosarcoma cells exposed to 5 mg MTX-HNTs showed a greater reduction in cell growth as compared to MTX group and 1 mg MTX-HNT group (**Figure 5-13** G-H). After 120 hours, in Group 4, osteosarcoma cells exposed to10 mg MTX-HNTs showed the greatest reduction in cell growth as compared to the MTX group, the 5 mg MTX-HNT and the 1 mg MTX-HNT group (**Figure 5-13** J-L). However, only a few dead cells were observed in all groups (**Figure 5-13** C, F, I and L).

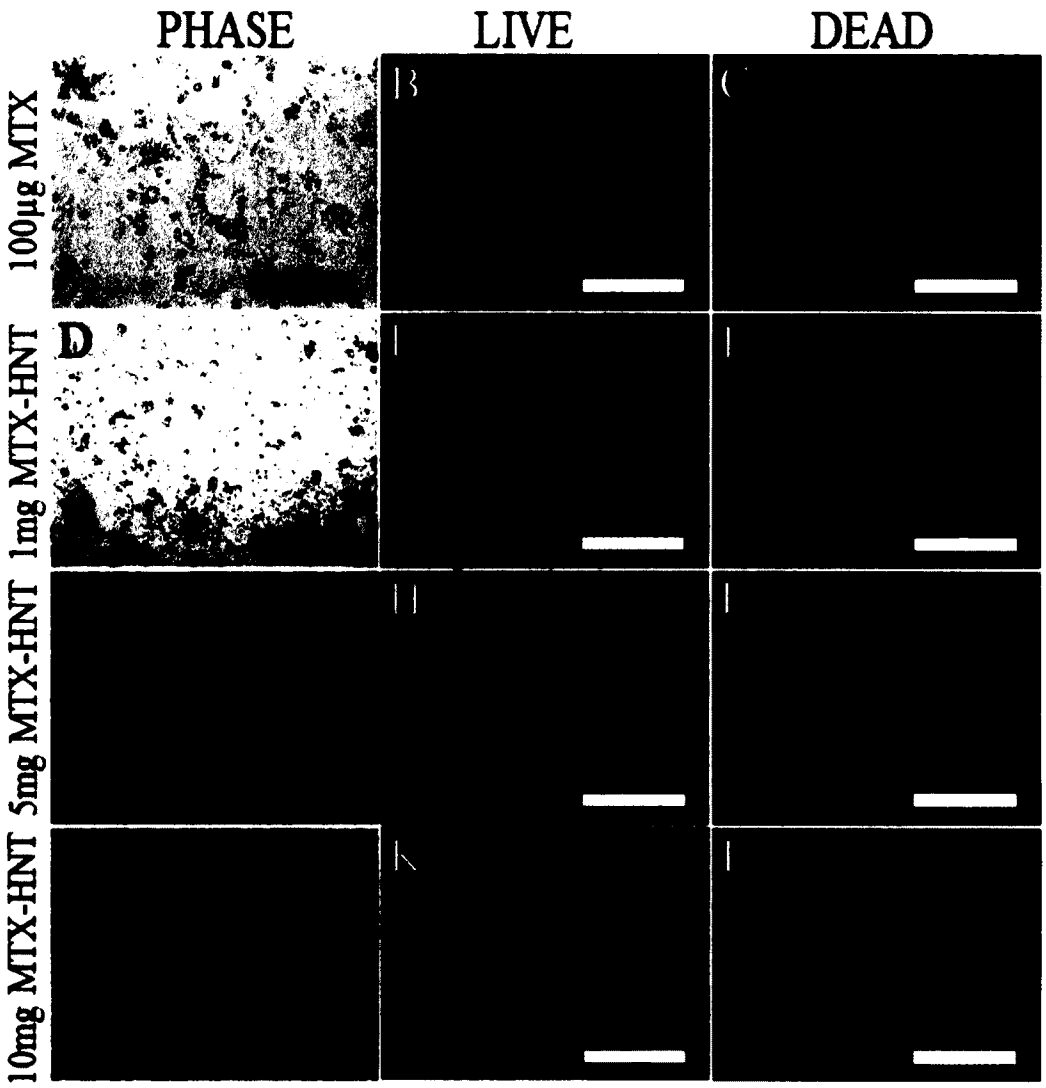


**Figure 5-13:** Cellular response to MTX and MTX loaded HNTs at 120 Hours Scale bars represent 500µm. (A-C) Group 1: Osteosarcoma cell cultures with MTX (100 µg) addition. (D-F) Group 2: Osteosarcoma cells exposed to 1 mg MTX-HNTs. (G-I) Group 3: Osteosarcoma cells exposed to 5 mg MTX-HNTs. (J-L) Group 4: Osteosarcoma cells exposed to 10 mg MTX-HNTs. A, D, G and J = Phase contrast; B, E, H and K = Live Dead assay showing live cells (green); C, F, I and L = Dead assay showing dead cells (red). The brown coloration in D, G and J is caused by the high concentration of HNTs. Haze shown in some of the images is also due to high concentrations of HNTs.

Osteosarcoma cells in monolayer culture continued to proliferate and maintained confluency after 168 hours (7 days) with little cell death observed (see **Figure 5-14** A-C). Osteosarcoma cells also began to show the effects of unloaded HNTs (**Figure 5-14** D-L). Cell proliferation and confluence are comparable to normal, untreated cells (compare **Figure 5-14** B and C with **Figure 5-14** E, H, K and F, I, L) but the HNT groups had many more dead cells. Also, the 5 mg and especially the 10 mg groups, are less confluent than the normal, untreated cells, which indicates a more cytotoxic response at 7 days.

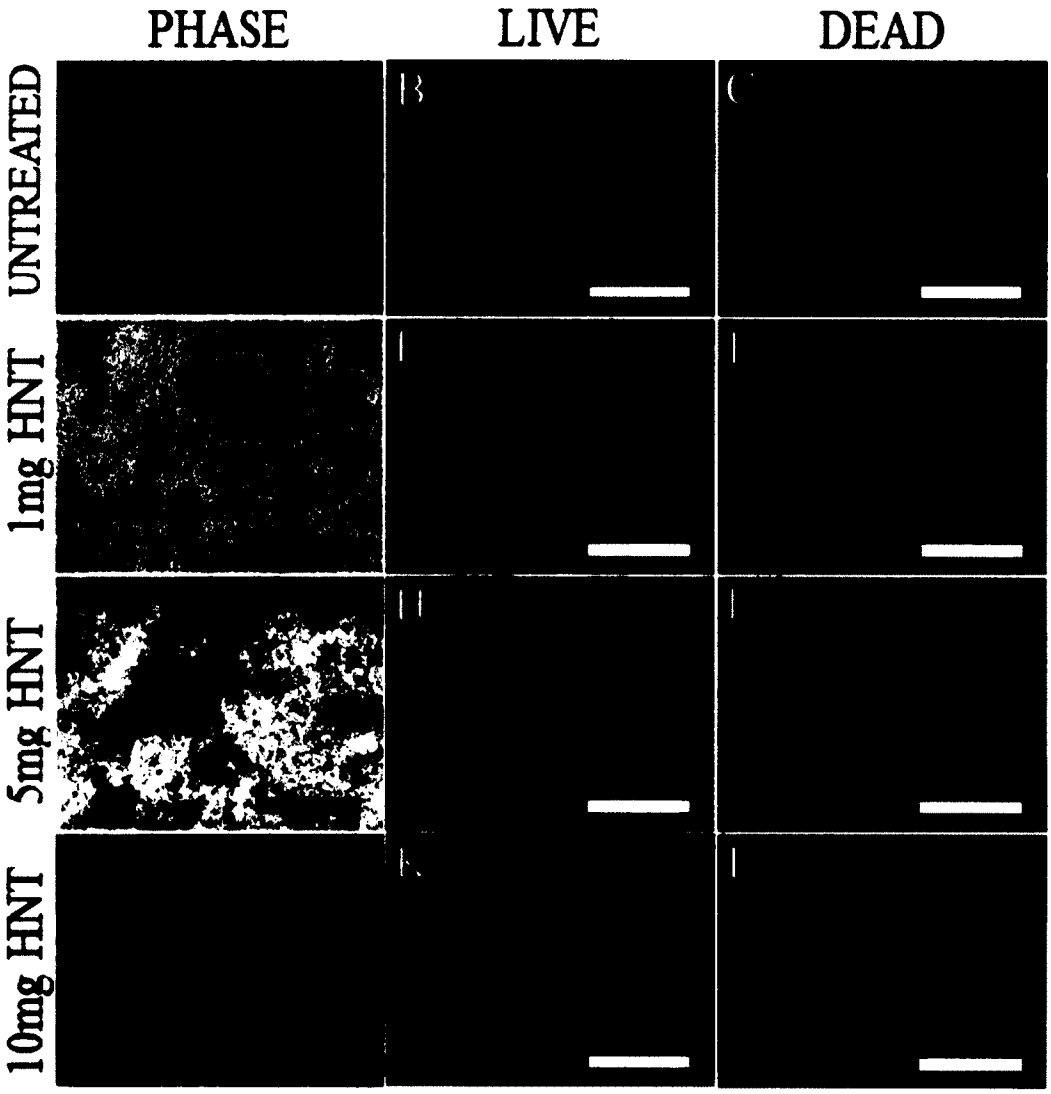


**Figure 5-14:** Cytotoxic response to HNTs at 168 Hours Scale bars represent 500μm (A-C) Group 1: Osteosarcoma cell cultures with no HNT addition. (D-F) Group 2: Osteosarcoma cells exposed to 1 mg HNTs. (G-I) Group 3: Osteosarcoma cells exposed to 5 mg HNTs. (J-L) Group 4: Osteosarcoma cells exposed to 10 mg HNTs. A, D, G and J = Phase contrast; B, E, H and K = Live Dead assay showing live cells (green); C, F, I and L = Dead assay showing dead cells (red). The brown coloration in D, G and J is caused by the high concentration of HNTs. Haze shown in some of the images is also due to high concentrations of HNTs.

After 168 hours, in MTX-treated groups, the reduction in cell growth was even greater than after 120 hours and the cellular response was very different from untreated cells (**Figure 5-15** A-C). After 168 hours, Group 2 osteosarcoma cells exposed to 1 mg MTX-HNTs showed a marked reduction in cell growth as compared to untreated control cells and cells treated with free MTX (**Figure 5-15** D-F). At 168 hours, in group 3, osteosarcoma cells exposed to 5mg MTX-HNTs showed a greater reduction in cell growth as compared to the MTX group and the 1mg MTX-HNT group (**Figure 5-15** G-H). After 168 hours, Group 4 osteosarcoma cells exposed to 10 mg MTX-HNTs showed the greatest reduction in cell growth as compared to the MTX group, the 5 mg MTX-HNT and the1 mg MTX-HNT group (**Figure 5-15** J-L). However, only a few dead cells were observed in all groups, and cells were more confluent than at the 120 hour time point, which may be attributed to the changing of the media which removed the majority of the drug that had been released (**Figure 5-15** C, F, I and L).

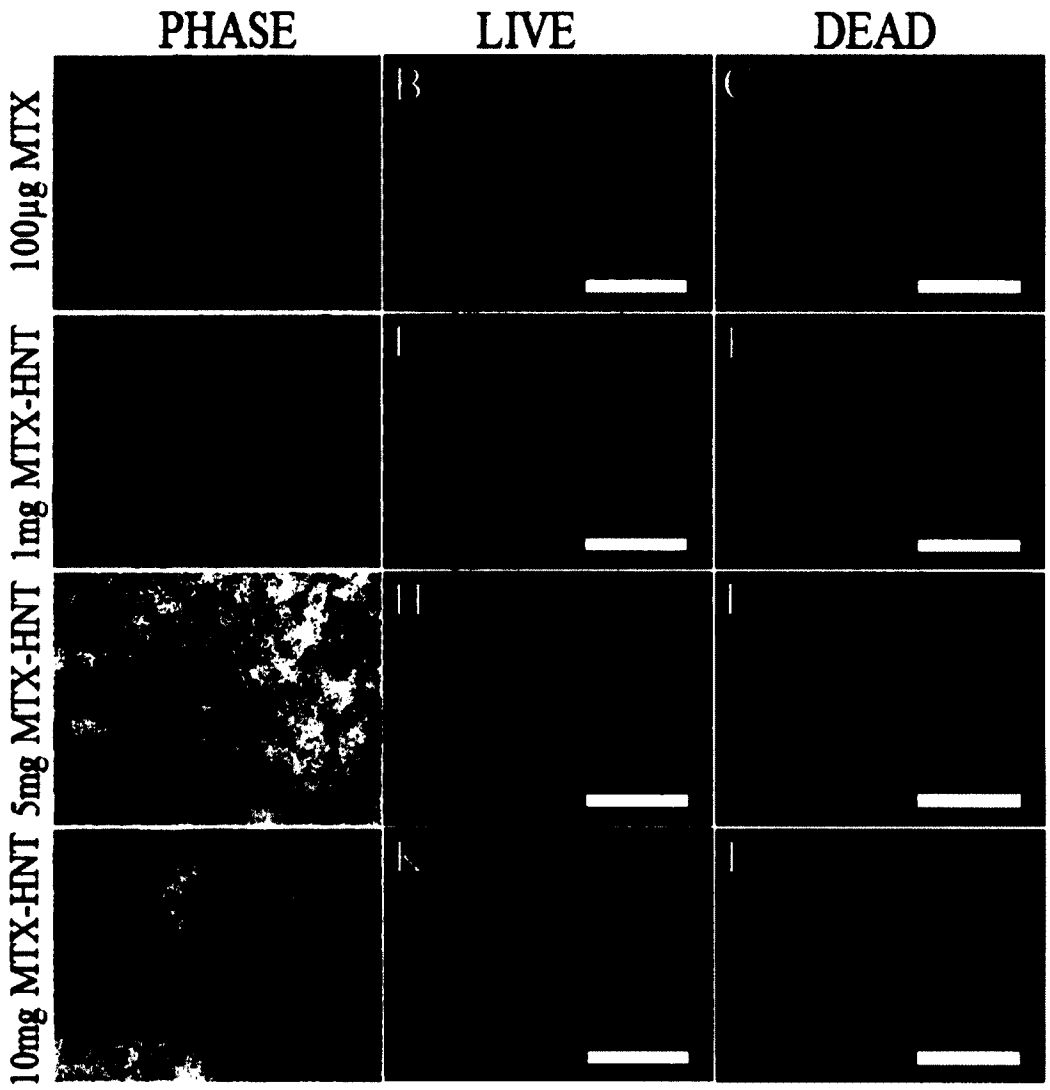


**Figure 5-15:** Cellular response to MTX and MTX loaded HNTs at 168 Hours Scale bars represent 500µm. (A-C) Group 1: Osteosarcoma cell cultures with MTX (100 µg) addition. (D-F) Group 2: Osteosarcoma cells exposed to 1 mg MTX-HNTs. (G-I) Group 3: Osteosarcoma cells exposed to 5 mg MTX-HNTs. (J-L) Group 4: Osteosarcoma cells exposed to 10 mg MTX-HNTs. A, D, G and J = Phase contrast; B, E, H and K = Live Dead assay showing live cells (green); C, F, I and L = Dead assay showing dead cells (red). The brown coloration in D, G and J is caused by the high concentration of HNTs. Haze shown in some of the images is also due to high concentrations of HNTs.

### 5.3.3 FE-SEM, TEM and Zeta Potential/Particle Size Analysis

FE-SEM and TEM images, as well as, zeta potential and particle size measurements were taken to characterize HNTs.

#### 5.3.3.1 *SEM TEM imaging*

**Figure 5-16** shows the SEM and TEM images of plain HNTs. Images show relative diameters, lengths and lumen size described in earlier chapters.

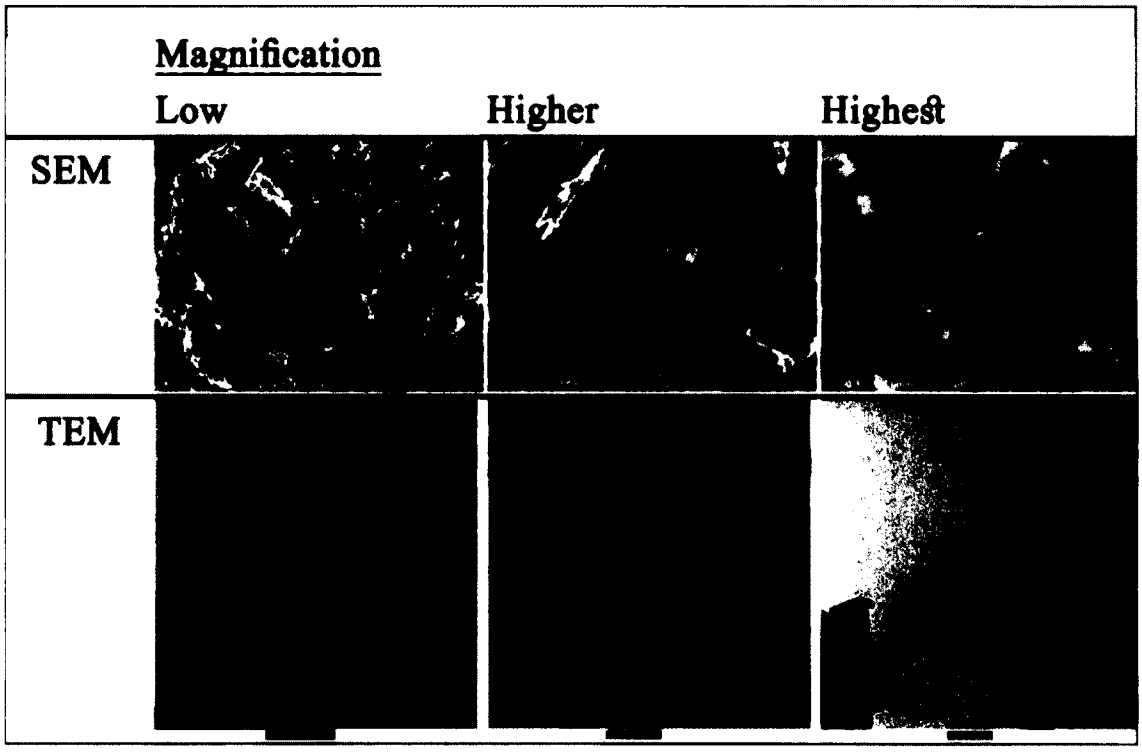


**Figure 5-16:** SEM and TEM Images of HNTs at different magnifications Scale bars for TEM are 500nm for low magnification 200 nm for Higher Magnification and 50nm for Highest Magnification. Scale Bars for SEM are 5μm for low magnification, 1μm for Higher Magnification and 500nm for Highest Magnification.

5.3.3.2 *Zeta Potential and Particle Size*

The average particle size of plain HNTs, methotrexate-loaded HNTs and pIRES2-EGFP-loaded HNTs was measured to compare and determine if loading had affected particle size. Results are plotted in **Figure 5-17**. For pIRES2-EGFP-loaded HNTs' particle size was measured to determine if surface adsorption or wrapping increased particle size. Plain HNTs and HNTs loaded with methotrexate shared similar particle sizes of 1522 nm ± 97.3 nm and 1513.4±562.8 nm respectively with no significant difference (Appendix A **Table A-2:** Results of IBM SPSS two-tailed Paired T-Test for Particle Size n = 4 samples.). The major difference in error between plain HNTs and methotrexate-loaded HNTs may be attributed to the formation of aggregates during the drying process. HNTs loaded with methotrexate may have some methotrexate on the surface causing them to stick together. Plasmid-loaded HNTs are noticeably larger than plain HNTs and methotrexate-loaded HNTs. On average pIRES2-EGFP-loaded HNTs were 4320.3 nm±609 nm in diameter. PIRES2-EGFP-loaded HNTs were almost 3 times the size of plain HNTs and methotrexate-loaded HNTs and this increased size may be attributed to the plasmid DNA adhering to the surface or wrapping around HNTs. The large error may be due to the formation of aggregates during the drying process.

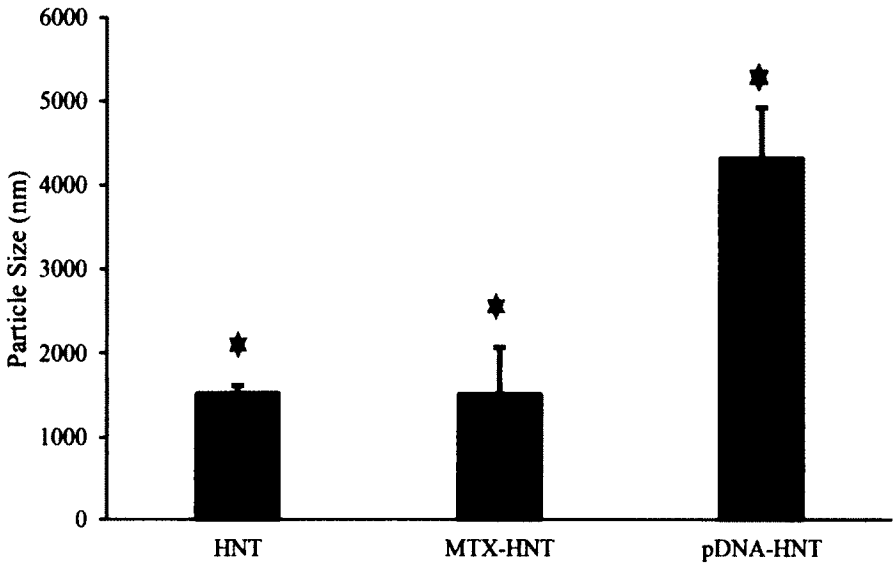


**Figure 5-17:** Mean Particle Size +/- standard deviation n = 4 samples. Statistical analysis was applied with IBM SPSS 22.0 at $\alpha = .05$, and the red stars indicate no significant difference exists the group and HNTs. The black stars indicate significant difference exists when group and HNTs are compared.

The zeta potential of plain HNTs, methotrexate-loaded HNTs and pIRES2-EGFP-loaded HNTs was measured to compare and determine if loading affected zeta potential. Results are plotted in **Figure 5-18**. For pIRES2-EGFP-loaded HNTs zeta potential was measured to determine if surface adsorption or wrapping changed the surface zeta potential of HNTs. With the loading of MTX and surface adsorption and/or loading of plasmid DNA, the zeta potential decreased slightly. The zeta potential was -41.6±3 mV for plain HNTs, -45±2.3 mV for MTX-HNT, and -51.4±2.1 mV for pIRES2-EGFP-HNT.

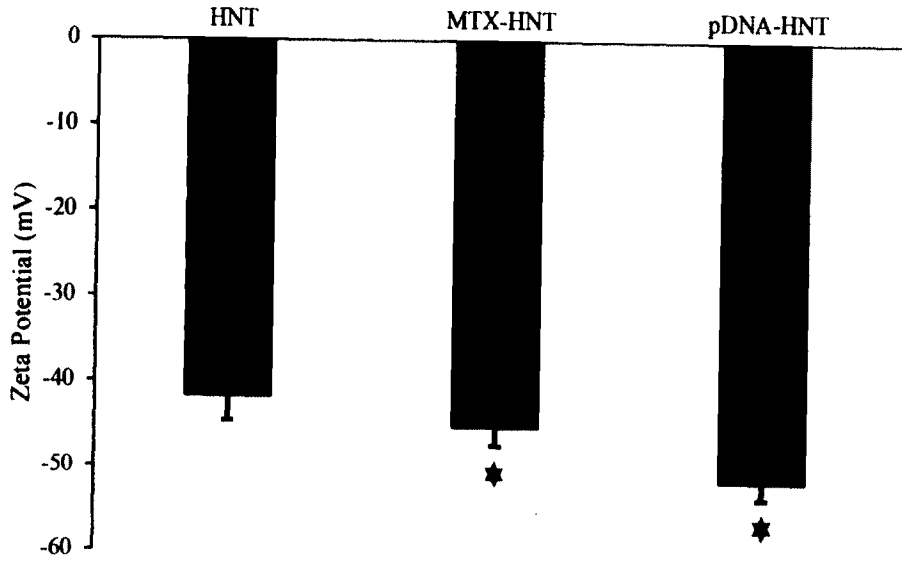


**Figure 5-18:** Mean Zeta Potential +/- standard deviation n = 4 samples. Statistical analysis was applied with IBM SPSS 22.0 at $\alpha = .05$,and the red stars indicate no significant difference exists the group and HNTs.

# CHAPTER 6

# AIR-BRUSHED HNT DOPED CHITOSAN FILMS FOR SUSTAINED AND LOCALIZED DELIVERY OF METHOTREXATE

## 6.1 Introduction

The previous chapter introduced HNTs as a drug delivery vector for methotrexate. Results suggest that MTX-loaded HNTs can release MTX and inhibit proliferation for up to seven days. Though capable of releasing drugs for seven days the release MTX from HNTs should be tailored to allow for a more controlled release. Here I discuss another potential application by pairing drug loaded HNTs with a novel air-brush sprayed film as a pre and post-surgical implant for patients with different types of cancer.

In Chapter 5, HNTs were used to deliver MTX to osteosarcoma cells to inhibit cellular growth. In the current chapter, HNTs are combined with novel air-brush sprayed chitosan films to improve their material and biological properties. The objective of adding MTX-HNTs to chitosan films was to tailor drug release, immobilize HNTs, and localize drug dosage. These MTX-HNT-doped chitosan films may be useful as post-surgical implants that reduce the recurrence of cancer in patients who have had cancerous tumors removed. They may also be used neo-adjuvantly to shrink different types of tumors.

Chitosan, individually and in combination with other polymers, has material and biological properties that make it suitable for drug delivery [87]. Chitosan is biodegradable, biocompatible, and capable of forming films through several methods [87]. Aside from the mentioned properties, chitosan can encapsulate free drugs, and it may be able to control the release based on film degradation.

The hypothesis of this project was that the combination of air-brush sprayed chitosan films and methotrexate-loaded HNTs could inhibit growth and proliferation of cells while modulating drug release *in vitro*.

## 6.2 Methods and Materials

All the plasticware, which include, syringes, centrifuge tubes, microcentrifuge tubes, 12 well plates, and pipettes were purchased from Mid Scientific, St. Louis, MO. Cell culture media, buffers, serum and LIVE/DEAD® Viability/Cytotoxicity Kit were purchased from Life Technologies, Grand Island, NY. Acetone, DMSO, Methotrexate, HNTs and XTT *in vitro* toxicology assay kits were obtained from Sigma-Aldrich, St. Louis, MO. ChitoClear® HQG10 chitosan was obtained from Primex, Siglufjörður, Iceland. Murine osteosarcoma cells CRL-2836 were obtained from ATCC, Manassas, VA.

### 6.2.1 Imaging

#### 6.2.1.1 *Camera Imaging*

To macroscopically view chitosan films, HNT chitosan films and MTX-HNT chitosan film images were taken with a 16-megapixel camera.

6.2.1.2 *Phase Contrast Imaging*

The Olympus BX51 fluorescent microscope was used in phase contrast mode to image chitosan films, MTX chitosan films, HNT chitosan films and MTX-HNT chitosan. The images allowed for the visualization of millimeter and micrometer scale features of the different film composites films.

6.2.1.3 *FE-SEM Imaging*

The HITACHI S 4800 Field Scanning Electron Microscope (FE-SEM) was used to image chitosan films, HNT chitosan films, and MTX-HNT chitosan films. The SEM microscope's high magnification allowed for a close comparison of the surface morphologies of chitosan films, HNT chitosan films, and MTX-HNT chitosan films. The comparison helped to assess the surface properties and to predict the behavior of the films *in vitro* conditions.

6.2.2 Release Study

The release profile study for methotrexate was done to understand the release of chemotherapeutic agents from HNT-embedded chitosan films. First, a calibration curve was created for MTX to compare with the drug elution profiles of the MTX-HNT chitosan films. Four sample sets of films were prepared using methods mentioned in 3.2.2, 1% HNT-MTX w/v chitosan, 5% HNT-MTX w/v and 10% HNT-MTX w/v chitosan and 1 mg/ml concentration of methotrexate in chitosan. After being spayed into a 12 will tissue culture dish in triplicates (see plate map **Table 6-1**), films were immersed in HBSS and mixed for 24-hour and 7-day time periods. Samples were centrifuged and the supernatants were collected for UV-vis. analysis (Nanodrop 2000c, ABS wavelength

300 nm). Samples were replenished with fresh HBSS. The details of sample collection and the overall procedure are provided in Section 3.2.6.

**Table 6-1:** 12-Well Plate Map for Chitosan Films Drug Release Study.

| | | | |
|---|---|---|---|
| **100 µg MTX Chitosan** | **1% MTX-HNT Chitosan** | **5% MTX-HNT Chitosan** | **10% MTX-HNT Chitosan** |
| **100 µg MTX Chitosan** | **1% MTX-HNT Chitosan** | **5% MTX-HNT Chitosan** | **10% MTX-HNT Chitosan** |
| **100 µg MTX Chitosan** | **1% MTX-HNT Chitosan** | **5% MTX-HNT Chitosan** | **10% MTX-HNT Chitosan** |

### 6.2.3 Cell Culture and Seeding

An osteosarcoma cell line was the model used to study *in vitro* cellular response to methotrexate-loaded chitosan composite. Osteosarcoma cells were plated in 25 $cm^2$ tissue culture flasks, and incubated at 37 °C under humidified 5% $CO_2$ and 95% air in complete DMEM containing 10% FBS and 1% PSA. Subconfluent cells were passaged with 0.25% trypsin, collected by centrifugation, suspended in complete DMEM and cultured at a 3:1 split into 25 $cm^2$ tissue culture flasks. These cultures were used for the viability and proliferation tests.

#### 6.2.3.1 *Cell Proliferation and Viability Studies*

In these experiments, osteosarcoma cells were used. Chitosan films were sprayed onto 12 well plates according to **Table 6-2** and **Table 6-3**. Osteosarcoma cells were seeded in 12-well plates containing films. Two of each plate were prepared for each time period, one for XTT cell proliferation assay and one for live/dead cell viability assay.

**Table 6-2:** Drug Free Film Plate Map for Cell Proliferation and Cytotoxcity studies.

| | | | |
|---|---|---|---|
| **Chitosan** | **1% HNT Chitosan** | **5% HNT Chitosan** | **10% HNT Chitosan** |
| **Chitosan** | **1% HNT Chitosan** | **5% HNT Chitosan** | **10% HNT Chitosan** |
| **Chitosan** | **1% HNT Chitosan** | **5% HNT Chitosan** | **10% HNT Chitosan** |

**Table 6-3:** MTX loaded Film Plate Map for Cell Proliferation and Cytotoxcity studies.

| | | | |
|---|---|---|---|
| **1 mg/ml MTX Chitosan** | **1% MTX-HNT Chitosan** | **5% MTX-HNT Chitosan** | **10% MTX-HNT Chitosan** |
| **1 mg/ml MTX Chitosan** | **1% MTX-HNT Chitosan** | **5% MTX-HNT Chitosan** | **10% MTX-HNT Chitosan** |
| **1 mg/ml MTX Chitosan** | **1% MTX-HNT Chitosan** | **5% MTX-HNT Chitosan** | **10% MTX-HNT Chitosan** |

6.2.3.2 *XTT Cell Proliferation Assay*

This assay is based on the ability of viable cells to reduce XTT dye. These wells were analyzed at 24, 72, 120 and 168 hours to evaluate if chitosan films and doped chitosan film composites reduced the cell proliferation. Cells seeded in 12 well plates were treated as mentioned in Section 6.2.3.1. The XTT assay was added, as detailed in Section 3.2.7.2, and analyzed with the absorbance microplate reader at 450 nm and 690 nm wavelengths.

6.2.3.3 *Live/Dead Assay*

This assay was used to determine if chitosan films and doped chitosan film composites resulted in cell death. Cells seeded in 12 well plates were treated as mentioned in Section 6.2.3.1. A live/dead assay was added as detailed in Section 3.2.7.3,

and cells were imaged at 24, 72, 120 and 168 hours under the Olympus BX51 fluorescent microscope with FITC and TRITC filters. Images were processed and quantified using Image J software.

## 6.3 Results and Discussion

### 6.3.1 Imaging

Various types of imaging were carried out to visualize chitosan films and identify features and/or properties that make them unique and ideal *in vitro*.

#### 6.3.1.1 *Camera Imaging*

Images were taken to visualize chitosan films embedded with HNTs, MTX and MTX-HNTs. **Figure 6-1** shows the images taken using a 16 MP camera. Films with 0% HNTs, without MTX have a clear and smooth appearance while films with 0% HNT and 1 mg/ml MTX concentration have a light yellow tint and a slightly more rough appearance. Films with 1, 5 and 10% HNTs have an increased roughness as the percentage of HNT in the films. The same trend is notice in MTX loaded HNT groups however, these groups have a yellow tint due to the loading of MTX.


**Figure 6-1:** Camera Images for Chitosan Films.

6.3.1.2 *Phase Contrast Imaging*

Phase contrast imaging was done to identify mm scale and μm scale feature of chitosan films. Imaging was carried out at 4x magnification (**Figure 6-2**) and 10x magnification (**Figure 6-3**)

**Figure 6-2** shows images of chitosan films at 4x magnification. Chitosan films with no drug or HNTs have sparsely located micron-scale chitosan particles throughout the film (**Figure 6-2**A). Chitosan films with a 1 mg/ml concentration of MTX have many ~50 μm bubbles, which may signify drug encapsulation within the films (**Figure 6-2**B).

In chitosan films with no drug and 1% HNTs, there are sparsely located micron scale chitosan particles throughout the film (**Figure 6-2**C) as well as a greater evenly distributed HNT particles. In chitosan films with a 1% MTX-HNTs, aggregates of MTX-HNT can be seen throughout the image and many of them seem to be encapsulated within bubbles which may signify MTX-HNT encapsulation within the films (**Figure 6-2**D). Additionally, it seems that HNTs loaded with MTX are much more pronounce than unloaded HNTs and MTX seems to also coat the surface.

Chitosan films with no drug and 5% HNTs had sparsely located micron scale chitosan particles throughout the film (**Figure 6-2**E) as well as a greater amount of evenly distributed HNT particles when compared to 1 %HNT chitosan films (**Figure 6-2**C). In chitosan films with a 5% MTX-HNTs, aggregates of MTX-HNT can be seen throughout the image and many of them seem to be encapsulated within bubbles, which may signify MTX-HNT encapsulation within the films (**Figure 6-2**F). Additionally, the 5%MTX-HNT films (**Figure 6-2**F) had many more MTX-HNT aggregates in than 1% MTX-HNT films (**Figure 6-2**D).

Chitosan films with no drug and 10% HNTs had sparsely located micron-scale chitosan particles throughout the film (**Figure 6-2**G) and more HNT particles when compared to 5% HNT chitosan films (**Figure 6-2**F), although not as evenly distributed. Chitosan films with a 10% MTX-HNTs had aggregates of MTX-HNT throughout the image, and many of them seem to be encapsulated with in bubble which may signify MTX-HNT encapsulation within the films (**Figure 6-2**H). Additionally, the MTX-HNT aggregates in 10%MTX-HNT are not evenly distributed like other groups, and MTX HNTs tended to clump together.

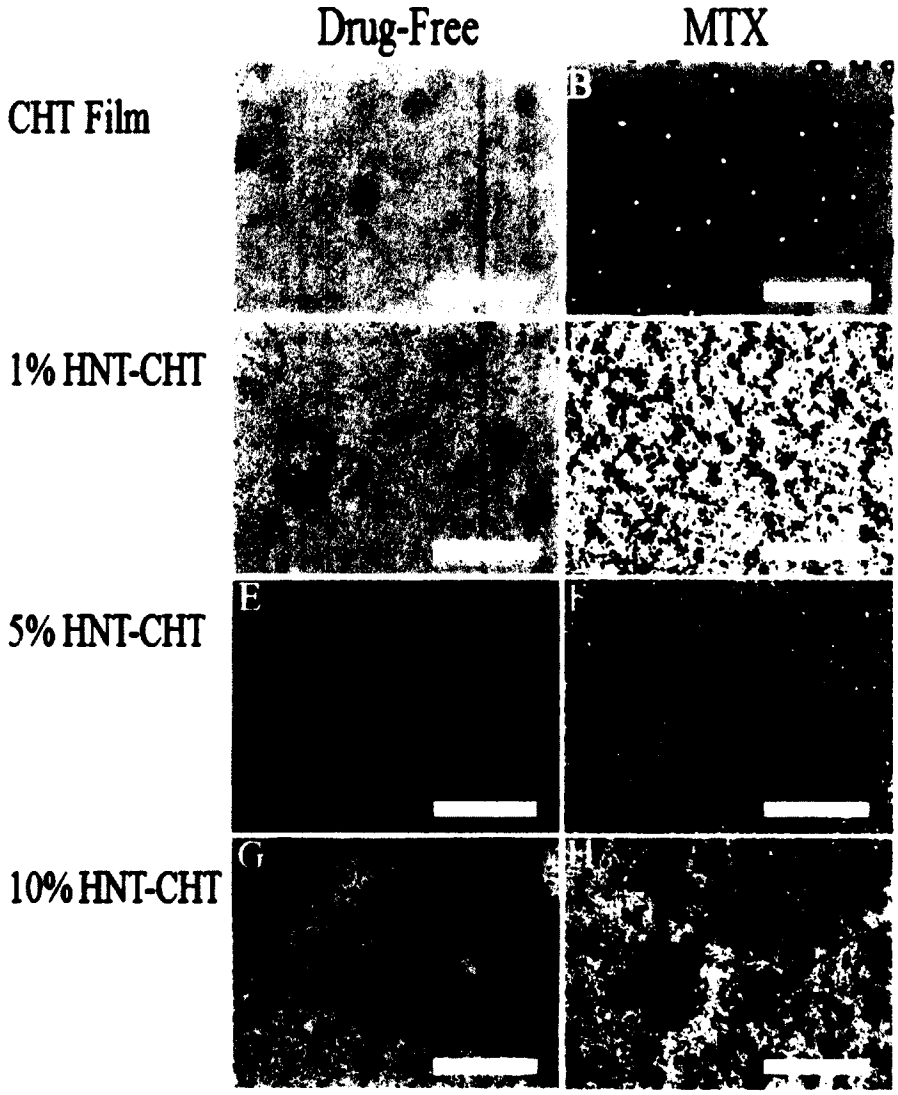


**Figure 6-2:** 4x Phase contrast images scale bars represent 500μm. A, C, E, and G are images of non-drug loaded films at 0% HNT, 1% HNT, 5% HNT and 10% HNT, respectively. B, D, F, and H are images of drug loaded films at 0% HNT, 1% HNT, 5% HNT and 10% HNT, respectively.

**Figure 6-3** shows images of chitosan films at 10x magnification. Images show the same trends as imaged at 4x magnification. Chitosan microparticles seen in images with no drug are ~1-20 microns in diameter (**Figure 6-3**A, C). Drug encapsulated

bubbles seen in the MTX-loaded 0% chitson films are ~20-40 microns in diameter (**Figure 6-3**B).

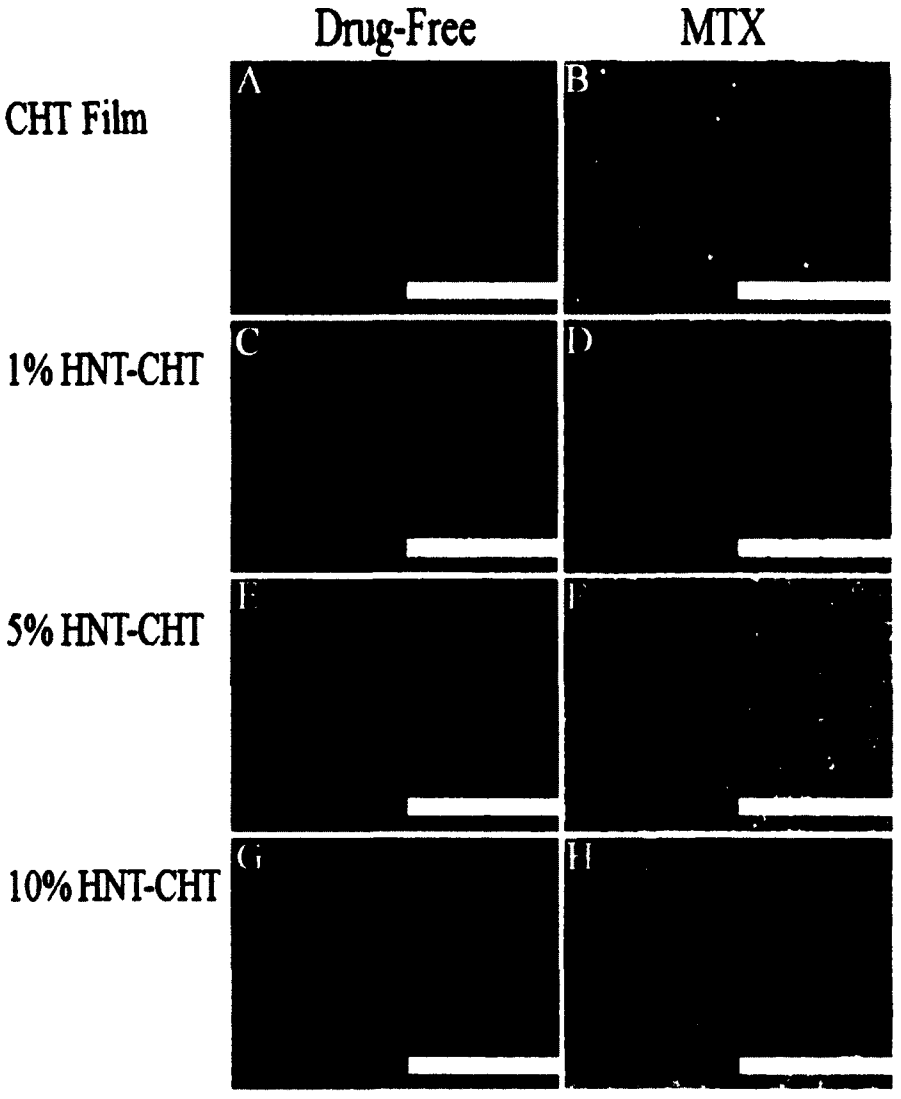


**Figure 6-3:** 10x Phase contrast images scale bars represent 200μm. A, C, E, and G are images of non-drug-loaded films at 0%, 1%, 5% and 10% HNT, respectively. B, D, F, and H are images of drug loaded films at 0%, 1%, 5% and 10% HNT, respectively.

6.3.1.3 *FE-SEM Imaging*

FE-SEM imaging was done to compare of the surface morphologies of chitosan films, HNT chitosan films, and MTX-HNT chitosan films. The comparison helped to assess the surface properties and identify micro and nano scale features of different film composites. **Figure 6-4** shows FE-SEM images of chitosan film composites with no methotrexate, while **Figure 6-5** shows FE-SEM images of chitosan film composites with methotrexate.

**Figure 6-4** shows FE-SEM images of chitosan film composites at different magnifications. Chitosan films alone show few features except the rare appearance of non-uniform 500 nm size particles (**Figure 6-4** A-C). The 1% HNT chitosan film images show a somewhat uniform distribution of HNTs and small sized aggregates (**Figure 6-4** D-F). The 5% HNT chitosan films images show many different sized HNTs aggregates and a few single HNTs (**Figure 6-4** G-I). The 10% HNT chitosan film images show many single HNTs but the majority of HNTs have aggregated into large clusters within the film (**Figure 6-4** J-L).

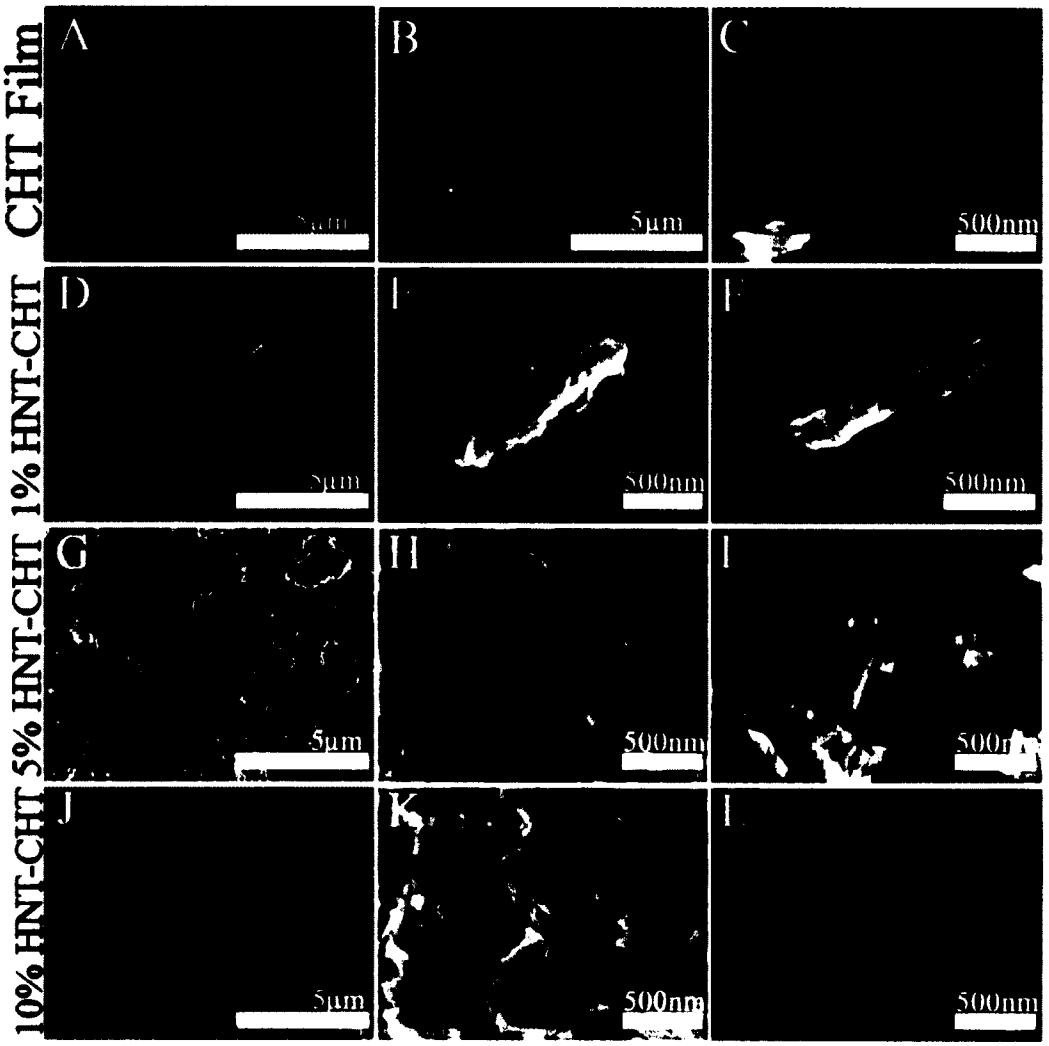


**Figure 6-4:** FE-SEM images of chitosan film composites without drug. A-C Chitosan films with 0% HNTs and without MTX. D-F Chitosan films with 1% HNTs and without MTX. G-I Chitosan films with 5% HNTs and without MTX. J-L Chitosan films with 10% HNTs and without MTX.

**Figure 6-5** shows FE-SEM images of chitosan film composites at different magnifications. 1% MTX-HNT chitosan film images show sparsely distributed HNTs (**Figure 6-5** D-F). The surface of the tubes has MTX coatings, and at higher magnifications, MTX crystals can be seen on the surface of the HNTs. The 5% HNT

chitosan films images show many small HNTs aggregates and a few single HNTs (**Figure 6-5** G-I). **Figure 6-5** H shows a pore resulting from MTX-HNTs protruding through the surface of the film. **Figure 6-5** I shows MTX-HNT completely immersed within the film. The 10% HNT chitosan film images show very few singular HNTs and most of the HNTs have aggregated into large clusters greater than 50 μm in diameter (**Figure 6-5** J-L). In all MTX-HNT (**Figure 6-5** D-L) groups, HNTs appear to be immersed within the film, although some may be protruding from the surface, creating pores.

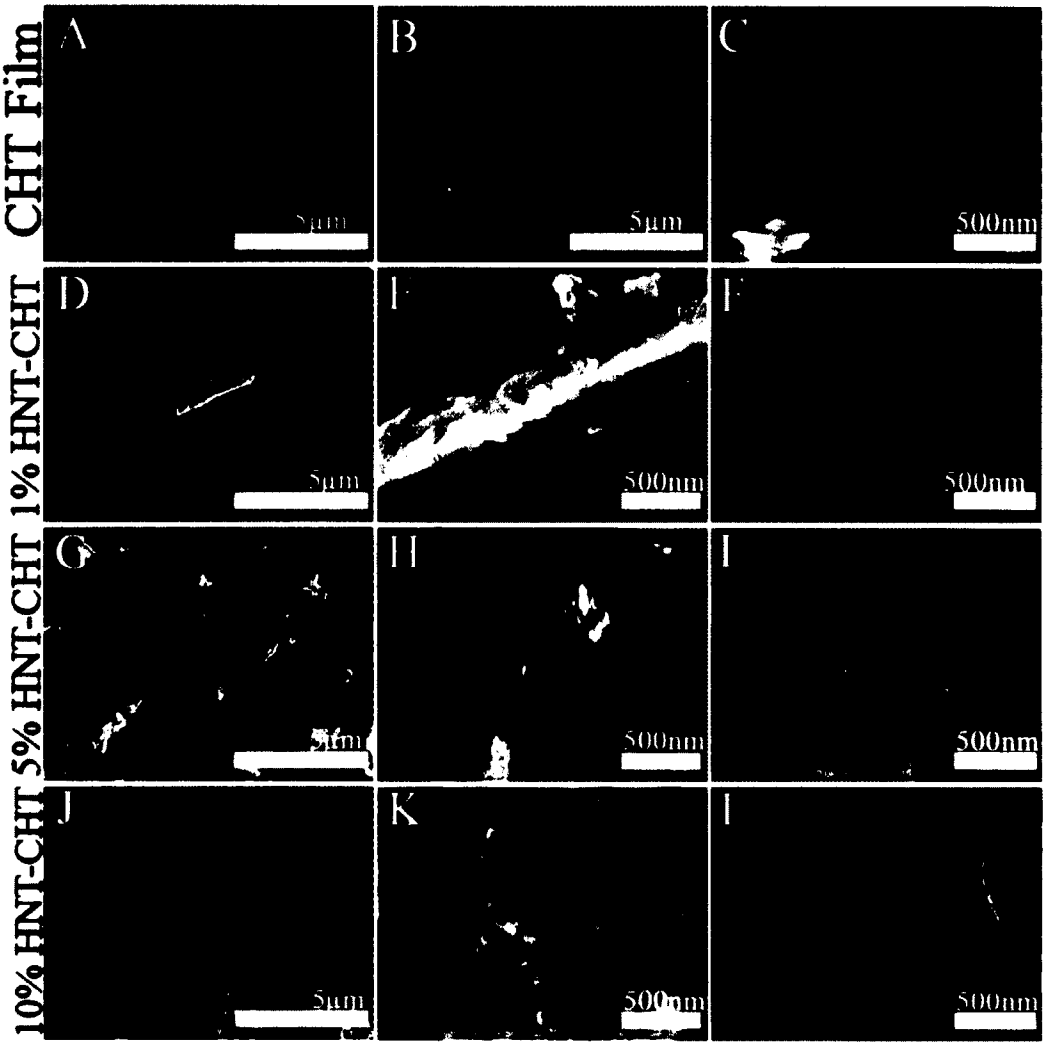


**Figure 6-5:** FE-SEM images of chitosan film composites with methotrexate. A-C Chitosan films with 0% HNTs and without MTX. D-F Chitosan films with 1% MTX-HNTs. G-I Chitosan films with 5% MTX-HNTs the circle indicates a pore, arrow points to pores. J-L Chitosan films with 10% MTX-HNTs.

### 6.3.2 Release Study

The release profile of MTX from MTX and MTX-HNT-doped chitosan films was determined to estimate the amount of drug eluted from the HNTs over a period of 24 hours and over 7 days (**Figure 6-6**). This study was carried out to determine if MTX and MTX-HNT-doped chitosan films elute enough to inhibit cell proliferation *in vitro*.

**Figure 6-6** shows the trend of the MTX release over a 24-hour time period for 1 mg/ml MTX chitosan films, 1% MTX-HNT chitosan films, 5% MTX-HNT chitosan films and 10% MTX-HNT chitosan films. The amount of MTX release was calculated from **Eq. 6-1**, which was derived from a standard curve for MTX concentrations absorbance values obtained at 300 nm wavelength via a NANODROP 2000 spectrophotometer.

$$y = 0.047x + 0.015, \qquad \textbf{Eq. 6-1}$$

where $y$ is the absorbance value and $x$ is the MTX concentration in μg.

The experiment was carried out in triplicate to reduce error and to check for reproducibility of results. The values are the mean of reading of MTX release from chitosan film composites at the respective time points from the three repetitions of the experiment. The error bars reflect the standard deviation.

**Figure 6-6** shows the cumulative release of the MTX for 24 hours in the microgram to nanogram range, which is comparable to the amount used for *in vitro* assays.

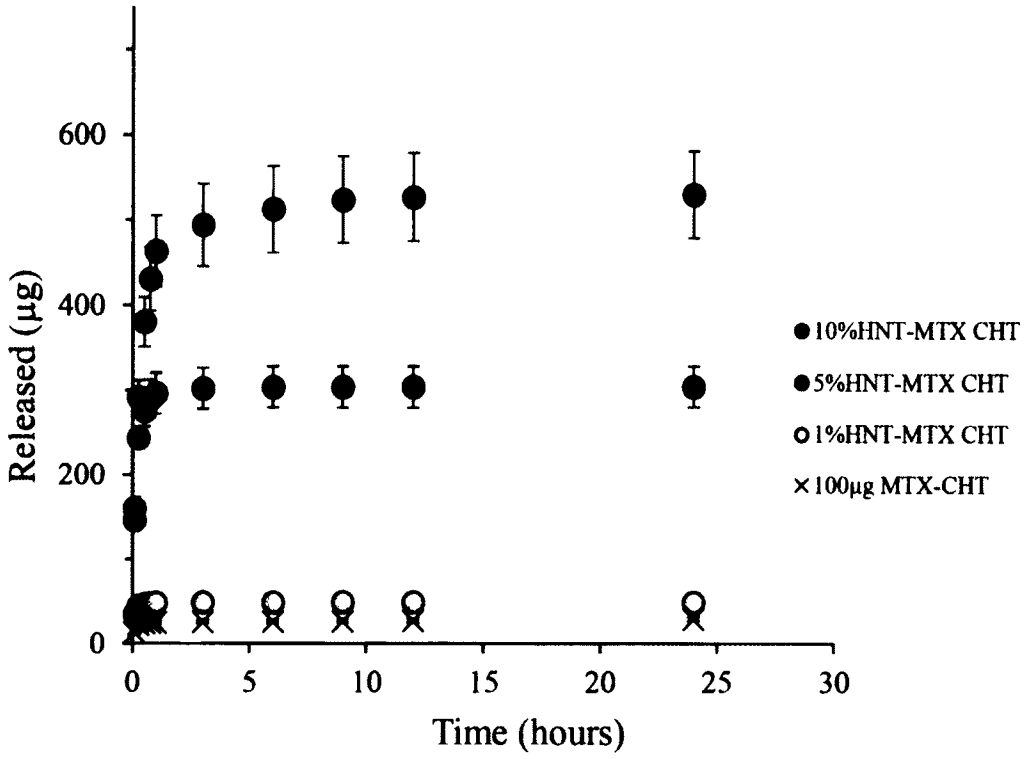


**Figure 6-6:** Mean Cumulative Release profile for Chitosan Composite Films at 24 hours mean of n = 9 for each concentration +/- standard deviation.

The graph of the release profile study for MTX from chitosan composite films for 7 days is given in **Figure 6-7**. The experiment was repeated three times to reduce error and to check for reproducibility of the results. The values are the means of the readings of MTX from chitosan composite films at the respective time points recorded from the repetitions of the experiments. The error bars reflect the standard deviation.

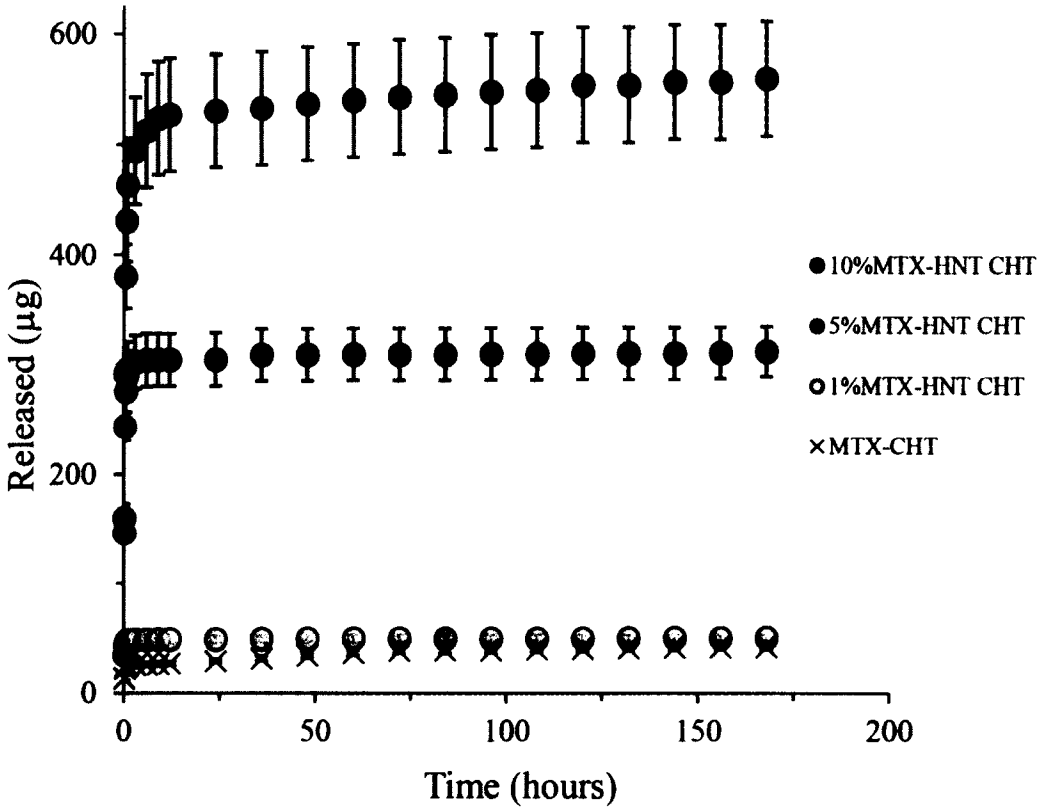


**Figure 6-7:** Mean Cumulative Release profile for chitosan film composites for Seven Days mean of n = 9 for each concentration +/- standard deviation.

The release of MTX from MTX-HNT chitosan films was extended and sustained for 7 days. In the first 24 hours, from the three different samples, an average of 54.5%± 6% of loaded MTX was released and after 7 days an average 56.4%±6% of loaded MTX was released. The film chitosan film alone on released 29.3%±2% within the first 24 hours and 42.6%±2.3% after 7 days. The release for 24 hours and 7 days were in the microgram and nanogram range for all samples and well within the range of MTX concentrations required for commonly *in vitro* assays.

The release profile of MTX from chitosan composite films suggest that the majority of the MTX localized in the films and this was responsible for the initial burst

release. Even with the ~80% of the drug being localized in the films, the release is in nano and micrograms, which is well within the range of MTX concentrations required for a cellular response in *in vitro* assays. Results obtained from the seven-day release profiles are promising, as HNTs release MTX continuously, even with the majority released in the first 24 hrs, as opposed to free drug which may be metabolized by the cells within the first 2-3 days. A sustained release of MTX is beneficial because film composite can be implanted, used to coat tumors and surrounding areas, stents and other fiducials once, yet sustain a release in the cancerous tissues for more than seven days thus reducing the need for multiple injections of chemotherapeutic drugs (prostate, breast and bone cancer). The approach may also be promising in that MTX-doped chitosan composite films could provide a localized and controlled drug release as a biodegradable chemotherapeutic patch for epithelial cell, mouth, and skin cancers for example. Films could be additionally doped with HNTs bearing DNA and/or p-GP blockers as a part of a sequential delivery and synergistic drug gene combination.

The release of MTX was not extended beyond seven days because *in vitro* experiments would only focus on the first 7 days and primarily on the first 3- 5 days. The comparison of the four composite films, 1 mg/ml MTX chitosan films, 1% MTX-HNT chitosan films, 5% MTX-HNT chitosan films and 10% MTX-HNT chitosan films, demonstrated films could sustain a release of low and high concentration for more than 7 days, and the release profile did not differ significantly when using different concentrations of HNTs.

**Figure 6-8** compares the percentage of drug release between MTX-loaded HNTs, MTX-HNT chitosan film composites and MTX chitosan films.

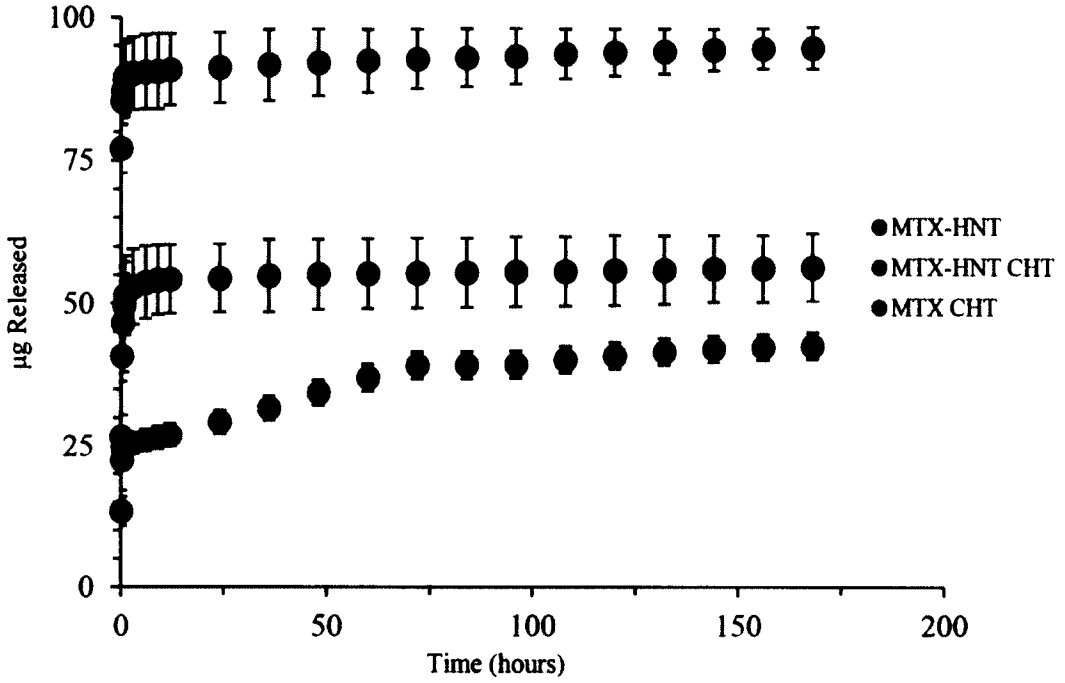


**Figure 6-8:** Seven Day Mean Release Comparison MTX-HNTs, MTX-HNT-CHT films and MTX-CHT films +/- standard deviation.

Initial studies of MTX release from HNTs (Chapter 5) showed that the majority of the drug loaded was released within the first 24 hours. The initial burst release was more than 70% of the drug loaded. The subsequent embedding of drug-loaded HNTs into chitosan films reduced the burst release by more than half. At 24 hours the MTX-HNT chitosan films only released 54% of the drug loaded while free MTX HNTs released 85% of the drug loaded. At 7 days free MTX-HNTs released more than 90 % of the drug loaded and MTX-HNT chitosan films only released 56%. Chitosan films controlled the release of MTX from HNTS effectively and reduced the release at 7 days by 34 %, thus, extending the release beyond 7 days.

### 6.3.3 Cell Culture and Seeding

#### 6.3.3.1 *XTT Cell Proliferation Assay*

A cell proliferation assay was performed to ascertain whether chitosan film composites could inhibit osteosarcoma cells proliferation. The cell proliferation of osteosarcoma cells incubated with MTX chitosan film composites were compared to proliferation of osteosarcoma cells treated with chitosan film composites with no drug. The negative control for this experiment was untreated cells. Following seeding and incubation, the plates were analyzed at 24, 72, 120 and 168 hours via XTT cell proliferation assay. The media in all plates was changed at 72 and 120 hours because cells in the control well were becoming confluent and the cells had used the majority of nutrients in the media.

After the absorbance was measured, the data were exported to Excel files. The data were subsequently processed and normalized by the absorbance at each time point of the untreated cells. IBM SPSS software and a paired t-test were used for statistical analysis (Appendix A **Table A-5**). **Figure 6-9** through **Figure 6-12** show graphs of the cell proliferation from 24-168 hours.

**Figure 6-9** shows the proliferation at 24 hours. At 24 hours the drug had yet to affect cellular proliferation in the groups treated with 1 mg/ml MTX chitosan films, 1% MTX-HNT chitosan films, 5% MTX-HNT chitosan films and 10% MTX-HNT chitosan films. The 100 μg (1 mg/ml) MTX chitosan film group proliverated more than any other group, and this activity may indicate that osteosarcoma cells proliferate more in the presence chitosan films; the chitosan film alone showed a similar level of proliferation. The methotrexate is not likely to have affected proliferation because at 24 hours it is not

completely metabolized and typically takes 1-3 days to elicit a response. This trend was also noticed in 5% and 10 % HNT groups as MTX groups showed more proliferation at 24 hours than their drug free counterparts. The presence of 5% and 10% concentrations of HNTs did seem to reduce the proliferation of cells to almost half when compared to untreated cells. The 1% HNT-MTX group was the only group at 24 hours that reduced proliferation when compared to the 1% HNT drug free group.

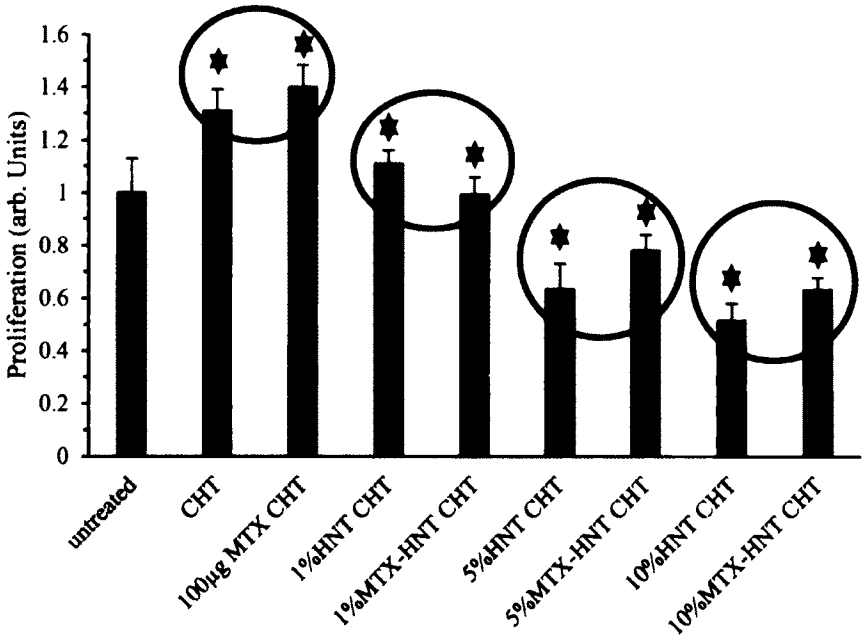


**Figure 6-9:** Mean Cell Proliferation at 24 hours of n = 9 samples ± standard deviation. Statistical analysis was applied with IBM SPSS 22.0 at $\alpha = .05$, and the black stars indicate significant difference exists when encircled groups are compared.

**Figure 6-10** shows the proliferation at 72 hours. At 72 hours the drug began to affect cellular proliferation in the groups treated in all groups. The chitosan film group showed a higher level of proliferation than any other group, suggesting that osteosarcoma cells proliferate more in the presence chitosan films. The 1% MTX-HNT group showed the most proliferation reduction when compared to 1%HNT, reducing proliferation by

nearly half. The 1% MTX-HNT was as effective as the 100 μg MTX chitosan films at inhibiting proliferation.

The presence of 5% and 10% concentrations of HNTs continued to stifle the proliferation of cells by more than half when compared to untreated cells. The 5% MTX-HNT reduced proliferation by nearly 60%, but 5 mg plain HNT reduced proliferation by ~50%, and it became difficult to determine if the effect was brought on by MTX or the HNTs. The 10% MTX-HNT and 10% HNT sets behaved similarly, and even though the 10% MTX-HNT showed the highest reduction in proliferation, the presence of MTX in this group had little effect by comparison to the 10% groups. At 72 hours the media was changed as it had begun to change colors, indicating that cells had absorbed the majority of the nutrients.

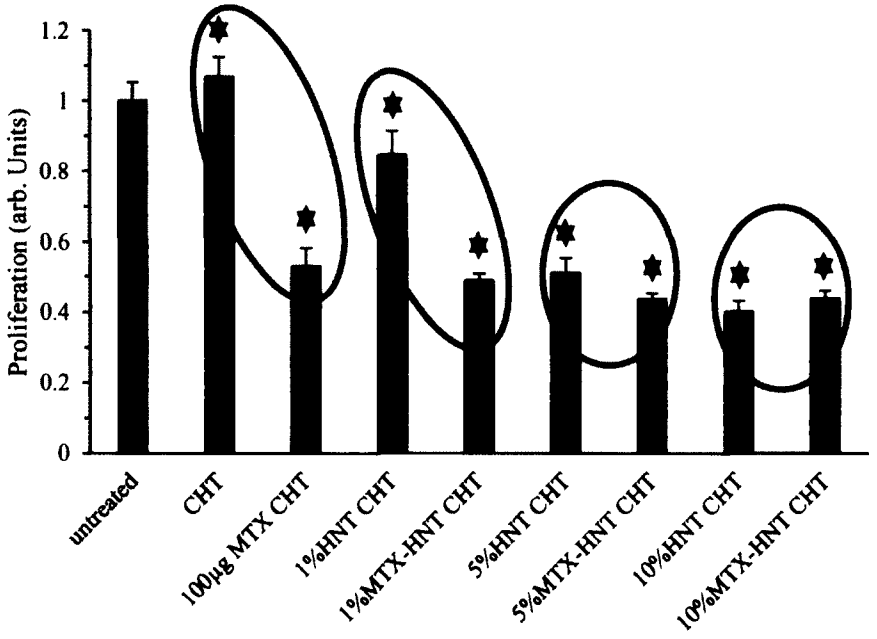


**Figure 6-10:** Mean Cell Proliferation at 72 hours of n = 9 samples ± standard deviation. Statistical analysis was applied with IBM SPSS 22.0 at $\alpha = .05$, and the black stars indicate significant difference exists when encircled groups are compared.

**Figure 6-11** shows the proliferation at 120 hours. At 120 hours, the drug continued to affect cellular proliferation in all groups treated with MTX. The chitosan film group showed a higher level of proliferation (almost twice the proliferation of untreated group). This increased proliferation may be caused by increased surface area in chitosan films for cell to proliferate and grow to. 1% HNT films showed a comparable amount of growth and proliferation. The 1% MTX-HNT group showed the most proliferation reduction when compared to 1% HNT reducing proliferation by nearly two thirds. The 1% MTX-HNT was more effective than 100 μg MTX chitosan films at inhibiting proliferation while the drug dosage was the same.

The presence of 5% and 10% concentrations of HNTs continued to stifle the proliferation of cells by more than half when compared to untreated cells. The 5% MTX-HNT reduced proliferation by more than 50%, but 5% HNT reduced proliferation by ~30%. The 10% HNT-MTX only reduced proliferation 5% more than the 10% HNT set even though the 10% HNT-MTX showed the highest reduction in proliferation. The presence of MTX in the 10% HNT group apparently had little effect by comparison of the 10% groups. At 120 hours the media was changed as it had begun to change colors, indicating cells had absorbed the majority of the nutrients.

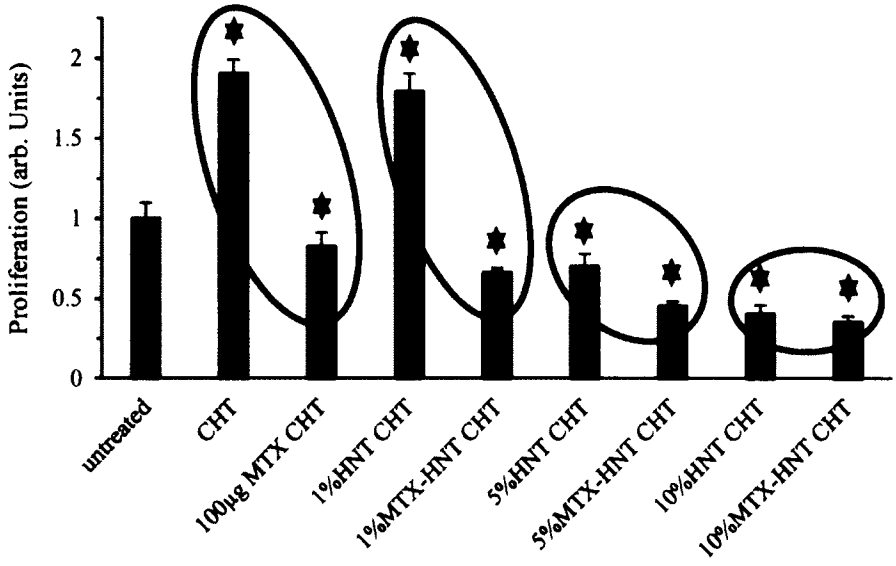


**Figure 6-11:** Mean Cell Proliferation at 120 hours of n = 9 samples ± standard deviation. Statistical analysis was applied with IBM SPSS 22.0 at $\alpha = .05$, and the black stars indicate significant difference exists when encircled groups are compared.

**Figure 6-12** shows the proliferation at 168 hours. At 168 hours, the drug continued to affect cellular proliferation in the in all groups treated with MTX. The chitosan film group continued to show a higher level of proliferation than any other group, although at this point it was comparable to untreated cells, possibly because cells finally proliferated throughout the entire chitosan film. The 1% MTX-HNT and 5% MTX-HNT groups showed the most proliferation reduction when compared to 1% HNT and 5% HNT, respectively. Proliferation was reduced by more than half by comparison to drug free groups. The 1% MTX-HNT was more effective than the 100 µg MTX chitosan films at inhibiting proliferation, even though the drug concentration was the same.

The presence of 5% and 10% concentrations of HNTs continued to stifle the proliferation of cells by more than half when compared to untreated cells. The 5% MTX-HNT reduced proliferation by 80% but 5% HNT reduced proliferation by ~58%. The

10% HNT-MTX only reduced proliferation 10% more than 10% HNT, even though the 10% HNT-MTX showed the highest reduction in proliferation.

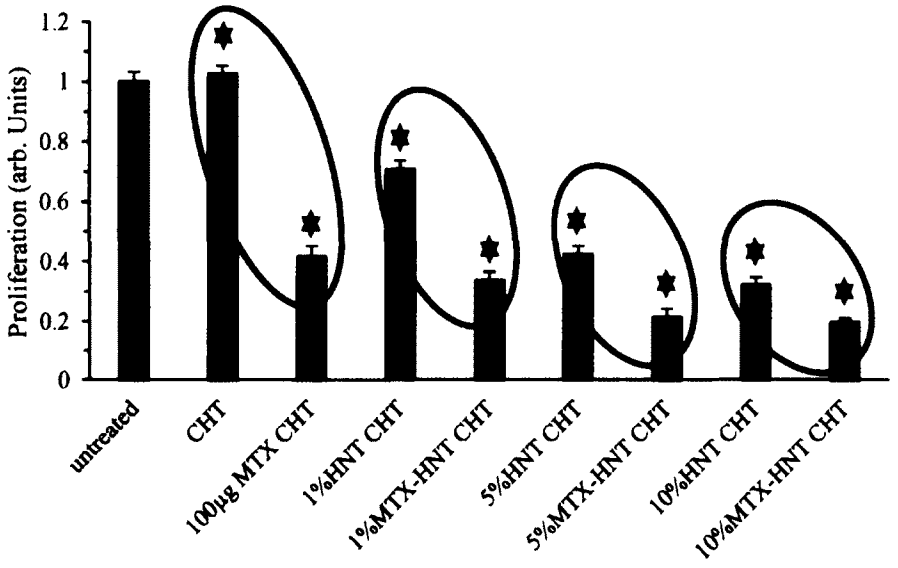


**Figure 6-12:** Mean Cell Proliferation at 168 hours of n = 9 samples ± standard deviation. Statistical analysis was applied with IBM SPSS 22.0 at $\alpha = .05$, and the black stars indicate significant difference exists when encircled groups are compared.

**Figure 6-13** compares cell proliferation over the 7 day period (168 Hours). Even though 5%MTX-HNT and 10%MTX-HNT chitosan films showed the largest reductions in proliferation over the 7 day period, 5 and 10% HNT films significantly reduced the cellular proliferation and limited the response shown from the drug released from the MTX-HNT groups. All groups were more effective than 100 µg MTX chitosan films at every time point after 24 hours, which may indicate that HNTs can localize the drug at the cell, as opposed to it being diluted in the media.

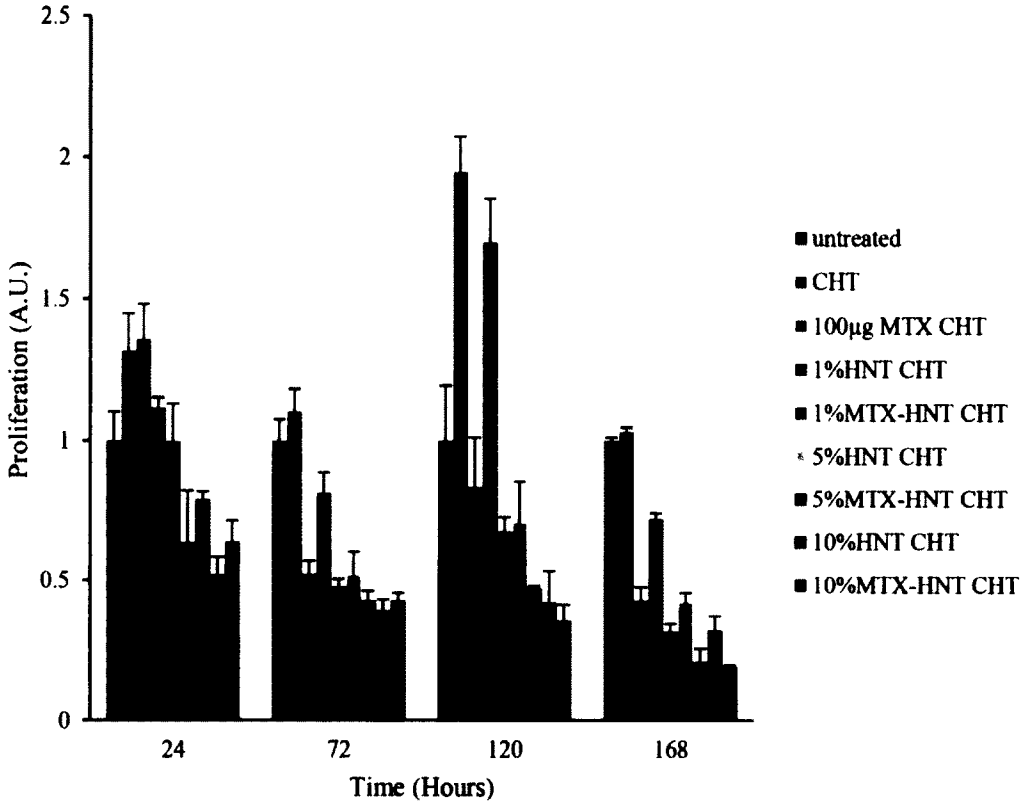


**Figure 6-13:** Seven Day Mean Proliferation Comparison normalized by untreated cells proliferation.

The 1% MTX-HNT chitosan film showed the highest reduction in proliferation when compared to 1% HNT chitosan films, by reducing proliferation by more than 60% by Day 7. The 1 % HNT chitosan films and 0% HNT chitosan stimulated cell growth until the cells became confluent, and at confluency, chitosan films showed the highest rate of proliferation while 1% HNT chitosan films show the lowest reduction in proliferation of all chitosan films embedded with HNTs. The 1% HNT chitosan films affected cell proliferation the least when administered alone and yielded the most anti-proliferative effect when loaded with methotrexate.

Cell proliferation seemed to return at 120 hours, but this return can be an effect of changing the media at 72 hours as it reduced the concentration of drug present. This effect was not noticed at 168 hours as cells did not recover from drug administration.

6.3.3.2 *Live/Dead Assay*

A live/dead cell viability assay was performed to determine whether MTX-loaded chitosan composite films induced cell death in osteosarcoma cells. The live/dead assay images of osteosarcoma cells incubated with MTX-loaded chitosan composite films were compared with live/dead images of osteosarcoma cells treated with drug free loaded chitosan composite films. The negative control for this experiment was untreated cells. Following seeding and incubation, the plates were treated with the live/dead cell viability assay kit and imaged at 24, 72, 120 and 168 hours via the Olympus BX51 fluorescent microscope with FITC and TRITC filters. The media in all plates was changed at 72 and 120 hours as cells in the control well were becoming confluent and the cells had used the majority of nutrients in the media.

The images were saved and processed with ImageJ software. **Figure 6-14** to **Figure 6-25** show live/dead results from 24-168 Hours.

Osteosarcoma cells in monolayer culture proliferated and became nearly confluent after 24 hours with little cell death observed (see **Figure 6-14** A-C).

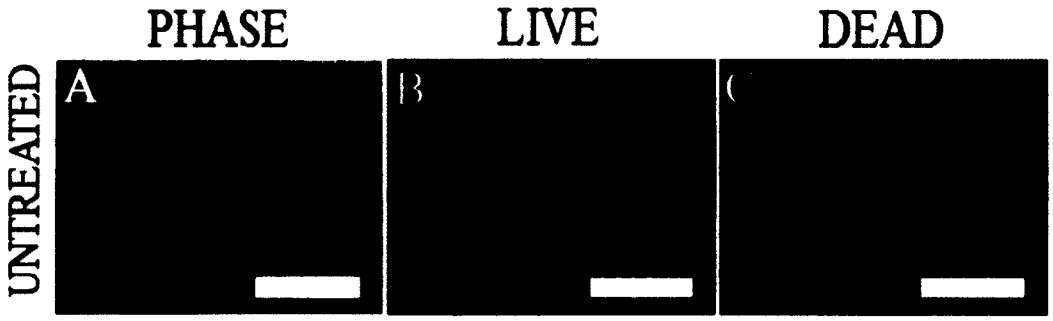


**Figure 6-14:** Untreated cells at 24 Hours scale bar indicate 500μm. A= Phase contrast; B= Live Dead assay showing live cells (green); C= Dead assay showing dead cells (red).

Osteosarcoma cells were also unaffected by the drug-free chitosan film composites (**Figure 6-15** A-L). Cells proliferated and achieved confluence comparable to normal, untreated cells (compare **Figure 6-14** B and C with **Figure 6-15** B, E, H, K and C, F, I, L).

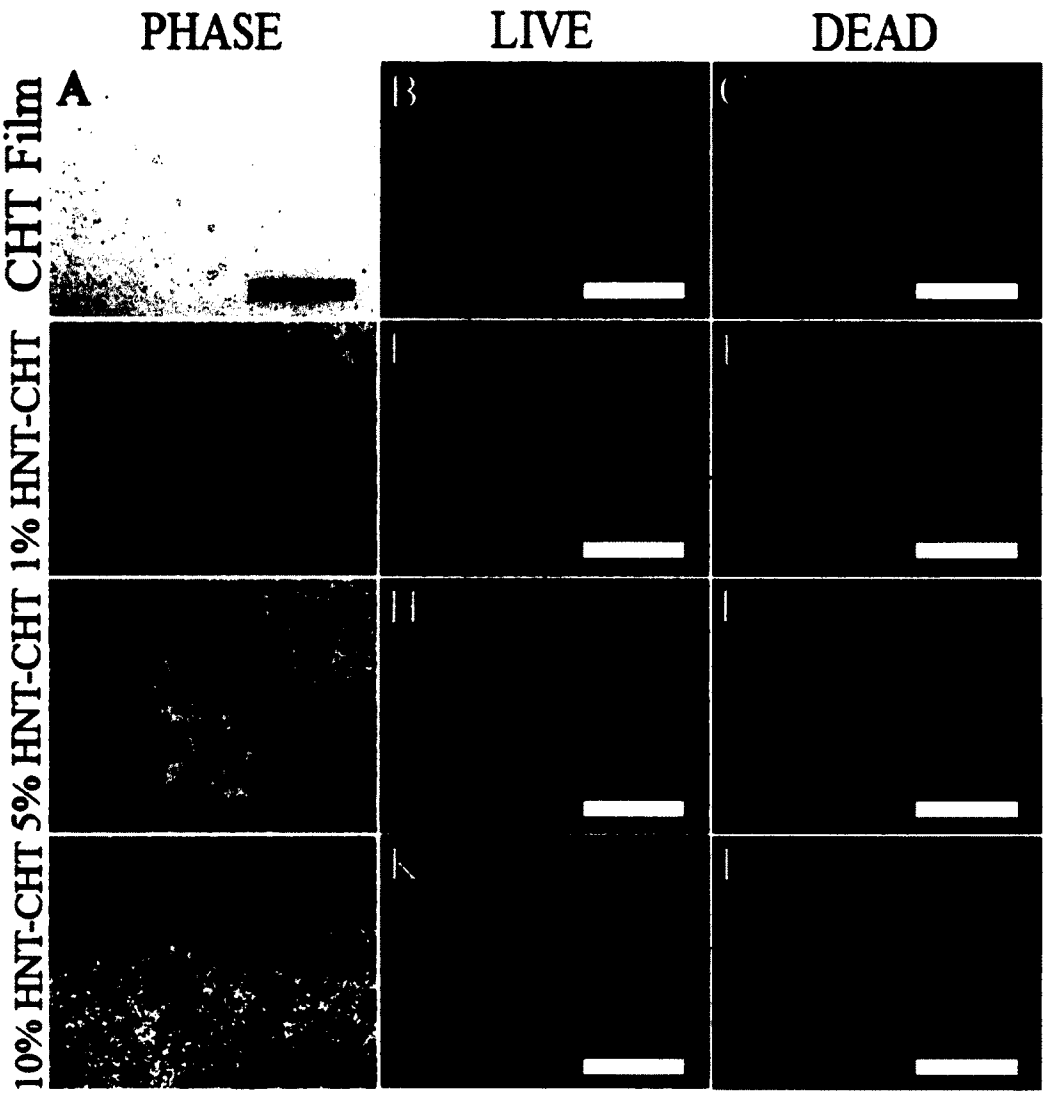


**Figure 6-15:** Cytotoxic response to Chitosan Film Composites at 24 Hours scale bar indicates 500μm. (A-C) Group 1: Osteosarcoma cell cultures with chitosan films. (D-F) Group 2: Osteosarcoma cells exposed to 1% HNT chitosan films. (G-I) Group 3: Osteosarcoma cells exposed to 5% HNT chitosan films (J-L) Group 4: Osteosarcoma cells exposed to % HNT chitosan films. A, D, G and J = Phase contrast; B, E, H and K = Live Dead assay showing live cells (green); C, F, I and L = Dead assay showing dead cells (red). The brown coloration in D, G and J is caused by the high concentration of HNTs.

HNTs could be seen clearly as particulate material (**Figure 6-16** D, G and J). At 24 hours, in MTX (100 μg) chitosan films groups, the cellular response was different from untreated cells and cell growth decreased (**Figure 6-16** A-C). At 24 hours, in Group 2, osteosarcoma cells exposed to 1% MTX-HNT chitosan films showed a similar reduction in cell growth as MTX (100 μg) chitosan films compared with untreated cells (**Figure 6-16** D-F). At 24 hours, in Group 3, osteosarcoma cells exposed to 5% MTX-HNT chitosan films showed a greater reduction in cell growth as compared to MTX group and 1% MTX-HNT chitosan films group (**Figure 6-16** G-I). At 24 hours, in Group 4, osteosarcoma cells exposed to 10% MTX-HNT chitosan films showed the greatest reduction in cell growth as compared to MTX group, 5% MTX-HNT chitosan films and 1% MTX-HNT chitosan film group (**Figure 6-16** J-l). However, only a few dead cells were observed in all groups (**Figure 6-16** C, F, I and L).

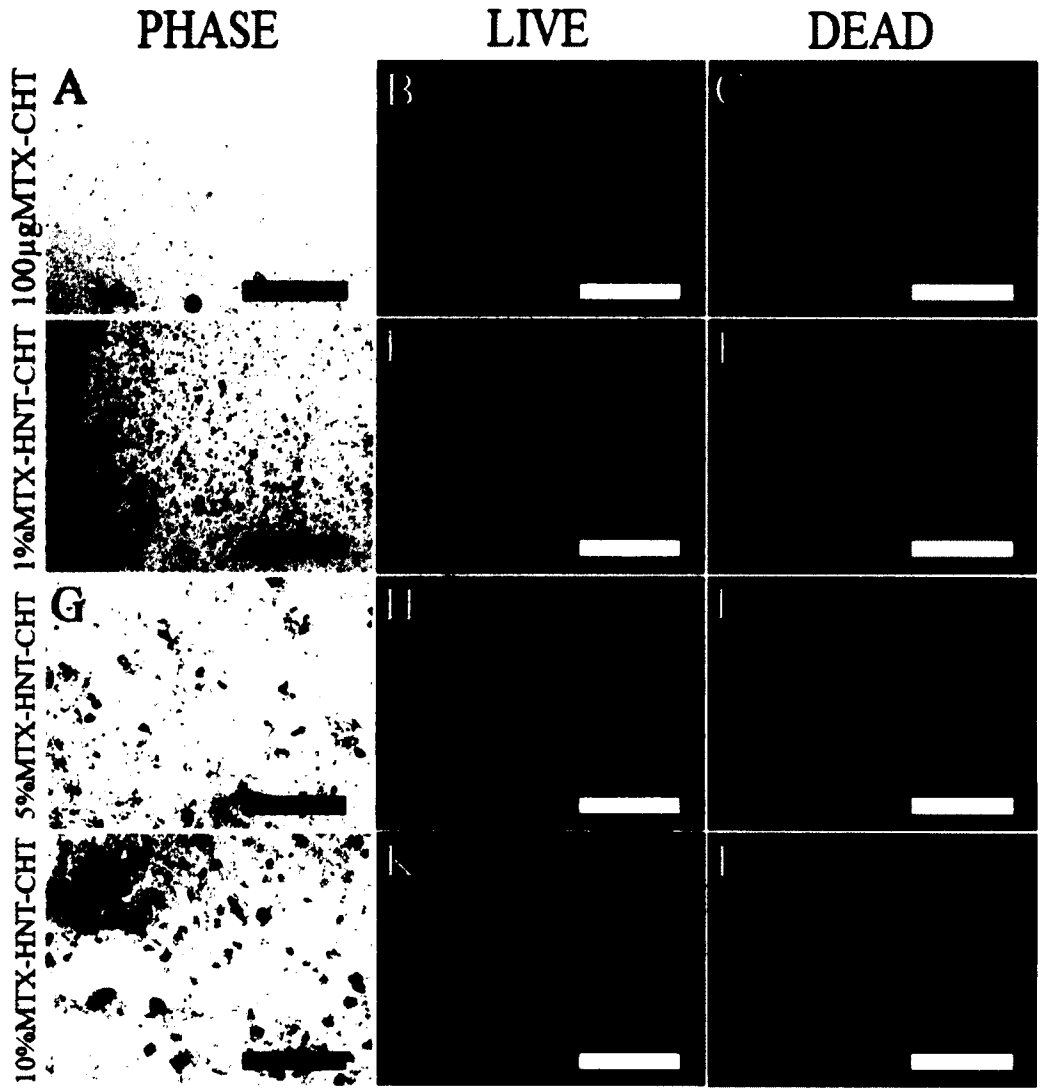


**Figure 6-16:** Cellular response to MTX-loaded chitosan film composites HNTs at 24 Hours. Scale bar represents 500µm (A-C) Group 1: Osteosarcoma cell cultures with MTX (100 µg) chitosan films addition. (D-F) Group 2: Osteosarcoma cells exposed to 1% MTX-HNT chitosan films. (G-I) Group 3: Osteosarcoma cells exposed to 5% MTX-HNT chitosan films. (J-L) Group 4: Osteosarcoma cells exposed to 10% MTX-HNT chitosan films. A, D, G and J = Phase contrast; B, E, H and K = Live Dead assay showing live cells (green); C, F, I and L = Dead assay showing dead cells (red). The brown coloration in D, G and J is caused by the high concentration of HNTs.

Osteosarcoma cells in monolayer culture proliferated and became confluent within 2-3 days with little cell death observed (see **Figure 6-17** A-C).

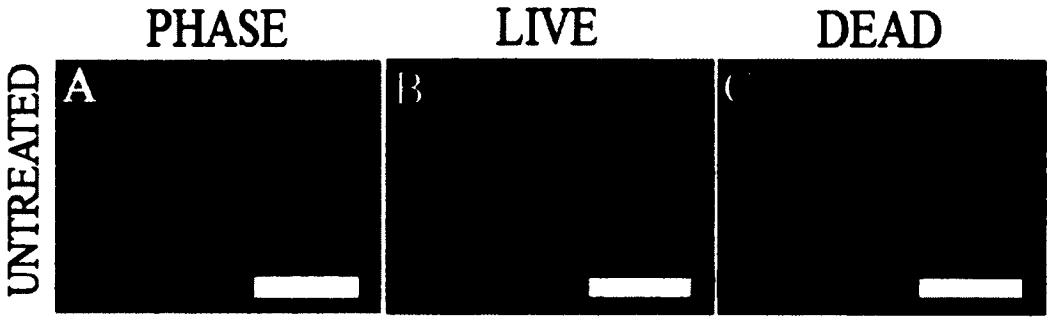


**Figure 6-17:** Untreated cells at 72 Hours. Scale bar represents 500μm A= Phase contrast; B= Live Dead assay showing live cells (green); C= Dead assay showing dead cells (red).

Osteosarcoma cells were also unaffected by chitosan composite films (**Figure 6-18** A-L). Cells proliferated and achieved confluence exceptionally well compared with normal, untreated cells (compare **Figure 6-17** B and C with **Figure 6-18** B, E, H, K and C, F, I, L).

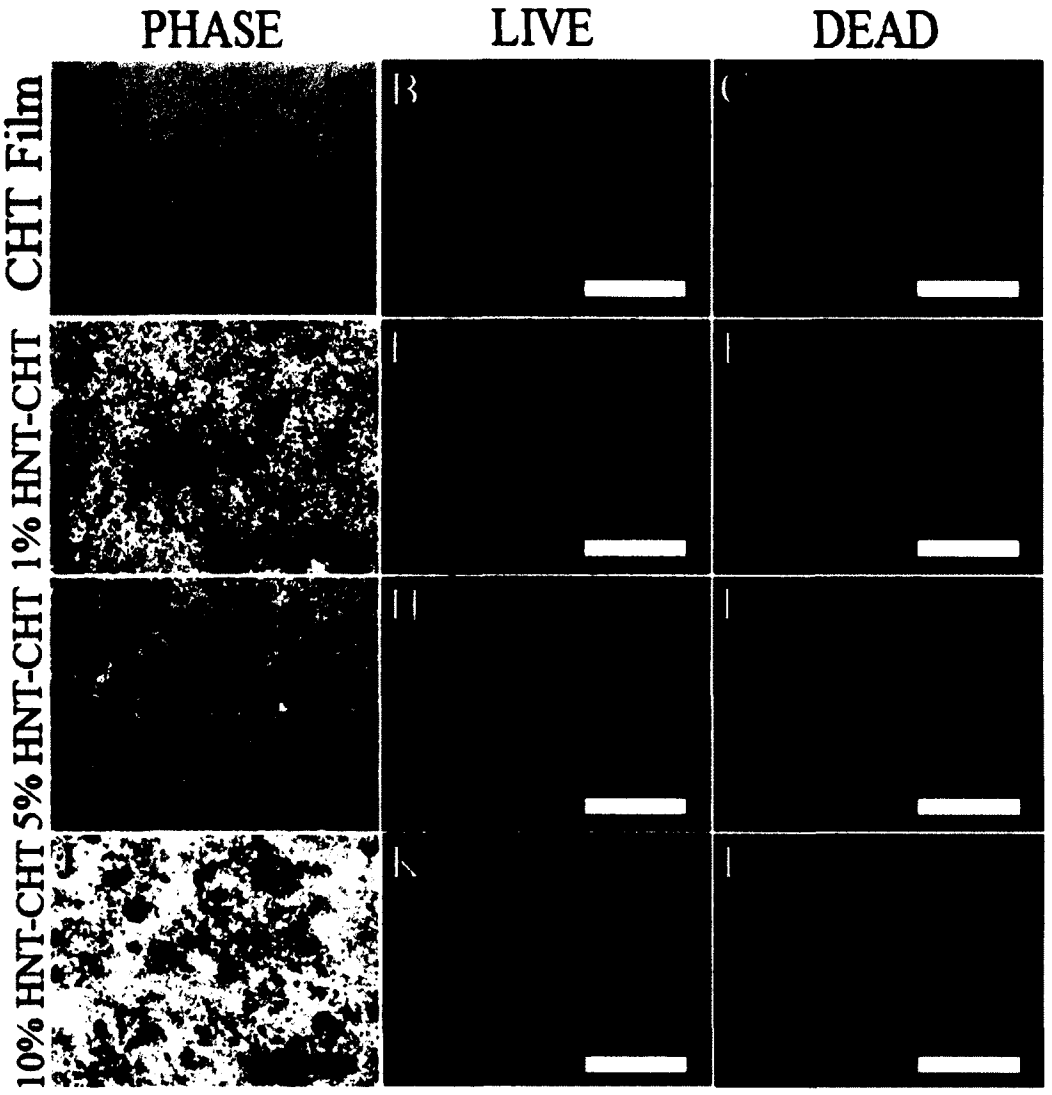


**Figure 6-18:** Cytotoxic response to Chitosan Film Composites at 72 Hours. Scale bar represents 500μm (A-C) Group 1: Osteosarcoma cell cultures with chitosan films. (D-F) Group 2: Osteosarcoma cells exposed to 1% HNT chitosan films. (G-I) Group 3: Osteosarcoma cells exposed to 5% HNT chitosan films (J-L) Group 4: Osteosarcoma cells exposed to % HNT chitosan films. A, D, G and J = Phase contrast; B, E, H and K = Live Dead assay showing live cells (green); C, F, I and L = Dead assay showing dead cells (red). The brown coloration in D, G and J is caused by the high concentration of HNTs.

At 72 hours, in MTX-treated groups, the cellular response was very different from untreated cells and the reduction in cell growth was even greater than at 24 hours (**Figure 6-19** A-C). At 72 hours, in Group 2, osteosarcoma cells exposed to 1% MTX-HNT chitosan films showed a marked reduction in cell growth compared with untreated cells and cells treated with (100 μg) MTX chitosan films (**Figure 6-19** D-F). This reduction was even greater than the reduction seen at 24 hours. At 72 hours, in Group 3, osteosarcoma cells exposed to 5% MTX-HNT chitosan films showed a greater reduction in cell growth than the MTX and 1% MTX-HNT chitosan film groups, but was greater than the reduction seen at 24 hours (**Figure 6-19** G-I). At 72 hours, in Group 4, osteosarcoma cells exposed to10% MTX-HNT chitosan films showed the greatest reduction in cell growth as compared to MTX group, 5% MTX-HNT chitosan films and 1% MTX-HNT chitosan films group and was similar to the cell growth at 24 hours (**Figure 6-19** J-L). However, only a few dead cells were observed in all groups (**Figure 6-19** C, F, I and L).

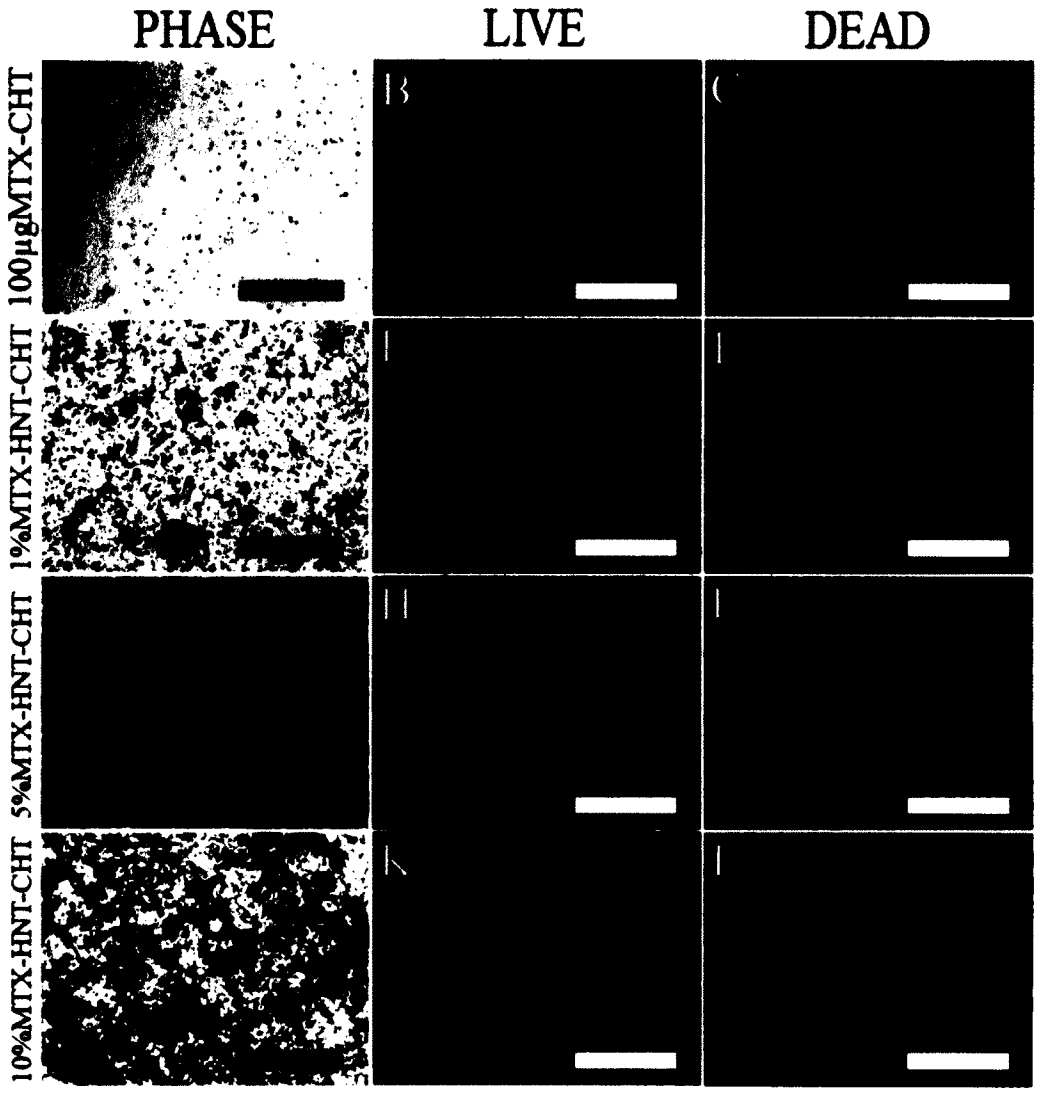


**Figure 6-19:** Cellular response to MTX-loaded chitosan film composites HNTs at 72 Hours. Scale bar represents 500µm (A-C) Group 1: Osteosarcoma cell cultures with MTX (100 µg) chitosan films addition. (D-F) Group 2: Osteosarcoma cells exposed to 1% MTX-HNT chitosan films. (G-I) Group 3: Osteosarcoma cells exposed to 5% MTX-HNT chitosan films. (J-L) Group 4: Osteosarcoma cells exposed to 10% MTX-HNT chitosan films. A, D, G and J = Phase contrast; B, E, H and K = Live Dead assay showing live cells (green); C, F, I and L = Dead assay showing dead cells (red). The brown coloration in D, G and J is caused by the high concentration of HNTs.

Osteosarcoma cells in monolayer culture continued to proliferate and maintained confluency within at 120 hours with little cell death observed (see **Figure 6-20** A-C).

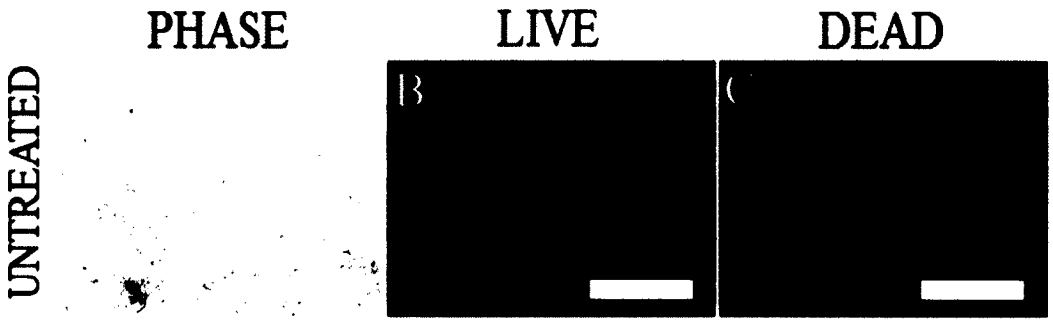


**Figure 6-20:** Untreated cells at 120 Hours. Scale bar represents 500μm A= Phase contrast; B= Live Dead assay showing live cells (green); C= Dead assay showing dead cells (red).

Osteosarcoma cells also began to show the effects of chitosan composite film groups (**Figure 6-21** A-L). Cells proliferated and achieved confluence comparable to normal, untreated cells (compare **Figure 6-20** B and C with **Figure 6-21** B and C, E, H, K and D, F, I, L) but the chitosan film composite groups had many more dead cells.

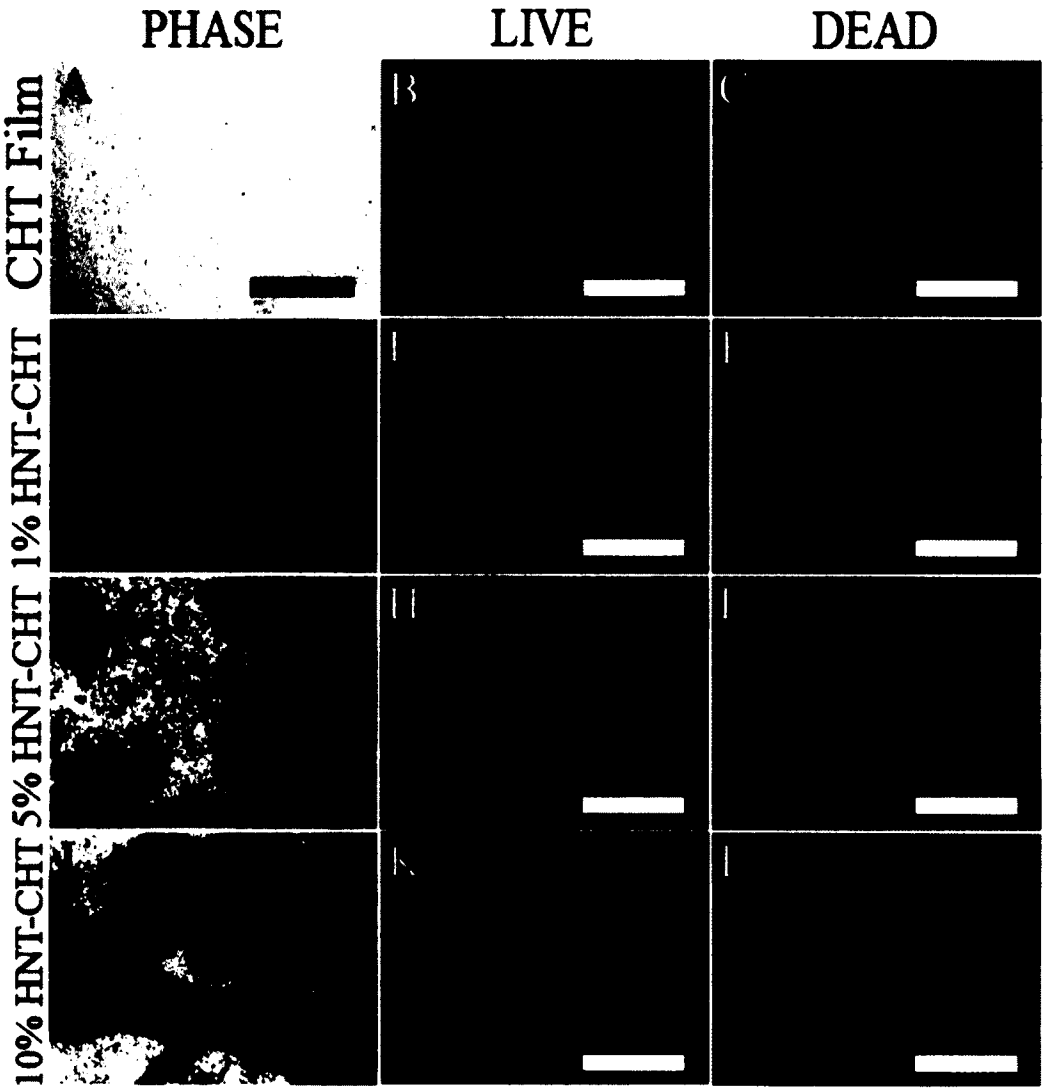


**Figure 6-21:** Cytotoxic response to Chitosan Film Composites at 120 Hours. Scale bar represents 500μm (A-C) Group 1: Osteosarcoma cell cultures with chitosan films. (D-F) Group 2: Osteosarcoma cells exposed to 1% HNT chitosan films. (G-I) Group 3: Osteosarcoma cells exposed to 5% HNT chitosan films (J-L) Group 4: Osteosarcoma cells exposed to % HNT chitosan films. A, D, G and J = Phase contrast; B, E, H and K = Live Dead assay showing live cells (green); C, F, I and L = Dead assay showing dead cells (red). The brown coloration in D, G and J is caused by the high concentration of HNTs.

At 120 hours, in MTX-treated groups, the cellular response was very different from untreated cells and the reduction in cell growth was even greater than at 72 hours (**Figure 6-22** A-C). At 120 hours, Group 2 osteosarcoma cells exposed to 1% MTX-HNT chitosan films showed less cell growth than control untreated cells and cells treated with (100 μg) MTX chitosan films (**Figure 6-22** D-F). This reduction was even greater than that seen at 72 hours. At 120 hours, in Group 3, osteosarcoma cells exposed to 5% MTX-HNT chitosan films showed a greater reduction in cell growth than the MTX group and the 1% MTX-HNT chitosan films group, and reduction was greater than seen at 72 hours (**Figure 6-22** G-H). At 120 hours, in Group 4, osteosarcoma cells exposed to 10% MTX-HNT chitosan films showed the greatest reduction in cell growth as compared to the MTX group, the 5% MTX-HNT chitosan film, and the 1% MTX-HNT chitosan film group and was greater than the reduction to the cell growth at 72 hours (**Figure 6-22** J-L). However, only a few dead cells were observed in all groups (**Figure 6-22** C, F, I and L).

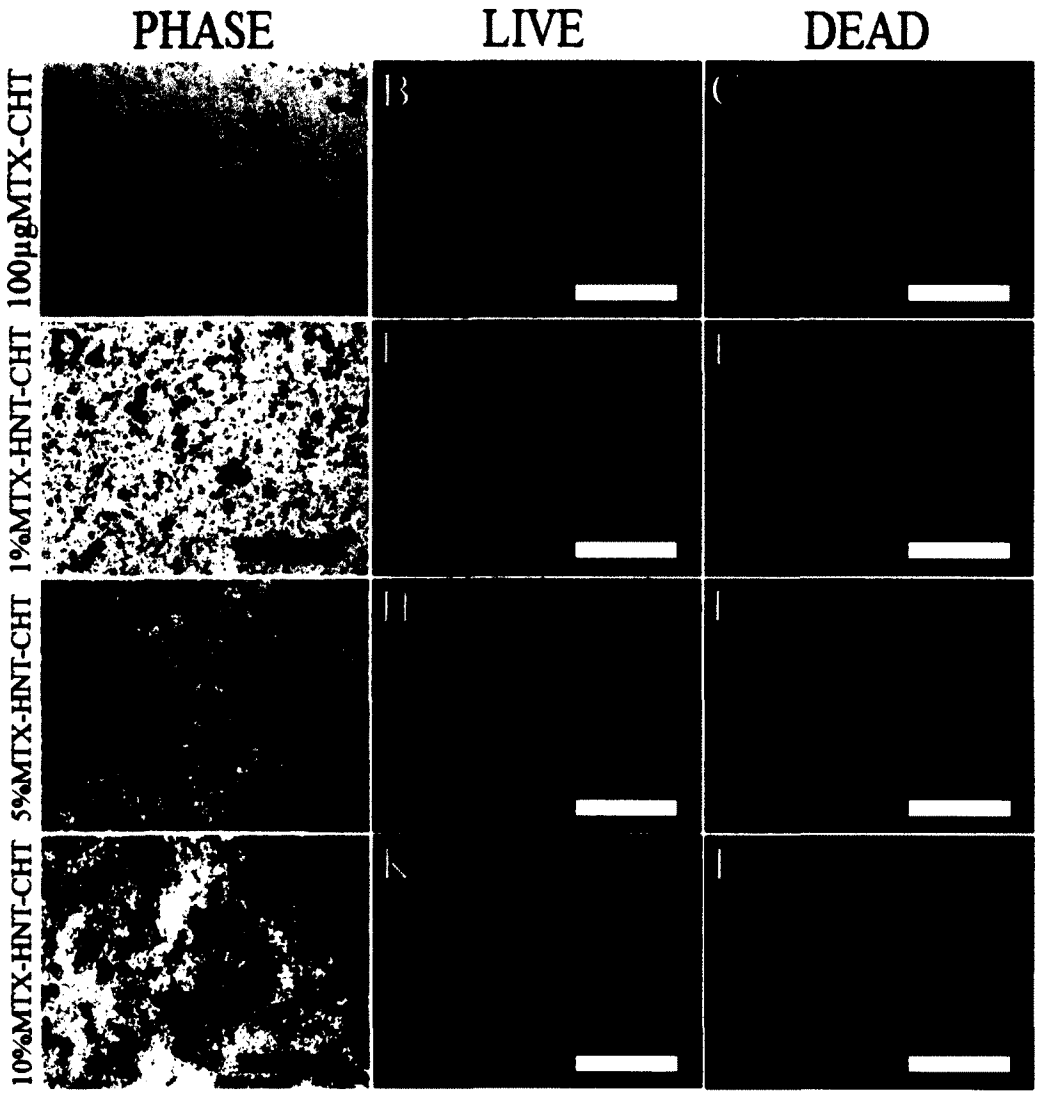


**Figure 6-22:** Cellular response to MTX-loaded chitosan film composite HNTs at 120 Hours. Scale bar represents 500µm (A-C) Group 1: Osteosarcoma cell cultures with MTX (100 µg) chitosan film addition. (D-F) Group 2: Osteosarcoma cells exposed to 1% MTX-HNT chitosan films. (G-I) Group 3: Osteosarcoma cells exposed to 5% MTX-HNT chitosan films. (J-L) Group 4: Osteosarcoma cells exposed to 10% MTX-HNT chitosan films. A, D, G and J = Phase contrast; B, E, H and K = Live Dead assay showing live cells (green); C, F, I and L = Dead assay showing dead cells (red). The brown coloration in D, G and J is caused by the high concentration of HNTs.

Osteosarcoma cells in monolayer culture continued to proliferate and maintained confluency at 168 hours with little cell death observed (see **Figure 6-23** A-C).

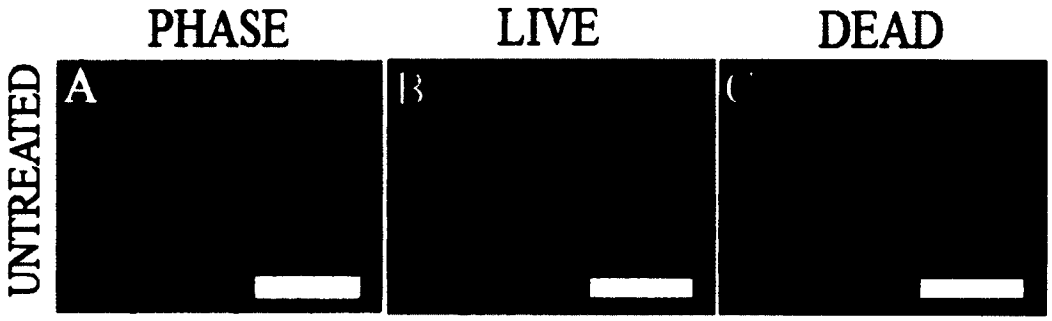


**Figure 6-23:** Untreated cells at 168 Hours. Scale bar represents 500μm A= Phase contrast; B= Live Dead assay showing live cells (green); C= Dead assay showing dead cells (red).

Osteosarcoma cells also began to show the effects of the chitosan composite film groups as they had reached full confluency and grown throughout the films (**Figure 6-24** A-L). Cells proliferated and achieved confluence comparable to normal, untreated cells (Compare **Figure 6-23** B and C with **Figure 6-24** B, E, H, K and C, F, I, L), but the chitosan composite film groups had many more dead cells. Also, confluency was reduced for 5% MTX-HNT chitosan films, and especially for 10% MTX-HNT chitosan film, compared to normal untreated cells, which indicates a more cytotoxic response at 7 days.

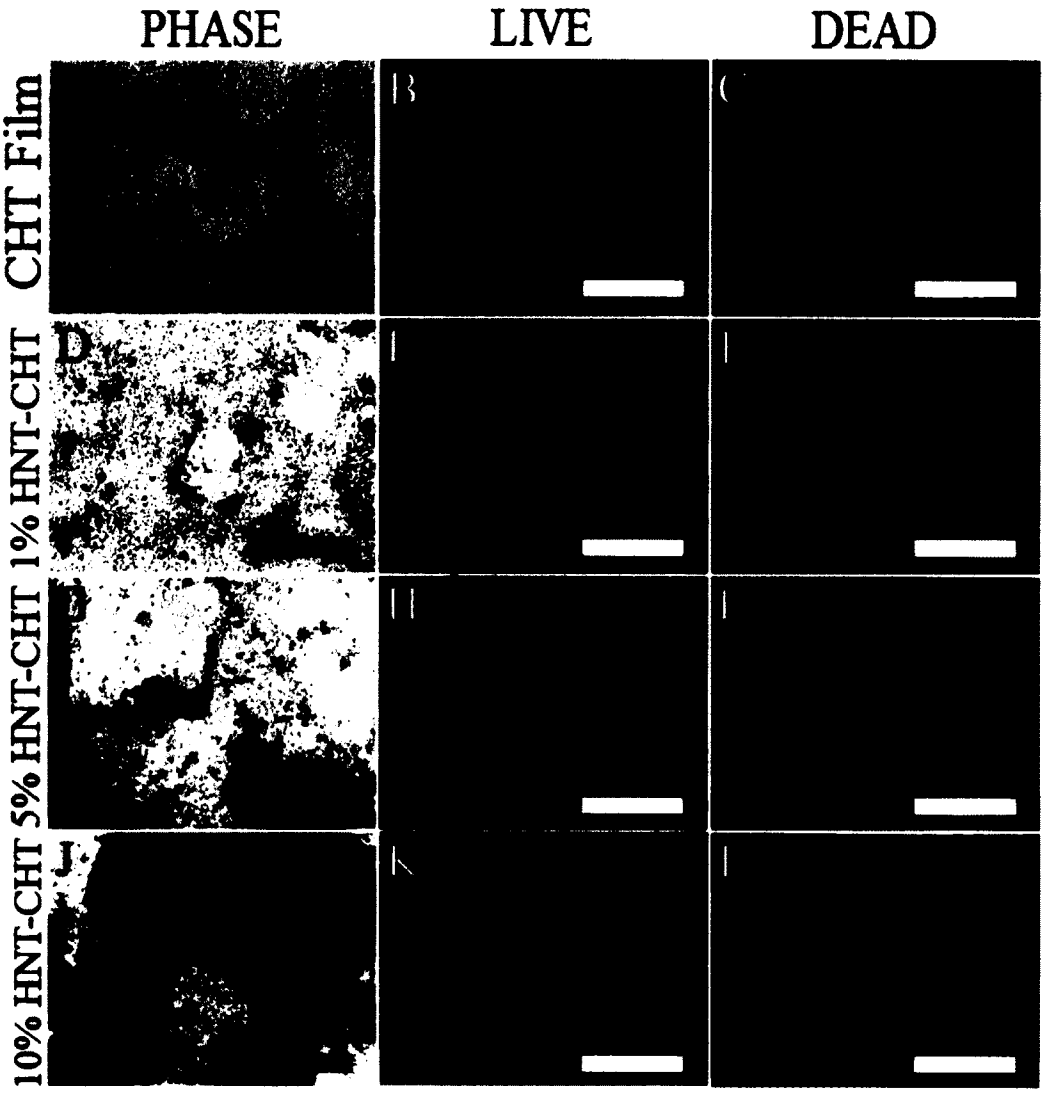


**Figure 6-24:** Cytotoxic response to Chitosan Film Composites at 168 Hours. Scale bar represents 500μm (A-C) Group 1: Osteosarcoma cell cultures with chitosan films. (D-F) Group 2: Osteosarcoma cells exposed to 1% HNT chitosan films. (G-I) Group 3: Osteosarcoma cells exposed to 5% HNT chitosan films (J-L) Group 4: Osteosarcoma cells exposed to % HNT chitosan films. A, D, G and J = Phase contrast; B, E, H and K = Live Dead assay showing live cells (green); C, F, I and L = Dead assay showing dead cells (red). The brown coloration in D, G and J is caused by the high concentration of HNTs.

At 168 hours, in MTX-treated groups, the cellular response was very different from untreated cells, and the reduction in cell growth remained constant (**Figure 6-25** A-L). At 168 hours, Group 2 osteosarcoma cells exposed to 1% MTX-HNT chitosan films showed a marked reduction in cell growth as compared to untreated control cells and cells treated with MTX (100 μg) chitosan films (**Figure 6-25** D-F). At 168 hours, Group 3 osteosarcoma cells exposed to 5% MTX-HNT chitosan films showed a greater reduction in cell growth as compared to the MTX group and the 1% MTX-HNT chitosan films group (**Figure 6-25** G-H). At 168 hours, Group 4 osteosarcoma cells exposed to 10% MTX-HNT chitosan films showed the greatest reduction in cell growth as compared to MTX group, 5% MTX-HNT chitosan films and the 1% MTX-HNT chitosan films group (**Figure 6-25** J-L). However, only a few dead cells were observed in all groups and cells were more confluent than at the previous time point, which may be attributed to the changing of the media, which removed the majority of the drug that had been released (**Figure 6-25** C, F, I and L).

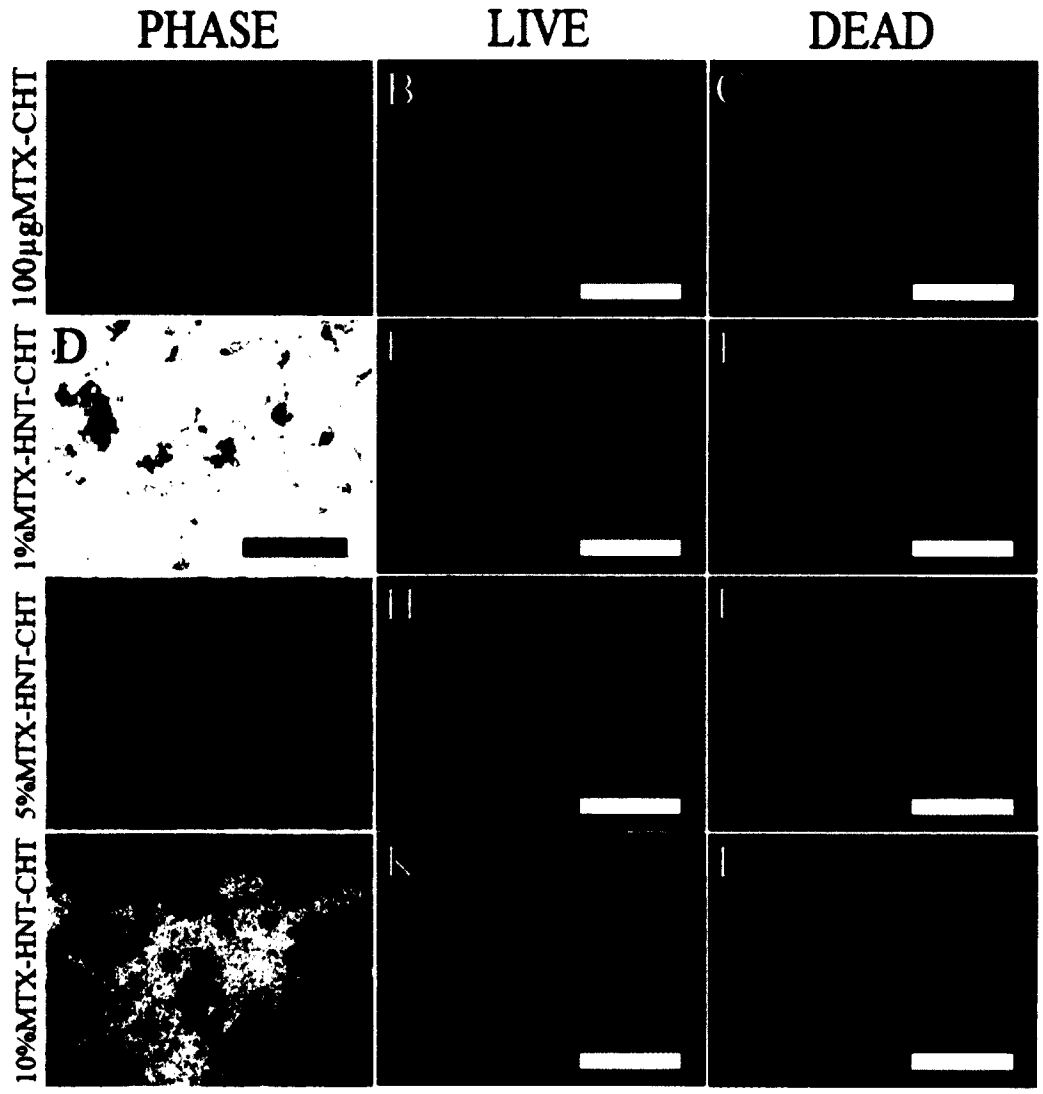


**Figure 6-25:** Cellular response to MTX loaded chitosan film composites HNTs at 168 Hours. Scale bar represents 500µm (A-C) Group 1: Osteosarcoma cell cultures with MTX (100µg) chitosan films addition. (D-F) Group 2: Osteosarcoma cells exposed to 1% MTX-HNT chitosan films. (G-I) Group 3: Osteosarcoma cells exposed to 5% MTX-HNT chitosan films. (J-L) Group 4: Osteosarcoma cells exposed to 10% MTX-HNT chitosan films. A, D, G and J = Phase contrast; B, E, H and K = Live Dead assay showing live cells (green); C, F, I and L = Dead assay showing dead cells (red). The brown coloration in D, G and J is caused by the high concentration of HNTs.

# CHAPTER 7

# CONCLUSIONS AND FUTURE WORK

Chapters 4, 5 and 6, discussed three projects with interrelated concepts and the novel applications of HNT for gene delivery, drug delivery, and enhancing drug delivery and material properties of chitosan composite films. The current chapter details the findings from recorded observations and integrates the concepts established in Chapters 4, 5 and 6. A plan for the future direction of this research is also provided.

Chapter 4 included a discussion of the possibility of using HNTs as a delivery platform for the transfection of osteosarcoma cells *in vitro*. The results suggest that HNTs alone were incapable of efficiently transfecting cells because the majority of plasmid DNA adsorbed to or wrapped around the surface. Surface localization of pDNA may be due to supercoiling, which can make plasmids too large to load into the lumen when paired with the lipid-based transfection agent Lipofectamine, HNTs enhanced the transfection efficiency of the transfection agent. Among the groups 0.5μg-pDNA-HNTs coated with Lipofectamine achieved better results than pDNA with Lipofectamine alone. This effect was sustained throughout the six-day testing period, whereas the Lipofectamine-pDNA group's fluorescence was reduced greatly by the sixth day. Therefore, HNTs loaded and coated with pDNA could be subsequently coated with lipids, and used as an effective delivery system for plasmid DNA. The release of plasmid DNA was sustained and extended, suggesting that plasmid DNA can be made available to

target cancer cells throughout a seven day period, which is crucial for a prolonged cellular response. In the future pDNA could be heat denature pror to loading in order due reduce super coiling and increase plasmid DNA loading.

Future research for his project would be developed in three stages. First, a calibration curve would be developed for a set concentration of Lipofectamine for transfecting differing concentrations of DNA based on cell density. Second, scanning and transmission electron microscopy imaging of pDNA loaded HNTs would be done to understand the level of wrapping/loading of HNTs. In addition, the pDNA-HNT to Lipofectamine ratio would be optimized for *in vitro* testing. After optimization, these HNT-pDNA-Lipofectamine complexes would be tested in other cancer cell lines. Still, more work could explore coatings for pDNA-HNT complexes for maximizing transfections efficiency. This work might involve coating pDNA-HNT complexes with DOTAP and comparing the efficiency to Lipofectamine. Chitosan film data presented in this work and recent advances in using chitosan nanoparticle for gene transfection[105][106] suggest that embedding pDNA-HNT complexes in chitosan films may provide a comparable transfection efficiency to Lipofectamine.

Chapter 5 discussed the concept of using HNTs as a drug delivery vector for chemotherapeutic drug methotrexate. The primary hypothesis tested if HNTs loaded with methotrexate could extend and sustain a release of methotrexate for seven days and sustain a localized reduction of cellular proliferation. Release profile data showed that HNTs could release methotrexate in microgram and nanogram concentrations for up to seven days. Cell proliferation and XTT viability assay results revealed that the cellular proliferation and growth were greatly reduced when compared with free drug. Reducing

prolifereation can shrink solid tumors and limit the growth of mircometastasis in vivo. A significant reduction in cancer cell groth and proliferation is vital in achieving remssion. Results also demonstrate that additional drug was required after the changing of media for free drug sets; however, in methotrexate-loaded HNT sets, further addition of drugs was not required, due to the continuous release of drug. SEM images revealed that drug was loaded into the HNTs and also adsorbed onto the surface of the HNTs. Results of the combined studies demonstrated that the drug was localized at the cells rather than being diluted in the media.

In future studies, HNTs can be coated with poly electrolyte films or by embedded MTX-HNTs within chitosan films to reduce the burst release seen within the first hour. HNT's lumen could also be etched with an acid to increase loading capacity. Other work may include merging the projects discussed in Chapters 4 and 5. This work would involve loading HNTs with methotrexate, coating with plasmid DNA that induces fluorescence expression and apoptosis, and subsequently coating with polyelectrolyte. This synergistic system would tag cancer cells, reduce or stop proliferation, and activate programmed cell death in targeted cancer cells.

Chapter 6 described the fabrication HNT enhanced chitosan film composites for localized and sustained drug delivery. The primary hypothesis of this project was that chitosan-HNT composite films could encapsulate methotrexate-loaded HNTs, reduce the burst release of drug from HNTs, sustain drug release for more than seven days, and maintain a reduced amount of cell proliferation and growth *in vitro*. Imaging revealed that films could encapsulate drug-loaded HNTs. Chitosan reduced the burst release by more than half and extended the release of drugs from HNTs to more than seven days.

HNT chitosan films released more methotrexate over a seven-day period than films complexed with only methotrexate. SEM imaging revealed that this increase was due to the presence of pores created by HNTs embedded in the chitosan films.

*In vitro* cell proliferation and viability assays indicated that films embedded with HNTs loaded with methotrexate were more effective at reducing proliferation than films complexed with free methotrexate. Reducing proliferation can shrink solid tumors and limit the growth of mircometastasis in vivo. A significant reduction in cancer cell growth and proliferation is vital in achieving remission. Additonally films sprayed into areas where tumors have been removed can eliminate the risk of recurrence in said region and composite films can act as a barrier reducing the amount of exposed leaky vasculature that feeds tumors.

These studies were carried out in murine osteosarcoma, and future research could be conducted on human osteosarcoma cell line. The release profile study could be extended to 21 days, as work presented here indicated only about half the drug was released over seven days. To understand the material properties of chitosan composite films and evaluate the effect of HNTs on film morphology, pore size analysis and TEM imaging can be performed on films. Pore size analysis would quantify the number of pores and the average pore size in chitosan composite films. Future research could also assess the effect of different concentrations of chitosan on film morphology and drug release-kinetics. In addition, HNTs can be loaded with different chemotherapeutic agents, like paclitaxel, while the film can be loaded with a synergist, like p-glyco-pump blocker tariquidar, creating a synergist, sequential drug release platform for combating multidrug resistant cancers.

All of the above-mentioned projects were tested *in vitro* due to time and resource constraints. Future studies can be carried out in 3 dimensional tumor models and eventually extend to *in vivo* animal models. Chapter 4 was limited to a green fluorescence plasmid and in the future this plasmid can be replaced with a genetic material that induces apoptosis. The scope of all of the projects in this dissertation was limited to extending and sustaining a localized drug release to tumors and surrounding tissues. The scope could be expanded to include genes (siRNA knockdown of p-GP expression) or drugs (tariquidar, miltefosine, etc.) that target these membrane proteins overexpressed in cancers and incorporate them into HNT-embedded films.

An investigative study of chitosan composite films, loaded with chemotherapeutic agents or genes, on cancer cell growth and proliferation with a comparison between murine osteosarcoma cell lines and human osteosarcoma cell lines can be useful in predicting the behavior of these constructs as adjuvant and neoadjuvant chemotherapeutic implants. Moreover, experiments can be designed for an extended period of 21 days or more advanced metrology techniques like BET pore size analysis can be used to quantify results discussed in this dissertation. Looking at the three projects, it can be concluded that HNTs hold promise as potential nanoparticle-based chemo and gene therapies for cancers and that chitosan composite films show potential as neo adjuvant and adjuvant implants and coatings for cancer therapy.

# RESULTS OF STATISTICAL ANALYSIS

# APPENDIX A

# APPENDIX A RESULTS OF STATISTICAL ANALYSIS

**Table A-1:** Results of IBM SPSS two-tailed Paired T-Test for Transfection Assay.

| Comparison (pairs) | Significant difference (P Value) 24 hours | Significant difference (P Value) 48 hours | Significant difference (P Value) 96 hours | Significant difference (P Value) 144 hours |
|---|---|---|---|---|
| **control vs. lipo 0.1μg** | .000 | .000 | .011 | .001 |
| **control vs. lipo 1μg** | .000 | .000 | .001 | .000 |
| **control vs. 0.5μg HNT-lipo** | .000 | .000 | .000 | .000 |
| **control vs. 1μg HNT-lipo** | .000 | .000 | .001 | .004 |
| **lipo 0.1μg vs. lipo 1μg** | .148 | .729 | .008 | .038 |
| **lipo 0.1μg vs. 0.5μg HNT-lipo** | .022 | .799 | .000 | .285 |
| **lipo 0.1μg vs. 1μg HNT-lipo** | .002 | .000 | .290 | .002 |
| **lipo 1μg vs. 0.5μg HNT-lipo** | .000 | .951 | .845 | .340 |
| **lipo 1μg vs. 1μg HNT-lipo** | .000 | .000 | .007 | .001 |
| **0.5μg HNT-lipo vs. 1μg HNT-lipo** | .000 | .000 | .000 | .000 |

**Table A-2:** Results of IBM SPSS two-tailed Paired T-Test for Particle Size n = 4 samples.

| Comparison (Pairs) | Significant Difference (P Value) |
|---|---|
| **HNT vs. MTX-HNT** | .842 |
| **HNT vs. pDNA-HNT** | .000 |
| **MTX-HNT vs. pDNA-HNT** | .000 |

**Table A-3:** Results of IBM SPSS two-tailed Paired T-Test for Zeta Potential n = 4 Samples.

| Comparison (Pairs) | Significant Difference (P Value) |
|---|---|
| **HNT vs. MTX-HNT** | .033 |
| **HNT vs. pDNA-HNT** | .000 |
| **MTX-HNT vs. pDNA-HNT** | .000 |

**Table A-4:** Results of IBM SPSS two-tailed Paired T-Test for HNT Proliferation Assay.

| Comparison (pairs) | Significant difference (P Value) 24 hours | Significant difference (P Value) 72 hours | Significant difference (P Value) 120 hours | Significant difference (P Value) 168 hours |
|---|---|---|---|---|
| **untreated vs. drug** | .092 | .000 | .000 | .000 |
| **untreated vs. 1mg HNT** | .224 | .000 | .018 | .000 |
| **untreated vs. 1mg HNT-MTX** | .004 | .000 | .000 | .000 |
| **untreated vs. 5mg HNT** | .081 | .000 | .000 | .000 |
| **untreated vs. 5mg HNT-MTX** | .000 | .000 | .000 | .000 |
| **untreated vs. 10mg HNT** | .000 | .000 | .000 | .000 |
| **untreated vs. 10mg HNT-MTX** | .000 | .000 | .000 | .000 |
| **drug vs. 1mg HNT** | .010 | .000 | .000 | .000 |
| **drug vs. 1mg HNT-MTX** | .001 | .045 | .001 | .050 |
| **drug vs. 5mg HNT** | .263 | .237 | .047 | .615 |
| **drug vs. 5mg HNT-MTX** | .000 | .004 | .000 | .000 |
| **drug vs. 10mg HNT** | .000 | .010 | .000 | .001 |
| **drug vs. 10mg HNT-MTX** | .000 | .005 | .000 | .000 |
| **1mg HNT vs. 1mg HNT-MTX** | .001 | .000 | .000 | .000 |
| **5mg HNT vs. 5mg HNT-MTX** | .000 | .002 | .000 | .000 |
| **10mg HNT vs. 10mg HNT-MTX** | .000 | .018 | .002 | .061 |

**Table A-5:** Results of IBM SPSS two-tailed Paired T-Test for Chitosan Film Proliferation Assay.

| Comparison (pairs) | **Significant difference (P Value) 24 hours** | **Significant difference (P Value) 72 hours** | **Significant difference (P Value) 120 hours** | **Significant difference (P Value) 168 hours** |
|---|---|---|---|---|
| untreated vs. CHT | .000 | .007 | .000 | .026 |
| untreated vs. 100mgMTX_CHT | .000 | .000 | .000 | .000 |
| untreated vs. 1%HNT_CHT | .066 | .002 | .000 | .000 |
| untreated vs. 1%MTX_HNT CHT | .851 | .000 | .000 | .000 |
| untreated vs. 5%HNT_CHT | .000 | .000 | .000 | .000 |
| untreated vs. 5%MTX_HNT_CHT | .004 | .000 | .000 | .000 |
| untreated vs. 10%HNT_CHT | .000 | .000 | .000 | .000 |
| untreated vs. 10%MTX_HNT_CHT | .000 | .000 | .000 | .000 |
| CHT vs. 100mgMTX_CHT | .007 | .000 | .000 | .000 |
| CHT vs. 1%HNT_CHT | .001 | .000 | .045 | .000 |
| CHT vs. 1%MTX_HNT CHT | .000 | .000 | .000 | .000 |
| CHT vs. 5%HNT_CHT | .000 | .000 | .000 | .000 |
| CHT vs. 5%MTX_HNT_CHT | .000 | .000 | .000 | .000 |
| CHT vs. 10%HNT_CHT | .000 | .000 | .000 | .000 |
| CHT vs. 10%MTX_HNT_CHT | .000 | .000 | .000 | .000 |
| 100mgMTX_CHT vs. 1%HNT_CHT | .000 | .000 | .000 | .000 |
| 100mgMTX_CHT vs. 1%MTX_HNT CHT | .000 | .079 | .002 | .001 |
| 100mgMTX_CHT vs. 5%HNT_CHT | .000 | .442 | .000 | .581 |
| 100mgMTX_CHT vs. 5%MTX_HNT_CHT | .000 | .002 | .000 | .000 |
| 100mgMTX_CHT vs. 10%HNT_CHT | .000 | .000 | .000 | .001 |
| 100mgMTX_CHT vs. 10%MTX_HNT_CHT | .000 | .001 | .000 | .000 |
| 1%HNT_CHT vs. 1%MTX_HNT CHT | .005 | .000 | .000 | .000 |
| 5%HNT_CHT vs. 5%MTX_HNT_CHT | .010 | .000 | .000 | .000 |
| 10%HNT_CHT vs. 10%MTX_HNT_CHT | .003 | .023 | .026 | .000 |

# BIBLIOGROPHY

[1] A. C. Society, "Cancer Facts and Figures 2014." [ Accessed Online Dec 9, 2015 Nov. 17, 2015]. Available: http://www.cancer.org/research/cancerfactsstatistics/cancerfactsfigures2014/index.

[2] N. C. Institute, "Cancer statistics." [Accessed Online Dec 9, 2015 Nov. 18, 2015]. Available: http://www.cancer.gov/about-cancer/what-is-cancer/statistics.

[3] A. C. Guyton M.D. and J. E. Hall Ph.D. "Cancer," in *Textbook of Medical Physiology*, 11TH ed. Elsevier Inc. Saunders WB, 2006, pp. 40–42.

[4] N. C. Institute, "Types of Treatment." [Accessed Online Dec 9, 2015 Nov. 120, 2015]. Available: http://www.cancer.gov/about-cancer/treatment/types.

[5] C. L. Haddox, G. Han, L. Anijar, O. Binitie, G. D. Letson, M. M. Bui, and D. R. Reed, "Osteosarcoma in Pediatric Patients and Young Adults : A Single Institution Retrospective Review of Presentation , Therapy , and Outcome," vol. 2014, 2014.

[6] A. C. Society, "what are the key statistics of osteosarcoma." [AccessedOnline Dec 9, 2015]. Available: http://www.cancer.org/cancer/osteosarcoma/detailedguide/osteosarcoma-key-statistics.

[7] G. Ottaviani and N. Jaffe, "The epidemiology of osteosarcoma." *Cancer Treat. Res.* vol. 152, pp. 3–13, 2009.

[8] A. C. Society, "Osteosarcoma a detailed guide," 2014. [Accessed Online Dec 9, 2015 Nov. 18, 2015]. Available: http://www.cancer.org/acs/groups/cid/documents/webcontent/003129-pdf.pdf.

[9] M. J. Klein and G. P. Siegal, "Osteosarcoma," *Am. J. Clin. Pathol.* vol. 125, no. 4, pp. 555–581, Apr. 2006.

[10] N. C. Institute, "Prostate Cancer," 2014. [Accessed Online Dec 9, 2015 Nov. 19, 2015]. Available: http://www.cancer.gov/types/prostate.

[11] A. C. Society, "Key statistics for Prostate Cancer." [Accessed Online Dec 9, 2015 Nov. 20, 2016]. Available: http://www.cancer.org/cancer/prostatecancer/detailedguide/prostate-cancer-key-statistics.

[12] M. Salam, *Principles and Practice of Urology*. Jaypee Brothers Medical P, 2013.

[13] A. C. Society, "Prostate Cancer," 2014. [Accessed Online Dec 9, 2015 Nov. 23, 2015. Available: http://www.cancer.org/acs/groups/cid/documents/webcontent/003134-pdf.pdf.

[14] A. C. Society, "Breast Cancer." [Accessed Online Dec 9, 2015 Nov. 27, 2015]. Available: http://www.cancer.org/acs/groups/cid/documents/webcontent/003090-pdf.pdf.

[15] T. Who and W. Group, "CHAPTER 1 WHO histological classification of tumours of the breast."

[16] B. Weigelt, H. M. Horlings, B. Kreike, M. M. Hayes, M. Hauptmann, L. F. a Wessels, D. de Jong, M. J. Van de Vijver, L. J. Van't Veer, and J. L. Peterse, "Refinement of breast cancer classification by molecular characterization of histological special types." *J. Pathol.* vol. 216, no. 2, pp. 141–50, Oct. 2008.

[17] Mary Ann Kosir MD, "Breast Cancer," *Merck Manuals*, 2008. [AccessedOnline Dec 9, 2015]. Available: http://www.merckmanuals.com/home/women-s-health-issues/breast-disorders/breast-cancer. [Accessed: 12-Mar-2015].

[18] F.-S. Liu, "Mechanisms of chemotherapeutic drug resistance in cancer therapy--a quick review." *Taiwan. J. Obstet. Gynecol.* vol. 48, no. 3, pp. 239–44, Sep. 2009.

[19] A. A. Stavrovskaya and T. P. Stromskaya, "Transport Proteins of the ABC Family and Multidrug Resistance of Tumor Cells," vol. 73, no. 5, pp. 592–604, 2008.

[20] S. V Ambudkar, C. Kimchi-Sarfaty, Z. E. Sauna, and M. M. Gottesman, "P-glycoprotein: from genomics to mechanism." *Oncogene*, vol. 22, no. 47, pp. 7468–85, Oct. 2003.

[21] X. Chang, "A molecular understanding of ATP-dependent solute transport by multidrug resistance-associated protein MRP1," *Cancer Metastasis Rev.* vol. 26, no. 1, pp. 15–37, 2007.

[22] Y.-N. Chen, L. A. Mickley, A. M. Schwartz, E. M. Acton, J. L. Hwang, and A. T. Fojo, "Characterization of adriamycin-resistant human breast cancer cells which display overexpression of a novel resistance-related membrane protein." *J. Biol. Chem.* vol. 265, no. 17, pp. 10073–10080, 1990.

[23] R. Clarke, F. Leonessa, and B. Trock, "Multidrug resistance/P-glycoprotein and breast cancer: review and meta-analysis." *Semin. Oncol.* vol. 32, no. 6 Suppl 7, pp. S9–15, Dec. 2005.

[24] W. J. Gradishar, S. Tjulandin, N. Davidson, H. Shaw, N. Desai, P. Bhar, M. Hawkins, and J. O'Shaughnessy, "Phase III trial of nanoparticle albumin-bound paclitaxel compared with polyethylated castor oil-based paclitaxel in women with breast cancer." *J. Clin. Oncol.* vol. 23, no. 31, pp. 7794–803, 2005.

[25] R. Duncan, "The dawning era of polymer therapeutics." *Nat. Rev. Drug Discov.* vol. 2, no. 5, pp. 347–60, 2003.

[26] P. a Vasey, S. B. Kaye, R. Morrison, C. Twelves, P. Wilson, R. Duncan, a H. Thomson, L. S. Murray, T. E. Hilditch, T. Murray, S. Burtles, D. Fraier, E. Frigerio, and J. Cassidy, "Phase I clinical and pharmacokinetic study of PK1 [N-(2-hydroxypropyl)methacrylamide copolymer doxorubicin]: first member of a new class of chemotherapeutic agents-drug-polymer conjugates. Cancer Research Campaign Phase I/II Committee." *Clin. Cancer Res.* vol. 5, pp. 83–94, 1999.

[27] Y. Fukumori and H. Ichikawa, "Nanoparticles for cancer therapy and diagnosis," *Adv. Powder Technol.* vol. 17, no. 1, pp. 1–28, 2006.

[28] T. Y. Kim, D. W. Kim, J. Y. Chung, S. G. Shin, S. C. Kim, D. S. Heo, N. K. Kim, and Y. J. Bang, "Phase I and pharmacokinetic study of Genexol-PM, a Cremophor-free, polymeric micelle-formulated paclitaxel, in patients with advanced malignancies," *Clin. Cancer Res.* vol. 10, no. 11, pp. 3708–3716, 2004.

[29] S. Mitra, U. Gaur, P. C. Ghosh, and a. N. Maitra, "Tumour Targeted Delivery of Encapsulated Dextran-Doxorubicin Conjugate Using Chitosan Nanoparticles as Aarrier," in *Journal of Controlled Release*, 2001, vol. 74, no. 1–3, pp. 317–323.

[30] H. S. Yoo, K. H. Lee, J. E. Oh, and T. G. Park, "In vitro and in vivo anti-tumor activities of nanoparticles based on {doxorubicin–PLGA} conjugates," *J. Control. Release*, vol. 68, no. 3, pp. 419–431, 2000.

[31] L. Brannon-Peppas and J. O. Blanchette, "Nanoparticle and targeted systems for cancer therapy," *Adv. Drug Deliv. Rev.* vol. 64, no. SUPPL. pp. 206–212, 2012.

[32] M. Ogris, G. Walker, T. Blessing, R. Kircheis, M. Wolschek, and E. Wagner, "Tumor-targeted gene therapy: Strategies for the preparation of ligand-polyethylene glycol-polyethylenimine/DNA complexes," *J. Control. Release*, vol. 91, pp. 173–181, 2003.

[33] T. Liu, G. Zhang, Y.-H. Chen, Y. Chen, X. Liu, J. Peng, M. H. Xu, and J. W. Yuan, "Tissue specific expression of suicide genes delivered by nanoparticles inhibits gastric carcinoma growth," *Cancer Biol. Ther.* vol. 5, no. 12, pp. 1683–1690, 2006.

[34] M. Morille, C. Passirani, A. Vonarbourg, A. Clavreul, and J. P. Benoit, "Progress in developing cationic vectors for non-viral systemic gene therapy against cancer," *Biomaterials*, vol. 29, pp. 3477–3496, 2008.

[35] S. Kommareddy and M. Amiji, "Antiangiogenic gene therapy with systemically administered sFlt-1 plasmid DNA in engineered gelatin-based nanovectors," *Cancer Gene Ther.* vol. 14, no. 5, pp. 488–498, 2007.

[36] I. P. Trougakos, A. So, B. Jansen, M. E. Gleave, and E. S. Gonos, "Silencing expression of the clusterin/apolipoprotein j gene in human cancer cells using small interfering RNA induces spontaneous apoptosis, reduced growth ability, and cell sensitization to genotoxic and oxidative stress," *Cancer Res.* vol. 64, no. 5, pp. 1834–1842, 2004.

[37] T. S. Zimmermann, A. C. H. Lee, A. Akinc, B. Bramlage, D. Bumcrot, M. N. Fedoruk, J. Harborth, J. A. Heyes, L. B. Jeffs, and M. John, "RNAi-mediated gene silencing in non-human primates," *Nature*, vol. 441, no. 7089, pp. 111–114, 2006.

[38] R. Cavalli, A. Bisazza, R. Bussano, M. Trotta, A. Civra, D. Lembo, E. Ranucci, and P. Ferruti, "Poly ( amidoamine ) -Cholesterol Conjugate Nanoparticles Obtained by Electrospraying as Novel Tamoxifen Delivery System," vol. 2011, 2011.

[39] U. B. Nielsen, D. B. Kirpotin, E. M. Pickering, K. Hong, J. W. Park, M. Refaat Shalaby, Y. Shao, C. C. Benz, and J. D. Marks, "Therapeutic efficacy of anti-ErbB2 immunoliposomes targeted by a phage antibody selected for cellular endocytosis." *Biochim. Biophys. Acta*, vol. 1591, no. 1–3, pp. 109–118, 2002.

[40] M. Rodolfo, C. Melani, C. Zilocchi, B. Cappetti, E. Luison, I. Arioli, M. Parenza, S. Canevari, and M. P. Colombo, "IgG2a induced by interleukin (IL) 12-producing tumor cell vaccines but not IgG1 induced by IL-4 vaccine is associated with the eradication of experimental metastases." *Cancer research*, vol. 58, no. 24. pp. 5812–7, 1998.

[41] K. Cho, X. Wang, G. Kim, A. Gjyrezi, P. Giannakakou, S. Nie, Z. Chen, and D. Shin, "Investigation of Taxol-resistance using folate-targeted ternary therapeutic nanoparticle," *Cancer Res.* vol. 67, no. 9 Supplement, p. 2311, 2007.

[42] K. Cho, X. Wang, S. Nie, Z. G. Chen, and D. M. Shin, "Therapeutic nanoparticles for drug delivery in cancer." *Clin. Cancer Res.* vol. 14, no. 5, pp. 1310–6, 2008.

[43] O. C. Farokhzad, J. Cheng, B. a Teply, I. Sherifi, S. Jon, P. W. Kantoff, J. P. Richie, and R. Langer, "Targeted nanoparticle-aptamer bioconjugates for cancer chemotherapy in vivo." *Proc. Natl. Acad. Sci. U. S. A.* vol. 103, no. 16, pp. 6315–20, 2006.

[44] S. K. S. Sahoo and V. Labhasetwar, "Enhanced antiproliferative activity of transferrin-conjugated paclitaxel-loaded nanoparticles is mediated via sustained intracellular drug retention." *Mol. Pharm.* vol. 2, no. 5, pp. 373–83, 2005.

[45] L. Xu, K. F. Pirollo, W. H. Tang, a Rait, and E. H. Chang, "Transferrin-liposome-mediated systemic p53 gene therapy in combination with radiation results in regression of human head and neck cancer xenografts." *Hum. Gene Ther.* vol. 10, pp. 2941–2952, 1999.

[46] A. Ediriwickrema, J. Zhou, Y. Deng, and W. M. Saltzman, "Biomaterials Multi-layered nanoparticles for combination gene and drug delivery to tumors," *Biomaterials*, vol. 35, no. 34, pp. 9343–9354, 2014.

[47] Q. Xu, Y. Xia, C.-H. Wang, and D. W. Pack, "Monodisperse double-walled microspheres loaded with chitosan-p53 nanoparticles and doxorubicin for combined gene therapy and chemotherapy," *J. Control. Release*, vol. 163, no. 2, pp. 130–135, 2012.

[48] H. Meng, M. Liong, T. Xia, Z. Li, Z. Ji, J. I. Zink, and A. E. Nel, "Engineered Design of Mesoporous Silica Nanoparticles to Deliver Doxorubicin and P-Glycoprotein siRNA to Overcome Drug Resistance in a Cancer Cell Line," vol. 4, no. 8, pp. 4539–4550, 2010.

[49] A. Lamprecht and J. Benoit, "Etoposide nanocarriers suppress glioma cell growth by intracellular drug delivery and simultaneous P-glycoprotein inhibition," vol. 112, pp. 208–213, 2006.

[50] T. Tsuruo, M. Naito, A. Tomida, N. Fujita, T. Mashima, H. Sakamoto, and N. Haga, "Molecular targeting therapy of cancer : drug resistance , apoptosis and survival signal," vol. 94, no. 1, pp. 15–21, 2003.

[51] M. Signore, L. Ricci-Vitiani, and R. De Maria, "Targeting apoptosis pathways in cancer stem cells," *Cancer Lett.* vol. 332, no. 2, pp. 374–382, 2013.

[52] A. Shapira, Y. D. Livney, H. J. Broxterman, and Y. G. Assaraf, "Nanomedicine for targeted cancer therapy: Towards the overcoming of drug resistance," *Drug Resist. Updat.* vol. 14, no. 3, pp. 150–163, 2011.

[53] S. Vijayaraghavalu, J. K. Dermawan, V. Cheriyath, and V. Labhasetwar, "Highly synergistic effect of sequential treatment with epigenetic and anticancer drugs to overcome drug resistance in breast cancer cells is mediated via activation of p21 gene expression leading to G2/M cycle arrest." *Mol. Pharm.* vol. 10, no. 1, pp. 337–52, 2013.

[54] M. J. Lee, A. S. Ye, A. K. Gardino, A. M. Heijink, P. K. Sorger, G. MacBeath, and M. B. Yaffe, "Sequential Application of Anticancer Drugs Enhances Cell Death by Rewiring Apoptotic Signaling Networks," *Cell*, vol. 149, no. 4, pp. 780–794, 2012.

[55] K. Mutoh, S. Tsukahara, J. Mitsuhashi, K. Katayama, and Y. Sugimoto, "Estrogen-mediated post transcriptional down- regulation of P-glycoprotein in," vol. 97, no. 11, 2006.

[56] C. Sarisozen, I. Vural, T. Levchenko, A. A. Hincal, and V. P. Torchilin, "ong-circulating PEG-PE micelles co-loaded with paclitaxel L and elacridar (GG918) overcome multidrug resistance," vol. 19, no. May, pp. 363–370, 2012.

[57] N. R. Patel, A. Rathi, D. Mongayt, and V. P. Torchilin, "Reversal of multidrug resistance by co-delivery of tariquidar ( XR9576 ) and paclitaxel using long-circulating liposomes," *Int. J. Pharm.* vol. 416, no. 1, pp. 296–299, 2011.

[58] H. L. Wong, A. M. Rauth, R. Bendayan, J. L. Manias, M. Ramaswamy, Z. Liu, S. Z. Erhan, and X. Y. Wu, "Research Paper A New Polymer Y Lipid Hybrid Nanoparticle System Increases Cytotoxicity of Doxorubicin Against Multidrug-Resistant Human Breast Cancer Cells," vol. 23, no. 7, pp. 1574–1585, 2006.

[59] B. D. Rege, J. P. Y. Kao, and J. E. Polli, "Effects of nonionic surfactants on membrane transporters in Caco-2 cell monolayers," *Eur. J. Pharm. Sci.* vol. 16, no. 4, pp. 237–246, 2002.

[60] N. Akhtar, A. Ahad, R. K. Khar, M. Jaggi, M. Aqil, Z. Iqbal, F. J. Ahmad, and S. Talegaonkar, "The emerging role of P-glycoprotein inhibitors in drug delivery: a patent review." *Expert Opin. Ther. Pat.* vol. 21, no. 4, pp. 561–76, 2011.

[61] L. Liang, "Micellar systems useful for delivery of lipophilic or hydrophobic compounds." Google Patents, 24-Nov-2004.

[62] G. Cornaire, J. Woodley, P. Hermann, A. Cloarec, C. Arellano, and G. Houin, "Impact of excipients on the absorption of P-glycoprotein substrates *in vitro* and *in vivo*," *Int. J. Pharm.* vol. 278, no. 1, pp. 119–131, 2004.

[63] Y. Lin, Q. Shen, H. Katsumi, N. Okada, T. Fujita, X. Jiang, and A. Yamamoto, "Effects of Labrasol and other pharmaceutical excipients on the intestinal transport and absorption of rhodamine123, a P-glycoprotein substrate, in rats." *Biol. Pharm. Bull.* vol. 30, no. 7, pp. 1301–1307, 2007.

[64] G. N. Shankar, "Orally-Absorbed Solid Dose Formulation for Vancomycin." Google Patents, 29-Oct-2007.

[65] J. Pachot and S. S. Chicq, "Galenic applications of self-emulsifying mixtures of lipidic excipients." Google Patents, 27-Aug-2010.

[66] A. Kozak, R. Duvdevani, and F. M. Younis, "Use of branched-chain fatty acids and derivatives thereof for the treatment of pain." Google Patents, 11-Feb-2003.

[67] P. Lienau, T. Backensfeld, A. Reichel, and T. Jung, "Pharmaceutical preparations, use of these preparations and process for increasing the biovailability of pharmaceutical substances to be administered perorally." Google Patents, 07-Oct-2003.

[68] M. Saraswathy and S. Gong, "Different Strategies to Overcome Multidrug Resistance in Cancer ." *Biotechnol. Adv.* vol. 31, no. JUNE 2013, pp. 1397–1407, 2015.

[69] W. E. Teo and S. Ramakrishna, "A review on electrospinning design and nanofibre assemblies," vol. 89, 2006.

[70] X. Hu, S. Liu, G. Zhou, Y. Huang, Z. Xie, and X. Jing, "Electrospinning of polymeric nanofibers for drug delivery applications," *J. Control. Release*, vol. 185, no. APRIL, pp. 12–21, 2014.

[71] Q. P. Pham, U. Sharma, and A. G. Mikos, "Electrospinning of polymeric nanofibers for tissue engineering applications: a review." *Tissue Eng.* vol. 12, no. 5, pp. 1197–211, 2006.

[72] S. Liu, G. Zhou, D. Liu, Z. Xie, Y. Huang, X. Wang, W. Wu, and X. Jing, "Inhibition of orthotopic secondary hepatic carcinoma in mice by doxorubicin-loaded electrospun polylactide nanofibers," *J. Mater. Chem. B*, vol. 1, no. 1, pp. 101–109, 2013.

[73] Y. Zhang, C. T. Lim, S. Ramakrishna, and Z.-M. Huang, "Recent development of polymer nanofibers for biomedical and biotechnological applications," *J. Mater. Sci. Mater. Med.* vol. 16, no. 10, pp. 933–946, 2005.

[74] M. Prabaharan, R. Jayakumar, and S. V Nair, "Electrospun nanofibrous scaffolds-current status and prospects in drug delivery," in *Biomedical applications of polymeric nanofibers*, Springer, 2012, pp. 241–262.

[75] N. Bhardwaj and S. C. Kundu, "Electrospinning: A fascinating fiber fabrication technique," *Biotechnol. Adv.* vol. 28, no. 3, pp. 325–347, 2010.

[76] J. D. Schiffman and C. L. Schauer, "A Review: Electrospinning of Biopolymer Nanofibers and their Applications," *Polym. Rev.* vol. 48, no. 2, pp. 317–352, 2008.

[77] B. Dalby, S. Cates, A. Harris, E. C. Ohki, M. L. Tilkins, P. J. Price, and V. C. Ciccarone, "Advanced transfection with Lipofectamine 2000 reagent: Primary neurons, siRNA, and high-throughput applications," *Methods*, vol. 33, no. 2, pp. 95–103, 2004.

[78] Y. Chu, M. Masoud, and G. Gebeyehu, "Transfection reagents." Google Patents, 20-Jan-2009.

[79] K. Y. Lee, L. Jeong, Y. O. Kang, S. J. Lee, and W. H. Park, "Electrospinning of polysaccharides for regenerative medicine," *Adv. Drug Deliv. Rev.* vol. 61, no. 12, pp. 1020–1032, 2009.

[80] K. E. Park, H. K. Kang, S. J. Lee, B.-M. Min, and W. H. Park, "Biomimetic nanofibrous scaffolds: preparation and characterization of PGA/chitin blend nanofibers," *Biomacromolecules*, vol. 7, no. 2, pp. 635–643, 2006.

[81] E.-R. Kenawy, G. L. Bowlin, K. Mansfield, J. Layman, D. G. Simpson, E. H. Sanders, and G. E. Wnek, "Release of tetracycline hydrochloride from electrospun poly(ethylene-co-vinylacetate), poly(lactic acid), and a blend," *J. Control. Release*, vol. 81, no. 1–2, pp. 57–64, 2002.

[82] X. Xu, X. Chen, P. Ma, X. Wang, and X. Jing, "The release behavior of doxorubicin hydrochloride from medicated fibers prepared by emulsion-electrospinning," *Eur. J. Pharm. Biopharm.* vol. 70, no. 1, pp. 165–170, 2008.

[83] J. Xie, R. S. Tan, and C. Wang, "Biodegradable microparticles and fiber fabrics for sustained delivery of cisplatin to treat C6 glioma in vitro," *J. Biomed. Mater. Res. Part A*, vol. 85, no. 4, pp. 897–908, 2008.

[84] D. Liu, S. Liu, X. Jing, X. Li, W. Li, and Y. Huang, "Necrosis of cervical carcinoma by dichloroacetate released from electrospun polylactide mats," *Biomaterials*, vol. 33, no. 17, pp. 4362–4369, 2012.

[85] T. Amna, M. S. Hassan, K.-T. Nam, Y. Y. Bing, N. A. M. Barakat, M.-S. Khil, and H. Y. Kim, "Preparation, characterization, and cytotoxicity of CPT/Fe2O3-embedded PLGA ultrafine composite fibers: A synergistic approach to develop promising anticancer material," *Int. J. Nanomedicine*, vol. 7, p. 1659, 2012.

[86] Y. Yu, L. Kong, L. Li, N. Li, and P. Yan, "Antitumor Activity of Doxorubicin-Loaded Carbon Nanotubes Incorporated Poly(Lactic-Co-Glycolic Acid) Electrospun Composite Nanofibers," *Nanoscale Res. Lett.* vol. 10, no. 1, pp. 1–9, 2015.

[87] D. B. Tada, S. Singh, D. Nagesha, E. Jost, C. O. Levy, E. Gultepe, R. Cormack, G. M. Makrigiorgos, and S. Sridhar, "Chitosan Film Containing Poly(D,L-Lactic-Co-Glycolic Acid) Nanoparticles: A Platform for Localized Dual-Drug Release," *Pharm. Res.* vol. 27, no. 8, pp. 1738–1745, 2010.

[88] R. Qi, J. Yu, and X. Shi, "Electrospun Poly ( lactide-co-glycolide )/ Nanotube Composite Nanofibers for Drug Encapsulation and Sustained Release," *Vacuum*.

[89] N. G. Veerabadran, R. R. Price, and Y. M. Lvov, "Clay Nanotubes for Encapsulation and Sustained Release of Drugs," *Nano*, vol. 02, no. 02, pp. 115–120, 2007.

[90] V. Vergaro, E. Abdullayev, Y. M. Lvov, A. Zeitoun, R. Cingolani, R. Rinaldi, and S. Leporatti, "Cytocompatibility and Uptake of Halloysite Clay Nanotubes," *Biomacromolecules*, vol. 11, no. 3, pp. 820–826, 2010.

[91] D. G. Shchukin, G. B. Sukhorukov, R. R. Price, and Y. M. Lvov, "Halloysite nanotubes as biomimetic nanoreactors," *Small*, vol. 1, no. 5, pp. 510–513, 2005.

[92] D. S. Kommireddy, I. Ichinose, Y. M. Lvov, and D. K. Mills, "Nanoparticle Multilayers: Surface Modification for Cell Attachment and Growth," *J. Biomed. Nanotechnol.* vol. 1, no. 3, pp. 286–290, 2005.

[93] V. Vergaro, Y. M. Lvov, and S. Leporatti, "Halloysite clay nanotubes for resveratrol delivery to cancer cells," *Macromol. Biosci.* vol. 12, pp. 1265–1271, 2012.

[94] L. T. University, "FE-SEM S4800 HITACHI." [Accessed Online Dec 9, 2015]. Available: http://www.latech.edu/ifm/resources/equipment/hitachi_s-4800.php.

[95] Tulane, "Tecnai G2 F30 TWIN 300 kV / FEG Transmission Electron Microscope." [Accessed Online Dec 9, 2015]. Available: http://tulane.edu/sse/cif/microscopy.cfm.

[96] Louisian Tech University, "Brookhaven Instruments ZetaPlus Potential and Particle Size Analyzer." [Accessed Online Dec 9, 2015]. Available: http://www.ifm.latech.edu/resources/equipment/zetaplus.php.

[97] "Nanodrop 2000." [Accessed Online Dec 9, 2015]. Available: http://www.nanodrop.com/Productnd2000overview.aspx.

[98] Invtirogen, "Qubit® 2.0 Fluorometer." [Accessed Online Dec 9, 2015]. Available: https://tools.thermofisher.com/content/sfs/manuals/mp32866.pdf.

[99] TCP Global, "Master Performance G22 Airbrush Kit with Master Compressor TC-20 & Air Hose." [Accessed Online Dec 9, 2015]. Available: http://www.tcpglobal.com/ABD-KIT-G222_2.html?sc=113&category=2738755.

[100] M. P. Link, A. M. Goorin, A. W. Miser, A. A. Green, C. B. Pratt, J. B. Belasco, J. Pritchard, J. S. Malpas, A. R. Baker, and J. A. Kirkpatrick, "The effect of adjuvant chemotherapy on relapse-free survival in patients with osteosarcoma of the extremity," *N. Engl. J. Med.* vol. 314, no. 25, pp. 1600–1606, 1986.

[101] L. Sun, "Drug coated clay nanoparticles for delivery of chemotherapeutics," *Curr. Nanosci.* vol. 11.

[102] "Halloysite Product Information." [Accessed Online Dec 9, 2015]. Available: http://www.sigmaaldrich.com/catalog/product/aldrich/685445?lang=en&region=US.

[103] W. Wei, "Halloysite nanotube composites for sustained release of antimocrobial agents (antiseptics and antibiotics)," Louisiana Tech, Ruston, 2013.

[104] N. Jaffe, "Osteosarcoma: review of the past, impact on the future. The American experience," in *Pediatric and Adolescent Osteosarcoma*, Springer, 2010, pp. 239–262.

[105] M. Alameh, D. DeJesus, M. Jean, V. Darras, M. Thibault, M. Lavertu, M. D. Buschmann, and A. Merzouki, "Low molecular weight chitosan nanoparticulate system at low N: P ratio for nontoxic polynucleotide delivery," *Int. J. Nanomedicine*, vol. 7, p. 1399, 2012.

[106] M. Jean, M. Alameh, M. D. Buschmann, and A. Merzouki, "Effective and safe gene-based delivery of GLP-1 using chitosan/plasmid-DNA therapeutic nanocomplexes in an animal model of type 2 diabetes," *Gene Ther.* vol. 18, no. 8, pp. 807–816, 2011.